Distribution Agreement

In presenting this thesis or dissertation as a partial fulfillment of the requirements for an advanced degree from Emory University, I hereby grant to Emory University and its agents the non-exclusive license to archive, make accessible, and display my thesis or dissertation in whole or in part in all forms of media, now or hereafter known, including display on the world wide web. I understand that I may select some access restrictions as part of the online submission of this thesis or dissertation. I retain all ownership rights to the copyright of the thesis or dissertation. I also retain the right to use in future works (such as articles or books) all or part of this thesis or dissertation.

Signature:

_____ _____

Matthew Tillman Date

A STRUCTURAL AND BIOCHEMICAL INVESTIGATION OF HOW LIPID MESSENGERS ACT THROUGH LIPID TRANSFER PROTEINS TO REGULATE METABOLISM AND LONGEVITY

By

Matthew Clyde Tillman
Doctor of Philosophy

Graduate Division of Biological and Biomedical Science
Molecular and Systems Pharmacology

_____
Eric A. Ortlund, Ph.D.
Advisor

_____
David E. Cohen, M.D., Ph.D.
Committee Member

_____
Dean P. Jones, Ph.D.
Committee Member

_____
Renhao Li, Ph.D.
Committee Member

Accepted:

_____
Lisa A. Tedesco, Ph.D.
Dean of the James T. Laney School of Graduate Studies

_____
Date

A STRUCTURAL AND BIOCHEMICAL INVESTIGATION OF HOW LIPID MESSENGERS ACT THROUGH LIPID TRANSFER PROTEINS TO REGULATE METABOLISM AND LONGEVITY

By

Matthew Clyde Tillman
B. S., Georgia Institute of Technology, 2013

Advisor: Eric A. Ortlund, Ph.D.

An abstract of
A dissertation submitted to the Faculty of the
James T. Laney School of Graduate Studies of Emory University in partial fulfillment of the
requirements for the degree of Doctor of Philosophy
in Graduate Division of Biological and Biomedical Science
Molecular and Systems Pharmacology
2020

Abstract

Lipids signal to control cellular homeostasis, metabolism, inflammation, and aging. Since lipids are hydrophobic, they are primarily sequestered within membranes, which limits their ability to signal through diffusion. Lipid transfer proteins (LTPs) solubilize lipids and mediate their signaling effects. LTPs are not simply passive carriers of lipids but are active participants in signaling that sense specific lipids that in turn regulate LTP function. In this study, we biochemically and structurally characterize two LTPs that control aging and lipid metabolism respectively. We determine the first structure of Lipid Binding Protein 8 (LBP-8), a fatty acid binding protein in *Caenorhabditis elegans* that extends lifespan through carrying lysosomal lipid signals into the nucleus to initiate expression of life prolonging genes. We identify a structurally conserved nuclear localization signal and describe a range of fatty acids LBP-8 is capable of binding, including life extending ligands such as oleic acid and oleoylethanolamide. Secondly, we characterize the functional role of the lipid binding StAR-related lipid transfer domain (StarD) of Thioesterase Superfamily Member 1 (Them1) to regulate lipid metabolism and thermogenesis in brown adipocytes. We show the StarD of Them1 acts as a lipid sensor, binding fatty acid and lysophosphatidylcholine species, which allosterically control the enzymatic activity of Them1. Furthermore, we also show how ADP and ATP allosterically control Them1 activity through a distinct mechanism. Together, lipids and ADP/ATP engage molecular switches that fine tune Them1 activity to regulate the thermogenic capacity of brown adipose tissue. Collectively, this work shows how lipids interact with LTPs to control their activity and vital biological processes.

A STRUCTURAL AND BIOCHEMICAL INVESTIGATION OF HOW LIPID MESSENGERS ACT THROUGH LIPID TRANSFER PROTEINS TO REGULATE METABOLISM AND LONGEVITY

By

Matthew Clyde Tillman
B. S., Georgia Institute of Technology, 2013

Advisor: Eric A. Ortlund, Ph.D.

A dissertation submitted to the Faculty of the
James T. Laney School of Graduate Studies of Emory University in partial fulfillment of the
requirements for the degree of Doctor of Philosophy
in Graduate Division of Biological and Biomedical Science
Molecular and Systems Pharmacology
2020

Acknowledgements

I would like to thank my dissertation committee for their continual guidance through my graduate research. My Ph.D. advisor, Dr. Eric Ortlund, has been a constant source of encouragement and excellent mentor. I am grateful for all of my colleagues in the Ortlund lab. I have learned so much from all of you through conversations about my project and watching you in your research. Most of all, I'm thankful to call you all my friend. I would have never pursued a career in research if it was not for the encouragement of Dr. Berkley Gryder. Thank you, old friend. Abbey, you challenge me to work harder, think smarter, and be the best I possibly can. Thank you for your support through these years of research. I owe the greatest thanks to God. Through the highs and lows of research, Jesus Christ is my constant source of joy and hope. The small findings that lie within this dissertation are just a glimpse of the wisdom of God. To God alone be the glory.

Table of Contents

ABBREVIATIONS

1,8-ANS: 1-anilinonaphthalene-8-sulfonic acid

AA: arachidonic acid

ACSL1: acyl-CoA synthetase 1

ADP: adenosine diphosphate

ACOT: acyl-Coa thioesterase

ANOVA: analysis of variance

ApoD: apolipoprotein D

AR: androgen receptor

ATP: adenosine triphosphate

BAT: brown adipose tissue

BFIT: brown fat inducible thioesterase

BPI/LBP/CETP N-terminal domain: bactericidal permeability-increasing protein/ lipopolysaccharide-binding protein/ cholesteryl ester transfer protein N-terminal domain

CD: circular dichroism

CERT: ceramide transfer protein

CoA: coenzyme A

CRABP: cellular retinoic acid binding protein

CRBP: cellular retinol binding protein

DGLA: dihomo-γ-linoleic acid

DNA: deoxyribonucleic acid

DSF: differential scanning fluorimetry

DTNB: 5,5′-dithiobis-(2-nitrobenzoic acid)

EGFP: enhance green fluorescent protein

EMS: enhanced mass spectrometry

ER: endoplasmic reticulum

FA: fatty acid

FABP: fatty acid binding protein

GL: glycerolipids

GLTP: glycolipid transfer protein

GP: glycerophospholipids

GR: glucocorticoid receptor

GST: glutathione S-transferase

HDX-MS: hydrogen-deuterium exchange mass spectrometry

iBAs: immortalized brown adipocytes

iLBPs: intracellular lipid-binding proteins

kD: kilodalton

Km: Michaelis constant

LBP-2: Lipid Binding Protein 2

LBP-3: Lipid Binding Protein 3

LBP-8: Lipid Binding Protein 8

LCFAs: long-chain fatty acids

LC/MS: liquid chromatography/mass spectrometry

LIPL-4: lysosomal acid lipase 4

LPC: lysophosphatidylcholine

LPCAT2: lysophosphatidylcholine acyltransferase 2

LRH-1: liver receptor homolog-1

LTP: lipid transfer protein

LXR: liver X receptor

MBP: maltose0binding protein

MCS: membrane contact sites

MD: molecular dynamics

ML: MD-2-related lipid-recognition

MOI: multiplicity of infection

MS: mass spectrometry

MST: microscale thermophoresis

NE: norepinephrine

NHR: nuclear hormone receptor

NLS: nuclear localization signal

NPC1 NTD: Niemann–Pick C1 N-terminal domain

NRs: nuclear receptors

OA: oleic acid

OCR: oxygen consumption rate

OEA: oleoylethanolamide

OSBP: oxysterol-binding protein

PBS: phosphate buffered saline

PC: phosphatidylcholine

PCA: protein-fragment complementation assays

PCTP: phosphatidylcholine transfer protein

PDB: protein data bank

PDGS: prostaglandin D synthase

PH: pleckstrin homology

PIP: phosphatidylinositol-4-phosphate

PIP2: phosphatidylinositol-4,5-bisphosphate

PIP3: phosphatidylinositol-3,4,5-triphosphate

PITP: phosphatidylinositol transfer protein

PK: polyketides

PKA: protein kinase A

PMA: phorbol 12-myristate 13-acetate

PPAR: peroxisome proliferator-activated receptor

PPIs: protein-protein interactions

PR: prenol lipids

PUFAs: polyunsaturated fatty acids

qRT-PCR: quantitative reverse transcription polymerase chain reaction

RABP: retinoic acid-binding protein

RARA: retinoic acid receptor α

RARB: retinoic acid receptor β

RBP: retinol-binding protein

RMSD: root mean squared deviation

RMSF: root mean squared fluctuation

SAM: sterile alpha motif

SCP2: sterol carrier protein 2

SEM: standard error of the mean

SL: saccharolipids

SP: sphingolipids

ST: sterol lipids

StAR: steroidogenic acute regulator protein

StarD: START domain

START: StAR related transfer

SUMO: small ubiquitin-like modifier

TCEP: tris(2-carboxyethyl)phosphine

TEV: tobacco etch virus

Them1: thioesterase superfamily member 1

T_m: thermal melting temperature

TNP-ATP: 2,4,6-trinitrophenol-adenosine triphosphate

UCP1: uncoupling protein 1

V_o: enzyme initial velocity

V_{max}: enzyme maximum velocity

ω-3 AA: ω-3 arachidonic acid

CHAPTER 1: INTRODUCTION

Lipids are signaling molecules

Lipids serve a vital role in energy storage and also construct membranes that allow for compartmentalization of biological processes necessary for life. In addition to these significant roles, lipids are signaling molecules that allow cells and tissues to communicate and respond to stimuli. Lipid signaling controls a wide range of biological processes including metabolism, inflammation, and aging [1-3]. Disruption of lipid signaling can lead to various diseases including metabolic disorders and cancer; therefore, a more thorough understanding of these signaling events is desired to aid in the development of novel therapeutics [2].

Lipids are divided into seven classes based on their chemical and biochemical properties: fatty acids (FA), glycerolipids (GL), glycerophospholipids (GP), sphingolipids (SP), sterol lipids (ST), prenol lipids (PR), saccharolipids (SL), and polyketides (PK) (see LIPID MAPS, http://www.lipidmaps.org/data/classification/LM_classification_exp.php). These lipid classes are diverse in structure and composition but share the common attribute of being hydrophobic. Given their hydrophobic nature, they are not readily solubilized in the aqueous environment of the cell; therefore, they are primarily sequestered within membranes. This creates a biophysical hurdle for lipids to overcome in order to signal to all cellular compartments since they do not easily diffuse between organelles.

Lipids are heterogeneously distributed within membranes of cellular organelles, laterally heterogeneous as evidenced by lipid domains/rafts, and asymmetrically distributed between the two membrane leaflets [4]. To achieve this level of heterogeneity, there must be mechanism other than simple diffusion to transport lipids throughout the cell. Lipids can be transferred through vesicular transport; however, lipid transport is still detected when this machinery is disrupted [5, 6]. Additionally, lipid transfer between the ER and plasma membrane occurs much quicker than can

be explained by vesicular transport [7, 8]. These findings suggest there are nonvesicular shuttling mechanisms.

Cytosolic lipid transfer proteins (LTPs)

Nonvesicular lipid transport was first postulated when isolated proteins were discovered to facilitate the transfer of lipids between radiolabeled donor membranes and unlabeled liposomes [9, 10]. In these early *in vitro* studies, lipid transfer proteins (LTPs), as they were later named, were identified to mediate an equilibrium reaction through efficiently and quickly transferring lipids between membranes. Since these early days, the number of identified LTPs and their understood functional roles have vastly expanded [11]. There are about 125 distinct genes that encode for LTPs that are grouped into ten families: calycin, StAR related transfer (START) domains (StarDs), MD-2-related lipid-recognition (ML), BPI/LBP/CETP N-terminal domain, oxysterol-binding protein (OSBP), phosphatidylinositol transfer protein (PITP), sterol carrier protein 2 (SCP2), Niemann–Pick C1 NTD (NPC1 NTD), CRAL-TRIO domain, and glycolipid transfer protein (GLTP) [12].

These distinct groups of LTPs adopt a range of conformational folds, with some containing β-barrels with few α-helices like the calycin family, while others contain only α-helices like the CRAL-TRIO and GLTP families[12]. However, all LTPs contain a hydrophobic pocket that accommodates a lipid, protecting lipids from the aqueous cellular environment. Most LTPs bind to a singular lipid, though some LTPs, like FABP1 (calycin family), contain a large interior cavity that are able to bind to multiple lipids, while others can oligomerize and form tunnels to shuttle several lipids such as CETP [13, 14]. Though LTPs are capable of binding to a wide range of lipids, they contain structural features that enable specificity. The shape and size

of the interior pocket of LTPs can specify which lipids bind. For instance, certain members of the StarD family, such as StarD1 and StarD3, contain an interior pocket size of 1014–1122 $Å^3$, which is close to the size of their natural ligand cholesterol, while other members, like StarD2, contain much larger pockets that can accommodate phospholipids [15]. LTPs also select for lipids through polar residues within the pocket that can engage electrostatically with polar moieties on the lipid. As an example, FABPs of the calycin family conserve an arginine and tyrosine residue that participate in hydrogen bonding with the carboxyl head group of fatty acids [16, 17].

The physiological roles of LTPs are vast and remain largely unexplored. Many LTPs are multidomain proteins, with each unit exhibiting a different function, making it technically difficult to assign a physiological role to LTPs. In general, LTPs are involved in metabolism, inflammation, and aging [18]. Disruption of LTPs can lead to diseases like Niemann–Pick disease type C from mutations in NPC1 and NPC2, and lipoid congenital adrenal hyperplasia from mutations in StarD1 [19, 20]. Specific LTPs in *C. elegans* expanded lifespan when overexpressed [3, 17, 21]. Deletion of certain LTPs like FABP4 and FABP5 increase insulin sensitivity and protects against atherosclerosis in mice [18]. Overviews of all LTP families have been published previously [11, 12, 22]. For the purpose of this study, we more closely examine the calycin and StarD families.

Structure and binding preference of calycins

Calycins are a sequence diverse group of ~20 kilodalton lipid binding proteins that share a common fold. The superfamily is divided into three main families: lipocalin, fatty acid binding protein (FABP), and avidin (Fig. 1). Lipocalins are found in prokaryotes and eukaryotes, while FABPs are only found in the animal kingdom and either evolved from lipocalins or

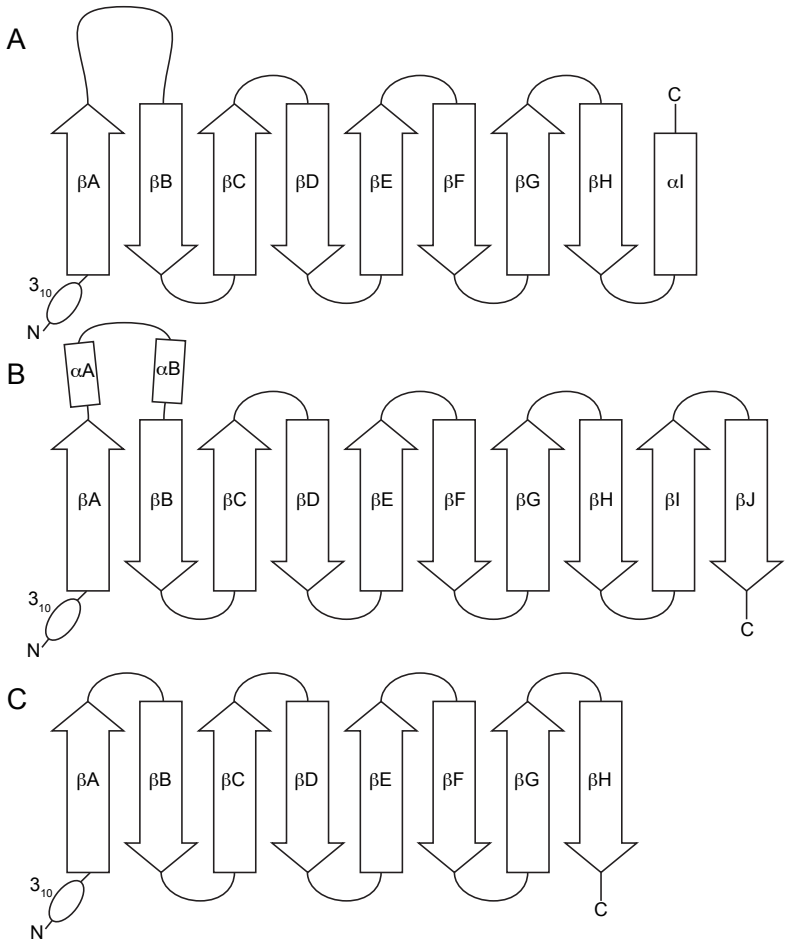

Figure 1. Schematic of structural features of calycin family members. *A.* Lipocalins contain eight antiparallel β-strands and one C-terminal α-helix. There is a large **Ω** loop between βA-βB strands that constructs the lid of the lipocalin. *B.* FABPs contain two more β-strands than lipocalins and do not contain a C-terminal α-helix. Additionally, FABPs contain two α-helices within the **Ω** loop between βA-βB strands. *C.* Avidins only contain eight β-strands, like lipocalins, but do not contain a C-terminal α-helix. There is only a small β-hairpin between βA-βB. All calycin members contain a N-terminal 3_{10} like helix. Figure adapted from Flower et. al.[23]

evolutionarily converged into a similar fold and function [24, 25]. The general conserved structure of calycins is a β-barrel consisting of anti-parallel β-sheets that encapsulate a hydrophobic molecule (Fig. 2). Lipocalins and avidins contain eight β-sheets, while FABPs contain ten (Fig. 1) [23, 26, 27]. All β-strands are connected by short β-hairpins except the first loop connecting βA-βB, which is a large Ω loop that serves as the lid for the β-barrel in lipocalins and FABPs (Fig. 1). In FABPs, this loop contains two α-helices that are important for lipid binding, membrane association, and localization (Fig. 1B, Fig. 2) [17, 28-31]. Lipocalins uniquely contain a C-terminal α-helix that packs back onto the β-barrel (Fig. 1A) [23, 27]. All calycins conserve a short N-terminal 3_{10}-like helix leading into the initial β-strand (Fig. 1).

Lipocalins are typically secreted, as opposed the FABPs that are primarily intracellular. The lipocalin family consists of kernel lipocalins that are closely related, like retinol-binding protein (RBP), retinoic acid-binding protein (RABP), apolipoprotein D (ApoD), and prostaglandin D synthase (PGDS), and a smaller subset of outlier lipocalins that are more divergent [27]. They bind a wide range of lipids such as retinol, retinoic acid, fatty acids, progesterone, prostaglandins, and pheromones, and are involved in transport, enzymatic synthesis, olfaction, and cell regulation [27, 32-35].

Human FABPs are subdivided into four groups based upon the lipids they bind [24]. Group I contains cellular retinol binding protein (CRBP) and cellular retinoic acid binding protein (CRABP) that bind to retinol derivatives [36, 37]. Group II contains FABP1 and FABP6, which have a large interior cavity that accommodates bile acids, acyl-CoA, heme, and multiple fatty acids [13, 38-40]. Group III contains FABP2 that binds to long-chain fatty acids (LCFAs) [39-41]. Group IV includes FABP3, FABP4, FABP5, FABP7, FABP8, and FABP9 that bind to LCFAs, eicosanoids, and retinols [37, 39, 41]. FABPs are thought to operate as monomers, but one study

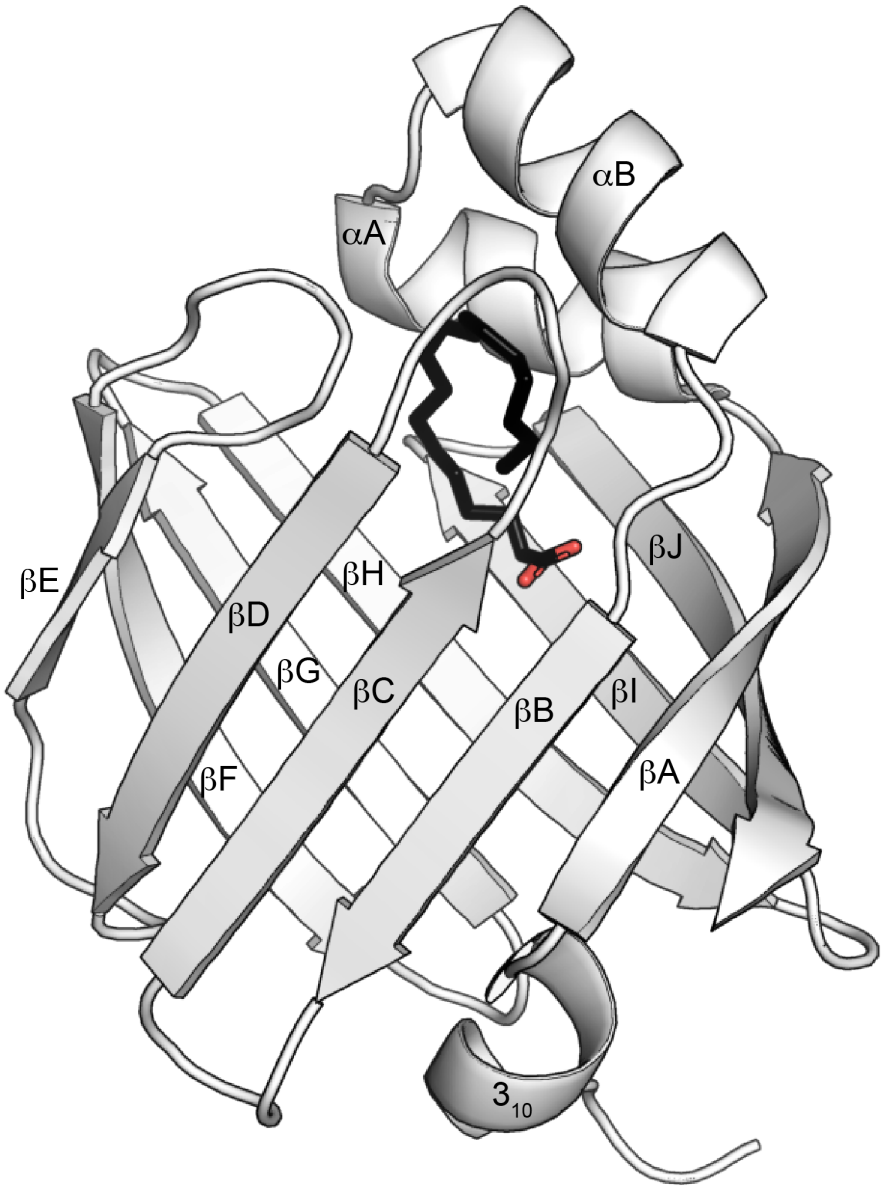

Figure 2. Structure of FABP5 bound to linoleic acid. Crystal structure of FABP5 (white) bound to linoleic acid (black) (PDB code: 4LKT) [28]. FABP5 contains ten β-strands forming a β-barrel and two α-helices that make up the lid. Linoleic acid is bound in the internal cavity of the protein, protected from solvent by the α-helical lid. All FABPs adopt this similar fold.

showed that FABP4 forms a dimer in solution, and interesting CRBPII and FABP5 structures were solved as domain swapped dimers, suggesting FABPs could operate as functional dimers [42-44]. Most FABPs acquire lipids through a "collisional" method that involves the α-helical lid inserting into the membrane surface, though some may acquire lipid by diffusion through the opposite end of the β-barrel [29]. The carboxyl head group of fatty acids and retinoic acid are stabilized through hydrogen bonding with a highly conserved arginine and tyrosine residue (Arg – X – Tyr) present in the last β-sheet (βJ), termed the P2 motif [24, 45]. These polar residues are important to stabilize fatty acids, but the bulky nonpolar residues surrounding the pocket are the main drivers of lipid binding, as site directed mutagenesis of these residues significantly disrupts binding [16]. Though many hydrophobic lipids are capable of binding to FABPs, only certain "activating" lipids induce specialized FABP functions. For instance, saturated fatty acids bind to FABP5, but only polyunsaturated fatty acids (PUFAs) stimulate FABP5 nuclear localization [28]. This occurs because PUFAs stabilize a patch of basic residues in the α-helical lid of FABP5 that make up a tertiary nuclear localization signal (NLS) [28]. Multiple other FABPs conserve this tertiary NLS, yet other NLS stabilizing lipids that stimulate nuclear localization still need to be identified [17, 42, 46].

Avidins are characterized by their high affinity for the vitamin biotin ($K_D = 10^{-15}$ M) [47]. They are similar in conformation to the lipocalins yet contain a much smaller loop between βA and βB [26]. The avidins bind to biotin as homotetramers, but recently, a subclass of bacterial avidins were discovered as dimers [48]. Biotin binds within the hydrophobic pocket, but the carboxyl tail of biotin is exposed to solvent [49]. Due to their high affinity for biotin, avidins have been utilized for various biochemical procedures [50].

Structure and binding preference of StarDs

Steroidogenic acute regulatory protein (StAR)-related lipid-transfer (START) domains (StarDs) are present in animals and plants, but absent in Archarbacteria [51]. Humans have 15 StarD containing proteins that are divided into six groups based upon phylogenetic analysis [52, 53]. The first group contains StarD1 and StaD3, which both bind to cholesterol [54]. The second group, consisting of StarD4, StarD5, and StarD6, also bind to cholesterol, but additionally bind to oxysterols and steroids [55-57]. The third group contains StarD2, StarD7, StarD10, and StarD11, which bind to phospholipids and ceramide [58-61]. The first three groups, other than StarD11, contain proteins that stand alone as ~30 kilodalton proteins, but the last three groups are multidomain proteins with a C-terminal StarD. Group four contains StarD8, StarD12, and StarD13, which have an N-terminal SAM (sterile alpha motif) domain that is involved in oligomerization and a central Rho-GAP domain that regulates GTPases [53]. The native ligands for these StarDs remains unknown. The fifth group, containing StarD14 and StarD15, have N-terminal thioesterase domains that hydrolyze acyl-CoA and acetyl-CoA respectively [62, 63]. The ligands for this group of StarDs is also unknown. Lastly, very little is known about the sole member of the last group, StarD9, though a recent study showed it is involved in mitotic spindle formation [64].

All StarDs share the same helix-grip fold consisting of a central curved antiparallel β-sheet surrounded by a C-terminal and N-terminal α-helix (α_A and α_D) (Fig. 3). Additionally, there are two Ω loops inserted between β_E and β_F (Ω_1) and β_G and β_H (Ω_2) (Fig. 3). The C-terminal α-helix folds onto the concaved β-sheet to form an amphipathic pocket that can accommodate lipid ligands. This helix serves as a gate for lipid binding, as it is unfolded in the

apo state, whereas ligand binding induces the closing of the helix onto the mouth of the pocket [54, 65]. Tryptophan 147 (StarD1 numbering), which is conserved in all human StarD family members,

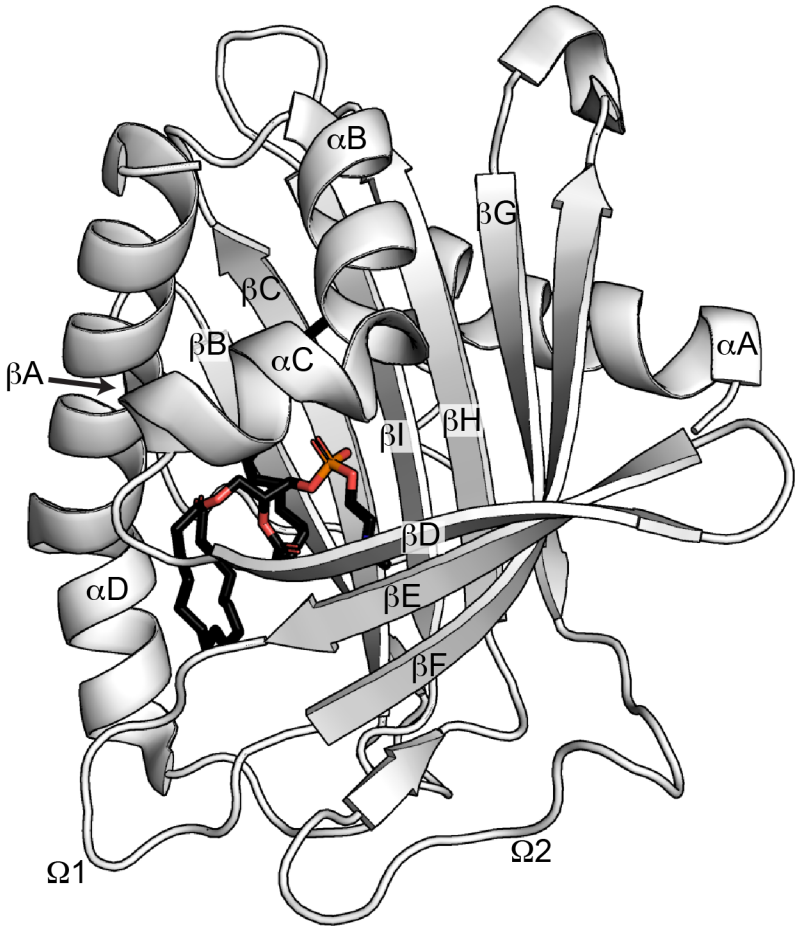

Figure 3. Structure of StarD2 bound to palmitoyl-linoleoyl phosphatidylcholine. Crystal structure of StarD2 (white) bound to palmitoyl-linoleoyl phosphatidylcholine (black) (PDB code: 1LN3) [66]. StarD2 contains nine antiparallel β-strands that are gripped by two α-helices (αA and αD). The C-terminal helix (αD) closes in on the mouth of the internal pocket where palmitoyl-linoleoyl phosphatidylcholine is bound. All StarDs fold adopt a similar fold.

contacts the C-terminal helix and likely aids in this gating function [15]. Additionally, the C-terminal helix, along with Ω_1, are involved with membrane association and lipid extraction [67]. StarD2 and StarD11 are the only StarDs with structures containing bound lipids, respectively phosphatidylcholine (PC) [59, 66] and ceramide [66, 68]. There are conserved bulky hydrophobic residues that encapsulate the acyl tails of lipids and basic/acidic residues that contact the polar components of lipids, such as the highly conserved arginine (StarD2 R78, StarD11 R442) that in StarD2 electrostatically interacts with the phosphate of phospholipids [66] and in StarD11 contacts the hydroxyl of ceramides [68]. There are structural features that are not conserved across StarD family members that allow for specificity in lipid binding. For instance, StarD2 contains residues that form an aromatic cage, which is not found in StarD11, that engage in cation-π interactions with the quaternary amine of choline [66].

Functions of LTPs

Though the functional roles of LTPs are diverse, they can be grouped into three main modes of action: lipid transporters that shuttle lipids between membranes, lipid chaperones that carry lipids to other proteins, and lipid sensors that regulate signaling and protein activity (Fig. 4). LTPs are not restricted to only one mode of action, but can participate in multiple functional roles, such as FABP5 [28, 69] and OSBP [70, 71].

Lipid Transporters

The transport of lipids from one membrane to another was the first described purpose of LTPs [9, 10]. Since the ER is the main site of lipid synthesis, many LTPs are responsible for distributing these newly synthesized lipids throughout the cell. LTPs can carry ER lipids to

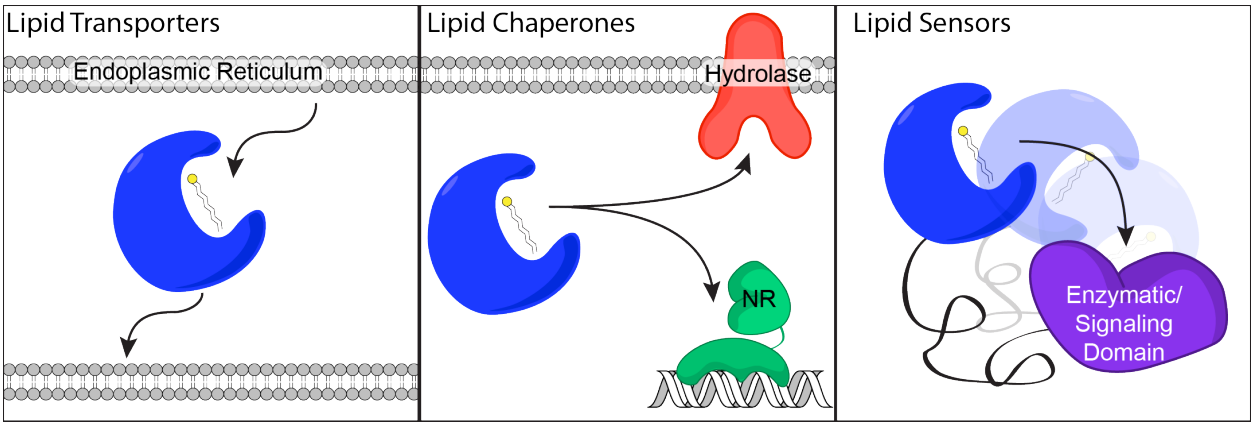

Figure 4. Schematic of functional roles of LTPs. LTPs participate in three distinct modes of action. First, LTPs can act as lipid transporters, shuttling lipids from one membrane to another (left). Since most lipids are synthesized in the endoplasmic reticulum (ER), LTPs often extract lipids from the ER and carry them to other organelle membranes. Lipids also work as lipid chaperones, transporting lipids to other proteins (middle). LTPs have been shown to transfer lipids to hydrolases that metabolize lipids and nuclear receptors (NR) to control gene transcription. Lastly, LTPs can serve as lipid sensors that detect the lipid environment and will undergo a conformational change once certain lipids bind, which in turn regulates the activity and signaling of an adjacent domain (right). Figure was adapted from Chiapparino et. al. [12]

distant membranes, but most lipid transfer occurs at membrane contact sites (MCS), which are small cytosolic gaps (10-20 nm) between the membranes of the ER and other organelles [72, 73]. Though lipids can spontaneously diffuse at these sites, LTPs greatly facilitate the transfer of lipids, and in some cases, allow for their transfer against concentration gradients [74, 75]. StarD7 is responsible for transporting PC synthesized in the ER to the mitochondria which is unable to synthesize its own [58, 76]. It contains an N-terminal mitochondrial targeting sequence and a transmembrane domain that anchors it in the mitochondrial membrane [58, 77]. The StarD is then able to shuttle PC from the ER to the mitochondria at MCS [77]. Furthermore, deletion of StarD7 grossly disrupts mitochondrial shape and respiration due to reduced levels of membrane PC [76]. StarD11, more commonly known as ceramide transfer protein (CERT), is responsible for transporting ceramide from the ER to the Golgi complex, where it can be converted into sphingomyelin [61, 78, 79]. CERT contains an N-terminal pleckstrin homology (PH) domain that associates with phosphatidylinositol-4-phosphate (PI4P) found in the Golgi [79] and a FFAT motif (two phenylalanines in an acidic tract) that interacts with ER resident membrane proteins [80], which work together to tether CERT to the Golgi and ER [78]. The StarD of CERT specifically extracts ceramide from ER membranes, and swings over to transfer the lipid to the Golgi membrane at MCS [79]. StarD3 contains an N-terminal MENTAL domain that anchors it to endosome membranes [81] and a FFAT motif like CERT that tethers it to the ER [82, 83]. This positions StarD3 at MCS where it transfers sterols from the ER to the endosome membrane [84]. In addition to the transfer of lipids by LTPs in the cytosol, LTPs are also secreted into the plasma to interact with lipoproteins and presumably transfer lipids between tissues [85]. FABP4 is secreted from adipocytes and at lower levels from macrophages [86-88]. FABP4 secretion is positively correlated with increased adiposity, insulin resistance, and other metabolic diseases [89].

Lipid Chaperones

In addition to LTPs transporting lipids to membranes, they also transport lipids directly to proteins such as enzymes, transmembrane transporters, nuclear receptors, or other LTPs. These protein-protein interactions and handoff of lipids regulate vital signaling processes involved in metabolism and homeostasis.

LTPs commonly shuttle their cargo to lipid metabolizing enzymes. For instance, FABP5 shuttles anandamide, an endocannabinoid that reduces stress, pain, and inflammation, to fatty acid amide hydrolase to be hydrolyzed [69]. Cellular retinol-binding protein 1 (CRBP1), a member of the calycin family, carries retinol from its plasma membrane transporter to retinol-metabolizing enzymes [90]. In addition to carrying lipids to enzymes, LTPs can carry lipids away from enzymes. For example, FABP4 enhances the activity of hormone sensitive lipase through removing fatty acids generated from lipolysis, thus relieving product inhibition [91].

There are several lines of evidence that FABPs commonly interact with nuclear receptors to regulate transcription. For one, many FABPs bind to the same endogenous lipids and drugs that activate nuclear receptors [92, 93]. Secondly, multiple FABPs contain nuclear localization signals (NLS) and are readily visualized within the nucleus [28, 42, 46]. Additionally, the presence of FABPs enhances the transcriptional activity of nuclear receptors [92, 94]. FABPs primarily target peroxisome proliferator-activated receptor family members (PPARα, PPARβ/δ, and PPARγ) and retinoic acid receptor α (RARA) nuclear receptors. The following FABP-nuclear receptor interactions have been identified at this point: FABP1 and FABP2 interact with PPARα [95], FABP5 interacts with PPARβ/δ [28], FABP4 interacts with PPARγ [42], and CRABPII interacts with RARA [46]. Though FABPs are capable of binding a wide range of lipids, these interactions with nuclear receptors are often driven by specific lipids. Activating ligands can stabilize the nuclear

localization signal on the FABP so that it can interact with importins, thus stimulating nuclear localization and interaction with nuclear receptors [28, 42, 46]. This however is not ubiquitous for all FABPs, as FABP1 and FABP2 freely diffuse into the nucleus without a nuclear localization signal and interact with PPARα in a ligand-specific fashion [95]. There are FABPs that conserve the nuclear localization signal found in FABP4, FABP5, and CRABPII, but it is not known if these FABPs also interact with nuclear receptors. There is much less known about StarDs interacting with nuclear receptors, though StarD2 has been reported to interact with PPARα and upregulate its activity [96]. Additionally, StarDs are joined to DNA-binding domains in plants acting as transcription factors, corroborating this potential role [51].

Lipid Sensors

Since many LTPs are multidomain proteins, this raises the possibility that ligand binding could regulate the activity of adjacent domains. This regulation can occur through lipid induced conformation changes that either alter protein localization or activity. Oxysterol binding protein (OSBP) is an example of a lipid transporter and sensor. OSBP contains a FAAT domain that localizes the protein to the ER. Once OSBP binds to sterols, a conformation change occurs that uncovers a PH domain that allows it to tether to other membranes that contain phosphatidylinositol-phosphates (PIP2 and PIP3) [70, 71]. Additionally, sterol bound OSBP acts as a scaffold, binding multiple phosphatases that cannot bind in the apo state [97]. This sterol-OSBP/phosphatase complex dephosphorylates pERK and regulates MAP kinase signaling, connecting sterol sensing with signaling pathways [97].

Many StarDs are contained within multidomain proteins containing enzymatic or signaling domains and potentially act as lipid sensors, though there is little experimental

evidence for this. StarD8, StarD12, and StarD13 all contain N-terminal Rho-GAP domains, but it is unknown if the StarDs regulate the activity of the Rho-GAP domains. StarD14 and StarD15 contain two N-terminal thioesterase domains that are regulated by the StarDs, as evidenced by significantly attenuated enzymatic activity when the StarDs are truncated [63, 98]. In StarD14, the enzymatic activity was recovered once the StarD was added back in *trans*, suggesting the StarD regulates enzymatic activity [63]. Similarly, StarD2 enhanced the activity of Them2, another thioesterase, when added in *trans* [99]. With these examples, it is clear that certain StarDs enhance the activity of specific thioesterase enzymes, but it is not known if lipid ligands regulate this process.

Questions and Hypotheses Addressed in this Work

There is still debate over the functional roles of LTPs. Are they passive carriers of lipids that nonspecifically bind to any hydrophobic molecule, or are they active participants in these signaling processes that have evolved specificity towards certain lipids? It is necessary to elucidate the functional roles and ligands of LTPs in order understand how they participate in cellular signaling to maintain homeostasis. Additionally, increased knowledge of how these LTPs work enables us to pharmacologically target them to regulate these important cellular processes. To address these questions, we characterize a lipid chaperone and lipid sensor in this work (Fig. 5). In **Chapter 2**, we structurally and biochemically characterize Lipid Binding Protein 8 (LBP-8) that serves as a lipid chaperone in *Caenorhabditis elegans.* In this work, we solve the first crystal structure of LBP-8 (calycin family), which enables us to identify a conserved NLS, explaining the molecular mechanism by which LBP-8 shuttles lysosomal lipids to the nucleus to regulate transcription of life extending genes. In **Chapter 3**, we elucidate the

mechanism by which StarD14 acts as a lipid sensor to regulate the thioesterase activity of its N-terminal domains. We show that the StarD binds to long-chain fatty acids and lysophosphatidylcholine species, which reciprocally alter enzyme activity. StarD14 suppresses fatty acid oxidation in brown adipocytes, limiting energy expenditure [100], but we show lysophosphatidylcholine reverses this through inhibiting StarD14, which in turn increases lipid metabolism. We more closely examine the enzymatic activity of StarD14 and how small molecules regulate its activity in **Chapter 4**. Finally, in **Chapter 5**, we discuss how this body of work supports our hypothesis that LTPs are active participants in lipid signaling to control essential biological processes.

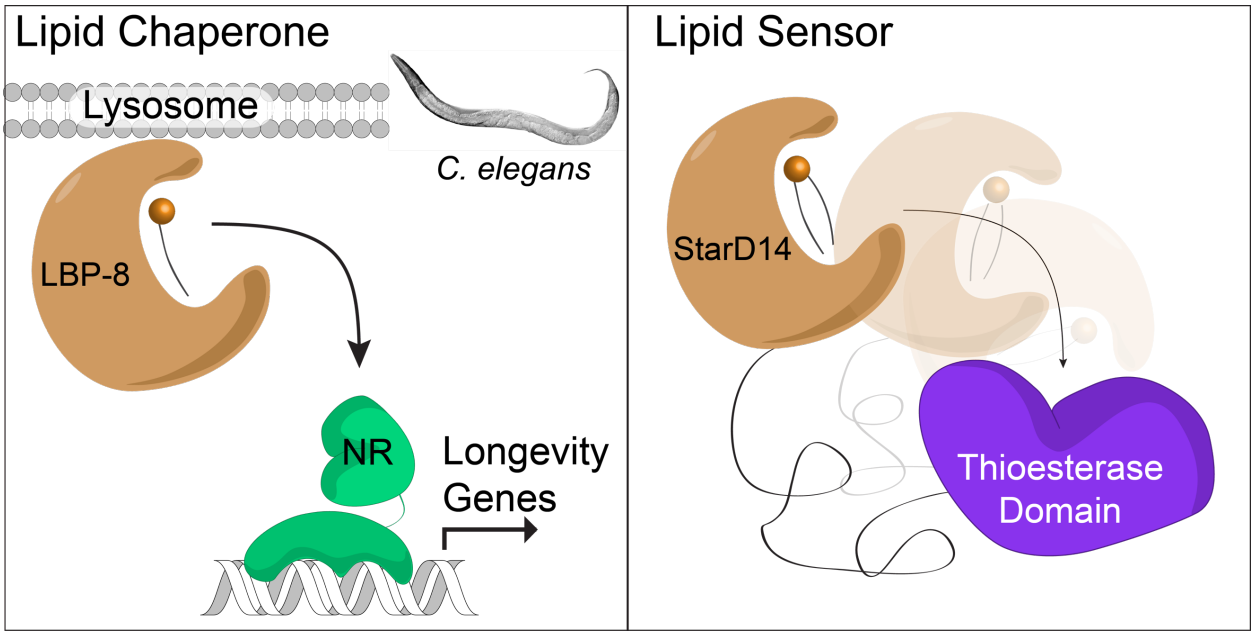

Figure 5. Schematic of LTPs studied in this work. *(Left panel)* In **Chapter 2**, I structurally and biochemically characterize LBP-8, which is expressed in *C. elegans.* LBP-8 acts as a lipid chaperone, carrying fatty acids from the lysosome to the nucleus to regulate the activity of nuclear receptors (NR) and expression of life-extending genes. *(Right panel)* In **Chapters 3** and **4**, I characterize StarD14, an LTP highly expressed in the brown adipose tissue of mammals. StarD14 acts as a lipid sensor, detecting specific lipids and regulating the activity of its N-terminal thioesterase domains.

References

1. Kennedy BK, Lamming DW. The Mechanistic Target of Rapamycin: The Grand ConducTOR of Metabolism and Aging. Cell Metab. 2016;23(6):990-1003. Epub 2016/06/16. doi: 10.1016/j.cmet.2016.05.009. PubMed PMID: 27304501; PMCID: PMC4910876.
2. Wymann MP, Schneiter R. Lipid signalling in disease. Nature reviews Molecular cell biology. 2008;9(2):162-76. Epub 2008/01/25. doi: 10.1038/nrm2335. PubMed PMID: 18216772.
3. Duffy J MA, Wang M. Lipid Metabolism, Lipid Signalling and Longevity2017:307-29. doi: 10.1007/978-3-319-44703-2_14.
4. Casares D, Escriba PV, Rossello CA. Membrane Lipid Composition: Effect on Membrane and Organelle Structure, Function and Compartmentalization and Therapeutic Avenues. International journal of molecular sciences. 2019;20(9). Epub 2019/05/06. doi: 10.3390/ijms20092167. PubMed PMID: 31052427; PMCID: PMC6540057.
5. Kaplan MR, Simoni RD. Intracellular transport of phosphatidylcholine to the plasma membrane. The Journal of cell biology. 1985;101(2):441-5. Epub 1985/08/01. doi: 10.1083/jcb.101.2.441. PubMed PMID: 4040519; PMCID: PMC2113683.
6. Vance JE, Aasman EJ, Szarka R. Brefeldin A does not inhibit the movement of phosphatidylethanolamine from its sites for synthesis to the cell surface. J Biol Chem. 1991;266(13):8241-7. Epub 1991/05/05. PubMed PMID: 2022641.
7. Daum G, Heidorn E, Paltauf F. Intracellular transfer of phospholipids in the yeast, Saccharomyces cerevisiae. Biochimica et biophysica acta. 1986;878(1):93-101. Epub 1986/08/14. doi: 10.1016/0005-2760(86)90347-4. PubMed PMID: 3524689.
8. Pagano RE. Lipid traffic in eukaryotic cells: mechanisms for intracellular transport and organelle-specific enrichment of lipids. Current opinion in cell biology. 1990;2(4):652-63. Epub 1990/08/01. doi: 10.1016/0955-0674(90)90107-p. PubMed PMID: 2252591.
9. Wirtz KW, Zilversmit DB. Exchange of phospholipids between liver mitochondria and microsomes in vitro. J Biol Chem. 1968;243(13):3596-602. Epub 1968/07/10. PubMed PMID: 4968799.
10. Helmkamp GM, Jr., Harvey MS, Wirtz KW, Van Deenen LL. Phospholipid exchange between membranes. Purification of bovine brain proteins that preferentially catalyze the transfer of phosphatidylinositol. J Biol Chem. 1974;249(20):6382-9. Epub 1974/10/25. PubMed PMID: 4371468.
11. Wong LH, Copic A, Levine TP. Advances on the Transfer of Lipids by Lipid Transfer Proteins. Trends in biochemical sciences. 2017;42(7):516-30. Epub 2017/06/06. doi: 10.1016/j.tibs.2017.05.001. PubMed PMID: 28579073; PMCID: PMC5486777.
12. Chiapparino A, Maeda K, Turei D, Saez-Rodriguez J, Gavin AC. The orchestra of lipid-transfer proteins at the crossroads between metabolism and signaling. Prog Lipid Res. 2016;61:30-9. Epub 2015/12/15. doi: 10.1016/j.plipres.2015.10.004. PubMed PMID: 26658141.
13. Sharma A, Sharma A. Fatty acid induced remodeling within the human liver fatty acid-binding protein. J Biol Chem. 2011;286(36):31924-8. Epub 2011/07/16. doi: 10.1074/jbc.M111.270165. PubMed PMID: 21757748; PMCID: PMC3173104.
14. Qiu X, Mistry A, Ammirati MJ, Chrunyk BA, Clark RW, Cong Y, Culp JS, Danley DE, Freeman TB, Geoghegan KF, Griffor MC, Hawrylik SJ, Hayward CM, Hensley P, Hoth LR, Karam GA, Lira ME, Lloyd DB, McGrath KM, Stutzman-Engwall KJ, Subashi AK, Subashi TA, Thompson JF, Wang IK, Zhao H, Seddon AP. Crystal structure of cholesteryl ester transfer

protein reveals a long tunnel and four bound lipid molecules. Nat Struct Mol Biol. 2007;14(2):106-13. Epub 2007/01/24. doi: 10.1038/nsmb1197. PubMed PMID: 17237796.
15. Thorsell AG, Lee WH, Persson C, Siponen MI, Nilsson M, Busam RD, Kotenyova T, Schuler H, Lehtio L. Comparative structural analysis of lipid binding START domains. PLoS One. 2011;6(6):e19521. Epub 2011/07/09. doi: 10.1371/journal.pone.0019521. PubMed PMID: 21738568; PMCID: PMC3127847.
16. Richieri GV, Ogata RT, Kleinfeld AM. Fatty acid interactions with native and mutant fatty acid binding proteins. Molecular and cellular biochemistry. 1999;192(1-2):77-85. Epub 1999/05/20. PubMed PMID: 10331661.
17. Tillman MC, Khadka M, Duffy J, Wang MC, Ortlund EA. Structural characterization of life-extending Caenorhabditis elegans Lipid Binding Protein 8. Scientific reports. 2019;9(1):9966. Epub 2019/07/12. doi: 10.1038/s41598-019-46230-8. PubMed PMID: 31292465; PMCID: PMC6620326.
18. Hotamisligil GS, Bernlohr DA. Metabolic functions of FABPs--mechanisms and therapeutic implications. Nature reviews Endocrinology. 2015;11(10):592-605. Epub 2015/08/12. doi: 10.1038/nrendo.2015.122. PubMed PMID: 26260145; PMCID: PMC4578711.
19. Bose HS, Sugawara T, Strauss JF, 3rd, Miller WL. The pathophysiology and genetics of congenital lipoid adrenal hyperplasia. N Engl J Med. 1996;335(25):1870-8. Epub 1996/12/19. doi: 10.1056/nejm199612193352503. PubMed PMID: 8948562.
20. Vanier MT. Complex lipid trafficking in Niemann-Pick disease type C. Journal of inherited metabolic disease. 2015;38(1):187-99. Epub 2014/11/27. doi: 10.1007/s10545-014-9794-4. PubMed PMID: 25425283.
21. Folick A, Oakley HD, Yu Y, Armstrong EH, Kumari M, Sanor L, Moore DD, Ortlund EA, Zechner R, Wang MC. Aging. Lysosomal signaling molecules regulate longevity in Caenorhabditis elegans. Science (New York, NY). 2015;347(6217):83-6. Epub 2015/01/03. doi: 10.1126/science.1258857. PubMed PMID: 25554789; PMCID: PMC4425353.
22. Hanada K. Lipid transfer proteins rectify inter-organelle flux and accurately deliver lipids at membrane contact sites. J Lipid Res. 2018;59(8):1341-66. Epub 2018/06/10. doi: 10.1194/jlr.R085324. PubMed PMID: 29884707; PMCID: PMC6071762.
23. Flower DR, North AC, Attwood TK. Structure and sequence relationships in the lipocalins and related proteins. Protein science : a publication of the Protein Society. 1993;2(5):753-61. Epub 1993/05/01. doi: 10.1002/pro.5560020507. PubMed PMID: 7684291; PMCID: PMC2142497.
24. Smathers RL, Petersen DR. The human fatty acid-binding protein family: evolutionary divergences and functions. Human genomics. 2011;5(3):170-91. Epub 2011/04/21. doi: 10.1186/1479-7364-5-3-170. PubMed PMID: 21504868; PMCID: PMC3500171.
25. Ganfornina MD, Gutierrez G, Bastiani M, Sanchez D. A phylogenetic analysis of the lipocalin protein family. Molecular biology and evolution. 2000;17(1):114-26. Epub 2000/02/10. doi: 10.1093/oxfordjournals.molbev.a026224. PubMed PMID: 10666711.
26. Flower DR. Structural relationship of streptavidin to the calycin protein superfamily. FEBS letters. 1993;333(1-2):99-102. Epub 1993/10/25. doi: 10.1016/0014-5793(93)80382-5. PubMed PMID: 8224179.
27. Flower DR. The lipocalin protein family: structure and function. Biochem J. 1996;318 (Pt 1):1-14. Epub 1996/08/15. doi: 10.1042/bj3180001. PubMed PMID: 8761444; PMCID: PMC1217580.

28. Armstrong EH, Goswami D, Griffin PR, Noy N, Ortlund EA. Structural basis for ligand regulation of the fatty acid-binding protein 5, peroxisome proliferator-activated receptor beta/delta (FABP5-PPARbeta/delta) signaling pathway. J Biol Chem. 2014;289(21):14941-54. Epub 2014/04/03. doi: 10.1074/jbc.M113.514646. PubMed PMID: 24692551; PMCID: PMC4031543.
29. Zamarreno F, Herrera FE, Corsico B, Costabel MD. Similar structures but different mechanisms: Prediction of FABPs-membrane interaction by electrostatic calculation. Biochimica et biophysica acta. 2012;1818(7):1691-7. Epub 2012/03/27. doi: 10.1016/j.bbamem.2012.03.003. PubMed PMID: 22446190.
30. Corsico B, Franchini GR, Hsu KT, Storch J. Fatty acid transfer from intestinal fatty acid binding protein to membranes: electrostatic and hydrophobic interactions. J Lipid Res. 2005;46(8):1765-72. Epub 2005/05/03. doi: 10.1194/jlr.M500140-JLR200. PubMed PMID: 15863832.
31. Corsico B, Liou HL, Storch J. The alpha-helical domain of liver fatty acid binding protein is responsible for the diffusion-mediated transfer of fatty acids to phospholipid membranes. Biochemistry. 2004;43(12):3600-7. Epub 2004/03/24. doi: 10.1021/bi0357356. PubMed PMID: 15035630.
32. Cogan U, Kopelman M, Mokady S, Shinitzky M. Binding affinities of retinol and related compounds to retinol binding proteins. Eur J Biochem. 1976;65(1):71-8. Epub 1976/05/17. doi: 10.1111/j.1432-1033.1976.tb10390.x. PubMed PMID: 945163.
33. Rankin TL, Ong DE, Orgebin-Crist MC. The 18-kDa mouse epididymal protein (MEP 10) binds retinoic acid. Biology of reproduction. 1992;46(5):767-71. Epub 1992/05/01. doi: 10.1095/biolreprod46.5.767. PubMed PMID: 1591333.
34. Balbin M, Freije JM, Fueyo A, Sanchez LM, Lopez-Otin C. Apolipoprotein D is the major protein component in cyst fluid from women with human breast gross cystic disease. Biochem J. 1990;271(3):803-7. Epub 1990/11/01. doi: 10.1042/bj2710803. PubMed PMID: 2244881; PMCID: PMC1149635.
35. Urade Y, Nagata A, Suzuki Y, Fujii Y, Hayaishi O. Primary structure of rat brain prostaglandin D synthetase deduced from cDNA sequence. J Biol Chem. 1989;264(2):1041-5. Epub 1989/01/15. PubMed PMID: 2642896.
36. Ong DE. Cellular retinoid-binding proteins. Archives of dermatology. 1987;123(12):1693-5a. Epub 1987/12/01. PubMed PMID: 2825608.
37. Napoli JL. Cellular retinoid binding-proteins, CRBP, CRABP, FABP5: Effects on retinoid metabolism, function and related diseases. Pharmacology & therapeutics. 2017;173:19-33. Epub 2017/01/31. doi: 10.1016/j.pharmthera.2017.01.004. PubMed PMID: 28132904; PMCID: PMC5408321.
38. Praslickova D, Torchia EC, Sugiyama MG, Magrane EJ, Zwicker BL, Kolodzieyski L, Agellon LB. The ileal lipid binding protein is required for efficient absorption and transport of bile acids in the distal portion of the murine small intestine. PLoS One. 2012;7(12):e50810. Epub 2012/12/20. doi: 10.1371/journal.pone.0050810. PubMed PMID: 23251388; PMCID: PMC3519535.
39. Storch J, McDermott L. Structural and functional analysis of fatty acid-binding proteins. J Lipid Res. 2009;50 Suppl:S126-31. Epub 2008/11/20. doi: 10.1194/jlr.R800084-JLR200. PubMed PMID: 19017610; PMCID: PMC2674722.
40. Lowe JB, Sacchettini JC, Laposata M, McQuillan JJ, Gordon JI. Expression of rat intestinal fatty acid-binding protein in Escherichia coli. Purification and comparison of ligand

binding characteristics with that of Escherichia coli-derived rat liver fatty acid-binding protein. J Biol Chem. 1987;262(12):5931-7. Epub 1987/04/25. PubMed PMID: 3553183.
41. Richieri GV, Ogata RT, Kleinfeld AM. Equilibrium constants for the binding of fatty acids with fatty acid-binding proteins from adipocyte, intestine, heart, and liver measured with the fluorescent probe ADIFAB. J Biol Chem. 1994;269(39):23918-30. Epub 1994/09/30. PubMed PMID: 7929039.
42. Gillilan RE, Ayers SD, Noy N. Structural basis for activation of fatty acid-binding protein 4. Journal of molecular biology. 2007;372(5):1246-60. Epub 2007/09/01. doi: 10.1016/j.jmb.2007.07.040. PubMed PMID: 17761196; PMCID: PMC2032018.
43. Assar Z, Nossoni Z, Wang W, Santos EM, Kramer K, McCornack C, Vasileiou C, Borhan B, Geiger JH. Domain-Swapped Dimers of Intracellular Lipid-Binding Proteins: Evidence for Ordered Folding Intermediates. Structure (London, England : 1993). 2016;24(9):1590-8. Epub 2016/08/16. doi: 10.1016/j.str.2016.05.022. PubMed PMID: 27524203; PMCID: PMC5330279.
44. Sanson B, Wang T, Sun J, Wang L, Kaczocha M, Ojima I, Deutsch D, Li H. Crystallographic study of FABP5 as an intracellular endocannabinoid transporter. Acta Crystallogr D Biol Crystallogr. 2014;70(Pt 2):290-8. Epub 2014/02/18. doi: 10.1107/s1399004713026795. PubMed PMID: 24531463; PMCID: PMC3940194.
45. Jakobsson E, Alvite G, Bergfors T, Esteves A, Kleywegt GJ. The crystal structure of Echinococcus granulosus fatty-acid-binding protein 1. Biochimica et biophysica acta. 2003;1649(1):40-50. Epub 2003/06/24. PubMed PMID: 12818189.
46. Sessler RJ, Noy N. A ligand-activated nuclear localization signal in cellular retinoic acid binding protein-II. Mol Cell. 2005;18(3):343-53. Epub 2005/05/04. doi: 10.1016/j.molcel.2005.03.026. PubMed PMID: 15866176.
47. Green NM. AVIDIN. 1. THE USE OF (14-C)BIOTIN FOR KINETIC STUDIES AND FOR ASSAY. Biochem J. 1963;89:585-91. Epub 1963/12/01. doi: 10.1042/bj0890585. PubMed PMID: 14101979; PMCID: PMC1202466.
48. Avraham O, Meir A, Fish A, Bayer EA, Livnah O. Hoefavidin: A dimeric bacterial avidin with a C-terminal binding tail. Journal of structural biology. 2015;191(2):139-48. Epub 2015/07/02. doi: 10.1016/j.jsb.2015.06.020. PubMed PMID: 26126731.
49. Pugliese L, Coda A, Malcovati M, Bolognesi M. Three-dimensional structure of the tetragonal crystal form of egg-white avidin in its functional complex with biotin at 2.7 A resolution. Journal of molecular biology. 1993;231(3):698-710. Epub 1993/06/05. doi: 10.1006/jmbi.1993.1321. PubMed PMID: 8515446.
50. Hofmann K, Kiso Y. An approach to the targeted attachment of peptides and proteins to solid supports. Proc Natl Acad Sci U S A. 1976;73(10):3516-8. Epub 1976/10/01. doi: 10.1073/pnas.73.10.3516. PubMed PMID: 185617; PMCID: PMC431147.
51. Schrick K, Nguyen D, Karlowski WM, Mayer KF. START lipid/sterol-binding domains are amplified in plants and are predominantly associated with homeodomain transcription factors. Genome biology. 2004;5(6):R41. Epub 2004/06/10. doi: 10.1186/gb-2004-5-6-r41. PubMed PMID: 15186492; PMCID: Pmc463074.
52. Alpy F, Tomasetto C. Give lipids a START: the StAR-related lipid transfer (START) domain in mammals. J Cell Sci. 2005;118(Pt 13):2791-801. Epub 2005/06/25. doi: 10.1242/jcs.02485. PubMed PMID: 15976441.

53. Alpy F, Legueux F, Bianchetti L, Tomasetto C. [START domain-containing proteins: a review of their role in lipid transport and exchange]. Medecine sciences : M/S. 2009;25(2):181-91. Epub 2009/02/26. doi: 10.1051/medsci/2009252181. PubMed PMID: 19239851.
54. Reitz J, Gehrig-Burger K, Strauss JF, 3rd, Gimpl G. Cholesterol interaction with the related steroidogenic acute regulatory lipid-transfer (START) domains of StAR (STARD1) and MLN64 (STARD3). The FEBS journal. 2008;275(8):1790-802. Epub 2008/03/12. doi: 10.1111/j.1742-4658.2008.06337.x. PubMed PMID: 18331352.
55. Letourneau D, Bedard M, Cabana J, Lefebvre A, LeHoux JG, Lavigne P. STARD6 on steroids: solution structure, multiple timescale backbone dynamics and ligand binding mechanism. Scientific reports. 2016;6:28486. Epub 2016/06/25. doi: 10.1038/srep28486. PubMed PMID: 27340016; PMCID: PMC4919784.
56. Rodriguez-Agudo D, Ren S, Wong E, Marques D, Redford K, Gil G, Hylemon P, Pandak WM. Intracellular cholesterol transporter StarD4 binds free cholesterol and increases cholesteryl ester formation. J Lipid Res. 2008;49(7):1409-19. Epub 2008/04/12. doi: 10.1194/jlr.M700537-JLR200. PubMed PMID: 18403318; PMCID: PMC2431108.
57. Rodriguez-Agudo D, Ren S, Hylemon PB, Redford K, Natarajan R, Del Castillo A, Gil G, Pandak WM. Human StarD5, a cytosolic StAR-related lipid binding protein. J Lipid Res. 2005;46(8):1615-23. Epub 2005/05/18. doi: 10.1194/jlr.M400501-JLR200. PubMed PMID: 15897605.
58. Horibata Y, Sugimoto H. StarD7 mediates the intracellular trafficking of phosphatidylcholine to mitochondria. J Biol Chem. 2010;285(10):7358-65. Epub 2010/01/01. doi: 10.1074/jbc.M109.056960. PubMed PMID: 20042613; PMCID: PMC2844184.
59. Kanno K, Wu MK, Scapa EF, Roderick SL, Cohen DE. Structure and function of phosphatidylcholine transfer protein (PC-TP)/StarD2. Biochimica et biophysica acta. 2007;1771(6):654-62. Epub 2007/05/15. doi: 10.1016/j.bbalip.2007.04.003. PubMed PMID: 17499021; PMCID: PMC2743068.
60. Olayioye MA, Vehring S, Muller P, Herrmann A, Schiller J, Thiele C, Lindeman GJ, Visvader JE, Pomorski T. StarD10, a START domain protein overexpressed in breast cancer, functions as a phospholipid transfer protein. J Biol Chem. 2005;280(29):27436-42. Epub 2005/05/25. doi: 10.1074/jbc.M413330200. PubMed PMID: 15911624.
61. Hanada K, Kumagai K, Tomishige N, Kawano M. CERT and intracellular trafficking of ceramide. Biochimica et biophysica acta. 2007;1771(6):644-53. Epub 2007/02/23. doi: 10.1016/j.bbalip.2007.01.009. PubMed PMID: 17314061.
62. Chen D, Latham J, Zhao H, Bisoffi M, Farelli J, Dunaway-Mariano D. Human brown fat inducible thioesterase variant 2 cellular localization and catalytic function. Biochemistry. 2012;51(35):6990-9. Epub 2012/08/18. doi: 10.1021/bi3008824. PubMed PMID: 22897136; PMCID: PMC4066737.
63. Han S, Cohen DE. Functional characterization of thioesterase superfamily member 1/Acyl-CoA thioesterase 11: implications for metabolic regulation. J Lipid Res. 2012;53(12):2620-31. Epub 2012/09/21. doi: 10.1194/jlr.M029538. PubMed PMID: 22993230; PMCID: PMC3494255.
64. Srivastava S, Panda D. A centrosomal protein STARD9 promotes microtubule stability and regulates spindle microtubule dynamics. Cell cycle (Georgetown, Tex). 2018;17(16):2052-68. Epub 2018/08/31. doi: 10.1080/15384101.2018.1513764. PubMed PMID: 30160609; PMCID: PMC6260213.

65. Roostaee A, Barbar E, Lehoux JG, Lavigne P. Cholesterol binding is a prerequisite for the activity of the steroidogenic acute regulatory protein (StAR). Biochem J. 2008;412(3):553-62. Epub 2008/03/18. doi: 10.1042/bj20071264. PubMed PMID: 18341481.
66. Roderick SL, Chan WW, Agate DS, Olsen LR, Vetting MW, Rajashankar KR, Cohen DE. Structure of human phosphatidylcholine transfer protein in complex with its ligand. Nat Struct Biol. 2002;9(7):507-11. Epub 2002/06/11. doi: 10.1038/nsb812. PubMed PMID: 12055623.
67. Iaea DB, Dikiy I, Kiburu I, Eliezer D, Maxfield FR. STARD4 Membrane Interactions and Sterol Binding. Biochemistry. 2015;54(30):4623-36. Epub 2015/07/15. doi: 10.1021/acs.biochem.5b00618. PubMed PMID: 26168008; PMCID: PMC4527246.
68. Kudo N, Kumagai K, Tomishige N, Yamaji T, Wakatsuki S, Nishijima M, Hanada K, Kato R. Structural basis for specific lipid recognition by CERT responsible for nonvesicular trafficking of ceramide. Proc Natl Acad Sci U S A. 2008;105(2):488-93. Epub 2008/01/11. doi: 10.1073/pnas.0709191105. PubMed PMID: 18184806; PMCID: PMC2206563.
69. Kaczocha M, Glaser ST, Deutsch DG. Identification of intracellular carriers for the endocannabinoid anandamide. Proc Natl Acad Sci U S A. 2009;106(15):6375-80. Epub 2009/03/25. doi: 10.1073/pnas.0901515106. PubMed PMID: 19307565; PMCID: PMC2669397.
70. Lehto M, Hynynen R, Karjalainen K, Kuismanen E, Hyvarinen K, Olkkonen VM. Targeting of OSBP-related protein 3 (ORP3) to endoplasmic reticulum and plasma membrane is controlled by multiple determinants. Experimental cell research. 2005;310(2):445-62. Epub 2005/09/07. doi: 10.1016/j.yexcr.2005.08.003. PubMed PMID: 16143324.
71. Ridgway ND, Dawson PA, Ho YK, Brown MS, Goldstein JL. Translocation of oxysterol binding protein to Golgi apparatus triggered by ligand binding. The Journal of cell biology. 1992;116(2):307-19. Epub 1992/01/01. doi: 10.1083/jcb.116.2.307. PubMed PMID: 1730758; PMCID: PMC2289278.
72. Levine T. Short-range intracellular trafficking of small molecules across endoplasmic reticulum junctions. Trends in cell biology. 2004;14(9):483-90. Epub 2004/09/08. doi: 10.1016/j.tcb.2004.07.017. PubMed PMID: 15350976.
73. Lebiedzinska M, Szabadkai G, Jones AW, Duszynski J, Wieckowski MR. Interactions between the endoplasmic reticulum, mitochondria, plasma membrane and other subcellular organelles. The international journal of biochemistry & cell biology. 2009;41(10):1805-16. Epub 2009/08/26. doi: 10.1016/j.biocel.2009.02.017. PubMed PMID: 19703651.
74. Lev S. Non-vesicular lipid transport by lipid-transfer proteins and beyond. Nature reviews Molecular cell biology. 2010;11(10):739-50. Epub 2010/09/09. doi: 10.1038/nrm2971. PubMed PMID: 20823909.
75. Stefan CJ, Manford AG, Baird D, Yamada-Hanff J, Mao Y, Emr SD. Osh proteins regulate phosphoinositide metabolism at ER-plasma membrane contact sites. Cell. 2011;144(3):389-401. Epub 2011/02/08. doi: 10.1016/j.cell.2010.12.034. PubMed PMID: 21295699.
76. Yang L, Na CL, Luo S, Wu D, Hogan S, Huang T, Weaver TE. The Phosphatidylcholine Transfer Protein Stard7 is Required for Mitochondrial and Epithelial Cell Homeostasis. Scientific reports. 2017;7:46416. Epub 2017/04/13. doi: 10.1038/srep46416. PubMed PMID: 28401922; PMCID: PMC5388865.
77. Horibata Y, Ando H, Satou M, Shimizu H, Mitsuhashi S, Shimizu Y, Itoh M, Sugimoto H. Identification of the N-terminal transmembrane domain of StarD7 and its importance for mitochondrial outer membrane localization and phosphatidylcholine transfer. Scientific reports.

2017;7(1):8793. Epub 2017/08/20. doi: 10.1038/s41598-017-09205-1. PubMed PMID: 28821867; PMCID: PMC5562819.
78. Hanada K. Intracellular trafficking of ceramide by ceramide transfer protein. Proceedings of the Japan Academy Series B, Physical and biological sciences. 2010;86(4):426-37. Epub 2010/05/01. doi: 10.2183/pjab.86.426. PubMed PMID: 20431265; PMCID: PMC3417804.
79. Hanada K, Kumagai K, Yasuda S, Miura Y, Kawano M, Fukasawa M, Nishijima M. Molecular machinery for non-vesicular trafficking of ceramide. Nature. 2003;426(6968):803-9. Epub 2003/12/20. doi: 10.1038/nature02188. PubMed PMID: 14685229.
80. Kawano M, Kumagai K, Nishijima M, Hanada K. Efficient trafficking of ceramide from the endoplasmic reticulum to the Golgi apparatus requires a VAMP-associated protein-interacting FFAT motif of CERT. J Biol Chem. 2006;281(40):30279-88. Epub 2006/08/10. doi: 10.1074/jbc.M605032200. PubMed PMID: 16895911.
81. Alpy F, Wendling C, Rio MC, Tomasetto C. MENTHO, a MLN64 homologue devoid of the START domain. J Biol Chem. 2002;277(52):50780-7. Epub 2002/10/24. doi: 10.1074/jbc.M208290200. PubMed PMID: 12393907.
82. Loewen CJ, Roy A, Levine TP. A conserved ER targeting motif in three families of lipid binding proteins and in Opi1p binds VAP. The EMBO journal. 2003;22(9):2025-35. Epub 2003/05/03. doi: 10.1093/emboj/cdg201. PubMed PMID: 12727870; PMCID: PMC156073.
83. Alpy F, Rousseau A, Schwab Y, Legueux F, Stoll I, Wendling C, Spiegelhalter C, Kessler P, Mathelin C, Rio MC, Levine TP, Tomasetto C. STARD3 or STARD3NL and VAP form a novel molecular tether between late endosomes and the ER. J Cell Sci. 2013;126(Pt 23):5500-12. Epub 2013/10/10. doi: 10.1242/jcs.139295. PubMed PMID: 24105263.
84. Wilhelm LP, Wendling C, Vedie B, Kobayashi T, Chenard MP, Tomasetto C, Drin G, Alpy F. STARD3 mediates endoplasmic reticulum-to-endosome cholesterol transport at membrane contact sites. The EMBO journal. 2017;36(10):1412-33. Epub 2017/04/06. doi: 10.15252/embj.201695917. PubMed PMID: 28377464; PMCID: PMC5430228.
85. Masson D, Jiang XC, Lagrost L, Tall AR. The role of plasma lipid transfer proteins in lipoprotein metabolism and atherogenesis. J Lipid Res. 2009;50 Suppl:S201-6. Epub 2008/11/22. doi: 10.1194/jlr.R800061-JLR200. PubMed PMID: 19023137; PMCID: PMC2674750.
86. Josephrajan A, Hertzel AV, Bohm EK, McBurney MW, Imai SI, Mashek DG, Kim DH, Bernlohr DA. Unconventional Secretion of Adipocyte Fatty Acid Binding Protein 4 Is Mediated By Autophagic Proteins in a Sirtuin-1-Dependent Manner. Diabetes. 2019;68(9):1767-77. Epub 2019/06/07. doi: 10.2337/db18-1367. PubMed PMID: 31171562; PMCID: PMC6702637.
87. Cao H, Sekiya M, Ertunc ME, Burak MF, Mayers JR, White A, Inouye K, Rickey LM, Ercal BC, Furuhashi M, Tuncman G, Hotamisligil GS. Adipocyte lipid chaperone AP2 is a secreted adipokine regulating hepatic glucose production. Cell Metab. 2013;17(5):768-78. Epub 2013/05/15. doi: 10.1016/j.cmet.2013.04.012. PubMed PMID: 23663740; PMCID: PMC3755450.
88. Villeneuve J, Bassaganyas L, Lepreux S, Chiritoiu M, Costet P, Ripoche J, Malhotra V, Schekman R. Unconventional secretion of FABP4 by endosomes and secretory lysosomes. The Journal of cell biology. 2018;217(2):649-65. Epub 2017/12/08. doi: 10.1083/jcb.201705047. PubMed PMID: 29212659; PMCID: PMC5800802.
89. Furuhashi M. Fatty Acid-Binding Protein 4 in Cardiovascular and Metabolic Diseases. Journal of atherosclerosis and thrombosis. 2019;26(3):216-32. Epub 2019/02/07. doi: 10.5551/jat.48710. PubMed PMID: 30726793; PMCID: PMC6402888.

90. Noy N. Signaling by retinol and its serum binding protein. Prostaglandins, leukotrienes, and essential fatty acids. 2015;93:3-7. Epub 2014/12/08. doi: 10.1016/j.plefa.2014.10.004. PubMed PMID: 25481334; PMCID: PMC4323939.
91. Jenkins-Kruchten AE, Bennaars-Eiden A, Ross JR, Shen WJ, Kraemer FB, Bernlohr DA. Fatty acid-binding protein-hormone-sensitive lipase interaction. Fatty acid dependence on binding. J Biol Chem. 2003;278(48):47636-43. Epub 2003/09/18. doi: 10.1074/jbc.M307680200. PubMed PMID: 13129924.
92. Tan NS, Shaw NS, Vinckenbosch N, Liu P, Yasmin R, Desvergne B, Wahli W, Noy N. Selective cooperation between fatty acid binding proteins and peroxisome proliferator-activated receptors in regulating transcription. Mol Cell Biol. 2002;22(14):5114-27. Epub 2002/06/22. doi: 10.1128/mcb.22.14.5114-5127.2002. PubMed PMID: 12077340; PMCID: PMC139777.
93. Velkov T. Interactions between Human Liver Fatty Acid Binding Protein and Peroxisome Proliferator Activated Receptor Selective Drugs. PPAR research. 2013;2013:938401. Epub 2013/03/12. doi: 10.1155/2013/938401. PubMed PMID: 23476633; PMCID: PMC3588188.
94. Kaczocha M, Vivieca S, Sun J, Glaser ST, Deutsch DG. Fatty acid-binding proteins transport N-acylethanolamines to nuclear receptors and are targets of endocannabinoid transport inhibitors. J Biol Chem. 2012;287(5):3415-24. Epub 2011/12/16. doi: 10.1074/jbc.M111.304907. PubMed PMID: 22170058; PMCID: PMC3270995.
95. Hughes ML, Liu B, Halls ML, Wagstaff KM, Patil R, Velkov T, Jans DA, Bunnett NW, Scanlon MJ, Porter CJ. Fatty Acid-binding Proteins 1 and 2 Differentially Modulate the Activation of Peroxisome Proliferator-activated Receptor alpha in a Ligand-selective Manner. J Biol Chem. 2015;290(22):13895-906. Epub 2015/04/08. doi: 10.1074/jbc.M114.605998. PubMed PMID: 25847235; PMCID: PMC4447964.
96. Kang HW, Kanno K, Scapa EF, Cohen DE. Regulatory role for phosphatidylcholine transfer protein/StarD2 in the metabolic response to peroxisome proliferator activated receptor alpha (PPARalpha). Biochimica et biophysica acta. 2010;1801(4):496-502. Epub 2010/01/05. doi: 10.1016/j.bbalip.2009.12.013. PubMed PMID: 20045742; PMCID: PMC2826570.
97. Wang PY, Liu P, Weng J, Sontag E, Anderson RG. A cholesterol-regulated PP2A/HePTP complex with dual specificity ERK1/2 phosphatase activity. The EMBO journal. 2003;22(11):2658-67. Epub 2003/05/30. doi: 10.1093/emboj/cdg255. PubMed PMID: 12773382; PMCID: PMC156752.
98. Horibata Y, Ando H, Itoh M, Sugimoto H. Enzymatic and transcriptional regulation of the cytoplasmic acetyl-CoA hydrolase ACOT12. J Lipid Res. 2013;54(8):2049-59. Epub 2013/05/28. doi: 10.1194/jlr.M030163. PubMed PMID: 23709691; PMCID: PMC3708356.
99. Kanno K, Wu MK, Agate DS, Fanelli BJ, Wagle N, Scapa EF, Ukomadu C, Cohen DE. Interacting proteins dictate function of the minimal START domain phosphatidylcholine transfer protein/StarD2. J Biol Chem. 2007;282(42):30728-36. Epub 2007/08/21. doi: 10.1074/jbc.M703745200. PubMed PMID: 17704541.
100. Zhang Y, Li Y, Niepel MW, Kawano Y, Han S, Liu S, Marsili A, Larsen PR, Lee CH, Cohen DE. Targeted deletion of thioesterase superfamily member 1 promotes energy expenditure and protects against obesity and insulin resistance. Proc Natl Acad Sci U S A. 2012;109(14):5417-22. Epub 2012/03/20. doi: 10.1073/pnas.1116011109. PubMed PMID: 22427358; PMCID: PMC3325675.

CHAPTER 2: STRUCTURAL CHARACTERIZATION OF LIFE-EXTENDING CAENORHABITIS ELEGANS LIPID BINDING PROTEIN 8

Matthew C. Tillman[1], Manoj Khadka[1], Jonathon Duffy[2], Meng C. Wang[2,3], and Eric A. Ortlund[1*]

From the [1]Department of Biochemistry, Emory University School of Medicine, 1510 Clifton Road, Atlanta, GA 30322; [2]Huffington Center on Aging and Department of Molecular and Human Genetics, Baylor College of Medicine, Houston, Texas; [3]Howard Hughes Medical Institute, Baylor College of Medicine, Houston, TX 77030, USA

This manuscript describes the first crystal structure of LBP-8, a fatty acid binding protein that extends life in *C. elegans*. Using this structure, we identify a conserved nuclear localization signal and key residues involved in lipid binding. Additionally, we describe the lipid binding preference of LBP-8 for monounsaturated fatty acyls, like oleic acid and oleoylethanolamide. This biochemical and structural analysis of LBP-8 helps to elucidate the molecule mechanism by which it extends lifespan. This manuscript was published in *Scientific Report,* July 2019.

MCT performed protein expression, purification, crystallization, X-ray data collection, solved the structure, mass spectrometry, binding experiments, differential scanning fluorimetry, fatty acid quantification, and circular dichroism. JD grew and lysed *C. elegans.* MK assisted in mass spectrometry data collection and analysis. MCT, MCW, and EAO designed the experiments and discussed the data. MCT, MCW, and EAO wrote the manuscript. All authors reviewed the manuscript.

Abstract

The lysosome plays a crucial role in the regulation of longevity. Lysosomal degradation is tightly coupled with autophagy that is induced by many longevity paradigms and required for lifespan extension. The lysosome also serves as a hub for signal transduction and regulates longevity via affecting nuclear transcription. One lysosome-to-nucleus retrograde signaling pathway is mediated by a lysosome-associated fatty acid binding protein LBP-8 in *Caenorhabditis elegans.* LBP-8 shuttles lysosomal lipids into the nucleus to activate lipid regulated nuclear receptors NHR-49 and NHR-80 and consequently promote longevity. However, the structural basis of LBP-8 action remains unclear. Here, we determined the first 1.3 Å high-resolution structure of this life-extending protein LBP-8, which allowed us to identify a structurally conserved nuclear localization signal and amino acids involved in lipid binding. Additionally, we described the range of fatty acids LBP-8 is capable of binding and show that it binds to life-extending ligands in worms such as oleic acid and oleoylethanolamide with high affinity.

Introduction

Lysosomes are catabolically active cellular organelles and serve a vital role as the recycling center of the cell. Lysosomes contain various hydrolases, including proteases, lipases, nucleases, etc. that degrade damaged macromolecules and organelles in their highly acidic interior through a process termed autophagy [1]. As we age, we acquire various forms of damaged cellular macromolecules such as aggregated proteins, mutated DNA, and damaged organelles [2]. Given its significance in the clearance of these cellular damages, autophagy has been associated with a variety of longevity mechanisms. In the past few decades, molecular genetics studies in model organisms, including yeasts, worms, flies and mice, have demonstrated a series of lifespan-extending paradigms [2]. Interestingly, many of these paradigms induce autophagy, and the autophagy activity is required for their pro-longevity effects [3]. Thus, the lysosome can be linked with the longevity regulation through its involvement in the autophagic process.

On other hand, the lysosome is not only the center for the degradation and recycling of cellular waste, but can also serve as the hub for organizing signal transduction and controlling nuclear transcription. With adequate amino acids, mTORC1 is recruited to the surface of the lysosome through its interaction with active Rag GTPases and Ragulator, and is then activated by the small GTPase Rheb [4]. The activation of mTORC1 can negatively regulate the nuclear translocation of TFEB, a master regulator of lysosome biogenesis, and affect lysosomal functions [4]. Both mTORC1 and TFEB have been implicated in the regulation of longevity [5-7]. More recently, Folick et. al. reported a lysosome-to-nucleus retrograde lipid messenger signaling pathway in the regulation of longevity in *C elegans*. Upregulation of *LIPL-4*, a lysosomal lipid hydrolase extends lifespan through a process dependent upon the activation of nuclear receptors NHR-49 and NHR-80 [8]. Both NHR-49, an orthologue of the peroxisome proliferator-activated receptors (PPARs) in

vertebrates, and NHR-80, an orthologue of HNF4-α, bind to lipids and activate transcription responses crucial for the longevity regulation [9, 10]. Folick et. al. further identified a Lipid Binding Protein 8 (LBP-8) that mediates the retrograde signaling between lysosomal lipid hydrolysis and nuclear transcription. Upon the induction of LIPL-4, the *lbp-8* gene is transcriptionally up-regulated, and the LBP-8 protein is translocated into the nucleus from the lysosome. Interestingly, LBP-8 itself is also sufficient to prolong lifespan through activating NHR-49 and NHR-80 [8].

LBP-8 is a member of a larger family of proteins termed the intracellular lipid-binding proteins (iLBPs), which includes both fatty acid binding proteins (FABPs), cellular retinoic acid binding proteins (CRABPs), and cellular retinoid binding proteins (CRBPs). It is estimated that the iLBP family evolved in the animal kingdom over 1,000 MYA [11]. There are nine *C. elegans* FABPs, while humans have ten FABPs that are tissue specifically expressed. The hFABPs predominately bind to long-chained fatty acids, but some hFABPs bind larger hydrophobic molecules, such as bile acids, heme, and acyl-CoA [12-14]. They have been characterized to shuttle hydrophobic molecules to various cellular compartments, but of relevance here, certain hFABPs have been shown to shuttle nuclear receptor ligands into the nucleus to regulate nuclear receptor transcription [15-18].

In this study, we characterized *C. elegans* LBP-8 using structural and biochemical techniques to further understand its function as a longevity promoting protein and to gain more insight into the family of iLBPs. We solved the structure of LBP-8 at 1.3 Å, which is the first structure of a *C. elegans* FABP, providing new insights into the diverse iLBP family. Additionally, we identified ligands that bind to LBP-8 in an unbiased manner using mass spectrometry (MS), supporting the role of LBP-8 as a shuttling protein for monounsaturated fatty acids and their derivatives.

Results

Overall structure of apo-LBP-8 and general comparison with other FABPs

Overexpression of LBP-8 extends lifespan in worms, but the molecular mechanism explaining ligand binding or lysosome-nuclear lipid shuttling is not understood. To gain insight into these processes, we determined the first crystal structure of *C. elegans* LBP-8 (Fig. 1A). A crystal structure of heart FABP bound to stearic acid (PDB code 3WVM) was used as a search model to determine the initial phases since it shares the highest sequence similarity (37 %) with LBP-8 of known structures [19]. The LBP-8 structure was solved in the C121 space group at high resolution (1.3 Å), with the asymmetric unit containing a monomer, which was consistent with size exclusion chromatography (Fig. 1B). Refinement and model statistics are summarized in Table 1. The crystal structure includes all 137 amino acids of wild type LBP-8, 92 waters, and two sulfate anions. LBP-8 adopts a typical lipocalin fold, present in all FABPs, consisting of a N-terminal alpha helix-turn-helix motif lid (αA- αB) and a twisted beta barrel containing ten antiparallel strands (βA-βJ) (Fig. 1A). The interior cavity is lined with polar and hydrophobic residues generating a solvent accessible surface area of 825 $Å^2$ and volume of 1170 $Å^3$ (Fig 1C) [20]. There are fragments of continuous electron density present throughout the pocket; however, we were unable to model in a fatty acid with confidence. We attempted to co-crystallize LBP-8 with oleoylethanolamide (OEA), palmitic acid, and stearic acid, but all crystals yielded weak and fragmented density within the pocket. We do predict that fatty acid is binding to LBP-8 based on lipid MS data (Table 2), therefore, the fragmented electron density likely reflects that only a fraction of the LBP-8 in the crystal bound to fatty acid, or the fatty acid does not adopt a preferred conformation in the pocket. A network of eleven waters are present in the putative lipid binding pocket and anchored via hydrogen bonds with amino acids glutamine 56 and arginine 132.

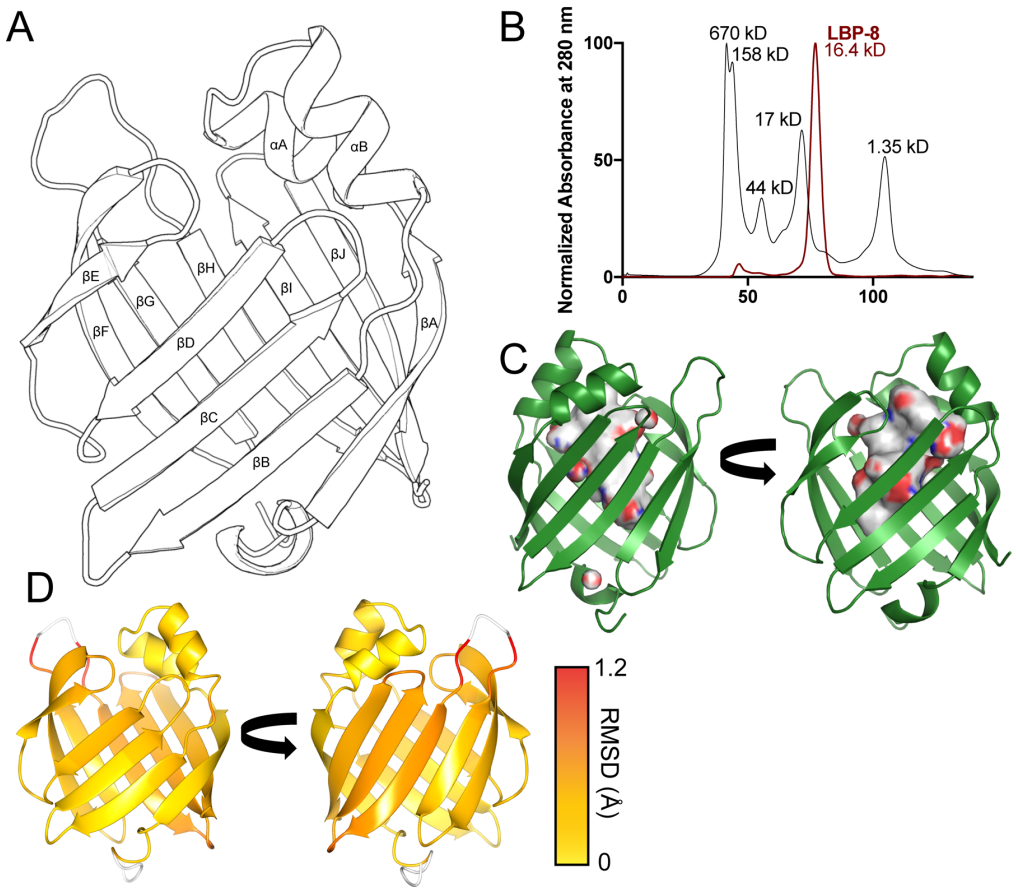

Figure 1. Structural overview of LBP-8. A. Tertiary structure of apo-LBP-8. The protein adopts typical lipocalin fold; a beta barrel (βA- (βJ) capped with an alpha helical lid (αA- αB). B. LBP-8 purifies as a monomer (16.4 kD). Size exclusion chromatography using HiLoad 16/60 Superdex 75 column comparing LBP-8 (red) and gel filtration standards (black). C. Surface representation of the interior cavity of LBP-8. Nonpolar surface is colored grey, polar surfaces are colored red and blue (red indicates oxygen, blue indicates nitrogen). D. ProSMART analysis conducted to determine r.m.s.d. between Cα backbone of LBP-8 and FABP4 bound linoleic acid (PDB 2Q9S). Root mean square deviations (range: 0 – 1.2 Å) between structures were mapped onto LBP-8 structure with a color scale depicting low (yellow) to high (red) deviations. Unaligned regions are colored in white.

Table 1: X-ray data collection and refinement statistics.

Data collection	LBP-8 Apo
Space group	C121
Cell dimensions	
a, *b*, *c* (Å)	46.9, 41.9, 70.9
α, β, γ (°)	90, 91.1, 90
Resolution (Å)	28.72 – 1.3 (1.347-1.3)
R_{pim}	0.018 (0.274)
$I / \sigma I$	33.3 (1.6)
Completeness (%)	96.3 (67.9)
Redundancy	6.9 (4.8)
Refinement	
Resolution (Å)	1.3
No. reflections	32686 (2491)
R_{work} / R_{free} (%)	19.04/21.01
No. atoms	
Protein	1142
Water	92
B-factors	
Protein	30.8
Ligand	37.6
Water	37.3
R.m.s. deviations	
Bond lengths (Å)	0.008
Bond angles (°)	0.9
Ramachandran favored (%)	100
Ramachandran outliers (%)	0
PDB accession code	6C1Z

Values in parenthesis indicate highest resolution shell (50.00-1.30 Å)

To identify conserved structural features between LBP-8 and other FABPs, we used the DALI server, which identifies similar protein structures based on root mean square deviations (r.m.s.d) [21]. This approach was critical since FABPs show low overall sequence conservation exemplified by the fact that the closest homolog by sequence is heart FABP at 49% similarity and 37% identity. Multiple FABP structures were found to be similar in 3D fold to LBP-8; however, we focused our analysis on the most similar structure that contained a bound fatty acid: FABP4 in complex with linoleic acid (PDB code 2Q9S) [17]. ProSMART ALIGN was used for alignment, superposition, and determining the structural conservation between the LBP-8 and FABP4 structure [22]. The main-chain dissimilarity scores were mapped onto the superposed structures with yellow depicting residues that have a similar local conformation, and gradually changing to red indicating comparative structural dissimilarity; white signifies unaligned residues (Fig. 1D). There are no major differences between the peptide backbones except for the loop between βG-βH, which is due to a three amino acids insertion in LBP-8. We additionally analyzed the structural conservation of side chains. Most side chain deviations were present in surface exposed residues, which is expected due to differential crystal packing and surface solvent interactions. The most divergent is an arginine side chain present in both structures (R81 in LBP-8 and R79 in FABP4). In FABP4, R79 is curled into the interior of the protein, where it can interact with D77 and solvent; however, in LBP-8, tyrosine 83 occupies this space, which positions R81 to the exterior surface.

The lipid sensing portal region

The portal region of FABPs, which is comprised of a helix-turn-helix motif (αA- αB), plays a vital role in protein-membrane interactions, protein localization, and ligand sensing. Many FABPs, such as FABP2, FABP3, FABP4, and FABP7 have been described as “collisional” FABPs

because they interact with the membrane via the alpha helical lid [23]. Positively charged residues within the αA and αB helices mediate electrostatic interactions with negatively charged phospholipid surfaces. Additionally, a hydrophobic patch within the turn region of the helix-turn-helix motif mediates insertion of the helical lid into the membrane [24, 25]. The LBP-8 structure contains two lysines (K24 and K34) and an arginine (R33) present in the alpha helical lid, and a hydrophobic patch (25-IGVGLLI-32) within the turn region, suggesting LBP-8 is a "collisional" FABP, and directly interacts with membranes or membrane proteins to acquire fatty acids (Fig. 2A-B). LBP-8 was previously shown to localize to the lysosome; therefore, we predict LBP-8 utilizes the collisional mechanism to obtain fatty acid ligands from lysosomal membranes [8].

The portal region of FABPs has also been reported to mediate nuclear localization. Though no nuclear localization sequence (NLS) is present in the primary sequence of FABPs, a three-dimensional structural NLS consisting of conserved lysines and an arginine was discovered in cellular retinoic acid binding protein 2 (CRABP-II), FABP4, and FABP5 [15-17]. The NLS is stimulated through the binding of "activating" ligands, which stabilize the NLS, supporting interaction with nuclear importins [16]. LBP-8 was previously reported to localize to the nucleus in *C. elegans* upon overexpression of *Lipl-4*; therefore, we sought to determine if LBP-8 also contained a structural NLS [8]. We performed a structural alignment of the ten human FABPs and two human CRABPs, and found that LBP-8 contained the conserved NLS sequence, along with FABP4, FABP5, PMP2, FABP12, and both CRABPs (Fig. 2C). We then aligned our LBP-8 structure with a structure of FABP5 in complex with linoleic acid (PDB code 4LKT), which drives nuclear localization, and found the LBP-8 NLS residues (K24, R33, and K34) directly overlaid with the FABP5 NLS residues (Fig. 2B). This suggests that these positive residues were co-opted into a role to drive active nuclear translocation through interaction with importins for FABPs, and

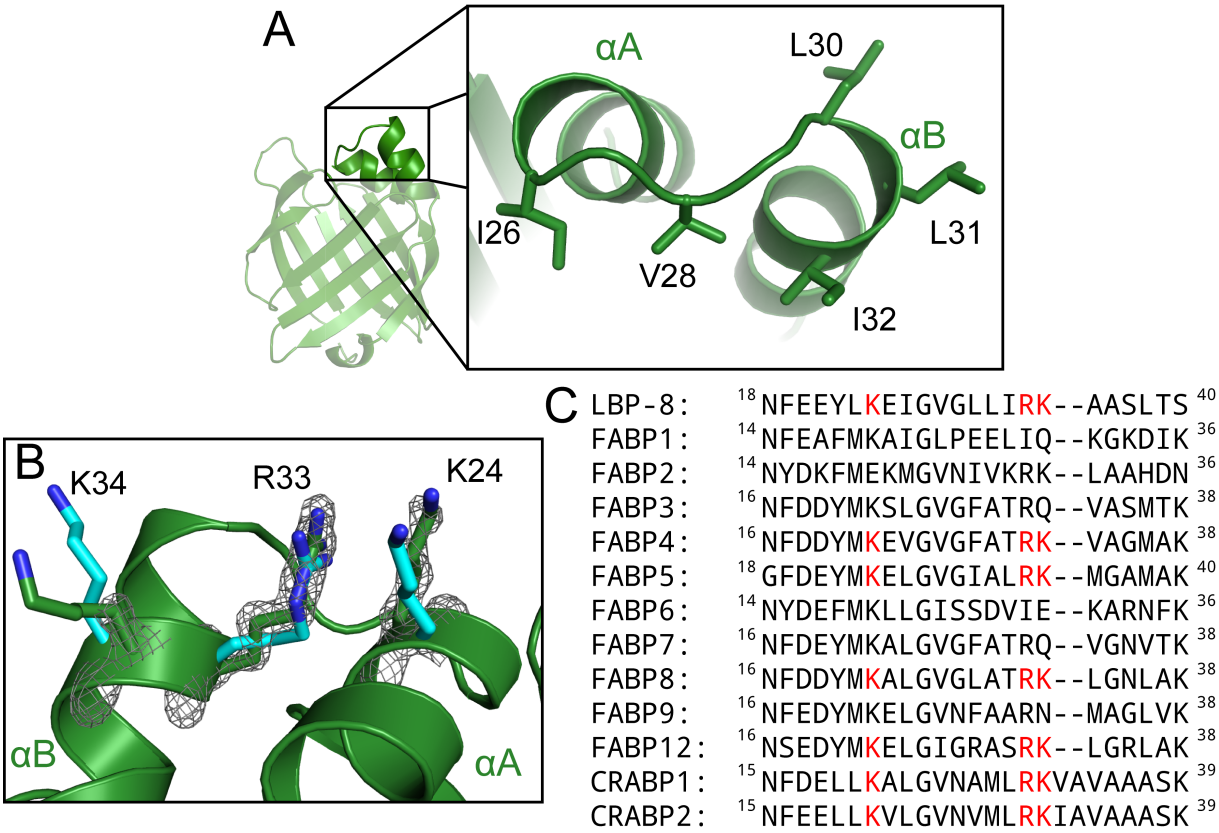

Figure 2. The portal region of LBP-8 contains a hydrophobic patch for interacting with membranes and conserved nuclear localization signal. A. Zoomed in view of the LBP-8 (green) portal region with hydrophobic residues depicted as sticks. B. Superposition of LBP-8 and FABP5 (PDB code 4LKT, cyan) with putative NLS residues depicted as sticks (C, green or cyan; N, blue). (C) Sequence alignment of LBP-8 with the human iLBPs. Residues that comprise the NLS are colored red.

this mechanism is likely conserved in LBP-8. Indeed, deletion of residues containing the putative NLS ablated nuclear translocation [8].

LBP-8 binds to a range of fatty acids with preference for monounsaturated fatty acids

Despite multiple attempts to crystallize LBP-8 in complex with fatty acids, only the apo-form of LBP-8 crystallized. Previously, we showed that LBP-8 bound to arachidonic acid (AA), ω-3 arachidonic acid (ω-3 AA), dihomo-γ-linoleic acid (DGLA), and oleoylethanolamide (OEA) in a dose dependent manner [8]. However, in order to identify all putative ligands, we took a discovery-based MS approach. Purified LBP-8 from *E. coli* was exposed to whole lipid extracts from *C. elegans*, re-purified through size-exclusion chromatography, and the bound fatty acids were identified through liquid chromatography/mass spectrometry (LC/MS) (Fig. 3A). Co-purified *E. coli* fatty acids were also determined by LC/MS and treated as background (Fig. 3B). To enhance signal and permit fatty acid quantification, we generated 3-picoylamide fatty acid derivatives, which selects for carboxyl containing lipids, and used precursor ion scan selecting for the loss of the 3-picoylamide ion [26]. Identification of the lipids from each experiment, and their relative percentages are recorded in Table 2. The major lipid species co-purified with LBP-8 from *E. coli* were palmitic acid (16:0) and oleic acid (18:1). Upon exposure to *C. elegans* lipid extracts, there was a shift in the binding preference of LBP-8. The relative amount of stearic acid (18:0) and palmitic acid (16:0) that co-purified with LBP-8 was greatly decreased, while there was an increase in the relative amount of myristic acid (14:0) and unsaturated fatty acids, such as arachadonic acid (20:4), linoleic acid (18:2), and palmitoleic acid (16:1). While the relative percentage of oleic acid decreased, it was still the most abundant fatty acid that bound to LBP-8. Additionally, two odd-chained fatty acids, heptadecanoic acid (17:0) and pentadecylic acid (15:0),

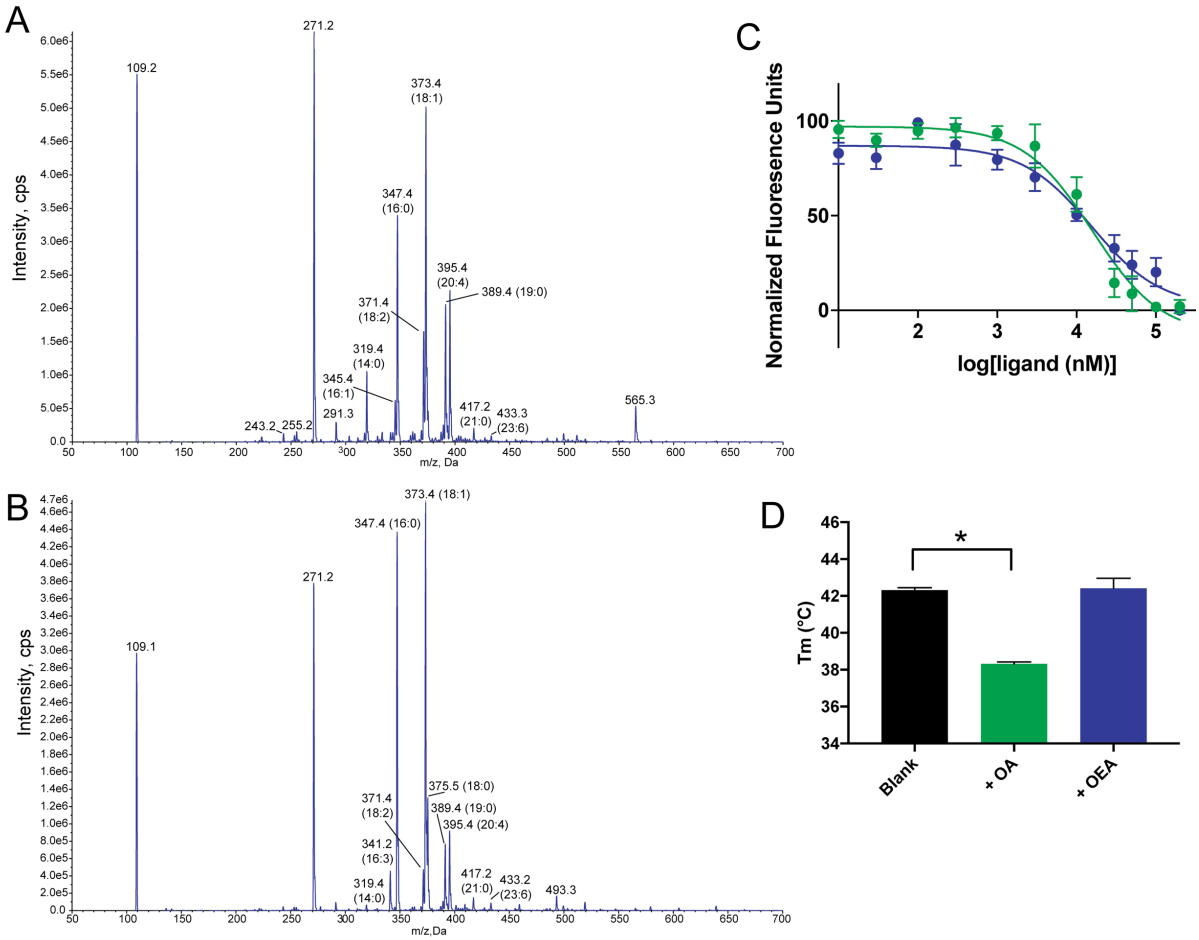

Figure 3. LBP-8 binds to a diverse array of saturated and unsaturated long-chained fatty acids. A. Mass spectra (positive mode) of carboxyl group containing lipids extracted from LBP-8 incubated with *C. elegans* lipid extracts. B. Mass spectra (positive mode) of carboxyl group containing lipids extracted from LBP-8 purified from *E. coli.* In both A and B, peaks are identified using fatty acid nomenclature (fatty acyl length: number of double bonds). C. Fluorescent ligand, 1,8-ANS, bound to LBP-8 was competed off with increasing amounts of oleic acid (green) and OEA (blue). Curves represent average of three independent replicates +/- SEM, conducted in triplicate, followed by normalization of curves. D. Oleic acid (OA, green) decreased the thermal melting temperature of LBP-8 compared to no ligand (Blank) and OEA (blue). Each bar represents the average of three independent replicates +/- SEM, each conducted

in triplicate. * $p < 0.05$ (significance was determined by one-way ANOVA followed by Dunnett's multiple comparisons test).

Table 2: Identification and relative quantification of lipids co-purified with LBP-8 via MS.

			Relative Percentage	
m/z (Da)	Adduct	Identified Lipid	*E. coli*	*C. elegans*
303.2	M + H	13:1	0.00%	0.48%
317.3	M + H	14:1	0.00%	0.74%
319.4	M + H	Myristic Acid (14:0)	0.47%	5.58%
333.4	M + H	Pentadecylic acid (15:0)	0.00%	0.78%
341.2	M + H	Hexadecatrienoic acid (16:3)	3.45%	0.85%
345.4	M + H	16:1	0.00%	3.56%
347.4	M + H	Palmitic Acid (16:0)	32.47%	19.44%
361.4	M + H	17:0	0.00%	0.92%
371.4	M + H	Linoleic Acid (18:2)	3.40%	9.27%
373.4	M + H	Oleic Acid (18:1)	35.72%	28.93%
375.5	M + H	Stearic Acid (18:0)	9.00%	2.29%
389.3	M + H	Nonadecylic Acid (19:0)	0.78%	1.52%
391.4	M + H	Hydroxy Stearic Acid	5.70%	11.24%
395.4	M + H	Arachadonic Acid (20:4)	6.82%	12.72%
417.2	M + H	Heneicosylic acid (21:0)	1.07%	1.14%
433.3	M + H	23:6	0.70%	0.54%
639.1	M + H	PS(20:3(8Z,11Z,14Z)/0:0)	0.44%	0.00%

co-purified with LBP-8 following exposure to *C. elegans* lipid extracts, which were not detectable in the LBP-8 purified from *E. coli.*

The lipid MS analysis suggested that LBP-8 does not bind to one fatty acid selectively but is capable of binding many fatty acids. However, LBP-8 does have a preference for unsaturated fatty acids, such as oleic acid, when presented with a variety of lipids. Previously, oleoylethanolamide (OEA), a monounsaturated fatty amide, was shown to bind to LBP-8 with higher affinity compared to other unsaturated fatty acids like arachidonic acid and dihomo-γ-linoleic acid. Due to the high abundance of oleic acid that co-purified with LBP-8, we sought to compare the affinity of LBP-8 for OEA and oleic acid. A fluorescence-based ligand binding assay was used to compare the affinity of oleic acid and OEA, and both had very similar Ki's, suggesting oleic acid, along with OEA, are high affinity ligands of LBP-8 (Fig. 3C).

To further analyze the effect of oleic acid binding to LBP-8, we conducted a thermal shift assay with LBP-8 in the presence of different ligands. To our surprise, oleic acid drastically destabilized LBP-8, decreasing the melting temperature (T_m) by ~4 °C compared to apo, while OEA had no effect on the melting temperature (Fig. 3D). Ligands typically stabilize a protein upon binding, but there are instances when ligands destabilize a protein [27, 28]. In this case, oleic acid selects for a less stable LBP-8 conformer.

Analysis of the ligand binding pocket

To gain insight into ligand binding, we compared the LBP-8 interior binding pocket with other FABPs. As stated previously, the interior cavity of LBP-8 has a solvent accessible surface area of 825 $Å^2$ and volume of 1170 $Å^3$ (Fig 1C) [20]. This interior cavity volume is similar to FABP9, smaller than FABP6 and FABP1, but larger than the other human FABPs (Table 3). While all

FABPs bind medium to long-chained fatty acids, FABP6 and FABP1 bind to larger hydrophobic molecules such as bile acids, heme, and acyl-CoA [29, 30].

Next, we compared the interior cavity side chains of LBP-8 with the other FABPs. The interior cavity of LBP-8 is lined with hydrophobic residues (F19, F60, L65, F67, F73, F94, F110, T112, and F134), which can stabilize fatty acyl tails of fatty acids via hydrophobic interactions. This is a trait found throughout the lipocalin family, with F19, F60, F67, and F73 being highly conserved residues. Additionally, the interior cavity is lined with several polar residues (Q56, Q121, Y123, and R132), which are capable of interacting with charged head groups of fatty acids via hydrogen bonding (Fig. 4A). Arginine 132 is highly conserved and is present in all human and *C. elegans* FABP isoforms; it has been shown to participate in electrostatic interactions with the head group of the bound fatty acid in many holo-FABP structures (Fig. 4A) [15, 19, 31]. The other interior polar residues in LBP-8 are not well conserved in human or *C. elegans* FABPs, suggesting R132 is likely an important residue for mediating lipid binding throughout the FABP family.

On the other hand, several amino acids that are highly conserved in other lipocalin family of proteins are not present in LBP-8. For instance, most *C. elegans* and human FABPs, excluding FABP1, FABP2, and FABP6, contain a tyrosine that is two residues downstream of the conserved arginine 132 (LBP-8 numbering), which also mediates electrostatic interactions with the head group of bound fatty acids (Fig. 4A) [11]. LBP-8 contains a phenylalanine (F134) at this position, which would disrupt the electrostatic interactions with the head group (Fig. 4A). Since FABP1, FABP2, and FABP6 also lack this tyrosine, we further compared LBP-8 to these FABPs, which are all capable of binding to hydrophobic molecules other than just medium to long chain fatty acids [29, 30]. A structure of the FABP2-oleic acid complex shows that the head group of oleic acid interacts with arginine 112 (LBP-8 numbering), resulting in fatty acid bound deeper in the pocket

Table 3: Interior cavity surface area and volume of human FABPs and LBP-8.

Protein	PDB code	Surface Area (Å^2)	Volume (Å^3)
Apo-FABP6	5L8I	1069.6	1482.8
FABP1	3STK	978.1	1429.2
LBP-8	**6C1Z**	**825**	**1170.3**
FABP7	5URA	770.6	1086.1
FABP3	5B27	768.1	1034.2
Apo-FABP2	1IFB	707.8	971.7
Apo-FABP9	4A60	703	1170.3
FABP8	3NR3	684.4	941.6
Apo-FABP5	4LKP	664.1	916.1
Apo-FABP4	3Q6L	636.5	936.6

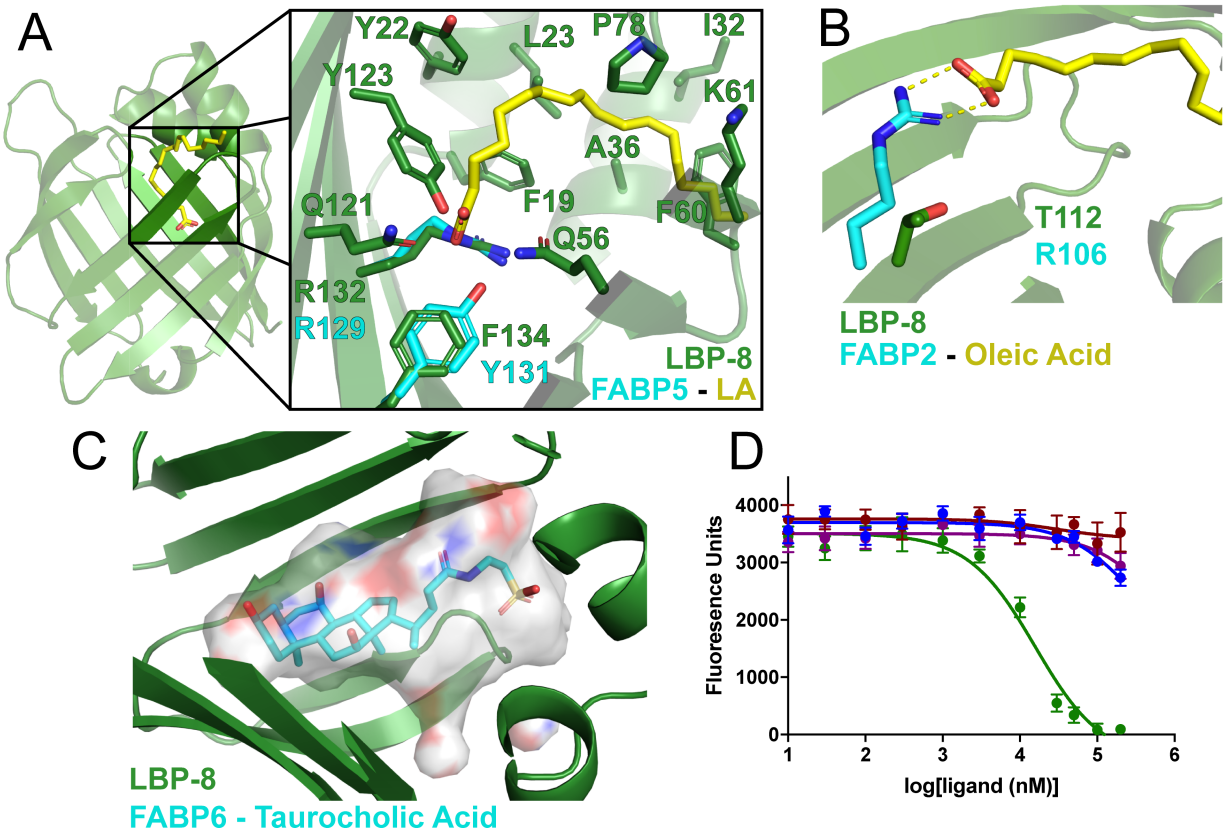

Figure 4. Comparison of ligand binding pocket of LBP-8 with FABPs. A. LBP-8 (green) is aligned with a structure of FABP5 (PDB code 4LKT, cyan) bound to linoleic acid (yellow). LBP-8 residues 3.5 Å away from linoleic acid are displayed. LBP-8 contains the conserved R132 that is also present in FABP5, R129, which electrostatically interacts with the head group of linoleic acid. FABP5 also contains a highly conserved tyrosine, Y131, which hydrogen bonds with the head group of linoleic acid, while LBP-8 contains a phenylalanine, F134. B. LBP-8 (green) is aligned with FABP2 (PDB code 2MO5, cyan) bound to oleic acid (yellow). The arginine, R106, electrostatically interacts with the head group of oleic acid, but LBP-8 contains a threonine, T112, at this residue. C. LBP-8 (green) is aligned with a structure of FABP6 in complex with taurocholic acid (PDB 1O1V, cyan). The solvent accessible surface of LBP-8's interior pocket is displayed in transparent white with charged surfaces colored red (negative) and blue (positive) around the ligand. D. Fluorescent ligand, 1,8-ANS, bound to LBP-8 was competed off with increasing amounts of oleic acid (green), cholic acid (blue). Taurocholic acid (red), and glycocholic acid (purple). Curves represent average of three independent replicates +/- SEM, conducted in triplicate.

compared to other holo-FABP structures (Fig. 4B). Although this residue is present in all FABPs except FABP1 and FABP6, the fatty acid only adopts this deep pocket conformation in FABP2. This conformation possibly occurs because of the absence of the conserved Y134 (LBP-8 numbering) at the C-terminus, leading to a new interaction site at R112 (LBP-8 numbering). However, LBP-8 has a threonine (T112) at this residue, like FABP1, rather than an arginine, which would not recapitulate the electrostatic interaction as seen in the FABP2-oleic acid structure (Fig. 4B). Similarly, FABP6 contains a serine at this residue.

Given LBP-8's pocket size and composition, we hypothesize that LBP-8 would bind a more diverse set of lipids similar to FABP1 and FABP6. In supporting this hypothesis, our lipid MS analysis identified a wide variety of lipids co-purified with LBP-8, including large lipids such as a phosphatidylserine species and a 23-carbon fatty acid, which have never been identified to bind to FABPs before now (Table 2). In order for the binding pocket to accommodate these lipids, we expect an opening of the portal region, enlarging the interior cavity, as seen in previous FABP structures [15]. To be noted, derivatization of lipids proceeding LC/MS prevented detection of non-carboxyl-containing lipids. Thus, there might be more lipids bound to LBP-8.

Bile acids such as cholic acid, taurocholic acid, and glycocholic acid are ligands for FABP6 and were significantly reduced in *lipl-4* transgenic worms that had extended lifespan in an LBP-8 dependent manner [8, 32]. Therefore, we postulated that these bile acids bound to LBP-8. We aligned a structure of FABP6 in complex with taurocholic acid with LBP-8 to determine if the LBP-8 pocket would accommodate bile acid binding. The ligand fit nicely within the solvent accessible surface of the pocket with only a few minor steric clashes (Fig. 4C). We then performed a fluorescence-based ligand binding assay with LBP-8 and cholic acid, taurocholic acid, and glycocholic acid. Compared with oleic acid, none of the bile acids bound or bound with very low

affinity (Fig. 4D). Further experimentation is required to determine if LBP-8 is capable of binding to larger lipid molecules, should these ligands be determined biologically relevant.

Mutational analysis of LBP-8 ligand binding pocket

Given the LBP-8 structure, we hypothesized that polar residues Q56, Q121, Y123, and R132 lining the interior cavity of LBP-8 stabilize the head group of fatty acids to mediate ligand binding (Fig. 4A). Though Q56, Q121 and Y123 are not conserved in human FABPs, they are apposed to the carboxyl head group of many fatty acids structurally aligned with LBP-8. Therefore, we created several mutational constructs that contained various combinations of these residues mutated to alanine. All constructs were purified successfully and eluted at the same volume as wild-type LBP-8 in size exclusion chromatography.

In order to test the impact of these residues on fatty acid binding, we first attempted to use a fluorescence-based competition assay, but many of our LBP-8 mutants had a significantly reduced binding to the fluorescent probe (1,8-ANS), preventing us from accurately comparing fatty acid binding to wild-type LBP-8 (Fig. 5A). Mutating asparagine 56 did not alter the affinity of the probe for LBP-8 but mutating the highly conserved arginine 132 significantly reduced probe affinity. All other constructs that included this arginine 132 mutant exhibited significantly lower affinity for probe. This led us to hypothesize that arginine 132 plays an essential role in fatty acid binding.

Since our fluorescent-based competition assay was insufficient to directly compare fatty acid binding between our constructs, we used another technique to probe fatty acid binding. Moving forward, we only utilized the R132A (R132A-LBP-8) and Q121A, Y123A, R132A (Triple-LBP-8) mutant constructs, since Q56 appeared to play an insignificant role in binding. We verified proper folding of these constructs with circular dichroism, which revealed no difference

between the wild-type and mutant proteins (Fig. 5B). We then used a coupled enzymatic reaction and colorimetric probe, to compare the total amount of fatty acid bound to wild type and mutant proteins when purified from *E. coli*. The R132A-LBP-8 protein had a similar amount of fatty acid bound compared to wild type protein. Surprisingly, the Triple-LBP-8 protein bound to a greater amount of fatty acids compared to wild type (Fig. 5C). Though our mutants had reduced affinity for 1,8-ANS, they actually bound to more fatty acid, suggesting the mechanism of binding for these ligands differ. These surprising results could be due to the generation of a larger and more hydrophobic pocket in our mutants, which would accommodate more fatty acid, yet disrupt 1,8-ANS binding.

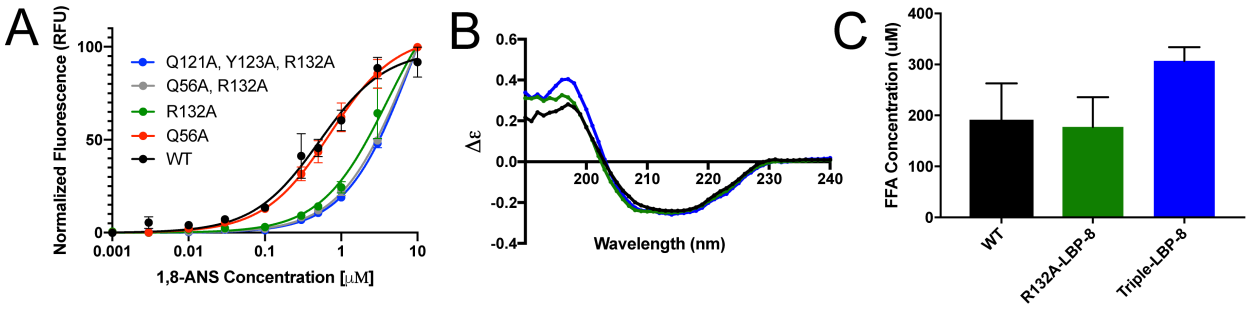

Figure 5. Analysis of ligand binding pocket mutants. A. Fluorescent probe, 1,8-ANS, was titrated into wild-type LBP-8 and mutant constructs. Curves depict average of experiment performed in triplicate +/- SEM, followed by normalization of curves. Mutant constructs with R132A mutant have significantly reduced affinity for 1,8-ANS. B. Circular dichroism spectra in molar extinction units (Δε) for WT-LBP-8 (black), R132A-LBP-8 (green), and Triple-LBP8 (blue) mutants. C. Average amount of fatty acid bound to 500 μM WT-LBP-8, R132A-LBP-8 and Triple-LBP-8 mutants. Each bar represents the average of three independent replicates +/- SEM.

Discussion

As a very conserved family of lipid binding proteins, FABPs share similarities in structure and fold, but there is vast diversity in sequence, ligand specificity, and function within the family. Much effort has been directed towards understanding the biology of human FABPs and we have high-resolution structures of all human FABPs, with the exception of FABP12. Yet, little is known about FABPs in other organisms, which in a way limits our understanding on the evolution of these proteins. Here, we have expanded our knowledge of the FABP family by reporting the first structure of a *C. elegans* FABP, LBP-8, and exploring its ligand specificity.

Though LBP-8 has little sequence similarity with human FABPs, it shares many of the same structural motifs. It contains a portal region similar to other FABPs, harboring a structural NLS present in many other FABPs. Additionally, LBP-8 binds to similar types of hydrophobic molecules known to bind to all FABPs, showing preference for long chained fatty acids. These congruent features support the conservation of FABP proteins on the structural basis, and the translatability of FABP biology across different species.

On the other hand, our studies also discover differences present in LBP-8 compared with human FABPs, many of which are found in the interior cavity. First, though LBP-8 contains a conserved arginine 132, it lacks a highly conserved tyrosine two residues downstream, which makes up what has been termed the P2 motif (Arg – x – Tyr) that is responsible for stabilizing the head group of bound fatty acids [11, 33, 34]. Additionally, LBP-8 lacks a conserved arginine at residue 112 that stabilizes the head group of fatty acids in FABP2. The absence of these conserved amino acids and having large pocket volume suggest that fatty acids can bind variably, possibly explaining why there was such diversity in our lipid MS data and disordered electron density within the interior of the crystal structure.

We attempted to ablate fatty acid binding through mutating conserved polar amino acids within the interior pocket, namely arginine 132, glutamine 121 and tyrosine 123, which we predicted to electrostatically interact with the carboxyl head group of fatty acids. To our surprise, mutating these residues did not reduce fatty acid binding, but rather increased binding. This suggests that though these conserved amino acids may play a role in orienting the carboxyl head group in the pocket, they do not drive fatty acid binding. A similar increase in ligand affinity, 30-fold, was discovered in human FABP2 upon mutating arginine 106 to an alanine, which disrupted the electrostatic interaction between the basic residue and the carboxyl head group of oleic acid [35]. Though the enthalpy of binding was decreased upon loss of the electrostatic interaction, this was more than compensated with an increase in entropy [35]. Our data concurs with this previous study which showed that binding to fatty acid is driven more entropically than enthalpically. The hydrogen bonding that occurs between a fatty acid head group and polar residues within the pocket are not necessary for binding. Hydrophobic effects appear to have a greater impact on binding than these hydrogen bonds. However, 1,8-ANS binds to LBP-8 through a very different mechanism than fatty acids. A previous crystal structure of human FABP3 bound to 1,8-ANS showed hydrogen bonding between the sulfonic acid group of the ligand and a water network coordinated by the highly conserved arginine 126 (R132 LBP-8 numbering) [36]. This explains why mutating arginine 132 in LBP-8 significantly reduced 1,8-ANS binding. Given this data, we suspect that entropy is the main driver in fatty acid binding, while enthalpy is the main driver of 1,8-ANS binding to LBP-8.

Our lipid MS analysis showed that LBP-8 bound to a diverse array of fatty acids. A low degree of lipid selectivity is a common trait found throughout the FABP family [37]. However, while FABPs are capable of binding an array of hydrophobic molecules, they have evolved to

selectively respond through conformational dynamics to a few lipids. For instance, polyunsaturated fatty acids binding to FABP5 activate its localization to the nucleus and the up-regulation of PPARβ/δ target genes, while saturated fatty acids binding does not activate these FABP5 functions [15]. Activating ligands allosterically communicate with an "activation switch", which is two hydrophobic residues that lie at the interface between the α2 helix of the portal region and the β2 loop (M35 and L60). Polyunsaturated fatty acids stabilize this switch, which stabilizes the NLS, stimulating nuclear localization [15]. Similarly, a PPARα agonist, GW7647, altered the conformation of residues on loops adjacent to the portal region of FABP1, which promoted interaction with PPARα and PPARα transactivation [38]. We hypothesize that the LBP-8 portal region and the surrounding loops mediate a similar ligand-controlled activation switch. In support of this, LBP-8 also contains hydrophobic residues (A35 and F60) at the same activation switch region found in FABP5. Despite the fact that many fatty acids are capable of binding to LBP-8, only select fatty acids may stimulate the life-extending effects of LBP-8. Consistently, although LBP-8 is capable of binding to saturated fatty acids, polyunsaturated fatty acids, monounsaturated fatty amide OEA, and monounsaturated fatty acid oleic acid, only OEA and oleic acid are shown to prolong *C. elegans* lifespan so far [8, 39].

Oleic acid plays a key role in many cellular events including remediation of inflammation, stimulation of lipid metabolism, and increased insulin sensitivity, yet the mechanisms by which oleic acid mediates all these effects aren't fully understood [40-42]. In this study, we showed LBP-8 co-purified with oleic acid, a monounsaturated fatty acid, from *C. elegans* lipid extracts. Additionally, oleic acid bound to LBP-8 with similar affinity as OEA, suggesting LBP-8 prefers monounsaturated fatty acyls. We propose LBP-8 is the main monounsaturated fatty acyl transporter to the nucleus to regulate aging.

Materials and Methods

Materials and reagents—Chemicals were purchased from Sigma, Fisher or Acros Organics. The vector for His-tagged tobacco etch virus (TEV) was a gift from John Tesmer (University of Texas at Austin). The pMCSG7 (LIC_HIS) vector was provided by John Sondek (University of North Carolina at Chapel Hill). DNA oligonucleotide primers were synthesized by IDT (Coralville, IA).

Cloning and mutagenesis—Full-length, wild-type *Caenorhabditis elegans* LBP-8 (residues 1 – 137) from was subcloned into pMCSG7-His vector. The NLS-deficient mutant (LBP-8 NLSm: K24A, R33A, and K34A) and lipid binding deficient mutants (combinations of Q121A, Y123A, and R132A) were generated in pMCSG7-His. All mutagenesis was accomplished using the megaprimer method [43].

Protein expression and purification—Full-length *Caenorhabditis elegans* LBP-8 in the pMCSG7 vector (wild-type and mutants) was transformed into *Escherichia coli* strain BL21 (DE3) cells and expressed as a His_6 fusion containing a tobacco etch virus protease cleavage site to facilitate tag removal. Cultures (1 liters in TB) were grown to an A_{600} of ~0.6 and induced with 0.5 mM isopropyl β-d-1-thiogalactopyranoside at 22 °C for ~18 hours. Cell mass was harvested, lysed through sonication in a buffer containing 20 mM Tris HCl pH 7.4, 150 mM NaCl, 25 mM imidazole, 5% glycerol, lysozyme, Dnase A, and 100 uM phenylmethylsulfonyl fluoride. LBP-8 was purified by nickel affinity chromatography and the His tag was cleaved by tobacco etch virus protease at 4 °C overnight with simultaneous dialysis into a buffer containing 20 mM Tris HCl pH 7.4, 150 mM NaCl, and 5% glycerol. Cleaved LBP-8 was purified from His tag through nickel affinity chromatography followed by gel filtration chromatography using a HiLoad 16/60

Superdex 75 column. For ligand binding studies, LBP-8 was unfolded and refolded to remove bound *E. coli* lipids. To do so, LBP-8 sequestered in inclusion bodies was solubilized and unfolded by resuspension and sonication in denaturing buffer (20 mM Tris HCl pH 8.0, 300 mM NaCl, 8 M urea, 5 mM 2-mercaptoethanol, and 25 mM imidazole). Unfolded LBP-8 was refolded on a 5 mL HisTrap FF affinity column using a linear gradient to remove urea, and then eluted using imidazole. Refolded LBP-8 was further purified by gel filtration chromatography using a HiLoad 16/60 Superdex 75 column.

Crystallization, data collection, structural refinement—Pure wild-type, full-length LBP-8 was concentrated to 15 mg mL^{-1} in 20 mM Tris HCl pH 7.4, 150 mM NaCl, and 5 % glycerol. Crystals of LBP-8 were grown over two weeks via sitting drop vapor diffusion at 4 °C from solutions containing 1 μL LBP-8, 1 μL mother liquor (2.81 M ammonium sulfate and 0.25 M potassium formate), and 0.7 μL LBP-8 seed stock. Crystals were cryoprotected by immersion in 2 M ammonium sulfate, 0.325 M potassium formate, and 20 % glycerol and flash frozen with liquid nitrogen. Data were collected remotely from the Southeast Regional Collaborative Access Team at the Advanced Photon Source, 22ID beamline (Argonne National Laboratories, Chicago, IL). Data were processed and scaled using HKL-2000 (HKL Research, Inc., Charlottesville, VA) [44] and phased by molecular replacement using Phaser-MR (Phenix, Berkeley, CA) [45]. The structure was phased using a previously solved crystal structure of human FABP3 (3WVM) as a search model [19]. Structure refinement and validation was performed using PHENIX (Phenix, Berkeley, CA) (version 1.11.1), and model building was performed in COOT (MRC Laboratory of Molecular Biology, Cambridge, UK) [45, 46]. PyMOL (version 1.8.2; Schrödinger, New York, NY) was used to visualize structures and generate figures.

LBP-8 lipid exchange with C. elegans lipids—A synchronous population of approximately 500,000 day 1, N2 worms were grown at 20°C on OP50. Worms were washed 3x in PBS, frozen into small pellets in liquid Nitrogen, and stored at -80°C. The worms were later cracked using a Cellcrusher. The cracked worms were then ground using a pestle and mortar, which had been chilled with liquid Nitrogen, until no intact worms remained. Liquid nitrogen was added to the sample in both the Cellcrusher and pestle and mortar as needed to maintain a cold temperature. Lipids were extracted from the *C. elegans* lysates using the Bligh and Dyer method [47]. Briefly, 1.6 grams of homogenized *C. elegans* lysates was resuspended in 5 ml methanol and 2.5 ml chloroform and vortexed for 30 minutes. Undissolved material was removed, followed by the addition of 2.5 ml 0.1 M NaCl. Additional methanol and chloroform were added to separate the aqueous and organic phase. The organic phase was collected and dried with nitrogen gas. Dried lipid extracts were resuspended in LBP-8 sizing buffer (20 mM Tris HCl pH 7.4, 150 mM NaCl, and 5% glycerol) plus 0.5 % DMSO, sonicated for 15 minutes, and rocked at 4 °C overnight to form lipid vesicles. The lipid vesicles were incubated with purified LBP-8 at 4 °C overnight while rocking. Nonspecifically bound lipids were removed through gel filtration chromatography using a HiLoad 16/60 Superdex 75 column.

Lipid derivatization and mass spectrometry—

Lipids were extracted from LBP-8 purified from *E. coli* before and after exchange with *C. elegans* lipid extracts using the Bligh and Dyer method as described above [47]. Fatty acid derivatives were generated as previously described here [26]. Briefly, dried lipid extracts were incubated with 200 μL of oxalyl chloride (2 M in dichloromethane) at 65 °C for 5 minutes, and then dried down with

nitrogen gas. Then, 3-picolylamide fatty acid derivatives were formed through incubation with 3-picolylamine at room temperature for 5 minutes and then dried down with nitrogen gas. The fatty acid derivatives were resuspended in a 1:1 methanol: water solution for mass spec analysis. The sample was directly injected into the ABSciex QTRAP5500 mass spectrometer. Data was collected in positive-ion mode using a precursor ion scan selected for the precursor ion of picolylamine (109 *m/z*). Data was acquired and analyzed using LipidSearch software.

Circular dichroism—Wild-type and mutant forms of LBP-8 were concentrated to ~0.8 mg/ml in 20 mM Tris HCl pH 7.4, 150 mM NaCl, and 5 % glycerol. Circular dichroism (CD) studies were performed on a Jasco J-810 spectropolarimeter with a 1 mm cell. Wavelength scans measuring ellipticity signal were performed at 25 °C from 190 to 300 nm at intervals of 0.2 nm. Each scan is the average of three independent spectral scans. Ellipticity degrees were converted to molar extinction to account for slight variations in protein concentration. The α-helix/ β-sheet ratios were calculated using the k2d3 server k2d3.ogic.ca/ [48].

Competitive fluorescence-based binding assay— Quantification of ligand binding was conducted via competition with the probe 1-anilinonaphthalene-8-sulfonic acid (1,8-ANS), a small molecule whose fluorescence increases drastically when surrounded by a hydrophobic environment and which has been shown to bind an array of iLBPs with varying affinity [49]. Briefly, binding of 1,8-ANS was carried out in PBS (137 mM NaCl, 2.7 mM KCl, 10 mM Na_2HPO_4, 2 mM KH_2PO_4, pH=8.0) in the presence of 250 nM LBP-8 that was unfolded and refolded to remove *E. coli* lipids and increasing amounts of fluorescent probe (0-30 μM). Blank measurements containing 1,8-ANS only were subtracted from each probe concentration tested, and the resulting fluorescent values

were fit with a One-Site binding curve to determine the binding constant, K_D. Competition assays were then carried out in the same buffer system using a constant concentration of 250 nM protein and 800 nM 1,8-ANS, with ligand added via 100X ethanol stocks to maintain an ethanol concentration of 1%. Following a one-hour incubation at 37 °C, data were collected on a BioTek Synergy NEO plate reader using an excitation wavelength of 360 nm and an emission wavelength of 525 nm. Blank wells containing only ligand and 1,8-ANS were subtracted from wells with protein at each ligand concentration tested. Data was processed in GraphPad Prism 7. All curves are the average of three independent experiments.

Differential scanning fluorimetry (DSF)—Purified LBP-8 protein (7 μM) that was unfolded then refolded to remove bound *E. coli* lipids was incubated for 30 minutes with 20 μM of oleic acid, cholic acid, or OEA at room temperature. Lipid ligands were dissolved in ethanol and diluted in water so that the percentage of ethanol was held at 1 % in the final reaction. SYPRO orange dye (Invitrogen) was then added at a 1:2000 dilution. Reactions were heated at a rate of 0.5°C per minute, using a StepOne Plus Real Time PCR System (ThermoFisher). Fluorescence was recorded at every degree using the ROX filter (602 nm). Data were analyzed by first subtracting baseline fluorescence (ligands + SYPRO with no protein) and then fitting the curves using the Bolzman equation (GraphPad Prism, v6) to determine the Tm. One-way ANOVA was used to compare Tm's of different ligands.

Fatty Acid Quantification—Lipids were extracted and dried down with nitrogen gas from equal amounts of purified WT and mutant forms of LBP-8 using the Bligh and Dyer method as described above [47]. The dried lipid extracts were resuspended in PBS (137 mM NaCl, 2.7 mM KCl, 10 mM

Na_2HPO_4, 2 mM KH_2PO_4, pH=8.0). The total amount of fatty acid for each sample was determined using the Free Fatty Acid Assay Kit (Colorimetric), Cell Biolabs, San Diego, CA, USA. Data was analyzed in GraphPad Prism 7. All data represents the average of three replicates.

Data Availability: The LBP-8 crystal structure dataset is available at the Protein Data Bank with the accession code 6C1Z. All other datasets generated and analyzed during the current study are available from the corresponding author on reasonable request.

References

1. Settembre C, Fraldi A, Medina DL, Ballabio A. Signals from the lysosome: a control centre for cellular clearance and energy metabolism. Nature reviews Molecular cell biology. 2013;14(5):283-96. Epub 2013/04/24. doi: 10.1038/nrm3565. PubMed PMID: 23609508; PMCID: PMC4387238.
2. Lopez-Otin C, Blasco MA, Partridge L, Serrano M, Kroemer G. The hallmarks of aging. Cell. 2013;153(6):1194-217. Epub 2013/06/12. doi: 10.1016/j.cell.2013.05.039. PubMed PMID: 23746838; PMCID: PMC3836174.
3. Hansen M, Rubinsztein DC, Walker DW. Autophagy as a promoter of longevity: insights from model organisms. Nature reviews Molecular cell biology. 2018;19(9):579-93. Epub 2018/07/15. doi: 10.1038/s41580-018-0033-y. PubMed PMID: 30006559.
4. Saxton RA, Sabatini DM. mTOR Signaling in Growth, Metabolism, and Disease. Cell. 2017;168(6):960-76. Epub 2017/03/12. doi: 10.1016/j.cell.2017.02.004. PubMed PMID: 28283069; PMCID: PMC5394987.
5. Johnson SC, Rabinovitch PS, Kaeberlein M. mTOR is a key modulator of ageing and age-related disease. Nature. 2013;493(7432):338-45. Epub 2013/01/18. doi: 10.1038/nature11861. PubMed PMID: 23325216; PMCID: PMC3687363.
6. Kennedy BK, Lamming DW. The Mechanistic Target of Rapamycin: The Grand ConducTOR of Metabolism and Aging. Cell Metab. 2016;23(6):990-1003. Epub 2016/06/16. doi: 10.1016/j.cmet.2016.05.009. PubMed PMID: 27304501; PMCID: PMC4910876.
7. Lapierre LR, De Magalhaes Filho CD, McQuary PR, Chu CC, Visvikis O, Chang JT, Gelino S, Ong B, Davis AE, Irazoqui JE, Dillin A, Hansen M. The TFEB orthologue HLH-30 regulates autophagy and modulates longevity in Caenorhabditis elegans. Nature communications. 2013;4:2267. Epub 2013/08/09. doi: 10.1038/ncomms3267. PubMed PMID: 23925298; PMCID: PMC3866206.
8. Folick A, Oakley HD, Yu Y, Armstrong EH, Kumari M, Sanor L, Moore DD, Ortlund EA, Zechner R, Wang MC. Aging. Lysosomal signaling molecules regulate longevity in Caenorhabditis elegans. Science (New York, NY). 2015;347(6217):83-6. Epub 2015/01/03. doi: 10.1126/science.1258857. PubMed PMID: 25554789; PMCID: PMC4425353.
9. Uno M, Nishida E. Lifespan-regulating genes in C. elegans. NPJ aging and mechanisms of disease. 2016;2:16010. Epub 2017/07/20. doi: 10.1038/npjamd.2016.10. PubMed PMID: 28721266; PMCID: PMC5514992.
10. Brandstadt S, Schmeisser K, Zarse K, Ristow M. Lipid-lowering fibrates extend C. elegans lifespan in a NHR-49/PPARalpha-dependent manner. Aging. 2013;5(4):270-5. Epub 2013/04/23. doi: 10.18632/aging.100548. PubMed PMID: 23603800; PMCID: PMC3651519.
11. Smathers RL, Petersen DR. The human fatty acid-binding protein family: evolutionary divergences and functions. Human genomics. 2011;5(3):170-91. Epub 2011/04/21. doi: 10.1186/1479-7364-5-3-170. PubMed PMID: 21504868; PMCID: PMC3500171.
12. Grober J, Zaghini I, Fujii H, Jones SA, Kliewer SA, Willson TM, Ono T, Besnard P. Identification of a bile acid-responsive element in the human ileal bile acid-binding protein gene. Involvement of the farnesoid X receptor/9-cis-retinoic acid receptor heterodimer. J Biol Chem. 1999;274(42):29749-54. Epub 1999/10/09. PubMed PMID: 10514450.
13. McArthur MJ, Atshaves BP, Frolov A, Foxworth WD, Kier AB, Schroeder F. Cellular uptake and intracellular trafficking of long chain fatty acids. J Lipid Res. 1999;40(8):1371-83. Epub 1999/08/03. PubMed PMID: 10428973.

14. Stewart JM, Slysz GW, Pritting MA, Muller-Eberhard U. Ferriheme and ferroheme are isosteric inhibitors of fatty acid binding to rat liver fatty acid binding protein. Biochemistry and cell biology = Biochimie et biologie cellulaire. 1996;74(2):249-55. Epub 1996/01/01. PubMed PMID: 9213434.
15. Armstrong EH, Goswami D, Griffin PR, Noy N, Ortlund EA. Structural basis for ligand regulation of the fatty acid-binding protein 5, peroxisome proliferator-activated receptor beta/delta (FABP5-PPARbeta/delta) signaling pathway. J Biol Chem. 2014;289(21):14941-54. Epub 2014/04/03. doi: 10.1074/jbc.M113.514646. PubMed PMID: 24692551; PMCID: PMC4031543.
16. Sessler RJ, Noy N. A ligand-activated nuclear localization signal in cellular retinoic acid binding protein-II. Mol Cell. 2005;18(3):343-53. Epub 2005/05/04. doi: 10.1016/j.molcel.2005.03.026. PubMed PMID: 15866176.
17. Gillilan RE, Ayers SD, Noy N. Structural basis for activation of fatty acid-binding protein 4. Journal of molecular biology. 2007;372(5):1246-60. Epub 2007/09/01. doi: 10.1016/j.jmb.2007.07.040. PubMed PMID: 17761196; PMCID: PMC2032018.
18. Hughes ML, Liu B, Halls ML, Wagstaff KM, Patil R, Velkov T, Jans DA, Bunnett NW, Scanlon MJ, Porter CJ. Fatty Acid-binding Proteins 1 and 2 Differentially Modulate the Activation of Peroxisome Proliferator-activated Receptor alpha in a Ligand-selective Manner. J Biol Chem. 2015;290(22):13895-906. Epub 2015/04/08. doi: 10.1074/jbc.M114.605998. PubMed PMID: 25847235; PMCID: PMC4447964.
19. Matsuoka S, Sugiyama S, Matsuoka D, Hirose M, Lethu S, Ano H, Hara T, Ichihara O, Kimura SR, Murakami S, Ishida H, Mizohata E, Inoue T, Murata M. Water-mediated recognition of simple alkyl chains by heart-type fatty-acid-binding protein. Angew Chem Int Ed Engl. 2015;54(5):1508-11. Epub 2014/12/11. doi: 10.1002/anie.201409830. PubMed PMID: 25491543; PMCID: PMC4471613.
20. Dundas J, Ouyang Z, Tseng J, Binkowski A, Turpaz Y, Liang J. CASTp: computed atlas of surface topography of proteins with structural and topographical mapping of functionally annotated residues. Nucleic acids research. 2006;34(Web Server issue):W116-8. Epub 2006/07/18. doi: 10.1093/nar/gkl282. PubMed PMID: 16844972; PMCID: PMC1538779.
21. Holm L, Rosenstrom P. Dali server: conservation mapping in 3D. Nucleic acids research. 2010;38(Web Server issue):W545-9. Epub 2010/05/12. doi: 10.1093/nar/gkq366. PubMed PMID: 20457744; PMCID: PMC2896194.
22. Nicholls RA, Fischer M, McNicholas S, Murshudov GN. Conformation-independent structural comparison of macromolecules with ProSMART. Acta Crystallogr D Biol Crystallogr. 2014;70(Pt 9):2487-99. Epub 2014/09/10. doi: 10.1107/s1399004714016241. PubMed PMID: 25195761; PMCID: PMC4157452.
23. Zamarreno F, Herrera FE, Corsico B, Costabel MD. Similar structures but different mechanisms: Prediction of FABPs-membrane interaction by electrostatic calculation. Biochimica et biophysica acta. 2012;1818(7):1691-7. Epub 2012/03/27. doi: 10.1016/j.bbamem.2012.03.003. PubMed PMID: 22446190.
24. Corsico B, Franchini GR, Hsu KT, Storch J. Fatty acid transfer from intestinal fatty acid binding protein to membranes: electrostatic and hydrophobic interactions. J Lipid Res. 2005;46(8):1765-72. Epub 2005/05/03. doi: 10.1194/jlr.M500140-JLR200. PubMed PMID: 15863832.
25. Corsico B, Liou HL, Storch J. The alpha-helical domain of liver fatty acid binding protein is responsible for the diffusion-mediated transfer of fatty acids to phospholipid

membranes. Biochemistry. 2004;43(12):3600-7. Epub 2004/03/24. doi: 10.1021/bi0357356. PubMed PMID: 15035630.
26. Li X, Franke AA. Improved LC-MS method for the determination of fatty acids in red blood cells by LC-orbitrap MS. Analytical chemistry. 2011;83(8):3192-8. Epub 2011/03/25. doi: 10.1021/ac103093w. PubMed PMID: 21428294; PMCID: PMC4439250.
27. Cimmperman P, Baranauskiene L, Jachimoviciute S, Jachno J, Torresan J, Michailoviene V, Matuliene J, Sereikaite J, Bumelis V, Matulis D. A quantitative model of thermal stabilization and destabilization of proteins by ligands. Biophysical journal. 2008;95(7):3222-31. Epub 2008/07/05. doi: 10.1529/biophysj.108.134973. PubMed PMID: 18599640; PMCID: PMC2547457.
28. Kabir A, Honda RP, Kamatari YO, Endo S, Fukuoka M, Kuwata K. Effects of ligand binding on the stability of aldo-keto reductases: Implications for stabilizer or destabilizer chaperones. Protein science : a publication of the Protein Society. 2016;25(12):2132-41. Epub 2016/09/07. doi: 10.1002/pro.3036. PubMed PMID: 27595938; PMCID: PMC5119574.
29. Storch J, McDermott L. Structural and functional analysis of fatty acid-binding proteins. J Lipid Res. 2009;50 Suppl:S126-31. Epub 2008/11/20. doi: 10.1194/jlr.R800084-JLR200. PubMed PMID: 19017610; PMCID: PMC2674722.
30. Hendrick AG, Muller I, Willems H, Leonard PM, Irving S, Davenport R, Ito T, Reeves J, Wright S, Allen V, Wilkinson S, Heffron H, Bazin R, Turney J, Mitchell PJ. Identification and Investigation of Novel Binding Fragments in the Fatty Acid Binding Protein 6 (FABP6). Journal of medicinal chemistry. 2016;59(17):8094-102. Epub 2016/08/09. doi: 10.1021/acs.jmedchem.6b00869. PubMed PMID: 27500412.
31. Marr E, Tardie M, Carty M, Brown Phillips T, Wang IK, Soeller W, Qiu X, Karam G. Expression, purification, crystallization and structure of human adipocyte lipid-binding protein (aP2). Acta crystallographica Section F, Structural biology and crystallization communications. 2006;62(Pt 11):1058-60. Epub 2006/11/02. doi: 10.1107/s1744309106038656. PubMed PMID: 17077479; PMCID: PMC2225221.
32. Kurz M, Brachvogel V, Matter H, Stengelin S, Thuring H, Kramer W. Insights into the bile acid transportation system: the human ileal lipid-binding protein-cholyltaurine complex and its comparison with homologous structures. Proteins. 2003;50(2):312-28. Epub 2002/12/18. doi: 10.1002/prot.10289. PubMed PMID: 12486725.
33. Jakobsson E, Alvite G, Bergfors T, Esteves A, Kleywegt GJ. The crystal structure of Echinococcus granulosus fatty-acid-binding protein 1. Biochimica et biophysica acta. 2003;1649(1):40-50. Epub 2003/06/24. PubMed PMID: 12818189.
34. Banaszak L, Winter N, Xu Z, Bernlohr DA, Cowan S, Jones TA. Lipid-binding proteins: a family of fatty acid and retinoid transport proteins. Advances in protein chemistry. 1994;45:89-151. Epub 1994/01/01. PubMed PMID: 8154375.
35. Richieri GV, Ogata RT, Kleinfeld AM. Fatty acid interactions with native and mutant fatty acid binding proteins. Molecular and cellular biochemistry. 1999;192(1-2):77-85. Epub 1999/05/20. PubMed PMID: 10331661.
36. Hirose M, Sugiyama S, Ishida H, Niiyama M, Matsuoka D, Hara T, Mizohata E, Murakami S, Inoue T, Matsuoka S, Murata M. Structure of the human-heart fatty-acid-binding protein 3 in complex with the fluorescent probe 1-anilinonaphthalene-8-sulphonic acid. Journal of synchrotron radiation. 2013;20(Pt 6):923-8. Epub 2013/10/15. doi: 10.1107/s0909049513021298. PubMed PMID: 24121341; PMCID: PMC3795557.

37. Richieri GV, Ogata RT, Zimmerman AW, Veerkamp JH, Kleinfeld AM. Fatty acid binding proteins from different tissues show distinct patterns of fatty acid interactions. Biochemistry. 2000;39(24):7197-204. Epub 2000/06/14. PubMed PMID: 10852718.
38. Patil R, Mohanty B, Liu B, Chandrashekaran IR, Headey SJ, Williams ML, Clements CS, Ilyichova O, Doak BC, Genissel P, Weaver RJ, Vuillard L, Halls ML, Porter CJH, Scanlon MJ. A ligand-induced structural change in fatty acid-binding protein 1 is associated with potentiation of peroxisome proliferator-activated receptor alpha agonists. J Biol Chem. 2019;294(10):3720-34. Epub 2019/01/02. doi: 10.1074/jbc.RA118.006848. PubMed PMID: 30598509; PMCID: PMC6416440.
39. Han S, Schroeder EA, Silva-Garcia CG, Hebestreit K, Mair WB, Brunet A. Mono-unsaturated fatty acids link H3K4me3 modifiers to C. elegans lifespan. Nature. 2017;544(7649):185-90. Epub 2017/04/06. doi: 10.1038/nature21686. PubMed PMID: 28379943; PMCID: PMC5391274.
40. Tardif N, Salles J, Landrier JF, Mothe-Satney I, Guillet C, Boue-Vaysse C, Combaret L, Giraudet C, Patrac V, Bertrand-Michel J, Migne C, Chardigny JM, Boirie Y, Walrand S. Oleate-enriched diet improves insulin sensitivity and restores muscle protein synthesis in old rats. Clinical nutrition (Edinburgh, Scotland). 2011;30(6):799-806. Epub 2011/06/28. doi: 10.1016/j.clnu.2011.05.009. PubMed PMID: 21700370.
41. Palomer X, Pizarro-Delgado J, Barroso E, Vazquez-Carrera M. Palmitic and Oleic Acid: The Yin and Yang of Fatty Acids in Type 2 Diabetes Mellitus. Trends in endocrinology and metabolism: TEM. 2018;29(3):178-90. Epub 2018/01/02. doi: 10.1016/j.tem.2017.11.009. PubMed PMID: 29290500.
42. Lim JH, Gerhart-Hines Z, Dominy JE, Lee Y, Kim S, Tabata M, Xiang YK, Puigserver P. Oleic acid stimulates complete oxidation of fatty acids through protein kinase A-dependent activation of SIRT1-PGC1alpha complex. J Biol Chem. 2013;288(10):7117-26. Epub 2013/01/19. doi: 10.1074/jbc.M112.415729. PubMed PMID: 23329830; PMCID: PMC3591621.
43. Vander Kooi CW. Megaprimer method for mutagenesis of DNA. Methods in enzymology. 2013;529:259-69. Epub 2013/09/10. doi: 10.1016/b978-0-12-418687-3.00021-5. PubMed PMID: 24011052.
44. Otwinowski Z, Minor W. [20] Processing of X-ray diffraction data collected in oscillation mode. Methods in enzymology. 1997;276:307-26. Epub 1997/01/01. doi: 10.1016/s0076-6879(97)76066-x. PubMed PMID: 27799103.
45. Adams PD, Afonine PV, Bunkoczi G, Chen VB, Davis IW, Echols N, Headd JJ, Hung LW, Kapral GJ, Grosse-Kunstleve RW, McCoy AJ, Moriarty NW, Oeffner R, Read RJ, Richardson DC, Richardson JS, Terwilliger TC, Zwart PH. PHENIX: a comprehensive Python-based system for macromolecular structure solution. Acta Crystallogr D Biol Crystallogr. 2010;66(Pt 2):213-21. Epub 2010/02/04. doi: 10.1107/s0907444909052925. PubMed PMID: 20124702; PMCID: PMC2815670.
46. Emsley P, Lohkamp B, Scott WG, Cowtan K. Features and development of Coot. Acta Crystallogr D Biol Crystallogr. 2010;66(Pt 4):486-501. Epub 2010/04/13. doi: 10.1107/s0907444910007493. PubMed PMID: 20383002; PMCID: PMC2852313.
47. Bligh EG, Dyer WJ. A rapid method of total lipid extraction and purification. Can J Biochem Physiol. 1959;37(8):911-7. Epub 1959/08/01. PubMed PMID: 13671378.
48. Tripathy C, Zeng J, Zhou P, Donald BR. Protein loop closure using orientational restraints from NMR data. Proteins. 2012;80(2):433-53. Epub 2011/12/14. doi: 10.1002/prot.23207. PubMed PMID: 22161780; PMCID: PMC3305838.

49. Kane CD, Bernlohr DA. A simple assay for intracellular lipid-binding proteins using displacement of 1-anilinonaphthalene 8-sulfonic acid. Anal Biochem. 1996;233(2):197-204. Epub 1996/01/15. doi: 10.1006/abio.1996.0028. PubMed PMID: 8789718.

Acknowledgements: MCT was funded by the T32 GM008602 NIH Pharmacology Training Grant. EAO was supported by R01DK115213 and the W. M. Keck Foundation. MCW was supported by R01AG045183, R01AT009050, DP1DK113644 and the HHMI. Crystallographic data were collected at Southeast Regional Collaborative Access Team (SER-CAT) 22-ID beamline at the Advanced Photon Source, Argonne National Laboratory, and was supported by the United States Department of Energy, Office of Science, Office of Basic Energy Sciences, under contract W-31–109-Eng-38. This study was supported in part by the Emory Integrated Lipidomics Core (EILC), which is subsidized by the Emory University School of Medicine and is one of the Emory Integrated Core Facilities. Additional support was provided by the Georgia Clinical & Translational Science Alliance of the National Institutes of Health under Award Number UL1TR002378. The content is solely the responsibility of the authors and does not necessarily reflect the official views of the National Institutes of Health.

Competing interest: The authors declare no competing interests.

CHAPTER 3: ALLOSTERIC REGULATION OF THIOESTERASE SUPERFAMILY MEMBER 1 BY FREE FATTY ACIDS AND LYSOPHOSPHATIDYLCHOLINE

Matthew C. Tillman[1], Norihiro Imai[2], Yue Li[3], Manoj Khadka[4], C. Denise Okafor[1], Puneet Juneja[5], Akshitha Adhiyaman[1], Susan J. Hagen[3], David E. Cohen[2], Eric A. Ortlund[1]*

[1]Department of Biochemistry, Emory University School of Medicine, 1510 Clifton Road, Atlanta, GA 30322. [2]Joan & Sanford I. Weill Department of Medicine, Weill Cornell Medical College, New York, NY. [3]Department of Surgery, Beth Israel Deaconess Medical Center, 330 Brookline Avenue, Boston, MA 02215. [4]Emory Integrated Lipidomics Core, Emory University, Atlanta, GA. [5] Robert P Apkarain Integrated Emory Integrated Electron Microscopy Core, Emory University, Atlanta, GA.

This manuscript describes the multifunctional role of the StarD of Them1 (StarD14). We show the StarD binds to fatty acids and lysophosphatidylcholine, which allosterically regulate Them1 activity. We further show that 18:1 lysophosphatidylcholine inhibits Them1 activity in live brown adipocytes. Additionally, we show the StarD localizes Them1 near the lipid droplet. Collectively, this work shows the StarD of Them1 serves as a lipid sensor to fine tune Them1 activity. This work is currently under review for publication.

M.C.T. performed affinity purification-MS, ligand binding assays, X-ray crystallography, thioesterase assays, negative stain electron microscopy, DSF assays, and wrote the paper; N.I. did Seahorse experiments; Y.L. performed cellular localization studies; M.K. assisted with affinity purification-MS and data analysis; C.D.O. performed MD simulations; P.J. did negative stain electron microscopy; A.A. assisted with thioesterase assays; S.J.H. assisted with experimental design; D.E.C. assisted with experimental design and edited the paper; E.A.O. mentored M.C.T., assisted with experimental design and data analysis, and edited the paper. All authors reviewed and edited the final manuscript.

Abstract

Non-shivering thermogenesis occurs in brown adipose tissue to generate heat in response to cold temperatures. Thioesterase superfamily member 1 (Them1) is transcriptionally upregulated in brown adipose tissue upon cold exposure and suppresses thermogenesis to conserve energy reserves. Them1 hydrolyzes long-chain fatty acyl-CoAs, preventing their use as fuel for thermogenesis. Them1 contains a C-terminal StAR-related lipid transfer domain (StarD) with unknown ligand or function. By complementary biophysical approaches, we show that StarD binds to long-chain fatty acids, products of Them1's enzymatic reaction, as well as lysophosphatidylcholine (LPC), which activate thermogenesis in brown adipocytes. Certain fatty acids stabilize the StarD and allosterically enhance Them1 catalysis of acyl-CoA, whereas 18:1 LPC destabilizes and inhibits activity, which we verify in cell culture. Additionally, we demonstrate that the StarD functions to localize Them1 near lipid droplets. These findings define the role of the StarD as a lipid sensor that allosterically regulates Them1 activity and localization.

Introduction

Brown adipose tissue (BAT) mediates non-shivering thermogenesis in both mice [1] and humans [1, 2]. A key function of non-shivering thermogenesis is to maintain core body temperature upon exposure to cold ambient temperatures. Because high rates of caloric consumption are required to generate heat, pharmacologic approaches to increasing BAT mass and activity are viewed as promising objectives in the management of obesity and related metabolic disorders [3].

In addition to activating thermogenesis in BAT, cold ambient temperatures lead to the transcriptional upregulation of genes that regulate energy expenditure including Thioesterase superfamily member 1 (synonyms brown fat inducible thioesterase (BFIT), steroidogenic acute regulatory lipid transfer-related domain 14 (StarD14) and acyl-Coa thioesterase 11 (Acot11)) [4, 5]. Expression is induced upon cold exposure, and this was originally believed to contribute to the thermogenic output of BAT [5]. However, rather than promoting energy use, Them1 proved to suppresses thermogenesis, thereby reducing the energy output of mice [6]. Mechanistically, Them1 hydrolyzes long-chain fatty acyl-CoAs that are derived from endogenous lipid droplets within brown adipocytes, preventing their use as fuel for thermogenesis [7, 8]. The genetic ablation of Them1 enhances the thermogeneic output of mice and protects against diet-induced obesity and metabolic disorders [6].

Them1 comprises two N-terminal thioesterase domains that hydrolyze acyl-CoA and a C-terminal StarD. The Them1 StarD is a member of the larger StarD family which is characterized by a highly conserved ~210 amino acid sequence found in both plant and animal proteins [9, 10]. Lipid ligands and functional roles have been proposed for several of the StarDs. For instance, cholesterol, 25-hydroxycholesterol, testosterone, phosphatidylcholine, phosphatidylethanolamine and ceramides bind to STARD1/STARD3/STARD4/STARD5 [11, 12], STARD5 [13], STARD6 [14],

STARD2/STARD7/STARD10 [15-17], STARD10 [17] and STARD11 [18], respectively. StarD1 and StarD3 bind and transport cholesterol to the mitochondria for steroidogenesis [11, 19, 20]. StarD2, StarD7, and StarD10 bind phosphatidylcholine and influence membrane lipid compositions [11, 16, 17, 21]. In the case of Them1, it is not known whether the StarD binds to lipid or whether lipid recognition plays a role in regulating thermogenesis.

We have shown that the Them1 StarD is necessary for full catalytic activity of the acyl-CoA thioesterase domains in the hydrolysis of long-chain fatty acyl-CoAs; purified recombinant acyl-CoA thioesterase domains alone exhibited significantly attenuated catalytic activity, and this was restored upon the addition of purified recombinant StarD [7]. This phenomenon is not restricted to Them1, evidenced by increased activity of the long-chain fatty acyl-CoA thioesterase, Them2, in the presence of StarD2 [16, 22, 23]. This study examines the effect of the StarD in brown adipocytes and explores the mechanism by which the StarD regulates acyl-CoA thioesterase (Acot) activity. We identify long-chain fatty acids and lysophosphatidylcholines (LPCs) as ligands for the Them1 StarD. Certain fatty acids allosterically enhance, whereas 18:1 LPC inhibits Them1 activity in a StarD-dependent manner. We further verify that 18:1 LPC relieves suppression of fatty acid oxidation by Them1 in brown adipocytes in an immortalized brown adipose cell line, in keeping with allosteric inhibition of Them1. Additionally, we discover the StarD is necessary for localizing Them1 to the lipid droplet.

Results

Them1 StarD binds long-chain fatty acids

To identify possible ligands for the Them1 StarD, we used affinity purification coupled with mass spectrometry following exposure of recombinantly expressed 6xHis tagged Them1 StarD to mixed-lipid liposomes (Fig. 1A). Because fatty acids are generated as a product of Them1's enzymatic reaction, we reasoned that these products may bind to the StarD to facilitate product release. Our initial strategy therefore involved a targeted quantitative free fatty acid assay [24]. This identified 15 fatty acid species that copurified with the Them1 StarD (Fig. 1B). Seven of the identified fatty acids were significantly enriched within the StarD samples over our negative control (maltose-binding protein (MBP)), namely, palmitoleic acid (16:1), oleic acid (18:1), linoleic acid (18:2), palmitic acid (16:0), arachidonic acid (20:4), eicosatrienoic acid (20:3), and heptadecenoic acid (17:1) (Fig. 1B). The StarD showed a preference for unsaturated fatty acids with a tail length from 16 to 20 carbons, but also bound to saturated fatty acids, such as palmitic acid (16:0), and to a lesser degree myristic acid.

To determine the fatty acid binding affinity, we attempted to use traditional fatty acid binding assays that rely on competitive displacement of a fluorescent probe such as 1-anilinonaphthalene-8-sulfonic acid (1,8-ANS) [25, 26]; however, the StarD did not bind to any of the probes tested. Therefore, we developed a fatty acid binding assay using microscale thermophoresis, which detects alterations in fluorescence along a temperature gradient induced by ligand binding to fluorophore-labeled protein [27, 28]. We tested the top three fatty acids that copurified most abundantly with the StarD from lipid extracts, namely, palmitoleic acid (16:1), palmitic acid (16:0), and oleic acid (18:1). In contrast to expectations, only palmitic acid generated a binding curve (Fig. 1C). Since palmitic acid is a saturated fatty acid, we also tested

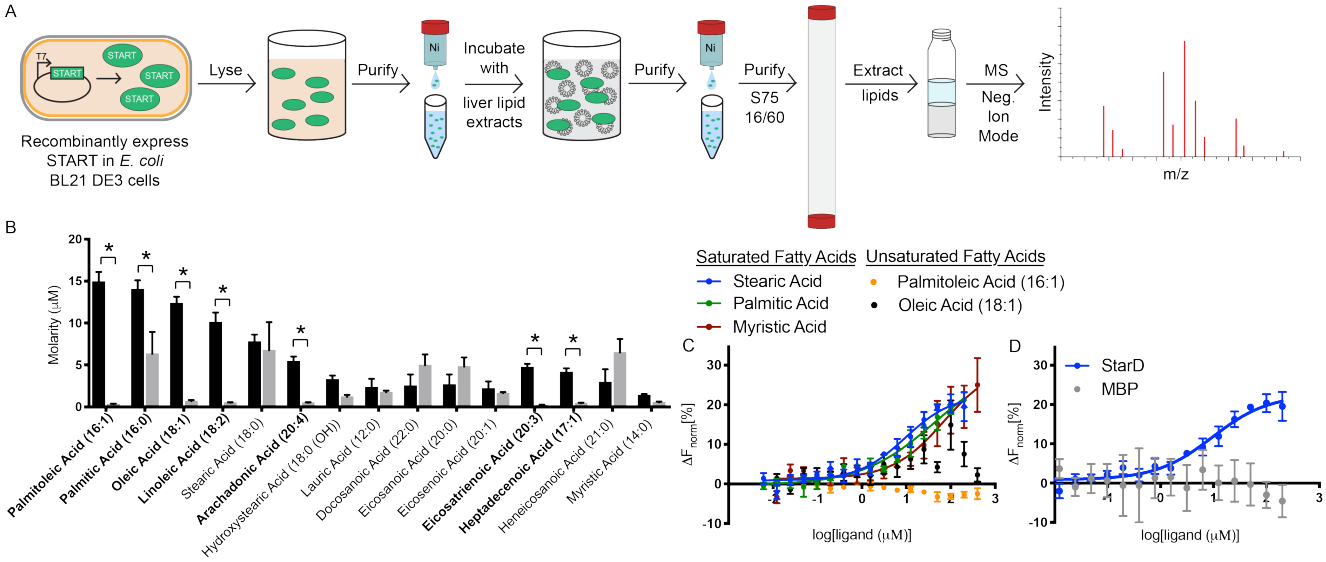

Figure 1. StarD of Them1 binds to long-chain fatty acids. *A.* Schematic of affinity purification mass spectrometry protocol. *B.* Concentration of 15 identified fatty acids bound to 1 milligram of Them1 StarD (black) or maltose-binding protein (MBP, gray) as determined by negative ion mode mass spectrometry through normalization to deuterated fatty acid standard. Bars indicate average of three technical replicates. Error bars display standard error of mean. Statistical analyses were conducted using 2-way ANOVA with Sidak's multiple comparisons test. *P<0.01. *C-D.* Fatty acid binding assay using microscale thermophoresis (MST). *C.* Them1 StarD labeled with Monolith RED-tris-NTA was kept constant at 50 nM, while the concentration of stearic acid (blue), palmitic acid (green), myristic acid (red), oleic acid (black), and palmitoleic acid (orange) were varied between 6.1 nM – 400 μM. Following an overnight incubation at 4 °C, StarD-FA solutions were loaded in standard Monolith NT.115 Capillaries (NanoTemper Technologies) and measured using a Monolith NT.115 instrument (NanoTemper Technologies). An MST-on time of 5 s was used for analysis, and baseline corrected normalized fluorescence values (ΔF_{norm}[%]) were plotted against fatty acid concentration. Curves were fit with a nonlinear regression model and Kd's are reported in Table 1 (n = 3 independent

measurements, error bars represent the standard error of the mean). *D.* MST binding assay via titration of stearic acid (6.1 – 200 μM) into Monolith RED-tris-NTA labeled Them1 StarD (blue) or MBP (gray) held constant at 50 nM. Procedure and analysis were conducted the same as described previously.

Table 1. Affinity of fatty acids for Them1 START domain determined by MST.

Saturated Fatty Acids	
Myristic Acid (14:0)	70.8 μM
Palmitic Acid (16:0)	45.9 μM
Stearic Acid (18:0)	9.5 μM
Unsaturated Fatty Acids	
Palmitoleic Acid (16:1)	N.A.
Oleic Acid (18:1)	N.A.

N.A.: Not Applicable

myristic acid (14:0) and stearic acid (18:0); two saturated fatty acids that also copurified with the StarD in our MS analysis. Both generated binding curves (Fig. 1C). Binding for fatty acid species occurred in the μM range (Table 1). To ensure these alterations in thermophoresis were not due to micelle formation at high fatty acid concentrations, we titrated stearic acid (critical micellar concentration ≈ 300 μM [29]) which is most prone to form micelles, into fluorescently labeled MBP and observed no changes in thermophoresis (Fig. 1D). These results suggest specific binding of saturated long-chain fatty acid to the Them1 StarD.

There were some discrepancies in the fatty acids identified to bind to the StarD by affinity purification-MS and by microscale thermophoresis techniques (Figs. 1C, D). This may be explained by differences in presentation of lipids to the StarD depending on the technique: the StarD was exposed to mixed lipid liposomes in our affinity purification-MS experiment whereas a single fatty acid was titrated into the StarD in the microscale thermophoresis experiment. Since unsaturated fatty acids copurified with the StarD and were detected by MS but did not bind in the microscale thermophoresis experiment, Them1 may have only accessed unsaturated fatty acids in the context of a membrane bilayer. Alternatively, unsaturated fatty acid binding may require the presence of other lipids to serve as intermediate ligands prior to lipid exchange.

Fatty acids bind within the hydrophobic pocket of Them1's StarD.

To visualize the StarD-fatty acid complex, we attempted to generate crystals in the presence of a range of fatty acids; however, only incubation with myristic acid yielded crystals that diffracted. The myristic acid–StarD structure was solved in the P 1 2_1 1 space group to a resolution of 3.09 Å, with the asymmetric unit containing four StarD monomers (Fig. 2A). Refinement and model statistics are summarized in Table 2.

One monomer contained continuous electron density within the interior of the domain that fit myristic acid (Fig. 2B). A polder map displayed clear density at a sigma level of 3.0, strongly supporting the presence of myristic acid binding at this location (Fig. 2C) [30]. The other three monomers did not contain this continuous electron density; therefore, we suspect either no FA was bound, or that FA was bound with low occupancy or high conformational mobility. In this connection, myristic acid exhibited a higher B factor than the average B factor for the protein, suggesting the ligand had some mobility in the pocket (Table 2). Because we crystallized two different states of the StarD (with and without myristic acid) in one crystal, we compared the structures of these two states using ProSMART analysis [31]. The root mean squared deviation (RMSD) between the apo monomers and the myristic acid bound monomer were mapped onto the structure of the StarD complexed with fatty acid, (one comparison in Fig. 2D; other comparisons in Supplemental Fig. 1A). There were no major conformational differences between the structures suggesting fatty acid does not induce an appreciable conformational change, albeit our data do not discern whether the apo domains are truly devoid of fatty acid. Furthermore, the positioning of the residues surrounding the fatty acid in the holo-monomer were unchanged in all other monomers. There were some dissimilarities in the N-terminal α-helix, but these changes are likely an artifact of crystal packing.

We next compared our structure with a structure of the Them1 StarD that was solved at higher resolution and in a different space group [32]. Our structure exhibits the same overall conformation with an average RMSD of 0.4 Å over aligned atoms [32]. The prior structure contained long, tubular electron density in the same location where we modeled a myristic acid. A buffer component (PEG molecule) was modeled into this density because no ligand was

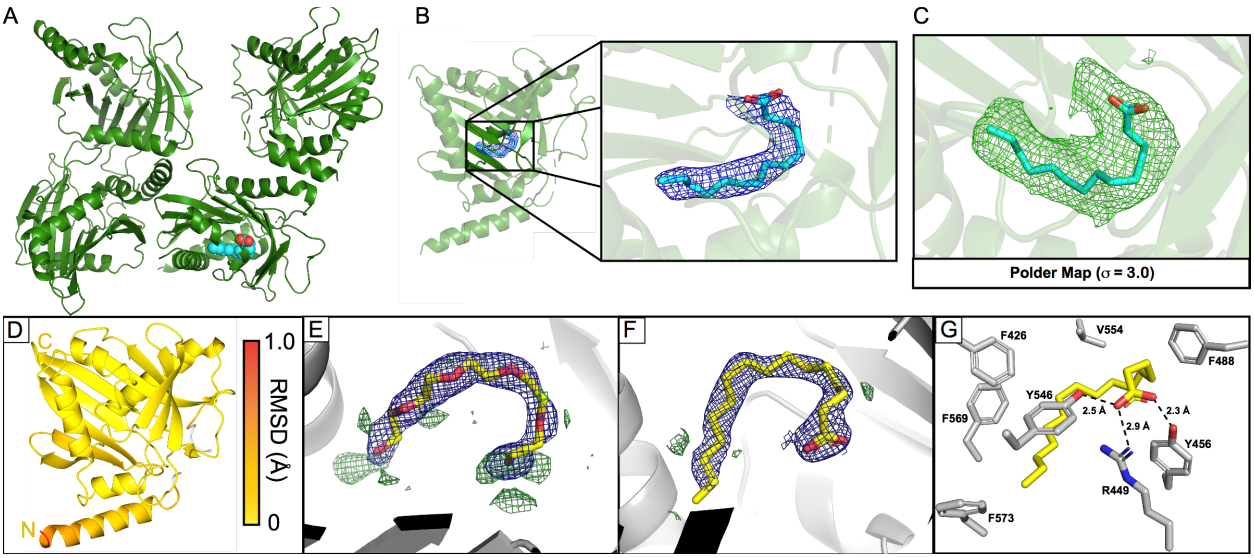

Figure 2. Fatty acids fit within crystal structure of Them1 StarD. *A.* Asymmetric unit cell of 3.09 Å structure of Them1 StarD contains 4 monomers (green), with one monomer bound to myristic acid (cyan). *B.* Zoomed in view of the lipid binding pocket of StarD where myristic acid (cyan) is modeled into $2F_o$-F_c map (blue mesh) contoured to σ = 1.0. *C.* Polder map (F_o-F_c map with bulk solvent removed, green) contoured to σ = 3.0 of region surrounding fatty acid. Myristic acid (cyan) fits nicely within this density. *D.* ProSMART analysis conducted to determine r.m.s.d. between Cα backbone of myristic acid bound StarD and apo-StarD monomers. Root mean square deviations (range: 0–1.0 Å) between monomers were mapped onto myristic acid bound StarD structure with a color scale depicting low (yellow) to high (red) deviations. Unaligned regions are colored in white. *E.* PEG molecule (yellow) modeled into electron density of previous Them1 StarD crystal structure (PDB code: 3FO5). *F.* Palmitic acid (16:0) (yellow) modeled into refined density from previous structure of StarD. All $2F_o$-F_c maps displayed in blue and contoured to σ = 1.0. All F_o-F_c maps displayed in green and contoured to σ = 2.0. *G.* Amino acids in close proximity surrounding palmitic acid. Distance between polar amino acids and carboxyl head group of fatty acid displayed as black dashed line.

Table 2. Myristic Acid—Them1 START domain X-ray data collection and refinement statistics.

Data collection	Myristic Acid—START
Space group	P 1 2_1 1
Cell dimensions	
a, *b*, *c* (Å)	65.08, 70.98, 127.22
α,β, γ (°)	90, 96.13, 90
Resolution (Å)	42.17 – 3.09 (3.20 – 3.09)
$CC_{1/2}$	0.647
R_{pim}	0.121 (0.71)
$I / \sigma I$	11.3 (1.4)
Completeness (%)	98.97 (96.86)
Redundancy	5.8 (5.3)
Refinement	
Resolution (Å)	3.09
Unique reflections	21201 (2040)
R_{work} / R_{free} (%)	21.76/27.72 (29.53/35.95)
No. non-hydrogen atoms	7515
Protein	7490
Ligands	16
Water	9
B-factors	88.73
Protein	88.73
Ligand	101.73
Water	60.46
Clashscore	5.72
R.m.s. deviations	
Bond lengths (Å)	0.004
Bond angles (°)	0.67
Ramachandran favored (%)	95.45
Ramachandran allowed (%)	4.32
Ramachandran outliers (%)	0.22
PDB accession code	6VVQ

Values in parenthesis indicate highest resolution shell

identified in the crystal structure (Fig. 2E) [32]. We observed branched electron density characteristic of a fatty acid carboxyl-head group; therefore, we modeled palmitic acid, a highly abundant *E. coli* fatty acid that copurifies with the StarD, into this density (Fig. 2F) [33]. Palmitic acid fit well within the density, providing strong support for placement of this fortuitously co-purified ligand. The palmitic acid carboxyl head group is contacted by polar residues arginine 449, tyrosine 456, and tyrosine 546 (Fig. 2G). The curved fatty acyl chain is enclosed by bulky, nonpolar amino acids, including phenylalanine 426, phenylalanine 488, valine 554, phenylalanine 569, and phenylalanine 573, which fully protect it from solvent (Fig. 2G).

To explain Them1's unexpected preference for fatty acids, which are smaller-sized lipids than typically bind StarDs, we analyzed the lipid binding pockets of all StarDs of known structure. These share a long, continuous C-terminal α-helix that packs across the mouth of a U-shaped incomplete β-barrel, forming the empty interior (Supplemental Fig. 1C). The conformation of this helix is radically different in Them1, whereby a kink, enabled by a highly conserved glycine 564 and a steric clash from α-helix α_0 (connecting thioesterase domain and the StarD), constricts the lipid-binding pocket [32]. Supplemental Table 1 displays the surface area ($Å^2$) and volume ($Å^3$) of each lipid binding pocket, which are also shown graphically (Supplemental Fig. 1B). Them1 possesses a smaller interior cavity than STARD2 and STARD11, which bind to phosphatidylcholine (PC) and ceramide respectively. All other StarD proteins contain an interior pocket with similar area and volume, though a different shape, when compared with Them1 StarD. These other StarD proteins have resisted efforts at co-crystallization with their cholesterol and sterol-like ligands [32, 34, 35]. Thus, the calculated size of the pocket size may not accurately reflect the ligand-bound state.

We superposed Them1 StarD with STARD2 bound to palmitoyl-linoleoyl phosphatidylcholine (PDB code: 1LN3) [36] and STARD11 bound to C16-ceramide (PDB code: 2E3P) [36, 37]. In both instances, the interior cavity of the Them1 StarD was unable to accommodate the same ligands (Supplemental Fig. 1D). Them1 StarD contains some equivalent structural features that enable StarD2 and StarD11 to bind to their respective ligands, such as arginine 449 (StarD2 R78, StarD11 R442), which electrostatically interacts with the phosphate of phospholipids in StarD2 [36] and a water mediated hydrogen bond with a ceramide hydroxyl in StarD11 [36, 37]. Additionally, these StarDs contain an acidic residue (Them1 D453, StarD2 D82, StarD11 E446) that participates in a salt bridge with the conserved arginine and engages in hydrogen bonding with the amide-nitrogen and hydroxyl of ceramide in StarD11 [37]. However, Them1 lacks the aromatic cage found in STARD2 that consists of tryptophan 101, tyrosine 114, and tyrosine 155, which together engage in cation-π interactions with the quaternary amine of choline [36]. Them1 only contains one structurally analogous aromatic residue (F488), though it also contains tyrosine 456 that could rotate and potentially occupy the same space as tryptophan 101 in STARD2 (Supplemental Fig. 1E). Additionally, Them1 does not conserve residues found in StarD11 (Y482, Q467, and N504) that participate in hydrogen bonding with ceramide [37]. Them1 lacks some necessary residues for recognition of the larger lipids present in StarD2 and StarD11, while coopting residues such as R449 and D453 to enable fatty acid binding.

Them1 StarD binds to lysophosphatidylcholine

To test whether long-chain fatty acids were the only ligands for the StarD of Them1, we repeated our affinity purification mass spectrometry experiment using a shotgun MS approach that examined all major phospholipid classes. Several lysophosphatidylcholine (LPC) species

including 18:2, 18:1, 20:4, 20:3, and 22:4 were highly enriched in our StarD samples, but absent in our negative control samples (Fig. 3A-C). LPC contains a single fatty acyl chain typically esterified at the *sn-1* position rather than the two fatty acyl chains present in phospholipids (Fig. 3D). The headgroup of LPC is considerably larger than the carboxyl head of a fatty acid; therefore, the StarD must conformationally change to expand the interior pocket to accommodate this larger lipid. Them1 StarD samples were not enriched for any phosphatidylethanolamine (PE), phosphatidylserine (PS), or phosphatidylinositol (PI) species. Some sphingomyelin (SM) and phosphatidylcholine (PC) species were enriched in the StarD samples at low levels.

It is an important signaling molecule that is implicated in the pathogenesis of cardiovascular disease, atherosclerosis, diabetes, and neurodegenerative diseases [38]. LPC also functions in lipid droplet formation because it is a precursor, along with fatty acyl-CoAs, for phosphatidylcholine molecules that are required to expand the membrane monolayer that coats lipid droplet membranes [39]. Upon stimulation of thermogenesis, levels of saturated LPC in brown adipocytes levels dramatically increase in brown adipocytes, which interestingly enhances thermogenesis [40].

Fatty acids enhance while 18:1 LPC inhibits Them1 acyl-CoA thioesterase activity

Since the StarD was previously shown to alter the enzymatic activity of Them1 [7], we reasoned fatty acids and LPC species may regulate Acot activity through interaction with the StarD. To test this, we monitored myristoyl-CoA hydrolysis in the presence of fatty acid or 18:1 LPC. Incubation with either 25 μM myristic acid or palmitic acid enhanced the maximum enzymatic velocity of ΔNterm-Them1 lacking the intrinsically disordered N-terminus (Fig. 4A,

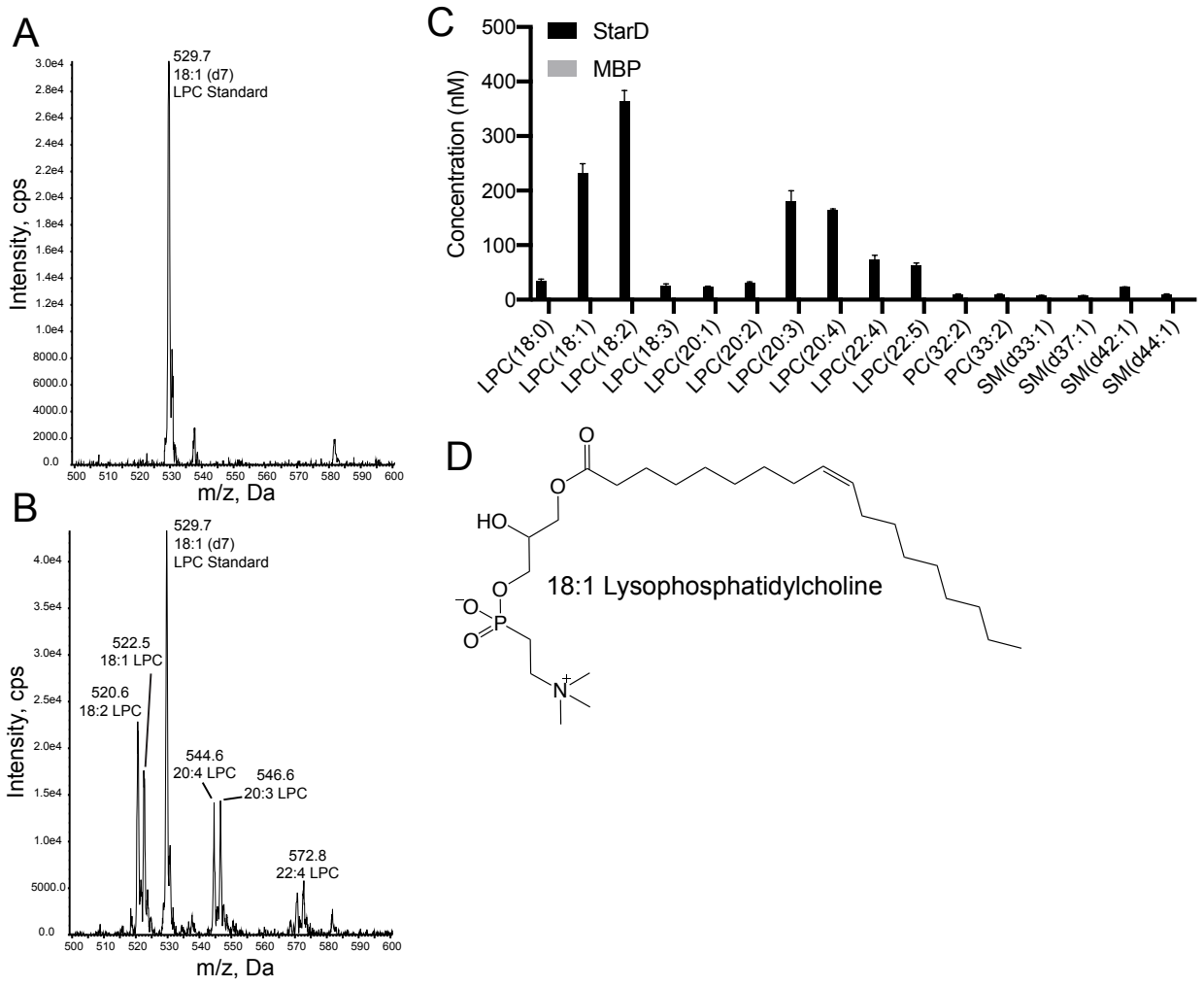

Figure 3. Them1 StarD domain binds to lysophosphatidylcholine. *A-B.* Mass spectra (precursor ion scan of *m/*z 184) of lipids containing a phosphatidylcholine head group that copurified with MBP *(A)* and Them1 StarD *(B)*. Lysophosphatidylcholine 18:1 (d7) standard was added to each sample for quantification of lipid concentrations. *C.* Graphical analysis of identified lysophosphotidylcholine species. Bars are an average of three technical replicates. Lysophosphotidylcholine species were not detected in MBP samples. *D.* Chemical structure of 18:1 lysophosphotidylcholine.

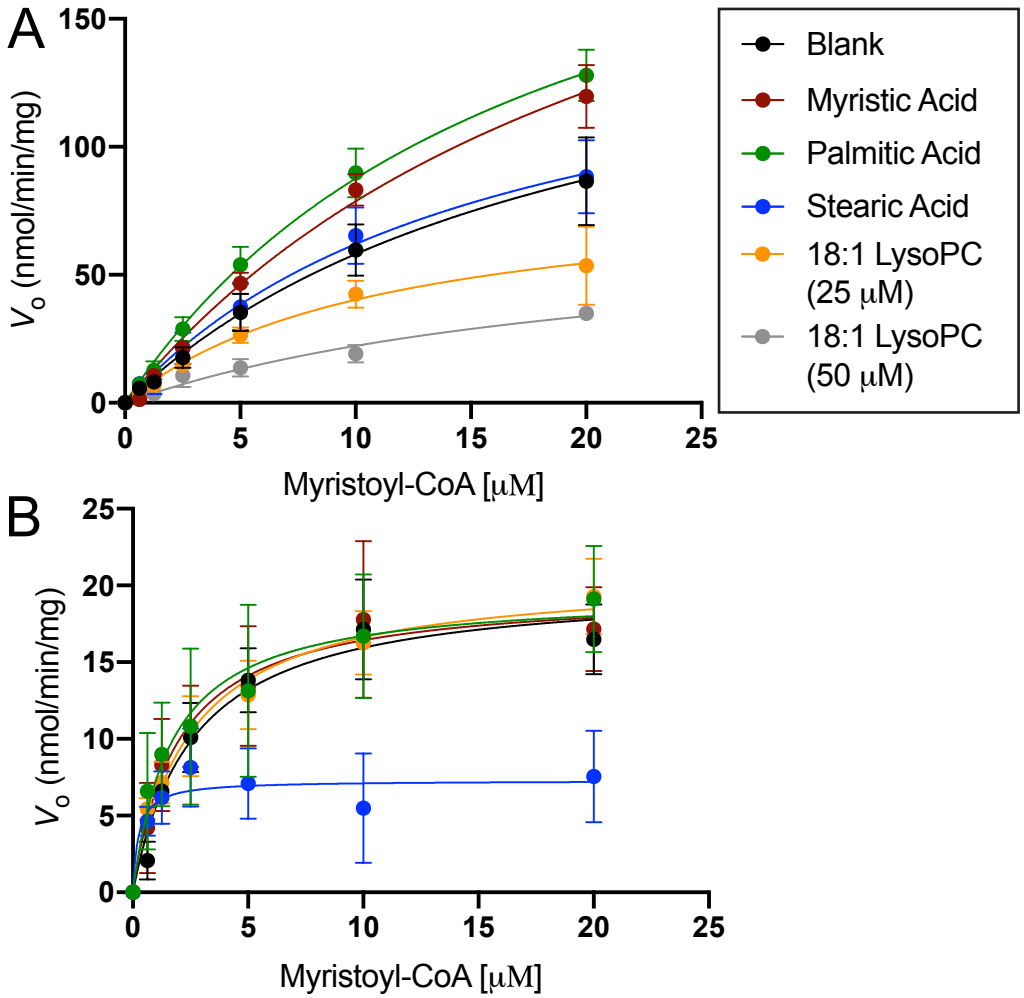

Figure 4. Fatty acids enhance while lysophosphatidylcholine inhibits Them1 activity in a StarD-dependent manner. ΔNterm-Them1 *(A)* and Δ Nterm-Them1_ΔStarD *(B)* (1 μM) were incubated with buffer (black) or 25 μM stearic acid (blue), palmitic acid (green), myristic acid (red), 18:1 lysophosphatidylcholine (orange), and 50 μM 18:1 lysophosphatidylcholine (gray) for 30 minutes at 37 °C prior to the addition of myristoyl-CoA. Saturation curves of V_0 plotted against increasing myrstoyl-CoA with solid lines indicating nonlinear analysis of the data. Each point corresponds to the average of a minimum of three replicates. Error bars represent standard error of the mean.

red and green). This enhancement in activity is dependent upon the StarD (Fig. 4B). Incubation with stearic acid did not alter the activity of ΔNterm-Them1; however, stearic acid suppressed enzymatic activity of Them1 when the StarD was absent, indicating the StarD relieves the inhibitory effects of stearic acid (Fig. 4A-B, blue).

Surprisingly, incubation with 25 μM 18:1 LPC greatly inhibited ΔNterm-Them1 activity (Fig. 4A, orange) in a StarD dependent manner (Fig. 4B). To determine whether this inhibition was dose dependent, we incubated ΔNterm-Them1 with twice the concentration of 18:1 LPC (50 μM) and observed greater inhibition (Fig. 4A, gray).

Them1 forms homotrimer containing a thioesterase domain core flanked by mobile StarDs

To understand how the StarD interacts with the thioesterase domains to influence catalytic activity we generated a model of full-length Them1 by joining the StarD structure with a homology model of the Them1 thioesterase domains created using the SWISS MODEL server [41-45] based on the structure of the ACOT12 (StarD15) thioesterase domains (56 % sequence identity and 69 % sequence similarity) [46]. Both structures contained a common α-helix that resides at the C-terminus of the thioesterase domains model and N-terminus of the StarD structure. We aligned this overlapping α-helix to generate a full-length model of Them1 with similarities to a previously reported model of intact ACOT12 (Fig. 5A) [46].

We used single particle negative stain electron microscopy to obtain a low-resolution map of Them1 to fit our structural model. ΔNterm-Them1 was purified as a stable trimer as determined by size exclusion chromatography and analytical ultracentrifugation (Supplemental Fig. 2A-B). Negative stain electron microscopy revealed a homogenous distribution of ΔNterm-

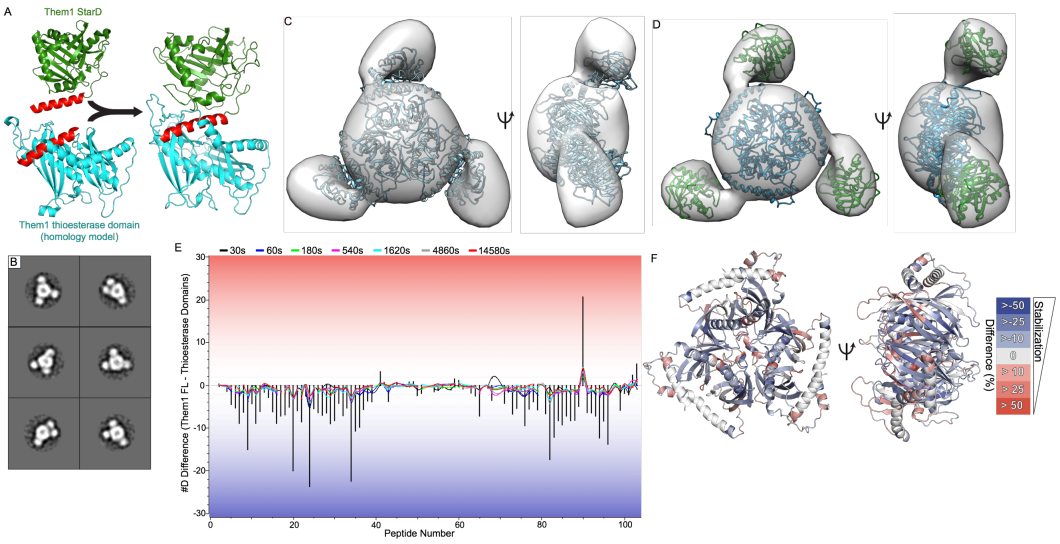

Figure 5. Them1 forms homotrimer with thioesterase domain core and flanking StarDs *A.* Generation of full-length Them1 model through structural alignment of linker helix (red) present in crystal structure of Them1 StarD (green) and homology model of Them1 thioesterase domains (blue). *B.* Subset of 2D class averages of Them1 using negative stain electron microscopy generated by Relion 3.0. *C.* 3D reconstruction of Them1 derived from subset of 2D class averages. Trimeric Them1 model fit into 3D reconstruction using Chimera. *D.* Separate StarDs (green) and thioesterase domains (blue) modeld into 3D reconstruction using Chimera. *E.* Butterfly plot overlayed with a residual plot displaying difference in deuterium uptake between ΔNterm-Them1 and ΔNterm-Them1_ΔStarD. Colored lines depict deuterium uptake difference (y-axis) for peptides (x-axis) at each time point (black: 30s, blue: 60s, green: 180s, pink: 540s, gray: 1620s, cyan: 4860s, red: 14580s). Bars display summed difference in deuterium uptake over all time points for each peptide. Negative values (blue) mean that removal of StarD increases the incorporation of deuterium for the cooresponding peptide. *F.* Percentage difference in deuterium uptake (Them1 – Them1_ΔStarD) at 60 seconds mapped onto homology model of Them1 thioesterase domains. Negative values (blue) indicate less deuterium exchange (greater protection) in intact Them1, indicating that StarD stabilizes the thioesterase domains.

Them1 trigonal particles with a diameter of 17 nm spread across the grid (Supplemental Fig. 2C). We generated 2D-classifications using Relion 3.0 [47] that revealed a trimeric complex consisting of a large spherical body flanked by three protruding lobes representing 3 fold symmetry (Fig. 5B, all class averages in Supplemental Fig. 2D). A 3D initial model was generated and refined using particles from selected class averages that revealed the trimeric complex (Fig. 5C). The central density of the 3D reconstruction accommodates the core heterotrimeric thioesterase domains; however, fitting the StarD within the peripheral density required relaxing the linker geometry of our model and independently fitting this domain (Fig. 5C-D).

The negative stain 2D class averages also revealed conformational flexibility between the StarD and thioesterase domains. The main central body of the map that accommodates the thioesterase domains is identical in all 2D class averages; however, the three exterior lobes that accommodate the StarDs are not perfectly arranged in a threefold symmetric frame in a few of the 2D class averages as seen in reprojections using C3 symmetry (Supplemental Fig. 2E). We postulate this flexibility is the result of a less ordered region lying between the domains (residues 365 – 383, *H. sapiens*), which was also disordered in our crystal structure of the StarD.

Them1 StarD stabilizes the thioesterase domains

To determine how the thioesterase and StarDs interact, we performed hydrogen-deuterium exchange MS (HDX-MS). This technique identifies regions of flexibility and rigidity by measuring the rate of exchange of deuterium with amide protons; high deuterium uptake signifies areas of flexibility and high solvent exposure, whereas low deuterium uptake signifies areas of rigidity and low solvent exposure [48]. Comparison of deuterium uptake of ΔNterm-

Them1 with ΔNterm-Them1-ΔStarD reveals a dramatic stabilizing effect driven by the StarD, as evidenced by a great reduction of deuterium incorporation throughout the thioesterase domains in the presence of the StarD (Fig. 5E-F). Heat maps showing identified peptides for each construct are provided in Supplemental Fig. 3. Although there is flexibility between the thioesterase and StarDs, the StarD significantly stabilizes the thioesterase domains.

Fatty acids stabilize while 18:1 LPC destabilizes StarD

Incubation with myristic acid, palmitic acid, or stearic acid did not alter the thermal melting temperature (T_m) of the StarD, as monitored by differential scanning fluorimetry (DSF); however, this is relative to StarD that copurifies with fatty acids from *E. coli* (Fig. 6A). Strikingly, 18:1 LPC destabilized the StarD by nearly 5 °C, which is in-line with the reduced catalytic activity driven by this ligand (Fig. 6A).

To determine how fatty acids enhanced Them1 activity, we performed 500 ns molecular dynamics simulations on Them1 comparing apo vs lipid-bound Them1. The presence of myristic acid substantially lowered the root mean squared fluctuations in the StarD and in some parts of the thioesterase domains, suggesting myristic acid generated a more stable complex than apo-Them1 (Fig. 6B-C). The C-terminal α-helix of the StarD, which plays a role in StarDs binding lipids [49, 50], was significantly stabilized by myristic acid (Fig. 6B-C). Next, we performed a community analysis, which identifies groups of residues that move in a coordinated manner throughout the simulation. Myristic acid significantly altered the communities within the StarD, changing their size and connectedness (Fig. 6D). In the apo state, multiple communities interface with the blue community of the thioesterase domains, but myristic acid shifts the communities so that only one is connected to the thioesterase domains (Fig. 6D). Although there are fewer

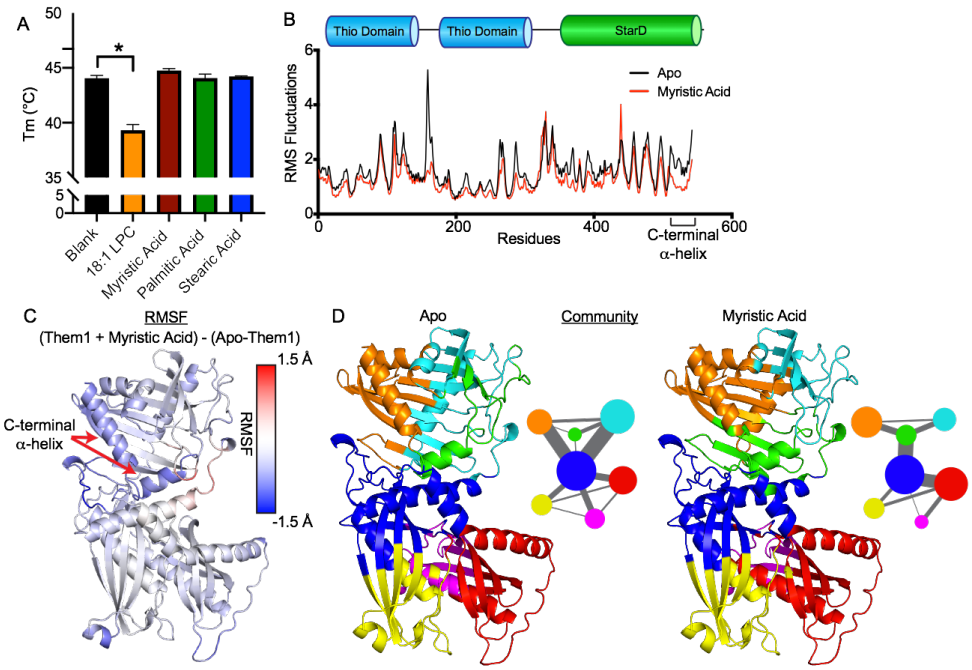

Figure 6. Fatty acids stabilize while 18:1 LPC destabilizes the StarD. *A.* Differential scanning fluorimetry of StarD incubated with either buffer (black), 18:1 LPC (orange), myristic acid (red), palmitic acid (green), and stearic acid (blue). LPC 18:1 significantly destabilizes the StarD. Bars depict average of three replicates. Error bars denote standard error of the mean. One-way ANOVA and Dunnett's multiple comparisons test were used to analyze StarD data. *B-D.* Molecular dynamics simulation for apo-Them1 and myristic acid bound Them1 over 500 ns. *B.* Root mean squared fluctuations (RMSFs) across Them1 residues for the apo (black) and myristic acid bound (red) states. *C.* Color coordinated difference in RMSFs between myristic acid bound and apo states (Them1-MYR – Them1-Apo) mapped onto full-length model of Them1. Myristic acid stabilizes the C-terminal α-helix; blue color corresponds to lower RMSFs in myrstic bound state than apo state. *D.* Community analysis that identifies residues that move in coordinated fashion thorughout the simulation. Circle size depicts number of residues within community and width of lines corresponds with strength of communication between communities. Myristic acid alters size and connectedness of communities.

connections between the communities in the myristic bound state, there are stronger connections linking the communities in the StarD (green) with communities within the thioesterase domains where acyl-CoA hydrolysis occurs (blue-red), potentially yielding a more active enzyme (Fig. 6D). Taken together, these data suggest fatty acids allosterically enhance Acot activity through stabilizing the StarD and altering dynamics within the thioesterase domains, while 18:1 LPC inhibits Acot activity through destabilizing the StarD.

18:1 LPC reverses Them1-mediated suppression of fatty acid oxidation

To test the effect of the StarD on Them1's capacity to suppress thermogenesis in live cells, we measured the oxygen consumption rate (OCR) of mouse-derived immortalized brown adipocytes (iBAs) that were transduced with EGFP alone, EGFP-tagged full-length Them1 (FL-Them1-EGFP), or a EGFP-tagged truncated variant containing only the N-terminal thioesterase domains (Them1_ΔStarD-EGFP) (Fig. 7A-B). We induced thermogenesis in the iBAs using norepinephrine (NE), which increased the OCR over basal levels (Fig 7B, green). As expected, Them1 suppressed NE-induced respiration (Fig. 7B, black). However, removal of the StarD did not reduce Them1-mediated suppression of OCR values, but slightly enhanced Them1 activity (Fig. 7B, red). The StarD in part attenuated Them1 activity, suggesting a role for feedback regulation by the StarD.

It was recently reported that LPC levels, specifically 16:0 and 18:0, were elevated in brown adipocytes upon induction of thermogenesis, and that 16:0 LPC enhanced UCP1 mediated respiration [40]. Since we identified that 18:1 LPC inhibits Them1 through the StarD (Fig. 6A-B), we hypothesized that 18:1 LPC regulates thermogenesis in brown adipocytes through interaction with Them1. To test this, we incubated iBAs transduced with FL-Them1-EGFP or

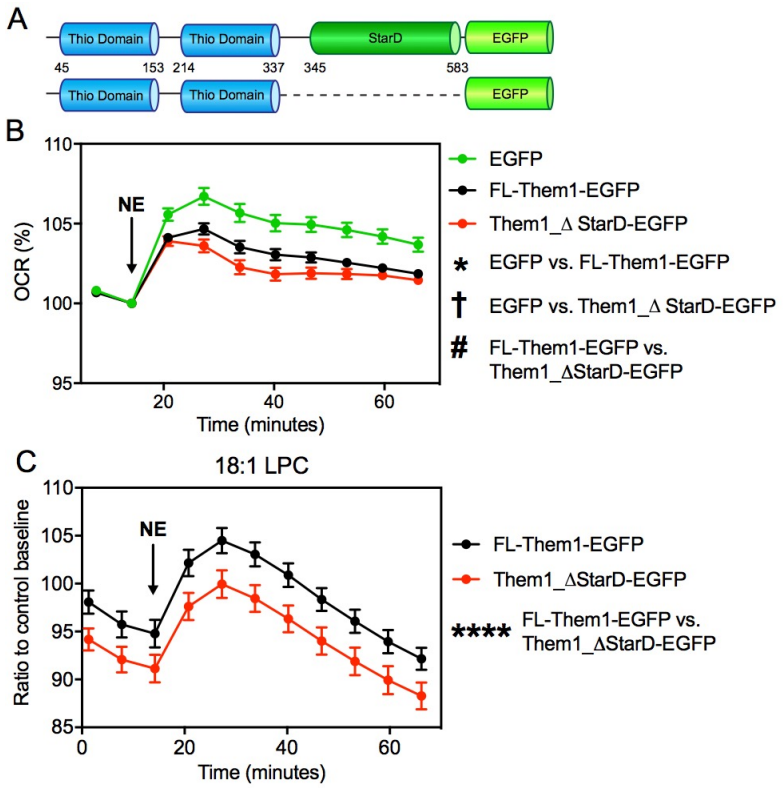

Figure 7. LPC 18:1 inhibits Them1 mediated suppression of thermogenesis in brown adipocytes. *A.* Schematic of adenovirus constructs of full-length Them1 (residues 1-594, top) and Them1_ΔStarD (residues 1-344, bottom) with C-terminal EGFP tags. ***B.*** OCR of iBAs following stimulation with 1 μM norepinephrine (NE). The iBAs were transduced with Ad-FL-Them1-EGFP (black), Ad-Them1_ΔStarD-EGFP (red), and Ad-EGFP (green). OCR values were normalized by the number of live cell nuclei and displayed as a percentage relative to the basal OCR. Graph shows combined data from 3 independent experiments. Statistical analyses were conducted via 2-way ANOVA with Tukey's correction. *P<0.001, between EGFP versus FL-Them1-EGFP, †P<0.001, between EGFP versus Them1_ΔStarD-EGFP, # P<0.001, between FL-Them1-EGFP versus Them1_ΔStarD-EGFP. *C.* OCR of iBAs transduced with Ad-FL-Them1-EGFP (black) or Ad-Them1_ΔStarD-EGFP (red) following stimulation with 1 μM NE. Cells were incubated with 25 μM LPC 18:1 or control buffer for one hour prior to the start of

experiment. OCR values were normalized by the number of live cell nuclei and displayed as ratios relative to the control baseline OCR for each genetic background. Graphs show combined data from 3 independent experiments. Statistical analyses were conducted via 2-way ANOVA with Tukey's correction. ****$P<0.0001$.

Them1_ΔStarD-EGFP with 25 μM 18:1 LPC for one hour prior to measuring NE induced respiration. In line with 18:1 LPC inhibition of Them1 through the StarD, respiration of iBAs transduced with FL-Them1-EGFP was enhanced in the presence of 18:1 LPC relative to Them1_ΔStarD-EGFP (Fig. 7C).

Them1 StarD is necessary for localization to the lipid droplet

To elucidate whether the StarD contributes to Them1 function by altering cellular localization, we visualized Them1 in iBAs stably transduced with the same viral Them1 constructs as above (FL-Them1-EGFP and Them1_ΔStarD-EGFP). FL-Them1-EGFP was primarily localized in puncta near the lipid droplet surface (Fig. 8A-C), as was previously shown by Li et al (REF). Removal of the StarD disrupted lipid droplet localization and led to puncta dispersed throughout the cytosol (Fig. 8D-F). Them1 suppresses thermogenesis in this condensed form, but phosphorylation of the N-terminus disperses Them1 within the cell, which abrogates Them1 mediated inhibition of thermogenesis [51]. To test whether the StarD alters this phosphorylation-mediated dissolution of Them1, we treated cells expressing just the thioesterase domains (Them1_ΔStarD-EGFP) with phorbol 12-myristate 13-acetate (PMA), a PKC activator that leads to Them1 phosphorylation [51]. After a 4 h treatment with PMA, Them1 was diffuse, demonstrating that the StarD is not essential for this process (Fig. 8G-H). These data reveal a spatiotemporal role for the Them1 StarD, whereby the StarD is necessary for positioning Them1 puncta near the lipid droplet. However, this process is distinct from the phosphorylation-regulated dynamics between puncta and diffuse Them1 that is critical for the suppression of thermogenesis.

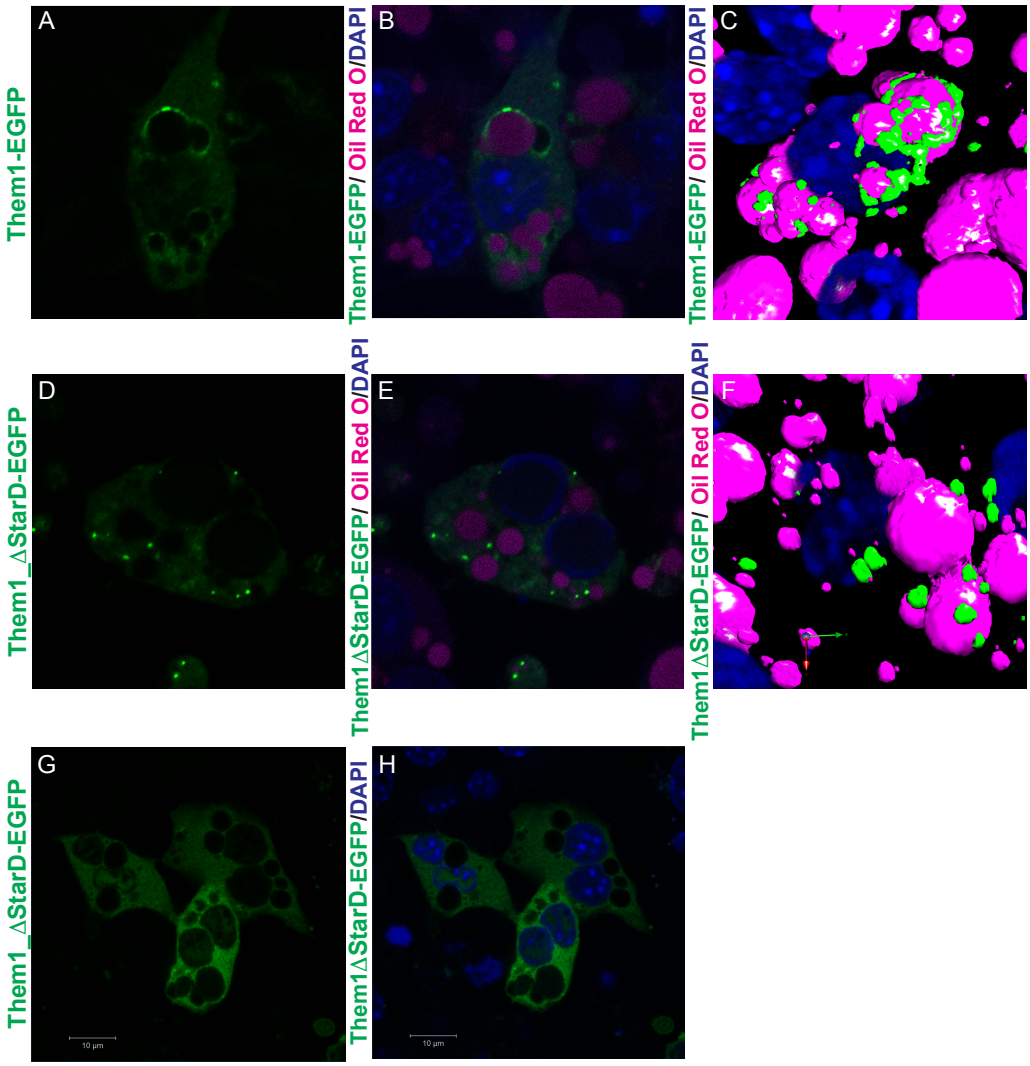

Figure 8. Them1 StarD drives localization to the lipid droplet and is not necessary for Them1 mediated suppression of thermogenesis. *A-F.* Confocal fluorescence microscopy of iBAs cells reconstituted with Ad-FL-Them1-EGFP *(A-C)* and Ad-Them1_ΔStarD-EGFP *(D-F).* Lipd droplets and nuceli were visualized through staining with Oil Red O and DAPI respectively. FL-Them1-EGFP localized with lipid droplets, while Them1_ΔStarD-EGFP did not associate with lipid droplets. *C, F.* 3D rendering of confocal fluorescence microscopy images. G-*H.* PMA treatment of iBAs induced dispression of Them1_ΔStarD-EGFP puncta.

Discussion

Them1 suppresses thermogenesis in BAT, limiting its capacity to oxidize endogenous fatty acids [6, 8]. Whereas we previously demonstrated that the C-terminal StarD is necessary for full catalytic activity of the enzyme [7], the current study elucidates the multifunctional role of the StarD to act as a lipid sensor to allosterically regulate Them1 activity and spatially localize Them1 near the lipid droplet.

We identified that both long-chain fatty acids and 18:1 LPC bind to the StarD and inversely alter Them1 stability and activity, establishing the StarD as a sensor that has evolved to bind specific lipids to tune enzymatic activity. The allosteric enhancement of activity by myristic and palmitic acid through a feedforward mechanism could drive Them1's preference to hydrolyze myristoyl-CoA and palmitoyl-CoA [7], distinguishing it from other thioesterases. When taken together with phosphorylation-dependent cellular dispersion of Them1 [51], the observation that 18:1 LPC as an allosteric inhibitor suggests multiple mechanisms have evolved to suppress Them1 activity in order to enhance thermogenesis. One study showed that induction of thermogenesis in brown adipocytes increased levels of 16:0 LPC, but decreased levels of 18:1 LPC [40]. However, another study showed that 18:1 LPC levels were increased in browning white adipose tissue of mice treated with a β3-adrenergic agonist [52]. Them1 potentially senses the nutritional state of these cells through the StarD and regulates its activity to conserve or oxidize lipids. Additionally, 18:1 LPC may spatiotemporally regulate Them1 activity to control lipid droplet membrane development. Since Them1 is localized to the lipid droplet surface, it could interfere with lipid droplet monolayer formation by hydrolyzing fatty acyl-CoAs, which are the substrates used by LPCAT2 to generate phosphatidylcholines for lipid droplet expansion [39].

However, this could be prevented through inhibition by LPC, which would be localized at the lipid droplet and is utilized by LPCAT2 to produce phosphatidylcholines.

Our data suggest the mechanism by which fatty acids enhance and 18:1 LPC inhibits Them1 activity is by differential stabilization of the StarD. The C-terminal α-helix of StarD is a gate for ligand binding, remaining unfolded in the apo state, and folding and encapsulating the pocket once ligand binds [49, 50]. Our molecular dynamic simulations showed myristic acid stabilized this helix, which is apposed to the thioesterase domains. We expect 18:1 LPC destabilizes this helix, which would then destabilize the thioesterase domains. Phospholipids are imperfect pharmacological tools due to their poor pharmacokinetics; however, these findings should aid in the development of small molecule allosteric inhibitors that enhance metabolism. Screening for compounds that destabilize the StarD and in turn inhibit Them1 activity could yield Them1-selective pharmacological tools to treat obesity and related metabolic disorders.

Our confocal fluorescence studies showed the StarD was responsible for localizing Them1 near the lipid droplet in brown adipocytes at a basal state. The StarD of Them1 could directly interact with the lipid droplet membrane or engage in protein-protein interactions at the lipid droplet surface. Previously it was shown that Them1 associated with phosphatidyl inositol-4-phosphate (PIP) through the StarD in a protein-lipid overlay assay, suggesting the StarD of Them1 is capable of directly interacting with a membrane surface [53]. There were no PIP species that copurified with the StarD in our affinity purification–MS technique, which would only detect high affinity ligands that remain bound through several washing steps; therefore, the StarD may engage in a low affinity interaction with PIP. Recently, it was shown that PIPs are present on the lipid droplet surface, which could potentially explain Them1 localization [54]. In our fitted model of Them1 in the low-resolution negative stain map, the StarDs are positioned on the

exterior of the trimeric complex, where the StarDs could cooperatively bind to the membrane surface, anchoring Them1 puncta to the lipid droplet. Although this localization was shown to be dispensable for Them1-mediated suppression of thermogenesis, the StarD of Them1 could perform other functions at the lipid droplet. For instance, many StarDs are involved in transporting specific lipids to cellular compartments; however, these possibilities remain to be explored [15, 17, 21].

In order to properly traffic acyl-CoAs into specific pathways to drive metabolism, the localization and activity of multiple acyl-CoA thioesterases and synthetases must be controlled [55]. The StarD of Them1 allows for fine tuning of Them1 function; regulating both activity and localization. This control is necessary for correct metabolism in BAT, enabling thermogenesis or preserving resources when needed.

Experimental Procedure

Materials and reagents—Chemicals were purchased from Sigma-Aldrich, Polysciences Inc., Cayman Chemical, and Avanti Polar Lipids. Cell culture media was purchased from Gibco. The vector for His-tagged tobacco etch virus (TEV) was a gift from John Tesmer (University of Texas at Austin). The pMCSG7 (LIC_HIS) vector was provided by Dr. John Sondek (University of North Carolina at Chapel Hill). The hSTARD14 pNIC28-Bsa4 vector was provided by Dr. Nicola Burgess-Brown (Structure Genomics Consortium). The pLVX-IRES-ZsGreen1 vector for stable cell line development was donated by Dr. Rafi Ahmed (Emory University). DNA oligonucleotide primers were synthesized by IDT (Coralville, IA).

Cell Culture—The *HEK293T* cells, which were used to generate the lentivirus, were purchased from the American Type Culture Collection and grown in Dulbecco's Modified Eagle Medium supplemented with 10 % fetal bovine serum (Atlanta Biologicals) and 1% penicillin–streptomycin. Cells were maintained using standard culture conditions. The Freestyle *HEK293F* cells, which were stably transduced, were purchased from Gibco and grown in Freestyle 293 expression medium supplemented with 1x antibiotic-antimycotic (Gibco). Freestyle *HEK293F* cells were grown in suspension culture using glass flasks and a Benchmark Scientific Orbi-Shaker CO_2 shaking at 120 rpm. Cells were maintained at a density of 0.1 – 4 million cells/ milliliter using standard culture conditions. The immortalized brown adipocytes (iBAs) used for localization and Seahorse experiments were a gift from Dr. Bruce Spiegelman (Harvard University). Prior to differentiation, iBAs were grown in Dulbecco's Modified Eagle Medium supplemented with 20 % fetal bovine serum and 1% penicillin–streptomycin. Differentiation of iBAs was induced through incubation in Dulbecco's Modified Eagle Medium supplemented with

10 % fetal bovine serum, 1% penicillin–streptomycin, 20 nM insulin, 1 nM triiodo-L-thyronine (T3), 1 μM rosiglitazone, 2 μg/ml dexamethasone, 125 μM indomethacin, and 500 μM 3-Isobutyl-1-methylxanthine (IBMX). After 48 hours, differentiated iBAs were transferred to maintenance medium containing Dulbecco's Modified Eagle Medium supplemented with 10 % fetal bovine serum, 1% penicillin–streptomycin, 20 nM insulin, 1 nM triiodo-L-thyronine (T3), 1 μM rosiglitazone, and 1 μM norepinephrine (NE). Cells were ready for experimentation after 48 hours in maintenance medium.

Protein expression and purification—The *Homo sapiens* Them1 START domain (residues 339 – 594 of isoform 2) in the pNIC28-Bsa4 vector was transformed in *Escherichia coli* strain BL21 (DE3) cells that were additionally transformed with the pG-Tf2 vector (codes groES-gorEL-tig chaperones). The START domains were expressed as a His_6 fusion containing a tobacco etch virus protease cleavage site to facilitate tag removal. Cultures (1 liters in TB) were grown to an A_{600} of ~0.6 - 0.8 and chaperone transcription was induced with 5 ng/mL tetracycline HCl at 18 °C for one hour, followed by START domain induction with 0.5 mM isopropyl β-d-1-thiogalactopyranoside at 18 °C for ~18 hours. Cell mass was harvested, lysed through sonication in a buffer containing 20 mM Tris HCl pH 7.4, 500 mM NaCl, 25 mM imidazole, 5% glycerol, lysozyme, Dnase A, 0.1 % Triton X-100, 5 mM beta-mercaptoethanol, and 100 uM phenylmethylsulfonyl fluoride. The START domain was purified by nickel affinity chromatography and the His tag was cleaved by tobacco etch virus protease at 4 °C overnight with simultaneous dialysis into a buffer containing 20 mM Tris HCl pH 7.4, 500 mM NaCl, and 5% glycerol when necessary. Cleaved START domain was purified from His tag through nickel

affinity chromatography followed by size exclusion chromatography (SEC) using a HiLoad 16/60 Superdex 75 column.

The *Mus musculus* Them1 thioesterase domains (ΔNterm-Them1_ΔStarD) (residues 43 – 365) in the pMCSG7 vector were transformed into *Escherichia coli* strain BL21 (DE3) pLysS cells. The thioesterase domains were expressed as a His_6 fusion containing a tobacco etch virus protease cleavage site. Cultures (1 liters in LB) were grown to an A_{600} of ~0.6 - 0.8, and thioesterase domain expression was induced with 0.5 mM isopropyl β-d-1-thiogalactopyranoside at 18 °C for ~18 hours. Cell mass was harvested, lysed through sonication in a buffer containing 20 mM Tris HCl pH 7.4, 500 mM NaCl, 25 mM imidazole, 5% glycerol, lysozyme, Dnase A, 5 mM beta-mercaptoethanol, and 100 uM phenylmethylsulfonyl fluoride. The thioesterase domains were purified by nickel affinity chromatography followed by SEC using a HiLoad 16/60 Superdex 200 column.

Wild-type *Mus musculus* Them1 containing both thioesterase domains and START domain (ΔNterm-Them1) (residues 43 – 594) was cloned along with a N-terminal His_6 tag followed by a tobacco etch virus protease cleavage site into the pLVX-IRES-ZsGreen1 lentiviral vector. Polyethylenimine, linear (MW 25,000) (Polysciences Inc.), was used to transfect the Them1 pLVX-IRES-ZsGreen1 vector along with the lentiviral packaging (Pax2) and envelope (MD2G) vectors at a mass ratio of 4:2:1 respectively into *HEK293T* cells according to manufacturer's instructions. After 48 and 72 hours, culture supernatant was collected and viral particles were precipitated through incubation with 10 % PEG 8000, 0.3 M NaCl, and PBS at 4 °C overnight. Viral particles were harvested through centrifugation at 1,500 x g for 30 minutes, decanted, and resuspended in DMEM. Several serial dilutions of lentivirus in DMEM were used to transduce Freestyle *HEK293F* cells. After 72 hours, multiplicity of infection (MOI) was

determined for cell lines through measuring GFP expression in limiting dilutions using a flow cytometer. Them1 (MOI of 50) grown in suspension culture was harvested at a cell density of 2 million cells/ milliliter. Cells were lysed through sonication in a buffer containing 20 mM Tris HCl pH 7.4, 500 mM NaCl, 25 mM imidazole, 5% glycerol, lysozyme, Dnase A, 0.1 % Triton X-100, 5 mM beta-mercaptoethanol, and 100 uM phenylmethylsulfonyl fluoride. Them1 was purified by nickel affinity chromatography followed by SEC using a HiLoad 16/60 Superdex 200 column.

Analytical Ultracentrifugation—Analytical ultracentrifugation experiments were carried out using a Beckman Coulter ProteomeLab™ XLI analytical ultracentrifuge equipped with both absorbance and interference optics and a four-hole An-60 Ti analytical rotor. Sedimentation velocity experiments were carried out at 10 °C and 50,000 rpm (200,000 × g) using 120-mm two-sector charcoal-filled Epon centerpieces with quartz windows. Each sample was scanned at 0-min time intervals for ~ 200 scans. ΔNterm-Them1 was run at ~0.5 mg/mL in buffer containing 20 mM bis-Tris pH 8.5, 500 mM NaCl, and 0.5 mM tris(2-carboxyethyl)phosphine (TCEP). Sedimentation boundaries were analyzed by the continuous distribution (c(s)) method using the program SEDFIT [56]. The program SEDNTERP, version 1.09, was used to correct the experimental s value (s*) to standard conditions at 20 °C in water ($s_{20,w}$) and to calculate protein partial specific volume [57]. Corrected $s_{20,w}$ was used for molecular weight calculation.

Lipid exchange with affinity-mass spectrometry—Bovine liver lipid extracts (Avanti Polar Lipids) suspended in chloroform was dried with nitrogen gas, followed by drying with a vacuum desiccator for at least an hour. Liposomes were generated through resuspending dried lipids in 20

mM Tris pH 7.4, 150 mM NaCl, and 5 % glycerol, agitating for one hour at room temperature, and sonicating for one hour in a bath sonicator. Purified His-tagged StarD and His-tagged MBP were incubated with liver lipid vesicles at 4 °C overnight with total lipid concentration in five-time excess to protein. Non-specifically bound lipids were removed through further purifying proteins with nickel affinity chromatography and SEC using a HiLoad 16/60 Superdex 75 column. Prior to running SEC, the column was cleaned by thoroughly washing with 70 % ethanol, followed by washing with deionized water and equilibration with 20 mM Tris pH 7.4, 150 mM NaCl, and 5 % glycerol. Glass washed three times with chloroform was used to collect, handle, and store samples proceeding SEC. Equal mass samples of StarD and MBP were collected in triplicate ranging from 0.5 – 1.0 mg depending on the experiment. SEC buffer was added to samples to make volume equal for all samples. Additionally, three SEC buffer samples of equal volume were collected as a negative control. Lipids were extracted from samples using the Bligh and Dyer method [58]. Samples were solubilized in 400 µL 1:1 v/v methanol: chloroform mix and spiked with either deuterated palmitic acid-d2 (Cayman Chemical) or deuterated lipid standards (SPLASH II LIPIDOMIX, Avanti Polar, Alabaster, Alabama). Fatty acids were analyzed using direct infusion mass spectrometry in Enhanced MS (EMS) mode over one minute and averaged. The profile mode data was collected in negative mode at scan rate of 10000 Da/s within the mass range 100-1000. The instrumental parameters used were as follows: curtain gas-20, CAD-Low, Ion spray voltage- - 4500, temperature – 350 °C and declustering potential - -100. The data was processed by extracting the peak area from the mass spectrum data and lipid was identified using mass with M-H adduct. Fatty acids were normalized to deuterated palmitic acid standard to quantify fatty acid species. The data is graphically represented as an average of three technical replicates +/- SEM. Phospholipids were analyzed through injecting ten µL of each

sample into the mass spectrometer for flow injection analysis. Several precursor ion scan methods were applied to specifically target phosphatidylcholine, phosphatidylethanolamine, sphingomyelin, ceramide, phosphatidylserine and phosphatidylinositol in the samples. Mass spectrometry data was collected for each precursor ion scan over one minute and averaged. The data was analyzed utilizing LipidView 1.2 (SCIEX, Framingham, MA, USA) with the following processing parameters: polarity-positive, precursor ion scan and neutral loss scan, mass tolerance- 0.5, minimum S/N-10, minimum % intensity-0. With these settings, the data were smoothed, deisotoped and searched for the peak list within a *m/z* range of 100-1000 and chromatographic range of 0.4-1.2 minute. The peak list generated through LipidView 1.2 was further interrogated using the LIPIDMAPS online tool. The identified lipids were semi quantified using deuterated lipid standards. Zero concentrations are represented as not determined (ND). The data is graphically represented as an average of three technical replicates +/- SEM. Statistical analyses were conducted using 2-way ANOVA with Sidak's multiple comparisons test.

Microscale thermophoresis—His-tagged *Homo sapiens* Them1 START domain was labeled using the Monolith His-Tag Labeling Kit RED-tris-NTA (NanoTemper Technologies). The labeling reaction was performed according to the manufacturer's instructions in PBS supplemented with 0.5 % Tween 20 at a concentration of 100 nM protein (molar dye:protein ratio = 1:1) at room temperature for 30 min. Fatty acids were dissolved in ethanol at 10 – 20 mM, and diluted in PBS supplemented with 0.5 % Tween 20 in a series of 16 1:1 dilutions, producing ligand concentrations ranging from 12.2 nM – 800 μM, with a constant final ethanol concentration of 4 %. Each ligand dilution was mixed with one volume of labeled START

domain, which led to a final concentration of START domain of 50 nM and final ligand concentrations ranging from 6.1 nM to 400 μM. START domain was incubated with fatty acid overnight at 4 °C, then loaded in standard Monolith NT.115 Capillaries (NanoTemper Technologies). MST was measured using a Monolith NT.115 instrument (NanoTemper Technologies) at an ambient temperature of 25°C. Instrument parameters were adjusted to 40 % LED power and medium MST power. Data of three independently pipetted measurements were fitted with a non-linear regression model in GraphPad Prism 8.0 using the signal from an MST-on time of 5 s.

Crystallization, data collection, structural refinement—Pure *Homo sapiens* Them1 START domain was incubated with myristic acid in 10-fold excess and concentrated to 10 mg mL^{-1} in 30 mM HEPES pH 7.5, 300 mM NaCl, 10 % glycerol, 0.5 mM tris(2-carboxyethyl)phosphine (TCEP). Crystals of START domain were grown over two weeks via hanging drop vapor diffusion at 4 °C from solutions containing 1 μL START domain and 1 μL mother liquor (0.1 M Tris HCl pH 9.4 and 27 % PEG 8000). Crystals were cryoprotected by immersion in 0.1 M Tris HCl pH 9.4, 27 % PEG 8000, and 20 % glycerol and flash frozen with liquid nitrogen. Data were collected remotely from the Southeast Regional Collaborative Access Team at the Advanced Photon Source, 22ID beamline (Argonne National Laboratories, Chicago, IL). Data were processed and scaled using HKL-2000 (HKL Research, Inc., Charlottesville, VA) [59] and phased by molecular replacement using Phaser-MR (Phenix, Berkeley, CA) [60]. The structure was phased using a previously solved crystal structure of Them1 START domain (3FO5) as a search model [32, 61]. Structure refinement and validation was performed using PHENIX (Phenix, Berkeley, CA) (version 1.11.1), and model building was performed in COOT (MRC Laboratory of Molecular

Biology, Cambridge, UK) [60, 62]. PyMOL (version 1.8.2; Schrödinger, New York, NY) was used to visualize structures and generate figures. Structure is deposited in PDB with ID: 6VVQ.

Acyl-CoA thioesterase activity assay—Myristic acid, palmitic acid, stearic acid, palmitoleic acid, and 18:1 lysophosphatidylcholine were dissolved in ethanol to a concentration of 1.78 mM (3.55 mM for 18:1 LPC at final 50 μM). Purified *Mus musculus* ΔNterm-Them1 or thioesterase domains at a concentration of 1.42 μM were incubated with 429 μM 5,5′-dithiobis-(2-nitrobenzoic acid) (DTNB) and 35 μM fatty acid or 18:1 lysophosphatidylcholine (71 μM for 18:1 LPC at final 50 μM) for 30 minutes at 37 °C in assay buffer containing 30 mM Hepes pH 7.5, 150 mM NaCl, and 5 % glycerol; ethanol concentration was 2 % across samples. Myristoyl-CoA (Sigma) was dissolved in 10 mM MES pH 5.5 to a concentration of 5 mM and further diluted in assay buffer. Myristoyl-CoA was added to protein-DTNB-lipid mixture to initiate reaction in a total reaction volume of 200 μL/ well, with final protein concentration at 1 μM, DTNB at 300 μM, lipid at 25 μM or 50 μM, and myristoyl-CoA ranging 0 – 20 μM. Plates were immediately introduced into a 37 °C temperature-controlled Synergy Neo 2.0 (BioTek) plate reader. Absorbance readings at 412 nm were read every 10 seconds for 1 hour. Enzyme initial velocities (V_0) were calculated through fitting a line to the rise in product formation in the early time points using GraphPad Prism 8.0 for each substrate concentration. The initial velocities were plotted against substrate concentrations and fitted with the Michaelis–Menten equation to yield the maximum velocity (V_{max}) and Km (the Michaelis constant) using GraphPad Prism 8.0. Values of kcat were calculated as kcat = Vmax/[E]. Each experiment was conducted with two technical replicates for each sample and repeated three times.

Negative Stain Electron Microscopy—Freshly purified *Mus musculus* ΔNterm-Them1 (residues 43 – 365) after SEC into a buffer containing 30 mM Hepes pH 7.5, 300 mM NaCl, and 0.5 mM TCEP was used for negative staining. Briefly, 4 ul of ΔNterm-Them1 was adsorbed on a carbon coated Cu–400 mesh grid (TedPella) grid for 1 minute and excess liquid was blotted with Whatman Filter paper 4, washed twice with 20 ul drop of water and stained with 0.75 % Uranyl formate for 30 sec, blotted and air dry. Negatively stained Them1 was imaged on Talos 120 C Microscope operating at 120 kV with Lab6 cathode at pixel size of 1.56 Å. Micrographs were recorded at low dose condition on the Ceta 16M camera (ThermoFisher).

2D classification and 3D Reconstruction—32000 particles were auto picked from 267 micrographs using EMAN2 e2boxer. Initial 2D classification was done using ISAC2 program in Sphire Package [63]. Final 6907 particle stack was imported to Relion 3.0 for further analysis. Ab-inito model reconstruction and 3D refinement was done using C1 and C3 symmetry respectively. Final 4457 particles were selected which gave the resolution of 23 Å with 0.5 FSC criteria. Final 3d volume with C3 symmetry was back projected and compared to 2D classes using EMAN2 for model validation. Model Visualization and analysis was done in Chimera. Map is deposited in EMDB data base with ID EMD-21414.

Molecular Dynamics Simulations—A model of Them1 monomer was prepared for molecular dynamics (MD) simulations. Them1 was prepared by aligning the thioesterase domains of ACOT12 bound to ADP and CoA (PDB code: 4MOB) and our myristic acid bound structure of the StarD. Using this model, apo and myristic-acid bound Them1 complexes were created. Complexes were solvated using an octahedral box of TIP3P water [64] with a 10 Å buffer

surrounding the complexes. Complexes were first neutralized and then adjusted to a final concentration of 150 mM NaCl by the addition of Na+ and Cl- ions. All complexes were prepared using xleap in AmberTools [65] and the parm99 forcefield [66] in Amber14 [67]. Parameters for ADP, CoA and myristic acid were obtained using Antechamber [68] in AmberTools. Using 5000 steps of steepest descent followed by 5000 steps of conjugate gradient, systems were minimized in two rounds. In the first round, restraints of 500 kcal/mol-A^2 were applied to all solute atoms. In the second round, restraints were removed from protein atoms and only maintained for the ligands. Systems were then heated from 0 to 300 K using a 100-ps run with constant volume periodic boundaries and restraints of 10-kcal/mol.A^2 applied to ligands (i.e. myristic acid, CoA and ADP). Equilibration was performed using 12 ns of MD in the NPT ensemble with 10-kcal/molA^2 restraints on small molecule atoms. Restraints were reduced to 1-kcal/molA^2 and equilibration performed for an additional 12 ns. All restraints were removed and 500-ns production simulations performed for each system. All bonds between heavy atoms and hydrogens were fixed with the SHAKE algorithm [69], allowing the use of a 2-fs time step. Long-range electrostatics were evaluated with a cutoff of 10 A.

For analysis, 25000 evenly-spaced frames were obtained from each simulation. The CPPTRAJ [70] module of AmberTools was used for structural averaging and calculations of root mean square fluctuations (RMSFs). Dynamic networks were produced for each system using the NetworkView plugin [71] of VMD [72]. Networks are constructed by defining all protein C-α atoms as nodes, using Cartesian covariance to measure communication within the network. Pairs of nodes that reside within a 4.5-Å cutoff for >75% of the simulation are connected via an edge. Edge weights are inversely proportional to the covariance between the nodes. Networks were subsequently partitioned into communities using the Girvan-Newman algorithm [73]. Communities

represent a group of nodes undergoing correlated motions. The minimum number of communities possible was generated while maintaining at least 98% maximum modularity.

Differential scanning fluorimetry (DSF)—Myristic acid, palmitic acid, stearic acid, and 18:1 lysophosphatidylcholine were dissolved in ethanol to a concentration of 2.5 mM. Purified His-tagged *Homo sapiens* Them1 START domain and His-tagged *Mus musculus* Them1 thioesterase domains at a concentration of 10 μM were incubated with 50 μM fatty acid or 18:1 lysophosphatidylcholine for 30 minutes at room temperature; ethanol concentration was constant at 2 % across samples. SYPRO orange dye (Invitrogen) was then added at a 1:1000 dilution. Reactions were heated at a rate of 0.5 °C per minute, using a StepOne Plus Real Time PCR System (ThermoFisher). Fluorescence was recorded at every degree using the ROX filter (602 nm). Technical triplicates were analyzed by first subtracting baseline fluorescence (ligands + SYPRO with no protein) and then fitting the curves using the Bolzman equation (GraphPad Prism 8.0) to determine the Tm. Experiment was performed with three replicates and the Tm's of different ligands were analyzed in Prism 8.0 with one-way ANOVA and Dunnett's multiple comparisons test.

Hydrogen-deuterium exchange mass spectrometry—HDX-MS experiments were performed on Them1 and the thioesterase domains in two replicates using a Waters nanoACQUITY UPLC HDX system coupled with a Synapt G2-Si mass spectrometer (Waters Corp, Milford, MA). The samples of ΔNterm-Them1 and ΔNterm-Them1_ΔStarD were prepared in 30 mM Hepes pH 7.5, 150 mM NaCl, and 0.5 mM TCEP at a final protein concentration of 6 μM. A PAL system autosampler (LEAP Technologies, Carrboro, NC) mixed the protein samples 1:7 (v/v) with

99.9% D_2O-containing buffer (10mM phosphate buffer, pD 7.0) at 20°C for variable time points between 0 and 14,580 seconds before quenching the reaction with an equal volume of pre-chilled quenching buffer (100 mM Na2PO4 pH 2.5, 5% Formic Acid, and 2% Acetonitrile) at 1°C. The quenched samples were digested with a Waters Enzymate BEH Pepsin Column (2.1 X 30 mm). Peptic peptides were then separated using a Waters ACQUITY UPLC BEH C18 column (1.7 µm 1.0 X 100 mm) at a flow rate of 40 µL/min for 11 minutes in a 5-85% linear gradient with a mobile phase of acetonitrile and 0.1% formic acid at 1°C. The mass spectrometer operated with the electrospray ionization source in positive ion mode, and data were acquired in resolution mode. A reference lock-mass of leucine enkephalin (Waters, Milford, MA) was acquired during sample data collection for internal calibration. Peptides were sequenced and identified through database searching of *Mus musculus* Them1 (residues 43 – 594) in ProteinLynx Global Server (ver. 3.0.3).

Confocal fluorescence microscopy— One day following differentiation, iBAs were transduced with adenovirus containing eGFP, *Mus musculus* full-length Them1-eGFP (residues 1-594), or Them1_ΔStarD-eGFP (residues 1-344) at a multiplicity of infection of 40. Three days following transduction, iBAs cells were washed three times with phosphate buffered saline (PBS) and then fixed with 4% paraformaldehyde in PBS for 20 min at room temperature. Cells were washed twice before staining with 0.3% Oil Red O solution in 60% isopropanol for 2 min at room temperature. The cells were washed twice with PBS and then mounted with ProLong Diamond Antifade Mountant with DAPI (ThermoFisher) to identify nuclei. The localization of fluorescence signal in cultured iBAs cells was evaluated using a Zeiss LSM880 confocal microscope system. The following wavelengths were used to image cellular components: the

405 nm laser was used for DAPI to stain nuclei; the 488 nm laser was used to evaluate EGFP that was linked to Them1; and the 543 nm laser was used to visualize lipid droplets that were stained with Oil Red O. Images were acquired through 2 μm z-stack slices at high resolution and assembled using Volocity image processing software.

O_2 consumption rates— OCR values were measured in iBAs using an Seahorse XFe96 analyzer (Seahorse Bioscience; North Billerica, MA, USA). iBAs were plated into Seahorse XF96 cell culture plate (Agilent) at a density of 1,000 cells / well and differentiated as described above. One day after induction of differentiation, cells were transduced with adenovirus containing eGFP, *Mus musculus* full-length Them1-eGFP (residues 1-594), or Them1_ΔStarD-eGFP (residues 1-344) at a multiplicity of infection of 40. Three days post-transduction, iBAs were incubated in the absence of CO_2 for 1 h at 37 °C in Krebs–Henseleit buffer (pH 7.4) containing 0.45 g/L glucose, 111 mM NaCl, 4.7 mM KCl, 2 mM $MgSO_4$-$7H_2O$, 1.2 mM Na_2HPO_4, 5 mM HEPES and 0.5 mM carnitine (Sigma–Aldrich). For LPC experiments, 16:0 and 18:1 LPC (Avanti Polar Lipids) were solubilized in DMSO at 10 mM, and further diluted into Krebs Henseleit buffer to a final concentration of 25 μM, allowed to incubate with cells at 37 °C for one hour prior to experimentation. OCR values were measured before and after the exposure of cells to 1 μM NE. OCR was normalized with total live cell count calculated through staining live cells with NucRed Live probe and measuring fluorescence with SpectraMax i3X plate reader at ex/em 625/715 nm. Three independent replicates were analyzed and compared with two-way ANOVA and Tukey's comparison test in Prism 8.0.

References

1. Smith RE, Horwitz BA. Brown fat and thermogenesis. Physiol Rev. 1969;49(2):330-425. Epub 1969/04/01. doi: 10.1152/physrev.1969.49.2.330. PubMed PMID: 4888392.
2. Cypess AM, Lehman S, Williams G, Tal I, Rodman D, Goldfine AB, Kuo FC, Palmer EL, Tseng YH, Doria A, Kolodny GM, Kahn CR. Identification and importance of brown adipose tissue in adult humans. N Engl J Med. 2009;360(15):1509-17. Epub 2009/04/10. doi: 10.1056/NEJMoa0810780. PubMed PMID: 19357406; PMCID: PMC2859951.
3. Cypess AM, Kahn CR. Brown fat as a therapy for obesity and diabetes. Current opinion in endocrinology, diabetes, and obesity. 2010;17(2):143-9. Epub 2010/02/18. doi: 10.1097/MED.0b013e328337a81f. PubMed PMID: 20160646; PMCID: PMC3593105.
4. Ricquier D, Mory G, Bouillaud F, Thibault J, Weissenbach J. Rapid increase of mitochondrial uncoupling protein and its mRNA in stimulated brown adipose tissue. Use of a cDNA probe. FEBS letters. 1984;178(2):240-4. Epub 1984/12/10. doi: 10.1016/0014-5793(84)80608-0. PubMed PMID: 6548975.
5. Adams SH, Chui C, Schilbach SL, Yu XX, Goddard AD, Grimaldi JC, Lee J, Dowd P, Colman S, Lewin DA. BFIT, a unique acyl-CoA thioesterase induced in thermogenic brown adipose tissue: cloning, organization of the human gene and assessment of a potential link to obesity. Biochem J. 2001;360:135-42. doi: 10.1042/0264-6021:3600135. PubMed PMID: WOS:000172466900015.
6. Zhang Y, Li Y, Niepel MW, Kawano Y, Han S, Liu S, Marsili A, Larsen PR, Lee CH, Cohen DE. Targeted deletion of thioesterase superfamily member 1 promotes energy expenditure and protects against obesity and insulin resistance. Proc Natl Acad Sci U S A. 2012;109(14):5417-22. Epub 2012/03/20. doi: 10.1073/pnas.1116011109. PubMed PMID: 22427358; PMCID: PMC3325675.
7. Han S, Cohen DE. Functional characterization of thioesterase superfamily member 1/Acyl-CoA thioesterase 11: implications for metabolic regulation. J Lipid Res. 2012;53(12):2620-31. Epub 2012/09/21. doi: 10.1194/jlr.M029538. PubMed PMID: 22993230; PMCID: PMC3494255.
8. Okada K, LeClair KB, Zhang Y, Li Y, Ozdemir C, Krisko TI, Hagen SJ, Betensky RA, Banks AS, Cohen DE. Thioesterase superfamily member 1 suppresses cold thermogenesis by limiting the oxidation of lipid droplet-derived fatty acids in brown adipose tissue. Molecular metabolism. 2016;5(5):340-51. Epub 2016/04/26. doi: 10.1016/j.molmet.2016.02.002. PubMed PMID: 27110486; PMCID: PMC4837299.
9. Schrick K, Nguyen D, Karlowski WM, Mayer KF. START lipid/sterol-binding domains are amplified in plants and are predominantly associated with homeodomain transcription factors. Genome biology. 2004;5(6):R41. Epub 2004/06/10. doi: 10.1186/gb-2004-5-6-r41. PubMed PMID: 15186492; PMCID: Pmc463074.
10. Soccio RE, Breslow JL. StAR-related lipid transfer (START) proteins: mediators of intracellular lipid metabolism. J Biol Chem. 2003;278(25):22183-6. Epub 2003/05/02. doi: 10.1074/jbc.R300003200. PubMed PMID: 12724317.
11. Alpy F, Legueux F, Bianchetti L, Tomasetto C. [START domain-containing proteins: a review of their role in lipid transport and exchange]. Medecine sciences : M/S. 2009;25(2):181-91. Epub 2009/02/26. doi: 10.1051/medsci/2009252181. PubMed PMID: 19239851.
12. Reitz J, Gehrig-Burger K, Strauss JF, 3rd, Gimpl G. Cholesterol interaction with the related steroidogenic acute regulatory lipid-transfer (START) domains of StAR (STARD1) and

MLN64 (STARD3). The FEBS journal. 2008;275(8):1790-802. Epub 2008/03/12. doi: 10.1111/j.1742-4658.2008.06337.x. PubMed PMID: 18331352.
13. Rodriguez-Agudo D, Ren S, Hylemon PB, Redford K, Natarajan R, Del Castillo A, Gil G, Pandak WM. Human StarD5, a cytosolic StAR-related lipid binding protein. J Lipid Res. 2005;46(8):1615-23. Epub 2005/05/18. doi: 10.1194/jlr.M400501-JLR200. PubMed PMID: 15897605.
14. Letourneau D, Bedard M, Cabana J, Lefebvre A, LeHoux JG, Lavigne P. STARD6 on steroids: solution structure, multiple timescale backbone dynamics and ligand binding mechanism. Scientific reports. 2016;6:28486. Epub 2016/06/25. doi: 10.1038/srep28486. PubMed PMID: 27340016; PMCID: PMC4919784.
15. Horibata Y, Sugimoto H. StarD7 mediates the intracellular trafficking of phosphatidylcholine to mitochondria. J Biol Chem. 2010;285(10):7358-65. Epub 2010/01/01. doi: 10.1074/jbc.M109.056960. PubMed PMID: 20042613; PMCID: PMC2844184.
16. Kanno K, Wu MK, Agate DS, Fanelli BJ, Wagle N, Scapa EF, Ukomadu C, Cohen DE. Interacting proteins dictate function of the minimal START domain phosphatidylcholine transfer protein/StarD2. J Biol Chem. 2007;282(42):30728-36. Epub 2007/08/21. doi: 10.1074/jbc.M703745200. PubMed PMID: 17704541.
17. Olayioye MA, Vehring S, Muller P, Herrmann A, Schiller J, Thiele C, Lindeman GJ, Visvader JE, Pomorski T. StarD10, a START domain protein overexpressed in breast cancer, functions as a phospholipid transfer protein. J Biol Chem. 2005;280(29):27436-42. Epub 2005/05/25. doi: 10.1074/jbc.M413330200. PubMed PMID: 15911624.
18. Hanada K, Kumagai K, Tomishige N, Kawano M. CERT and intracellular trafficking of ceramide. Biochimica et biophysica acta. 2007;1771(6):644-53. Epub 2007/02/23. doi: 10.1016/j.bbalip.2007.01.009. PubMed PMID: 17314061.
19. Alpy F, Stoeckel ME, Dierich A, Escola JM, Wendling C, Chenard MP, Vanier MT, Gruenberg J, Tomasetto C, Rio MC. The steroidogenic acute regulatory protein homolog MLN64, a late endosomal cholesterol-binding protein. J Biol Chem. 2001;276(6):4261-9. Epub 2000/10/29. doi: 10.1074/jbc.M006279200. PubMed PMID: 11053434.
20. Lin D, Sugawara T, Strauss JF, 3rd, Clark BJ, Stocco DM, Saenger P, Rogol A, Miller WL. Role of steroidogenic acute regulatory protein in adrenal and gonadal steroidogenesis. Science (New York, NY). 1995;267(5205):1828-31. Epub 1995/03/24. doi: 10.1126/science.7892608. PubMed PMID: 7892608.
21. Yang L, Na CL, Luo S, Wu D, Hogan S, Huang T, Weaver TE. The Phosphatidylcholine Transfer Protein Stard7 is Required for Mitochondrial and Epithelial Cell Homeostasis. Scientific reports. 2017;7:46416. Epub 2017/04/13. doi: 10.1038/srep46416. PubMed PMID: 28401922; PMCID: PMC5388865.
22. Wei J, Kang HW, Cohen DE. Thioesterase superfamily member 2 (Them2)/acyl-CoA thioesterase 13 (Acot13): a homotetrameric hotdog fold thioesterase with selectivity for long-chain fatty acyl-CoAs. Biochem J. 2009;421(2):311-22. Epub 2009/05/02. doi: 10.1042/bj20090039. PubMed PMID: 19405909; PMCID: PMC3086008.
23. Kang HW, Niepel MW, Han S, Kawano Y, Cohen DE. Thioesterase superfamily member 2/acyl-CoA thioesterase 13 (Them2/Acot13) regulates hepatic lipid and glucose metabolism. FASEB J. 2012;26(5):2209-21. Epub 2012/02/22. doi: 10.1096/fj.11-202853. PubMed PMID: 22345407; PMCID: PMC3336778.
24. Cajka T, Fiehn O. Comprehensive analysis of lipids in biological systems by liquid chromatography-mass spectrometry. Trends in analytical chemistry : TRAC. 2014;61:192-206.

Epub 2014/10/14. doi: 10.1016/j.trac.2014.04.017. PubMed PMID: 25309011; PMCID: PMC4187118.
25. Pastukhov AV, Ropson IJ. Fluorescent dyes as probes to study lipid-binding proteins. Proteins. 2003;53(3):607-15. Epub 2003/10/28. doi: 10.1002/prot.10401. PubMed PMID: 14579352.
26. Norris AW, Spector AA. Very long chain n-3 and n-6 polyunsaturated fatty acids bind strongly to liver fatty acid-binding protein. J Lipid Res. 2002;43(4):646-53. Epub 2002/03/22. PubMed PMID: 11907148.
27. Duhr S, Braun D. Why molecules move along a temperature gradient. Proc Natl Acad Sci U S A. 2006;103(52):19678-82. Epub 2006/12/14. doi: 10.1073/pnas.0603873103. PubMed PMID: 17164337; PMCID: PMC1750914.
28. Seidel SA, Dijkman PM, Lea WA, van den Bogaart G, Jerabek-Willemsen M, Lazic A, Joseph JS, Srinivasan P, Baaske P, Simeonov A, Katritch I, Melo FA, Ladbury JE, Schreiber G, Watts A, Braun D, Duhr S. Microscale thermophoresis quantifies biomolecular interactions under previously challenging conditions. Methods (San Diego, Calif). 2013;59(3):301-15. Epub 2012/12/29. doi: 10.1016/j.ymeth.2012.12.005. PubMed PMID: 23270813; PMCID: PMC3644557.
29. Mukerjee P. MKJ. Critical Micelle Concentrations of Surfactant Systems. Nat Stand Ref Data Ser. 1971;NSRDS-NBS 36(National Bureau of Standards).
30. Liebschner D, Afonine PV, Moriarty NW, Poon BK, Sobolev OV, Terwilliger TC, Adams PD. Polder maps: improving OMIT maps by excluding bulk solvent. Acta crystallographica Section D, Structural biology. 2017;73(Pt 2):148-57. Epub 2017/02/09. doi: 10.1107/s2059798316018210. PubMed PMID: 28177311; PMCID: PMC5297918.
31. Nicholls RA, Fischer M, McNicholas S, Murshudov GN. Conformation-independent structural comparison of macromolecules with ProSMART. Acta Crystallogr D Biol Crystallogr. 2014;70(Pt 9):2487-99. Epub 2014/09/10. doi: 10.1107/s1399004714016241. PubMed PMID: 25195761; PMCID: PMC4157452.
32. Thorsell AG, Lee WH, Persson C, Siponen MI, Nilsson M, Busam RD, Kotenyova T, Schuler H, Lehtio L. Comparative structural analysis of lipid binding START domains. PLoS One. 2011;6(6):e19521. Epub 2011/07/09. doi: 10.1371/journal.pone.0019521. PubMed PMID: 21738568; PMCID: PMC3127847.
33. Shaw MK, Ingraham JL. Fatty Acid Composition of Escherichia coli as a Possible Controlling Factor of the Minimal Growth Temperature. Journal of bacteriology. 1965;90(1):141-6. Epub 1965/07/01. PubMed PMID: 16562009; PMCID: PMC315606.
34. Horvath MP, George EW, Tran QT, Baumgardner K, Zharov G, Lee S, Sharifzadeh H, Shihab S, Mattinson T, Li B, Bernstein PS. Structure of the lutein-binding domain of human StARD3 at 1.74 A resolution and model of a complex with lutein. Acta crystallographica Section F, Structural biology communications. 2016;72(Pt 8):609-18. Epub 2016/08/05. doi: 10.1107/s2053230x16010694. PubMed PMID: 27487925; PMCID: PMC4973302.
35. Tan L, Tong J, Chun C, Im YJ. Structural analysis of human sterol transfer protein STARD4. Biochemical and biophysical research communications. 2019;520(2):466-72. Epub 2019/10/15. doi: 10.1016/j.bbrc.2019.10.054. PubMed PMID: 31607485.
36. Roderick SL, Chan WW, Agate DS, Olsen LR, Vetting MW, Rajashankar KR, Cohen DE. Structure of human phosphatidylcholine transfer protein in complex with its ligand. Nat Struct Biol. 2002;9(7):507-11. Epub 2002/06/11. doi: 10.1038/nsb812. PubMed PMID: 12055623.

37. Kudo N, Kumagai K, Tomishige N, Yamaji T, Wakatsuki S, Nishijima M, Hanada K, Kato R. Structural basis for specific lipid recognition by CERT responsible for nonvesicular trafficking of ceramide. Proc Natl Acad Sci U S A. 2008;105(2):488-93. Epub 2008/01/11. doi: 10.1073/pnas.0709191105. PubMed PMID: 18184806; PMCID: PMC2206563.
38. Law SH, Chan ML, Marathe GK, Parveen F, Chen CH, Ke LY. An Updated Review of Lysophosphatidylcholine Metabolism in Human Diseases. International journal of molecular sciences. 2019;20(5). Epub 2019/03/09. doi: 10.3390/ijms20051149. PubMed PMID: 30845751; PMCID: PMC6429061.
39. Cotte AK, Aires V, Fredon M, Limagne E, Derangere V, Thibaudin M, Humblin E, Scagliarini A, de Barros JP, Hillon P, Ghiringhelli F, Delmas D. Lysophosphatidylcholine acyltransferase 2-mediated lipid droplet production supports colorectal cancer chemoresistance. Nature communications. 2018;9(1):322. Epub 2018/01/24. doi: 10.1038/s41467-017-02732-5. PubMed PMID: 29358673; PMCID: PMC5778070.
40. Schweizer S, Liebisch G, Oeckl J, Hoering M, Seeliger C, Schiebel C, Klingenspor M, Ecker J. The lipidome of primary murine white, brite, and brown adipocytes-Impact of beta-adrenergic stimulation. PLoS biology. 2019;17(8):e3000412. Epub 2019/08/02. doi: 10.1371/journal.pbio.3000412. PubMed PMID: 31369546; PMCID: PMC6692052.
41. Waterhouse A, Bertoni M, Bienert S, Studer G, Tauriello G, Gumienny R, Heer FT, de Beer TAP, Rempfer C, Bordoli L, Lepore R, Schwede T. SWISS-MODEL: homology modelling of protein structures and complexes. Nucleic acids research. 2018;46(W1):W296-w303. Epub 2018/05/23. doi: 10.1093/nar/gky427. PubMed PMID: 29788355; PMCID: PMC6030848.
42. Bienert S, Waterhouse A, de Beer TA, Tauriello G, Studer G, Bordoli L, Schwede T. The SWISS-MODEL Repository-new features and functionality. Nucleic acids research. 2017;45(D1):D313-d9. Epub 2016/12/03. doi: 10.1093/nar/gkw1132. PubMed PMID: 27899672; PMCID: PMC5210589.
43. Guex N, Peitsch MC, Schwede T. Automated comparative protein structure modeling with SWISS-MODEL and Swiss-PdbViewer: a historical perspective. Electrophoresis. 2009;30 Suppl 1:S162-73. Epub 2009/06/12. doi: 10.1002/elps.200900140. PubMed PMID: 19517507.
44. Benkert P, Biasini M, Schwede T. Toward the estimation of the absolute quality of individual protein structure models. Bioinformatics (Oxford, England). 2011;27(3):343-50. Epub 2010/12/08. doi: 10.1093/bioinformatics/btq662. PubMed PMID: 21134891; PMCID: PMC3031035.
45. Bertoni M, Kiefer F, Biasini M, Bordoli L, Schwede T. Modeling protein quaternary structure of homo- and hetero-oligomers beyond binary interactions by homology. Scientific reports. 2017;7(1):10480. Epub 2017/09/07. doi: 10.1038/s41598-017-09654-8. PubMed PMID: 28874689; PMCID: PMC5585393.
46. Swarbrick CM, Roman N, Cowieson N, Patterson EI, Nanson J, Siponen MI, Berglund H, Lehtio L, Forwood JK. Structural basis for regulation of the human acetyl-CoA thioesterase 12 and interactions with the steroidogenic acute regulatory protein-related lipid transfer (START) domain. J Biol Chem. 2014;289(35):24263-74. Epub 2014/07/09. doi: 10.1074/jbc.M114.589408. PubMed PMID: 25002576; PMCID: PMC4148856.
47. Zivanov J, Nakane T, Forsberg BO, Kimanius D, Hagen WJ, Lindahl E, Scheres SH. New tools for automated high-resolution cryo-EM structure determination in RELION-3. eLife. 2018;7. Epub 2018/11/10. doi: 10.7554/eLife.42166. PubMed PMID: 30412051; PMCID: PMC6250425.

48. Chalmers MJ, Busby SA, Pascal BD, He Y, Hendrickson CL, Marshall AG, Griffin PR. Probing protein ligand interactions by automated hydrogen/deuterium exchange mass spectrometry. Analytical chemistry. 2006;78(4):1005-14. Epub 2006/02/16. doi: 10.1021/ac051294f. PubMed PMID: 16478090.
49. Roostaee A, Barbar E, Lavigne P, LeHoux JG. The mechanism of specific binding of free cholesterol by the steroidogenic acute regulatory protein: evidence for a role of the C-terminal alpha-helix in the gating of the binding site. Bioscience reports. 2009;29(2):89-101. Epub 2008/08/30. doi: 10.1042/bsr20080111. PubMed PMID: 18729825.
50. Roostaee A, Barbar E, Lehoux JG, Lavigne P. Cholesterol binding is a prerequisite for the activity of the steroidogenic acute regulatory protein (StAR). Biochem J. 2008;412(3):553-62. Epub 2008/03/18. doi: 10.1042/bj20071264. PubMed PMID: 18341481.
51. Li YA, L.H.; Hagen, S.J.; Cohen, D.E. N-Terminal Phosphorylation of Thioesterase Superfamily Member 1 (Them1) Regulates its Subcellular Localization in Brown Adipocytes. FASEB Journal2017.
52. He P, Hou B, Li Y, Xu C, Ma P, Lam SM, Gil V, Yang X, Yang X, Zhang L, Shui G, Song J, Qiang G, Liew CW, Du G. Lipid Profiling Reveals Browning Heterogeneity of White Adipose Tissue by Beta3-Adrenergic Stimulation. Biomolecules. 2019;9(9). Epub 2019/09/06. doi: 10.3390/biom9090444. PubMed PMID: 31484405; PMCID: PMC6770315.
53. Chen D, Latham J, Zhao H, Bisoffi M, Farelli J, Dunaway-Mariano D. Human brown fat inducible thioesterase variant 2 cellular localization and catalytic function. Biochemistry. 2012;51(35):6990-9. Epub 2012/08/18. doi: 10.1021/bi3008824. PubMed PMID: 22897136; PMCID: PMC4066737.
54. Du X, Zhou L, Aw YC, Mak HY, Xu Y, Rae J, Wang W, Zadoorian A, Hancock SE, Osborne B, Chen X, Wu JW, Turner N, Parton RG, Li P, Yang H. ORP5 localizes to ER-lipid droplet contacts and regulates the level of PI(4)P on lipid droplets. The Journal of cell biology. 2019. Epub 2019/10/28. doi: 10.1083/jcb.201905162. PubMed PMID: 31653673.
55. Cooper DE, Young PA, Klett EL, Coleman RA. Physiological Consequences of Compartmentalized Acyl-CoA Metabolism. J Biol Chem. 2015;290(33):20023-31. Epub 2015/07/01. doi: 10.1074/jbc.R115.663260. PubMed PMID: 26124277; PMCID: PMC4536410.
56. Schuck P. Size-distribution analysis of macromolecules by sedimentation velocity ultracentrifugation and lamm equation modeling. Biophysical journal. 2000;78(3):1606-19. Epub 2000/02/29. doi: 10.1016/s0006-3495(00)76713-0. PubMed PMID: 10692345; PMCID: PMC1300758.
57. Laue TMS, B.D., Ridgeway, T.M.; Pelletier, S.L. Computer-aided interpretation of analytical sedimentation data for proteins. Royal Society of Chemistry, Cambridge. 1992;Analytical ultracentrifugation in biochemistry and polymer science:90–125.
58. Bligh EG, Dyer WJ. A rapid method of total lipid extraction and purification. Can J Biochem Physiol. 1959;37(8):911-7. Epub 1959/08/01. PubMed PMID: 13671378.
59. Otwinowski Z, Minor W. [20] Processing of X-ray diffraction data collected in oscillation mode. Methods in enzymology. 1997;276:307-26. Epub 1997/01/01. doi: 10.1016/s0076-6879(97)76066-x. PubMed PMID: 27799103.
60. Adams PD, Afonine PV, Bunkoczi G, Chen VB, Davis IW, Echols N, Headd JJ, Hung LW, Kapral GJ, Grosse-Kunstleve RW, McCoy AJ, Moriarty NW, Oeffner R, Read RJ, Richardson DC, Richardson JS, Terwilliger TC, Zwart PH. PHENIX: a comprehensive Python-based system for macromolecular structure solution. Acta Crystallogr D Biol Crystallogr.

2010;66(Pt 2):213-21. Epub 2010/02/04. doi: 10.1107/s0907444909052925. PubMed PMID: 20124702; PMCID: PMC2815670.
61. Matsuoka S, Sugiyama S, Matsuoka D, Hirose M, Lethu S, Ano H, Hara T, Ichihara O, Kimura SR, Murakami S, Ishida H, Mizohata E, Inoue T, Murata M. Water-mediated recognition of simple alkyl chains by heart-type fatty-acid-binding protein. Angewandte Chemie (International ed in English). 2015;54(5):1508-11. Epub 2014/12/11. doi: 10.1002/anie.201409830. PubMed PMID: 25491543; PMCID: PMC4471613.
62. Emsley P, Lohkamp B, Scott WG, Cowtan K. Features and development of Coot. Acta Crystallogr D Biol Crystallogr. 2010;66(Pt 4):486-501. Epub 2010/04/13. doi: 10.1107/s0907444910007493. PubMed PMID: 20383002; PMCID: PMC2852313.
63. Moriya T, Saur M, Stabrin M, Merino F, Voicu H, Huang Z, Penczek PA, Raunser S, Gatsogiannis C. High-resolution Single Particle Analysis from Electron Cryo-microscopy Images Using SPHIRE. Journal of visualized experiments : JoVE. 2017(123). Epub 2017/06/02. doi: 10.3791/55448. PubMed PMID: 28570515; PMCID: PMC5607996.
64. Jorgensen WL, Chandrasekhar, J., Madura, J.D., Impey, R.W., and Klein, M.L. . Comparison of simple potential functions for simulating liquid water. The Journal of chemical physics. 1983;79:926-35.
65. Case D, and Kollman, P. AmberTools 122012.
66. Wang J, Cieplak, P., and Kollman, P.A. How well does a restrained electrostatic potential (RESP) model perform in calculating conformational energies of organic and biological molecules? ournal of computational chemistry. 2000;21:1049-74.
67. Armstrong EH, Goswami D, Griffin PR, Noy N, Ortlund EA. Structural basis for ligand regulation of the fatty acid-binding protein 5, peroxisome proliferator-activated receptor beta/delta (FABP5-PPARbeta/delta) signaling pathway. J Biol Chem. 2014;289(21):14941-54. Epub 2014/04/03. doi: 10.1074/jbc.M113.514646. PubMed PMID: 24692551; PMCID: PMC4031543.
68. Wang J, Wang, W., Kollman, P.A., and Case, D.A. Antechamber: an accessory software package for molecular mechanical calculations. J Am Chem Soc. 2001;222(U403).
69. Ryckaert J-P, Ciccotti, G., and Berendsen, H.J. Numerical integration of the cartesian equations of motion of a system with constraints: molecular dynamics of n-alkanes. Journal of Computational Physics. 1977;23:327-41.
70. Roe DR, Cheatham TE, 3rd. PTRAJ and CPPTRAJ: Software for Processing and Analysis of Molecular Dynamics Trajectory Data. Journal of chemical theory and computation. 2013;9(7):3084-95. Epub 2013/07/09. doi: 10.1021/ct400341p. PubMed PMID: 26583988.
71. Sethi A, Eargle J, Black AA, Luthey-Schulten Z. Dynamical networks in tRNA:protein complexes. Proc Natl Acad Sci U S A. 2009;106(16):6620-5. Epub 2009/04/09. doi: 10.1073/pnas.0810961106. PubMed PMID: 19351898; PMCID: PMC2672494.
72. Humphrey W, Dalke A, Schulten K. VMD: visual molecular dynamics. Journal of molecular graphics. 1996;14(1):33-8, 27-8. Epub 1996/02/01. doi: 10.1016/0263-7855(96)00018-5. PubMed PMID: 8744570.
73. Newman ME. Modularity and community structure in networks. Proc Natl Acad Sci U S A. 2006;103(23):8577-82. Epub 2006/05/26. doi: 10.1073/pnas.0601602103. PubMed PMID: 16723398; PMCID: PMC1482622.
74. Tian W, Chen C, Lei X, Zhao J, Liang J. CASTp 3.0: computed atlas of surface topography of proteins. Nucleic acids research. 2018;46(W1):W363-w7. Epub 2018/06/04. doi: 10.1093/nar/gky473. PubMed PMID: 29860391; PMCID: PMC6031066.

Acknowledgements

The authors thank Dr. Peter E. Prevelige at UAB for his assistance with HDX-MS, Dr. Pete Lollar and Dr. Anamika Patel at Emory University for their assistance with AUC, and Dr. Bruce Spiegelman of the Dana-Farber Cancer Institute at Harvard Medical School for providing the iBAs cells. This work was supported by the National Institutes of Health (RO1 DK 103046 to D.E.C., S.J.H, and E.O.). M.C.T. was funded by the T32 GM008602 NIH Pharmacology Training Grant. Crystallographic data were collected at Southeast Regional Collaborative Access Team (SER-CAT) 22-ID beamline at the Advanced Photon Source, Argonne National Laboratory, and was supported by the United States Department of Energy, Office of Science, Office of Basic Energy Sciences, under contract W-31–109-Eng-38. This study was supported in part by the Emory Integrated Lipidomics Core (EILC), which is subsidized by the Emory University School of Medicine and is one of the Emory Integrated Core Facilities. Additional support was provided by the Georgia Clinical & Translational Science Alliance of the National Institutes of Health under Award Number UL1TR002378. The content is solely the responsibility of the authors and does not necessarily reflect the official views of the National Institutes of Health.

Competing Interests

The authors declare no competing interests.

Materials & Correspondence:

Correspondence and requests for materials should be addressed to E.A.O.

Supplemental Table 1.

Protein Name	PDB	Ligand	Surface Area (Å^2)	Volume (Å^3)
STARD1	3P0L		329.5	196.6
			378.6	217.8
			375.6	217.4
STARD2	1LN3	Palmitoyl-Linoleoyl Phosphatidylcholine	1041.9	897.9
		Palmitoyl-Linoleoyl Phosphatidylcholine	1060.2	927.9
	1LN1	Dilinoleoylphosphatidylcholine	841.7	723.9
	1LN2	Dilinoleoylphosphatidylcholine	1043.3	883.1
		Dilinoleoylphosphatidylcholine	1079.1	913.1
STARD3	5I9J		539.7	230.1
	1EM2		575.2	404.8
STARD4	1JSS		408.6	262.9
			455.1	295.2
STARD5	2R55		381.7	186.1
			377.8	182.9
STARD6	2MOU		189.6	58.2
STARD11	2E3M		616.8	436.6
	2E3N	C6-ceramide	587.3	418.9
	2E3O	C16-ceramide	622.7	428.1
	2E3P	C16-ceramide	614.2	387.7
		C16-ceramide	620.1	429.4
	2E3Q	C18-ceramide	612.2	413.5
	2E3R	C18-ceramide	619.7	437.7
		C18-ceramide	626.5	437.4
	2E3S	C24-ceramide	692.5	486.0
	2Z9Y	C10-diacylglycerol	516.3	326.6
STARD13	2PSO		566.1	358.7
			434.2	261.5
			573.4	386.8
Them1	3FO5		389.4	203.9
			316.3	170.6
			323.5	175.9
			233.2	132.6
		Myristic Acid	315.8	178.5
			308.7	189.8

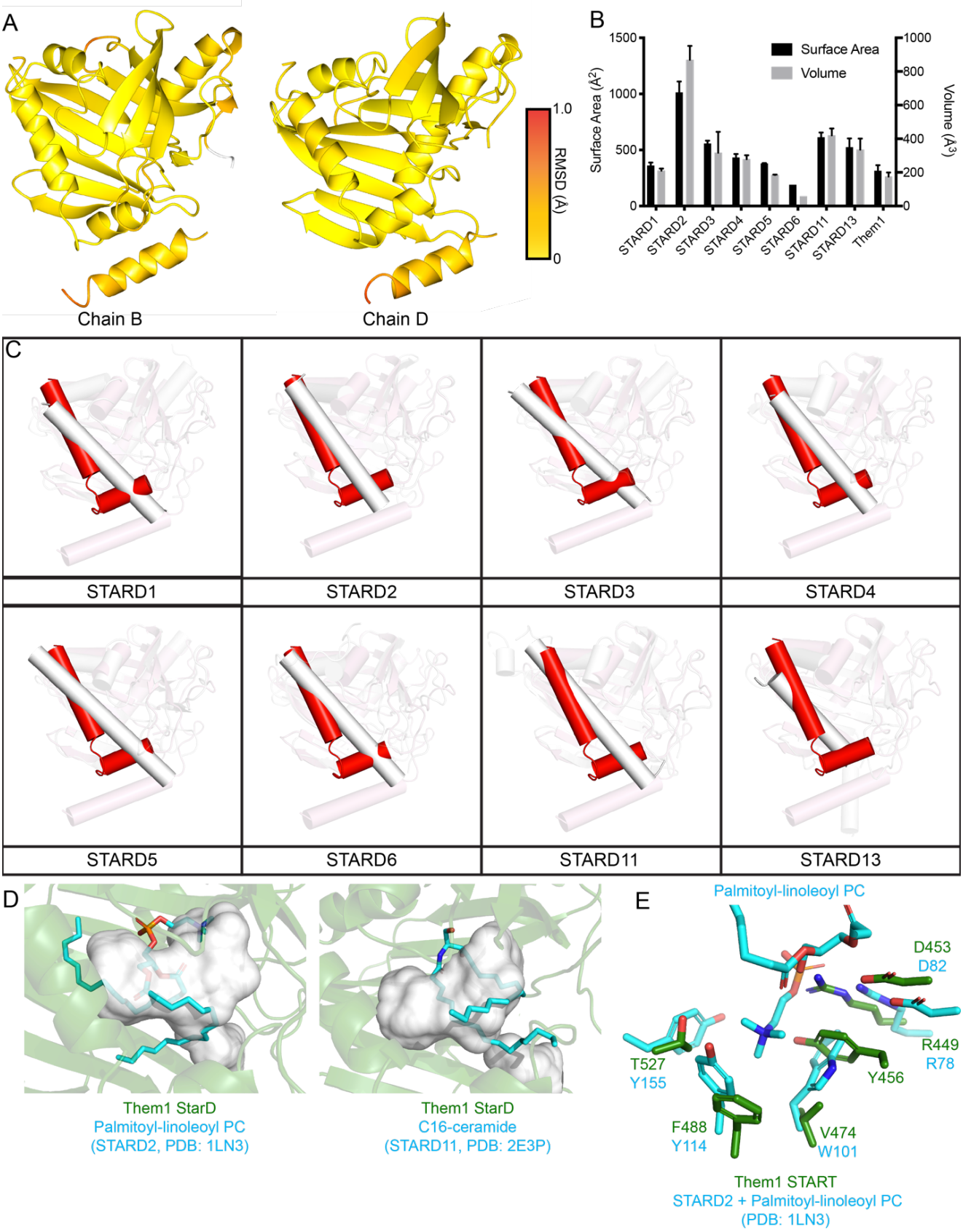
A
Chain B
Chain D
1.0
RMSD (Å)
0
B
Surface Area
Volume
Surface Area (Å²)
Volume (Å³)
1500
1000
500
0
1000
800
600
400
200
0
STARD1
STARD2
STARD3
STARD4
STARD5
STARD6
STARD11
STARD13
Them1
C
STARD1
STARD2
STARD3
STARD4
STARD5
STARD6
STARD11
STARD13
D
Them1 StarD
Palmitoyl-linoleoyl PC
(STARD2, PDB: 1LN3)
Them1 StarD
C16-ceramide
(STARD11, PDB: 2E3P)
E
Palmitoyl-linoleoyl PC
D453
D82
R449
R78
T527
Y155
Y456
F488
Y114
V474
W101
Them1 START
STARD2 + Palmitoyl-linoleoyl PC
(PDB: 1LN3)

Supplemental Figure 1. Structure of Them1 StarD suggests small lipids bind. *A.* ProSMART analysis conducted to determine r.m.s.d. between Cα backbone of myristic acid bound StarD and apo-StarD monomers (chain B and D). Root mean square deviations (range: 0–1.0 Å) between monomers were mapped onto chains B or D of the StarD structure with a color scale depicting low (yellow) to high (red) deviations. Unaligned regions are colored in white. *B.* Graphical representation of Table 3. Bars depict average surface area (black) and volume (gray) for each StarD structure as determined from the CASTp server [74]. Error bars display standard error of the mean. *C*. Alignment of Them1 StarD structure (red) with known structures of all other StarDs (white). The C-terminus of each comparison is emphasized to display structural dissimilarity. *D.* Structural alignment of the StarD of Them1 (green) with StarD2 bound to palmitoyl-linoleoyl phosphatidylcholine (left; PDB code: 1LN3) and StarD11 bound to C16-ceramide (right; PDB code: 2E3P). Only ligands of StarD2 and StarD11 displayed as cyan spheres. Ligands from StarD2 and StarD11 structures do not fit into the interior cavity of the StarD of Them1 that is colored white. *E.* Zoomed in view of the binding pocket of StarD2 (cyan, PDB code: 1LN3) and the StarD of Them1 (green) displaying residues surrounding palmitoyl-linoleoyl phosphatidylcholine from the StarD2 structure. The Them1 StarD contains conserved R449 and D453 that are also found in StarD2, that could participate in electrostatic interactions with the phosphate group of the PC. The StarD of Them1 lacks the aromatic cage present in StarD2 (W101, Y114, Y153), though it contains Y456 that could occupy the same space as W101 in StarD2.

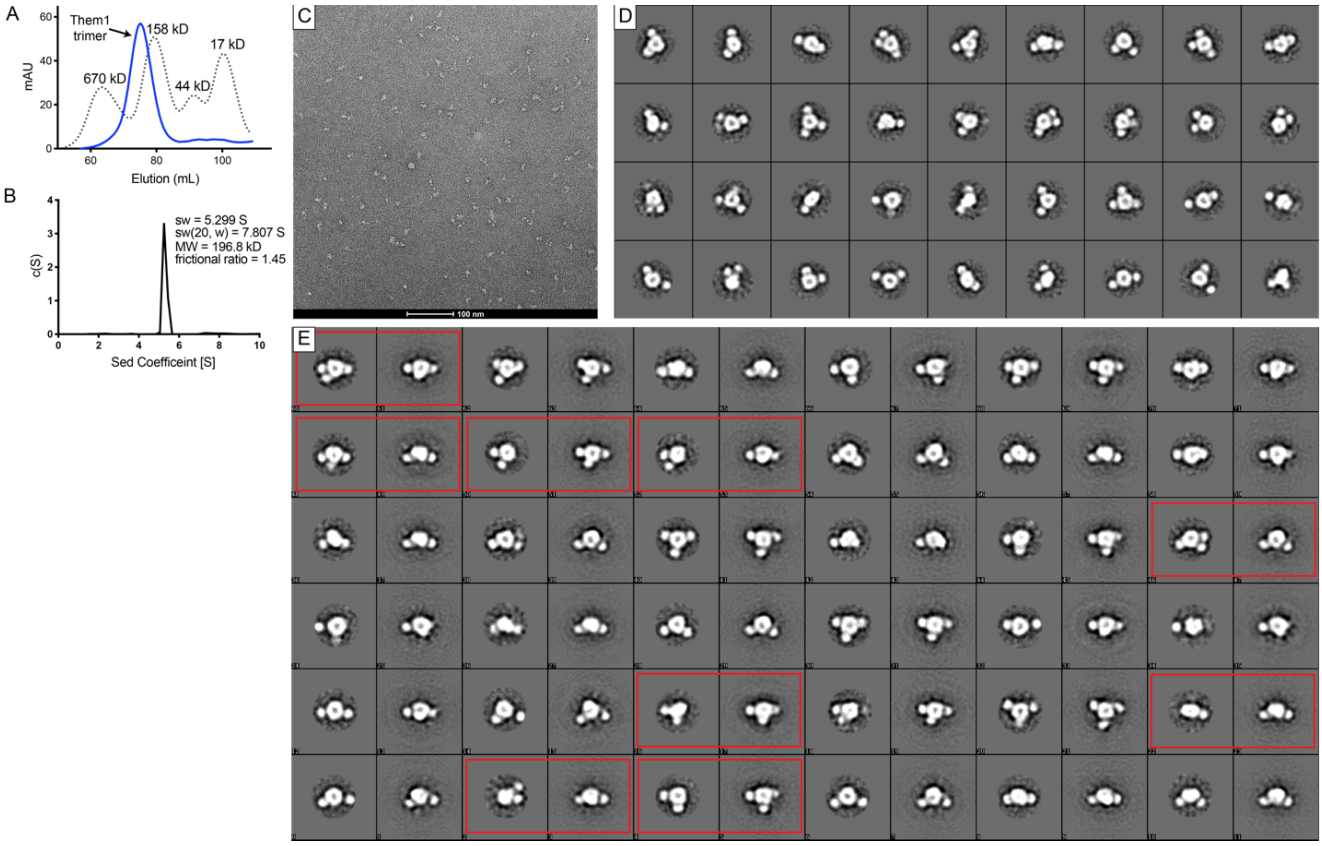

Supplemental Figure 2. Negative stain single particle electron microscopy of Them1. *A-B.* ΔNterm-Them1 purifies as a homogenous trimeric complex (~196.5 kD) as determined by size exclusion chromatography *(A)* and analytical ultracentrifugation *(B)*. *A.* Size exclusion chromatography of ΔNterm-Them1 (blue) and standards (dotted line). *B. c(s)* distribution from sedimentation velocity analytical ultracentrifugation of ΔNterm-Them1 complex. *C.* One image of ΔNterm-Them1 stained with uranyl formate spread across carbon coated Cu mesh grid collected on Talos 120 C Microscope at a magnification of 96,000X. *D.* 2D Class averages of Them1 using Relion 3.0. *E.* Comparison of 2D class averages (left) and reprojections (right) of 3D model generated with C3 symmetry to match the class average. Red rectangles highlight when reprojections of 3D model do not match class averages.

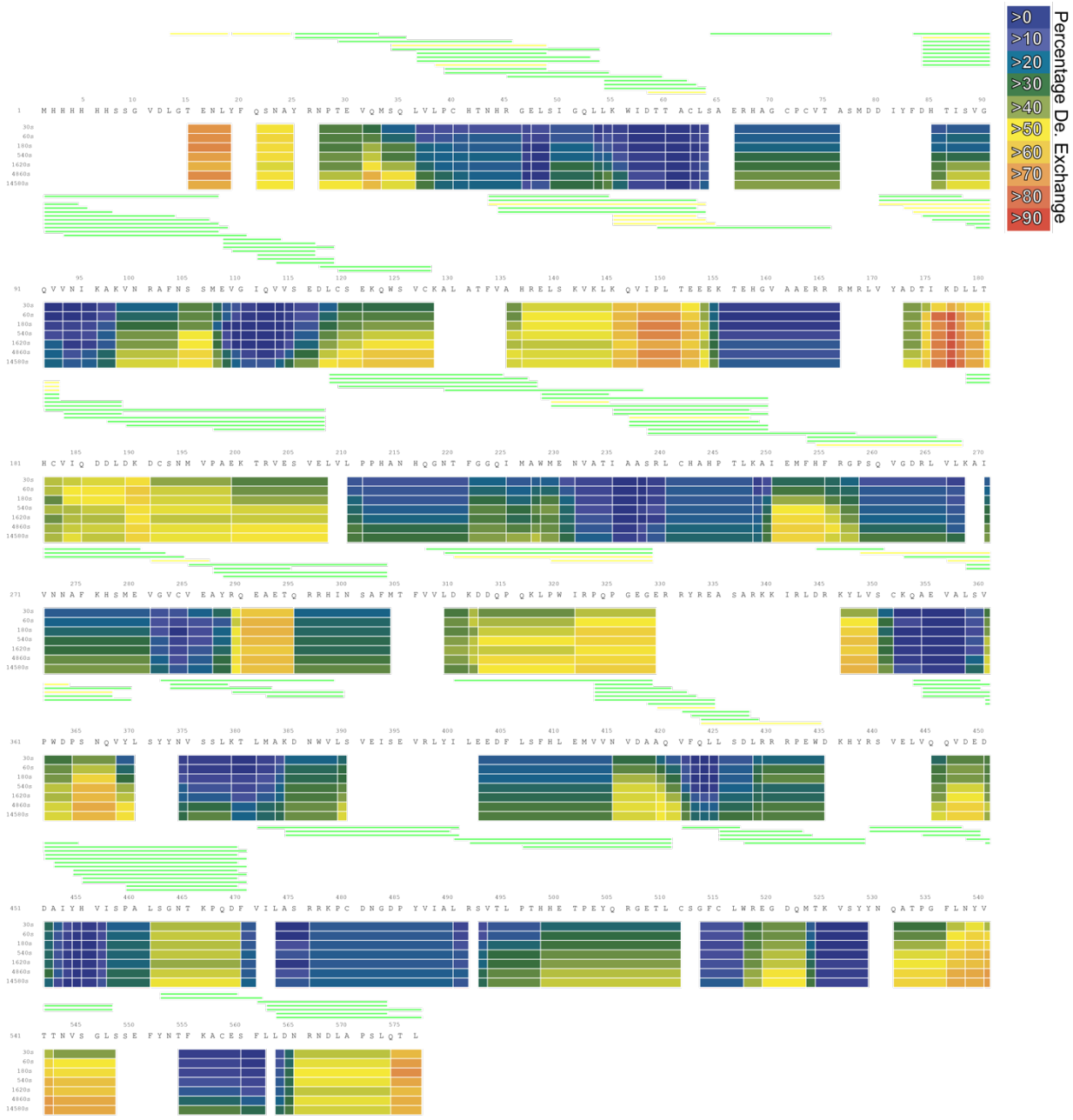
Percentage De. Exchange
>0
>10
>20
>30
>40
>50
>60
>70
>80
>90
30s
60s
180s
540s
1620s
4860s
14580s

Supplemental Figure 3. HDX-MS heatmap of Them1 and thioesterase domains. Identified peptides are displayed above sequence and colored according to the identification confidence (green = high confidence; yellow = medium confidence). Below sequence is a heatmap corresponding to the percentage deuterium incorporation across the sequence at each time point. ΔNterm-Them1 (top) is globally more stable than the thioesterse domains alone (bottom).

CHAPTER 4: BIOCHEMICAL CHARACTERIZATION OF THEM1 ENZYMATIC ACTIVITY AND REGULATION BY SMALL MOLECULES

Matthew C. Tillman[1], Anamika Patel[1], Akshitha Adhiyaman[1], Eric A. Ortlund[1]

[1]*Department of Biochemistry, Emory University School of Medicine, 1510 Clifton Road, Atlanta, GA 30322.*

This manuscript elucidates the enzymatic mechanism of Them1 using mutagenesis and uncovers the molecular mechanism by which ADP and ATP regulate Them1 activity through altering the thermal stability of the protein. Additionally, we show preliminary data of progress towards determining a high-resolution structure of full-length Them1 and the thioesterase domains. This work is currently not published and not in review.

M.C.T. performed mutagenesis, protein purification, thioesterase assays, DSF assays, protein crystallography, and wrote paper. A.P. performed AUC and Cryo EM. A.A. performed thioesterase assays. E.A.O. mentored M.C.T., assisted with experimental design and data analysis, and edited the paper.

Abstract

Maintaining the balance between free fatty acids and acyl-CoA is an essential process that effects lipid metabolism and signaling. In brown adipose tissue, thioesterase superfamily member 1 (Them1) hydrolyzes acyl-CoA into fatty acids, which suppresses the thermogenic capacity of the tissue. Them1 is a member of the type II acyl-CoA thioesterase (ACOT) family, containing two hot-dog fold thioesterase domains and a C-terminal lipid binding domain. Them1 function is tightly controlled through several distinct mechanisms. Phosphorylation of the Them1 N-terminus region leads to dispersion away from the lipid droplet-mitochondrial interface where it actively suppresses thermogenesis. Several compounds, including lipids and ADP/ATP, allosterically regulate Them1 activity, enabling Them1 to sense the energetic and nutrient status of the cell to fine tune its function. Up to this point, the mechanism by which Them1 hydrolyzes acyl-CoA and how ADP/ATP regulate Them1 activity have remained unknown. We show Them1 conserves the same enzymatic mechanism found throughout the type II ACOT family. Additionally, we show ADP/ATP directly bind to Them1 and alter the thermal stability of the protein. Furthermore, we identify key residues involved in ADP/ATP binding, and find there is a clinically reported mutation in one of these residues that is linked to a lipid storage myopathy.

Introduction

Once fatty acids enter a cell, they are esterified to coenzyme A (CoA) by acyl-CoA synthetase, activating them for use in protein acylation, complex lipid synthesis, and lipid metabolism [1]. The availability of acyl-CoA is tightly regulated by acyl-CoA thioesterases (ACOTs), which catalyze the reverse reaction, generating free fatty acids and CoA [2]. In brown adipose tissue, acyl-CoA synthetase 1 (ACSL1) converts fatty acids into acyl-CoA to serve as fuel for thermogenesis [3]. ACOT11 antagonizes this process by hydrolyzing acyl-CoA, preventing their use as substrate for β-oxidation [4]. In line with this, genetic ablation of ACOT11 in mice results in increased energy expenditure due to elevated thermogenic output [5]. In addition, these mice were protected against diet-induced obesity, hepatic steatosis, and insulin insensitivity, highlighting the potential of ACOT11 as a pharmacological target to treat these disorders [5].

ACOT11, also known as thioesterase superfamily member 1 (Them1), is a member of the type II ACOT family of thioesterases, which share a similar hot-dog domain fold. Them1 contains two hot-dog domains like other type II ACOT family members ACOT7, ACOT8, ACOT9, and ACOT12 [2]. This differs from ACOT13, which contains only one hot-dog domain that oligomerizes to form an active enzyme [6]. Them1, like ACOT12 [7], also contains a C-terminal StAR-related lipid transfer domain (StarD) that binds to fatty acids and lysophosphatidylcholine (**Chapter 4**) . Them1 can hydrolyze both acetyl-CoA and long-chain acyl-CoA, but its preferred substrate is myristoyl-CoA and palmitoyl-CoA [8].

There are several discrete mechanisms that regulate Them1 activity. For one, phosphorylation of the N-terminus distributes Them1 throughout the cell and lowers Them1 mediated suppression of thermogenesis [9]. Two, fatty acids and lysophosphatidylcholine bind to the StarD and reciprocally regulate Them1 enzymatic activity, as discussed in **Chapter 4**. Lastly,

ATP and ADP were previously shown to inversely regulate acyl-CoA catalysis, with ADP inhibiting and ATP enhancing Them1 activity [8]. Despite these findings, we still lack key knowledge of how this enzyme is regulated by ADP/ATP, which reflect the energy state of the cell. In this study, we elucidate the enzymatic mechanism of Them1 and how ADP/ATP regulate Them1 activity. Additionally, we report progress into solving the structure of Them1 and its thioesterase domains.

Results

Enzymatic Mechanism of Them1

There is currently no structure of Them1's thioesterase domains; therefore, we created a homology model using the SWISS MODEL server [10-14] from the structure of a close paralog, ACOT12 [7], that shares 50 % sequence identity and 65 % similarity. Using this model, we set out to elucidate the enzymatic mechanism for acyl-CoA hydrolysis. We aligned our model with the structure of other known type II ACOTs, namely ACOT7 [15], ACOT12 [7], and ACOT13 [6]. Both ACOT7 and ACOT12 were crystalized with coenzyme A, while ACOT13 was crystallized with the nonhydrolyzable substrate, undecane-2-one-coenzyme A. The coenzyme A is located similarly in all structures; however, the positioning of the thioether bond present in undecane-2-one-coenzyme A bound to ACOT13 is significantly different than the location of the free thiol in coenzyme A bound to ACOT7 and ACOT12. Since the undecane-2-one-coenzyme A compound is a close mimic of Them1's preferred substrate palmitoyl-CoA [8], and the catalytic mechanism of ACOT13 is elucidated [6], we used this structural comparison to identify residues involved in Them1's enzymatic reaction.

ACOT13 differs from Them1, as it only contains one hot-dog fold thioesterase domain. However, ACOT13 dimerizes, forming two active sites, and adopts a similar fold as our Them1 model. ACOT13 hydrolyzes acyl-CoA through an aspartic acid (D65)/ serine (S83) assisted attack of a water molecule that reacts with the thioester [6]. The tertiary transition state is stabilized by asparagine (N50), which further drives hydrolysis [6]. With this model, we identified two putative Them1 active sites through structural alignment with the ACOT13 dimer. Active site 1 is highly conserved across Them1 homologs and consists of aspartic acid 74, threonine 91, and asparagine 232 (Fig. 1A, C). Active site 2 is also conserved consisting of asparagine 59 and glutamic acid 247 but lacks a polar residue where serine 83 is located in ACOT13 (Fig. 1B, C).

We generated three thioesterase domain mutant constructs of active site 1 in which aspartic acid 74 and asparagine 232 were mutated to alanine individually or in combination. Mutation of these residues significantly disrupted hydrolysis of myrsitoyl-CoA, suggesting these residues are essential for Them1 Acot activity (Fig. 2). We did not mutate threonine 91 since mutagenesis of serine 83 in ACOT13 did not significantly alter activity [6]. These data suggest that Them1 hydrolyzes acyl-CoA in a similar mechanism as ACOT13; in which, aspartic acid 74 and threonine 91 attack of a water molecule that reacts with the thioester, and asparagine 232 coordinately stabilizes the tertiary transition state (Fig. 3). Since there was low residual Acot activity of the active site 1 mutants, we propose that there may be some low-level of activity in active site 2.

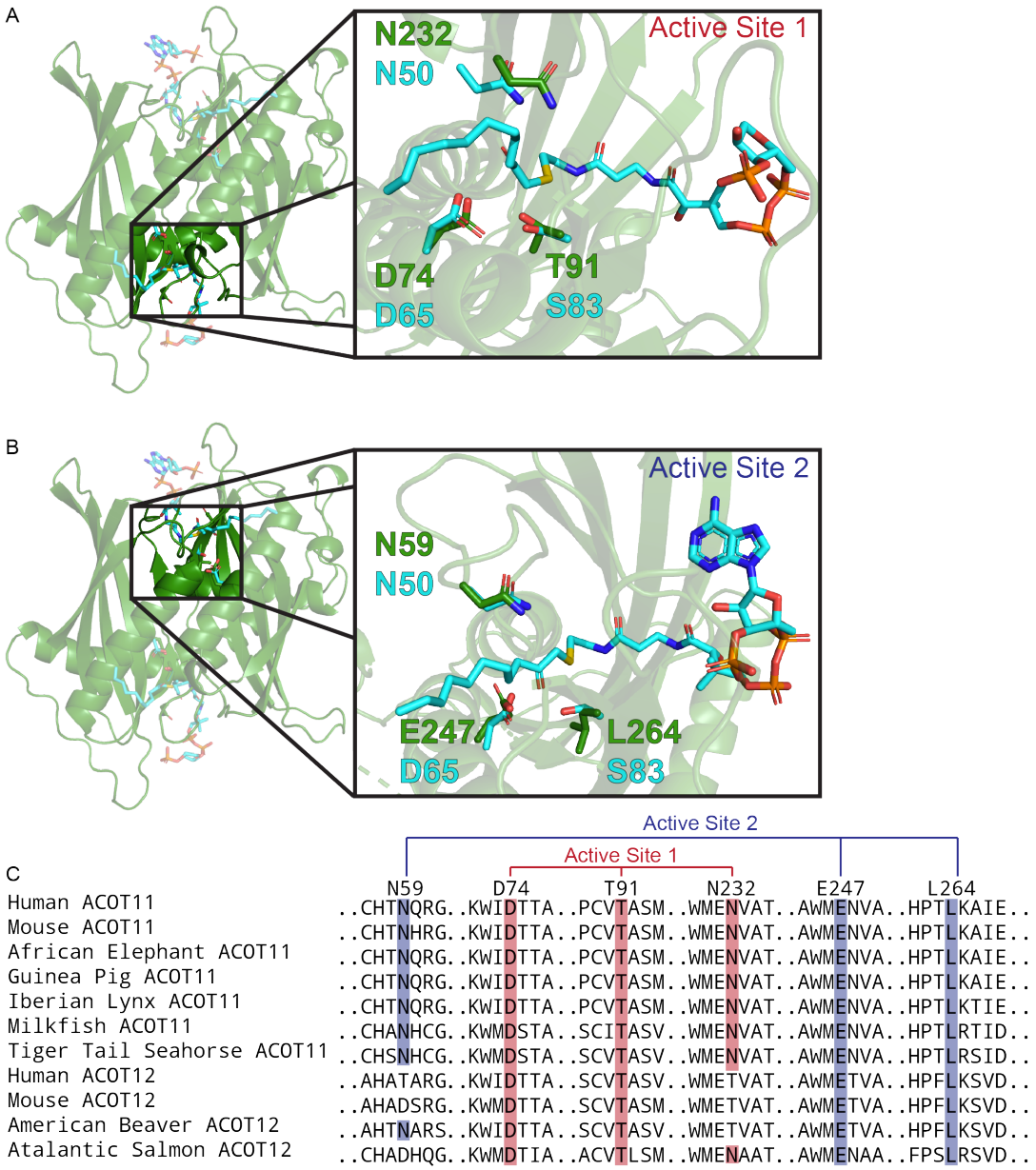

Figure 1. Them1 contains two putative active sites. *A-B.* Structural alignment on Them1 thioesterase domains model (green) with ACOT13 bound to undecane-2-one-coenzyme A (cyan) (PDB code: 3F5O). ACOT13 active site residues and putative Them1 active site residues are displayed as sticks. Zoomed in view of putative active site 1 (*A*) and active site 2 (*B*). *C.* Multiple sequence alignment of Them1 putative active site residues across Them1 homologs. Both putative active sites are highly conserved.

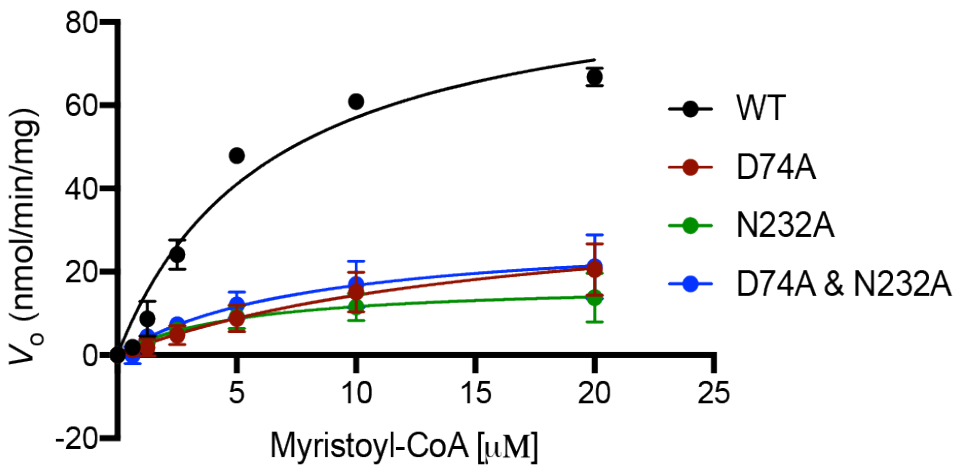

Figure 2. Asp74 and N232 are essential for catalysis of myristoyl-CoA. Thioesterase activity of wild type (black), D74A (red), N232A (green), and D74A & N232A (blue) *Homo Sapiens* Them1 thioesterase domains (1 μM) towards increasing amounts of myristoyl-CoA. Saturation curves of V_0 plotted against increasing myrstoyl-CoA with solid lines indicating nonlinear analysis of the data. Each point corresponds to the average of three replicates. Error bars represent standard error of the mean.

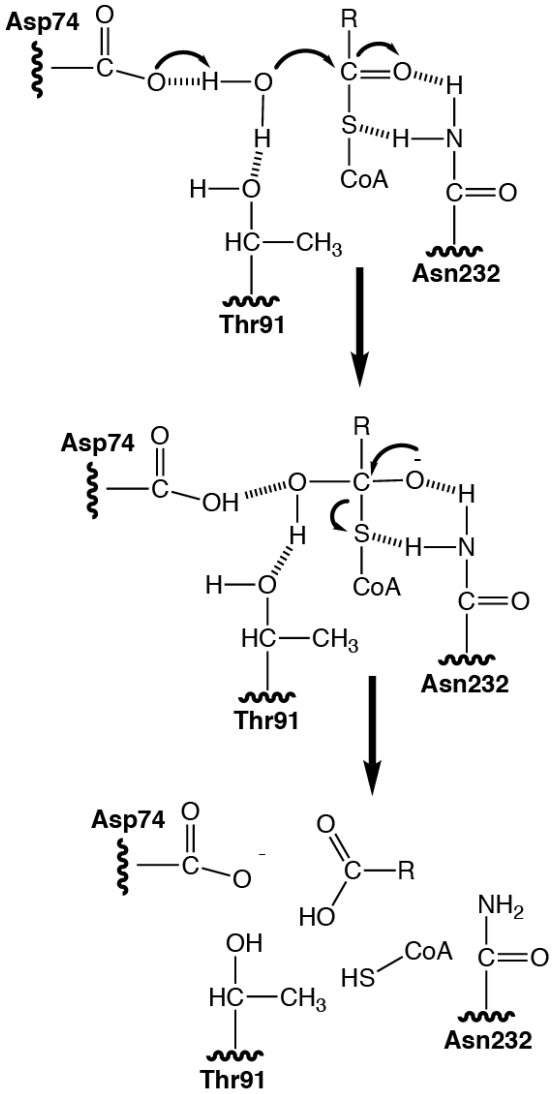

Figure 3. Enzymatic mechanism of Them1. Aps74 and Thr91 coordinate a water to attack the thioester carbon of acyl-CoA, forming a tertiary transition state that is stabilized by Asn232. The transition state collapses, releasing a free fatty acid and CoA. Schematic adapted from Cao. et. al. [6]

ADP and ATP bind to Them1 to regulate activity

The molecular mechanism by which the N-terminus and lipids through the StarD control Them1 activity have been elucidated, but how ADP/ATP mechanistically regulate Them1 is unknown. To test if ADP/ATP directly interacts with Them1, we titrated fluorescent an ATP analog, 2,4,6-trinitrophenol-ATP (TNP-ATP), into Them1 to measure binding. TNP-ATP bound to Them1 with an affinity of 21.5 μM (Fig. 4A). To determine if ADP/ATP altered Them1 oligomerization, we measured the size of the thioesterase domains using size exclusion chromatography and analytical ultracentrifugation in the presence of excess amounts of ADP or ATP. Regardless of the presence of ADP or ATP, the thioesterase domains remained primarily a trimer, suggesting, ADP and ATP do not alter the oligomeric state of Them1 (Fig. 4B-C). We then used differential scanning fluorometry (DSF) [16] to test if ADP/ATP alter the thermal stability of Them1. ATP slightly increased the thermal melting temperature (T_m) of Them1, however, ADP increased the T_m of Them1 ~2 degrees Celsius (Fig. 4D). To determine if this stabilization by ADP/ATP is distinct from Them1's interaction with substrate, we performed the same DSF experiment in the presence of CoA. Incubation with CoA alone greatly stabilized Them1 by ~4 °C. When ADP or ATP along with CoA were incubated with Them1, ADP and ATP increased the T_m relative to CoA alone to the same extent as when CoA was not present (Fig. 4D). Since the stabilization from ADP/ATP and CoA were additive, this suggests these molecules bind and stabilize discretely.

The thioesterase domains of ACOT12 were co-crystallized with ADP; therefore, we structurally aligned our Them1 model with the ACOT12-ADP structure to identify residues involved in ADP binding (Fig. 5A). Them1 residues within 3 Å of the ADP molecule were as follows: Lys285, Asn289, Cys301, Ser318, Arg347, Arg348, and Glu351. Asn289, Ser318,

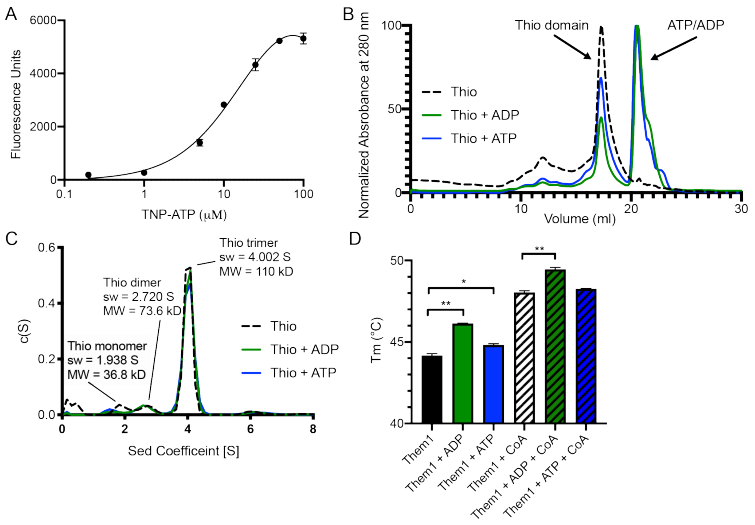

Figure 4. ADP/ATP directly bind and differentially stabilize Them1. *A.* TNP-ATP, which has enhanced fluorescence when bound to protein, was titrated into Them1 and lysozyme. Specific binding was calculated through subtracting background fluorescence (lysozyme + TNP-ATP) from Them1 samples at each TNP-ATP concentration. Curve represents average of two replicates. Error bars denote standard error of the mean. *B-C*. ATP and ADP do not alter the oligomerization of *Mus musculus* Them1 thioesterase domains as determined by size exclusion chromatography *(B)* and analytical ultracentrifugation *(C). B.* Size exclusion chromatography of thioesterase domains incubated with buffer (dotted line), ADP (green), or ATP (blue). *C.c(s)* distribution from sedimentation velocity analytical ultracentrifugation of thioesterase domains incubated with buffer (dotted line), ADP (green), or ATP (blue). The thioesterase domains purify primarily as a trimeric complex (~110 kD). *D.* Differential scanning fluorimetry of Them1 thioesterase domains incubated with either buffer (black), ADP (green), ATP (blue), CoA (striped), CoA + ADP (green striped), or CoA + ATP (blue striped). ADP and CoA discretely stabilize the thioesterase domains. Bars depict average of three replicates. Error bars denote standard error of the mean. One-way ANOVA and Dunnett's multiple comparisons test were used to analyze StarD data.

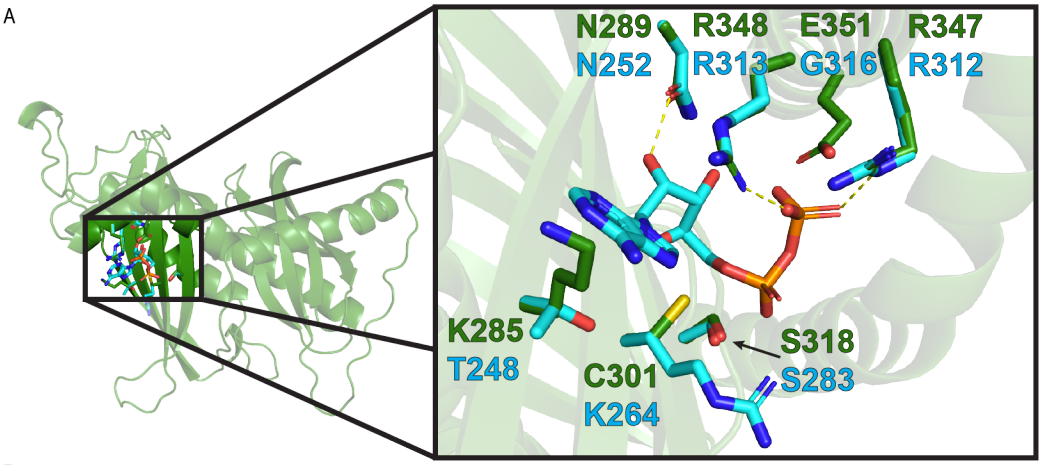

B

```
                                K285 N289       C301       S318     R347 R348 E351
Human ACOT11                  ..LVLKAIVNNAF..VGVCVEA..HINSAFM..DGERRYREASA..
Mouse ACOT11                  ..LVLKAIVNNAF..VGVCVEA..HINSAFM..EGERRYREASA..
African Elephant ACOT11       ..LVLKAIVNNAF..VGVCVEA..HINSAFM..DGERRYREASA..
Guinea Pig ACOT11             ..LVFKAIVNNAF..VGVCVEA..HINSAFM..DGERRYREAQA..
Iberian Lynx ACOT11           ..LVLKAIVNNAF..VGVCVEA..HINSAFM..DGERRYREASA..
Milkfish ACOT11               ..LVLKAIVNNAF..VGVCAEA..HINTAFM..DGKRRFQEAIA..
Tiger Tail Seahorse ACOT11    ..LVLKSIVNNAF..VGVCAEA..HINSAFM..DGKRRYQEAIA..
Human ACOT12                  ..LVFTAIVNNTF..VGVRVEA..HINSAFL..DDFRRYRGAIA..
Mouse ACOT12                  ..LVFSAIVNNTF..VGVRVEA..HINSAFL..DDFRRYQGAIA..
American Beaver ACOT12        ..LVFSATVNNTF..VGVRVEA..HINSAFL..DDFRRYQGAIA..
Atalantic Salmon ACOT12       ..LVFKAVVNNTF..VGVRVEA..HINSAFL..DGERRYLSAIV..
```

Figure 5. ADP/ATP binding site in Them1 is conserved. *A.* Structural alignment on Them1 thioesterase domains model (green) with ACOT12 bound to ADP (cyan) (PDB code: 4MOB). Residues 3 Å away from ADP are displayed as sticks. N289, R347, and R348 of Them1 are in position to electrostatically interact with ADP. *B.* Multiple sequence alignment of Them1 residues that putatively interact with ADP across Them1 homologs. N289, R347, and R348 are highly conserved.

Arg347, and Arg348 are highly conserved in Them1 homologs and present in ACOT12 (Fig. 5B). The two arginine residues and Ser318 are in position to electrostatically interact with the phosphate groups of ADP, and the asparagine residue is able to hydrogen bond with the hydroxyl groups of the ribose sugar (Fig. 5A). ADP/ATP also differentially regulate Acot activity of ACOT12, and interestingly, mutation of the conserved arginine residues ablates the effect of ADP/ATP on ACOT12 [7]. In the current alignment, Lys285 sterically clashes with ADP; therefore, ADP or Lys285 would adopt a slightly different conformation in a Them1-ADP crystal structure (Fig. 5A). Additionally, Glu351 of Them1 would potentially charge repulse the ADP phosphates in its current modeled location (Fig. 5A). The additional phosphate of ATP would sterically clash with Glu351, potentially explaining why ADP is more stabilizing than ATP.

Preliminary crystals of Them1 thioesterase domains

In order to better understand how ADP/ATP regulates Them1 activity and how Them1 interacts with its substrate, we set out to solve the crystal structure of the thioesterase domains of Them1 bound to ADP and CoA. We attempted to purify the thioesterase domains with several different N-terminal solubility tags, such as maltose binding protein (MBP), small ubiquitin-like modifier (SUMO), and glutathione S-transferase (GST); however, the protein would aggregate out of solution once concentrated. We hypothesized these issues with protein solubility were due to the removal of the C-terminal StarD, potentially exposing a hydrophobic patch leading to protein aggregation. Therefore, we generated an N-terminal His-tagged thioesterase domain construct with a C-terminal MBP tag with a simple four residue (Asn-Ala-Ala-Ala) linker between the last predicated helix of the thioesterase domains and MBP (Thio-MBP). The first 42 residues, which are predicted to be intrinsically disordered, were also removed to aid in

purification and crystallization. We were able to successfully purify Thio-MBP through Ni^{2+} affinity chromatography, ion-exchange chromatography, and size-exclusion chromatography (Fig. 6A-C). Thio-MBP purified as a trimer, just as full-length Them1 (**Chapter 4**) (Fig. 6C). The C-terminal MBP tag prevented protein aggregation as Thio-MBP was concentrated. We identified several buffer conditions that generated crystalline material through sitting-drop vapor diffusion, as diagramed in Table 1. We further optimized these conditions to produce single crystals that we were able to loop (Fig. 6D-E). However, these crystals did not diffract, preventing us from solving a structure.

Preliminary Cryo-EM structure of Them1

In **Chapter 4**, we reported a Them1 model, containing both the thioesterase domains and StarD, fitted into a negative stain map. This low-resolution map lacks detail needed to truly elucidate how the StarD interacts with the thioesterase domains. Therefore, we set out to determine a high-resolution cryo-EM structure of Them1 bound to ADP and CoA, which would enhance our understanding of how the StarD and ADP control Them1 activity. We purified ΔNterm-Them1 from *HEK293F* cells as described in **Chapter 4**. We optimized buffer conditions (20 mM Hepes pH 7.5 and 150 mM NaCl), protein concentration (0.2 mg/mL), and cryo grid freezing techniques (Vitrobot: 4°C, 100 % humidity) and screened the sample through an in house JEOL JEM1400 microscope for homogenous particle distribution and ice quality (Fig. 7). In order to solve a structure of Them1, we need to collect a large data set on the FEI Talos 200kV Artica instrument.

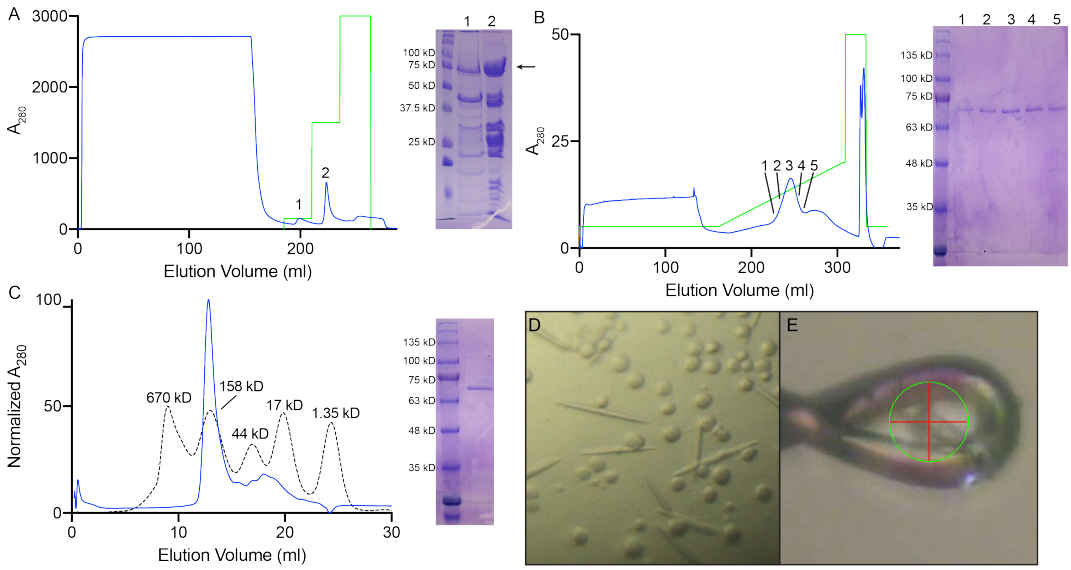

Figure 6. Purification and crystallization of trimeric Thio-MBP. *A.* Nickle affinity chromatography with His-tagged Thio-MBP. Blue line depicts A_{280} and green line displays elution steps with increasing amounts of elution buffer (20 mM Tris pH 7.4, 500 mM NaCl, 5 % glycerol, 500 mM imidazole; 5 %, 50 %, and 100 %). SDS-PAGE of protein elution at 5 % step (1) and 50 % step (2) of elution buffer. Arrow shows Thio-MBP at ~75 kD. *B.* Anion exchange chromatography with His-tagged Thio-MBP. Blue line depicts A_{280} and green line displays elution gradient with increasing amounts of elution buffer (20 mM Tris pH 7.4, 1 M NaCl; gradient: 10 – 40 % elution buffer over 30 column volumes). Thio-MBP eluted between 20 – 35 % elution buffer as determined by SDS-PAGE. *C.* Size exclusion chromatography of His-tagged Thio-MBP using S200 10/300 column. Lines depict normalized A_{280} for Thio-MBP (blue) and BioRad standards (dotted black). Thio-MBP purifies as a trimeric complex. SDS-PAGE verifies purity of Thio-MBP. *D.* Rod shaped crystals of Thio-MBP grown in 0.1 M Hepes pH 7.5, 0.066 M $MgCl_2$, 25 % PEG 400, 2 mM ADP, and 2 mM CoA at 4 mg/ml protein. *E.* Image of Thio-MBP crystal within loop from Advanced Photon Source, Argonne National Laboratory, 22ID beamline camera.

Table 1. Crystallization conditions that yield Thio-MBP crystals.

Buffer	Salt	Precipitant
0.1 M Hepes Na salt pH 7.5	0.2 M $MgCl_2$	30 % PEG 400
0.1 M Hepes pH 7.5	0.02 M $MgCl_2$	22 % Polyacrylic acid 5100 Na salt
0.2 M Na. Malonate		20 % PEG 3350
1.1 M Na. Malonate	0.1 M Hepes pH 7.0	0.5 % Jeffamine ED-2003

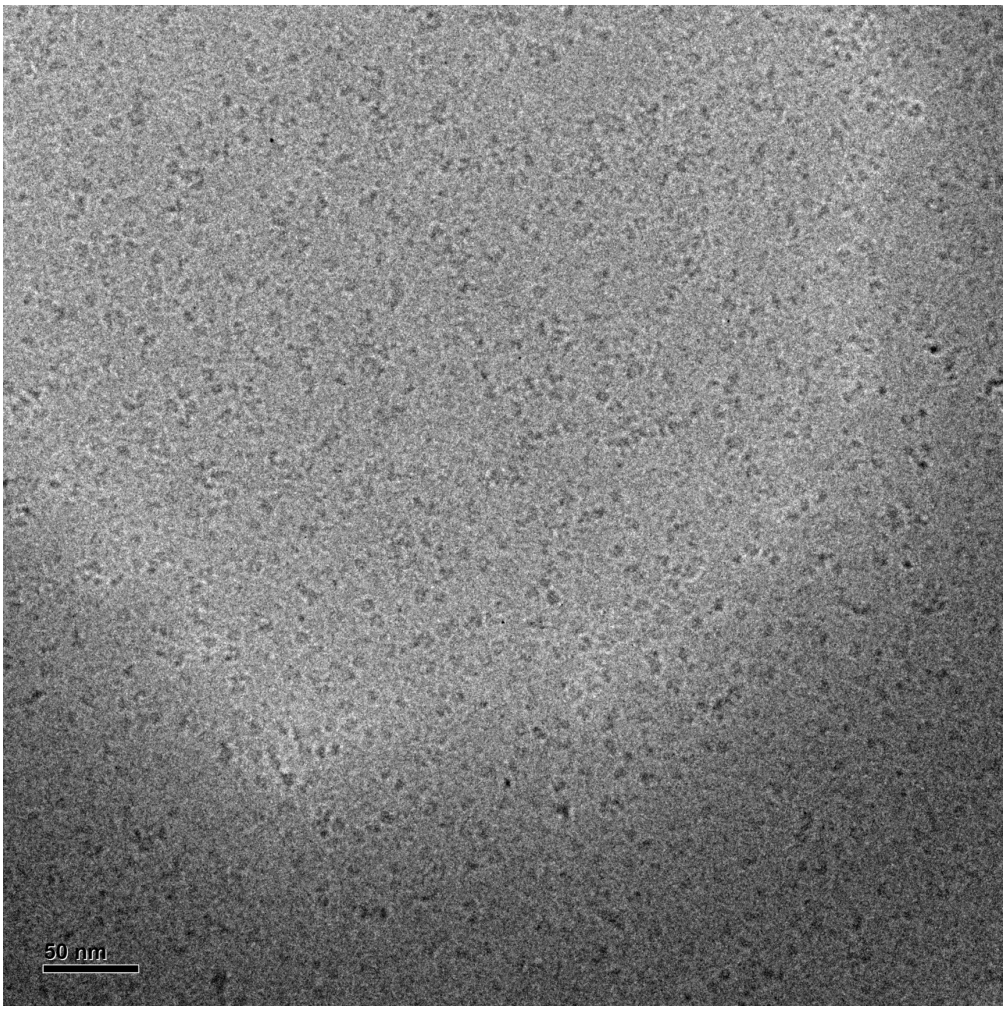

Figure 7. Preliminary cryo-EM image of Them1 homogenously spread across grid. Homogenous distribution of Them1 on frozen C-flat grid. Image obtained on a JEOL JEM1400 microscope at 40X magnification.

Discussion

Them1 regulates the availability of acyl-CoA that is used to fuel thermogenesis in brown adipose tissue. It does so through breaking the thioester bond of acyl-CoA to generate free fatty acids and CoA. The current study elucidates this enzymatic mechanism and identifies how ATP/ADP interact with Them1 to control its activity. Additionally, we show progress in determining the structure of Them1 and its thioesterase domains.

Them1, ACOT7 [15], and ACOT13 [6] all conserve the same enzymatic mechanism that utilizes aspartic acid and asparagine residues to catalyze the hydrolysis of acyl-CoA. This mechanism is likely conserved across all type II ACOTs, but this still needs to be tested. Given the high level of conservation at the site of catalysis for ACOTs, development of a specific ACOT11 inhibitor targeted for this site will be problematic; therefore, development of an allosteric inhibitor to achieve this goal is a more fruitful endeavor. Though Them1 contains two active sites, only one active site is responsible for the majority of catalysis. ACOT7 similarly contains two active sites with only one being catalytic [15]. Mutagenesis of the less active catalytic site in ACOT7 to the necessary Asp/Asn residues enhanced the enzymes ability to hydrolyze acyl-CoA, showing the enzyme contains the proper protein architecture to catalyze the reaction but lacks the necessary reactive amino acids to carry it out. It is likely that Them1, and other ACOTs containing two hot-dog domains, arose from a gene duplication event, and over time the second active site lost its activity since evolution selected more for the presence of Acot activity and not the quantity.

Our data show that ATP and ADP bind to Them1 and alter the thermal stability of the protein, which in turn regulates its activity. It is likely other nucleotides bind to Them1 and regulate its activity, as GDP and GTP also bind and regulate ACOT12 [7] as well as a bacterial

ACOT [17]. In ACOT12, ADP suppresses activity and is predicted to stabilize the enzyme by anchoring the C-terminal α-helix of the thioesterase domain and the α-helix between the hot dog domains, while ATP enhances activity presumably through clashing with these helices, allowing more flexibility between the domains [7]. Our data suggests that ADP and ATP interact with Them1 similarly. Taken together with the stabilizing effects of the StarD that enhance activity (**Chapter 4**), there is a complex interplay between rigidity and flexibility driven by compounds to regulate Them1 activity.

The importance of ADP/ATP regulation is highlighted by the presence of a missense mutation in Them1 (Arg348Trp) in a patient diagnosed with a lipid storage myopathy [18]. Based on our structural alignment, this mutation disrupts ADP/ATP binding, preventing Them1 from sensing the energy state of the cellular environment to regulate its activity. Though the patient also had mutations in electron transfer flavoprotein dehydrogenase, a key mitochondrial protein in the electron transport chain, our data suggests the mutation in Them1 has functional consequences as well.

A structure of Them1 and its thioesterase domains would enhance our understanding of how Them1 is regulated. Currently, there is only a low-resolution negative stain map of Them1, making it difficult to determine how the StarD interacts with the thioesterase domains. This study reports progress in structural studies with full-length Them1 and its thioesterase domains, but further optimization is required to obtain structures. The C-terminal MBP tag attached to the thioesterase domains, presumably mimicking the StarD, enabled us to purify and crystallize the domain. To obtain better crystals, the composition and length of the linker between the thioesterase domains and the MBP tag could be optimized. Additionally, we only further

screened one crystallization condition, while there are more conditions to explore that have yielded crystalline material (Table 1).

The dynamic between fatty acids and acyl-CoA must be tightly controlled for basic cellular processes such as lipid metabolism and lipid synthesis [1, 2]. ACOTs play a key role in regulating this process. This is evidenced by disease arising when ACOT activity and regulation is disrupted [18]. Therefore, studies like this are necessary to understand the pathogenesis of disease and potential therapeutic remedies.

Methods

Materials and reagents—Chemicals were purchased from Sigma-Aldrich, Polysciences Inc., and Cayman Chemical. The pMCSG7 (LIC_HIS) vector was provided by Dr. John Sondek (University of North Carolina at Chapel Hill). Codon-optimized Them1 DNA was synthesized by Genewiz (South Plainfield, NJ). DNA oligonucleotide primers were synthesized by IDT (Coralville, IA).

Protein expression and purification—The *Mus musculus* (residues 43 – 365) and codon optimized wild-type and mutant (D74A, N232A, and D74A-N232A) *Homo sapiens* (residues 41 – 364) Them1 thioesterase domains in the pMCSG7 vector were transformed into *Escherichia coli* strain BL21 (DE3) pLysS cells. The thioesterase domains were expressed as a His_6 fusion containing a tobacco etch virus protease cleavage site. Cultures (1 liters in LB) were grown to an A_{600} of ~0.6 - 0.8, and thioesterase domain expression was induced with 0.5 mM isopropyl β-d-1-thiogalactopyranoside at 18 °C for ~18 hours. Cell mass was harvested, lysed through sonication in a buffer containing 20 mM Tris HCl pH 7.4, 500 mM NaCl, 25 mM imidazole, 5% glycerol,

lysozyme, Dnase A, 5 mM beta-mercaptoethanol, and 100 uM phenylmethylsulfonyl fluoride. The thioesterase domains were purified by nickel affinity chromatography followed by SEC using a HiLoad 16/60 Superdex 200 column.

For crystallization work, maltose binding protein derived from pMCSG9 was inserted at the 3' end of the of the codon-optimized *Homo sapiens* (residues 41 – 364) Them1 thioesterase domains gene within the pMCSG7 vector, with a small linker coding for Asn-Ala-Ala-Ala between the two genes (Thio-MBP). Cultures (1 liters in LB) were grown to an A_{600} of ~0.6 - 0.8, and Thio-MBP expression was induced with 0.5 mM isopropyl β-d-1-thiogalactopyranoside at 18 °C for ~18 hours. Cell mass was harvested, lysed through sonication in a buffer containing 20 mM Tris HCl pH 7.4, 500 mM NaCl, 25 mM imidazole, 5% glycerol, lysozyme, Dnase A, 5 mM beta-mercaptoethanol, and 100 uM phenylmethylsulfonyl fluoride. Thio-MBP was purified by nickel affinity chromatography and diluted into a buffer containing 20 mM Tris HCl pH 7.4 and 100 mM NaCl. Thio-MBP was further purified through anion exchange chromatography, in which it eluted between 200 - 350 mM NaCl, followed by SEC using a HiLoad 16/60 Superdex 200 column.

Them1 was expressed and purified as previously described in **Chapter 4**. Briefly, *HEK293T* cells were stably transduced with pLVX-IRES-ZsGreen1 lentiviral vector containing wild-type *Mus musculus* Them1 including both thioesterase domains and START domain (residues 43 – 594). Them1 (MOI of 50) grown in suspension culture was harvested at a cell density of 2 million cells/ milliliter, and lysed through sonication in a buffer containing 20 mM Tris HCl pH 7.4, 500 mM NaCl, 25 mM imidazole, 5% glycerol, lysozyme, Dnase A, 0.1 % Triton X-100, 5 mM beta-mercaptoethanol, and 100 uM phenylmethylsulfonyl fluoride. Them1

was purified by nickel affinity chromatography followed by SEC using a HiLoad 16/60 Superdex 200 column.

Crystallization—Pure Thio-MBP was incubated with 2.5 mM ADP and CoA and concentrated to 5 mg mL^{-1} in 30 mM HEPES pH 7.5, 150 mM NaCl, 5 % glycerol, 0.5 mM tris(2-carboxyethyl)phosphine (TCEP). Crystals of Thio-MBP were grown via hanging drop vapor diffusion at 16 °C from solutions containing 1 μL Thio-MBP and 1 μL mother liquor (0.1 M Hepes HCl pH 7.5, 66 μM $MgCl_2$, and 25 % PEG 400).

TNP-ATP Binding Assay—Quantitation of ATP binding was conducted with a fluorescent analog of ATP, TNP-ATP (triethylammonium salt) (Cayman Chemical), which displays enhanced fluorescence when bound to a protein [19]. TNP-ATP was dissolved in 30mM Hepes pH 7.5, 100 mM NaCl, and 0.5 mM TCEP, and titrated (100 – 0.2 μM) into 4.5 μM of pure Them1 or chicken egg white lysozyme (Affymetrix) in the same buffer. Fluorescence values were obtained on a BioTek Synergy NEO plate reader using an excitation wavelength of 403 nm and an emission wavelength of 540 nm. Blank measurements containing lysozyme and TNP-ATP were subtracted from each probe concentration tested, and the resulting fluorescent values were fit with a One-Site binding curve to determine the binding constant, K_D. Curve is the average of two replicates.

Acyl-CoA thioesterase activity assay—Purified wild-type and mutant ((D74A, N232A, and D74A-N232A) *Homo sapiens* Them1 thioesterase domains in 30 mM Hepes pH 7.5, 150 mM NaCl, and 5 % glycerol, were incubated with 0.3 mM 5,5′-dithiobis-(2-nitrobenzoic acid)

(DTNB) for 30 minutes at 37 °C prior to measuring Acot activity. Protein concentrations were calculated using the Pierce™ BCA Protein Assay Kit (Thermo Scientific) and diluted to a final assay concentration of 1 μM. Acot activity was initiated upon the addition of myristoyl-CoA ranging from 0 – 20 μM. Plates were immediately introduced into a 37 °C temperature-controlled Synergy Neo 2.0 (BioTek) plate reader. Absorbance readings at 412 nm were read every 10 seconds for 1 hour. Enzyme initial velocities (V_0) were calculated through fitting a line to the rise in product formation in the early time points using GraphPad Prism 8.0 for each substrate concentration. The initial velocities were plotted against substrate concentrations and fitted with the Michaelis–Menten equation to yield the maximum velocity (V_{max}) and Km (the Michaelis constant) using GraphPad Prism 8.0. Values of kcat were calculated as kcat = Vmax/[E]. Each experiment was conducted with two technical replicates for each sample and repeated three times.

Analytical Ultracentrifugation—Mus musculus Them1 thioesterase domain samples were incubated with 200 μM ADP or ATP and SEC into 20 mM bis-Tris pH 8.5, 500 mM NaCl, and 0.5 mM tris(2-carboxyethyl)phosphine (TCEP) was used to remove nonspecifically bound nucleotide. Analytical ultracentrifugation experiments were carried out using a Beckman Coulter ProteomeLab™ XLI analytical ultracentrifuge equipped with both absorbance and interference optics and a four-hole An-60 Ti analytical rotor. Sedimentation velocity experiments were carried out at 10 °C and 50,000 rpm (200,000 × g) using 120-mm two-sector charcoal-filled Epon centerpieces with quartz windows. Each sample was scanned at 0-min time intervals for ~ 200 scans. Samples were run at ~0.5 mg/mL. Sedimentation boundaries were analyzed by the continuous distribution (c(s)) method using the program SEDFIT [20]. The program SEDNTERP,

version 1.09, was used to correct the experimental s value (s*) to standard conditions at 20 °C in water ($s_{20,w}$) and to calculate protein partial specific volume [21]. Corrected $s_{20,w}$ was used for molecular weight calculation.

Differential scanning fluorimetry (DSF)— Purified *Mus musculus* Them1 thioesterase domains at a concentration of 10 μM was incubated with ADP, ATP, and/or CoA at a concentration of 200 μM for 30 minutes at room temperature. SYPRO orange dye (Invitrogen) was then added at a 1:1000 dilution. Reactions were heated at a rate of 0.5 °C per minute, using a StepOne Plus Real Time PCR System (ThermoFisher). Fluorescence was recorded at every degree using the ROX filter (602 nm). Technical triplicates were analyzed by first subtracting baseline fluorescence (ligands + SYPRO with no protein) and then fitting the curves using the Bolzman equation (GraphPad Prism 8.0) to determine the Tm. Experiment was performed with three replicates and the Tm's of different ligands were analyzed in Prism 8.0 with one-way ANOVA and Dunnett's multiple comparisons test. **P< .0001; *P< 0.01.

Cryo EM with Them1—Purified Them1 was diluted to 0.2 mg/ml in 20 mM Hepes pH 7.5 and 150 mM NaCl. 3 μL of protein was deposited to a CF-1.2/1.3-3Cu grid that had been glow discharged for 20 seconds in negative mode. Temperature (4 °C) and humidity (100 %) were controlled by a FEI Vitrobot IV. Excess protein solution was blotted away for 3 seconds with vitrobot filter paper with a force of 0 prior to being plunged in liquid ethane. Frozen grids were visualized on JEOL JEM1400 microscope.

References

1. Grevengoed TJ, Klett EL, Coleman RA. Acyl-CoA metabolism and partitioning. Annual review of nutrition. 2014;34:1-30. Epub 2014/05/14. doi: 10.1146/annurev-nutr-071813-105541. PubMed PMID: 24819326; PMCID: PMC5881898.
2. Tillander V, Alexson SEH, Cohen DE. Deactivating Fatty Acids: Acyl-CoA Thioesterase-Mediated Control of Lipid Metabolism. Trends in endocrinology and metabolism: TEM. 2017;28(7):473-84. Epub 2017/04/08. doi: 10.1016/j.tem.2017.03.001. PubMed PMID: 28385385; PMCID: PMC5474144.
3. Ellis JM, Li LO, Wu PC, Koves TR, Ilkayeva O, Stevens RD, Watkins SM, Muoio DM, Coleman RA. Adipose acyl-CoA synthetase-1 directs fatty acids toward beta-oxidation and is required for cold thermogenesis. Cell Metab. 2010;12(1):53-64. Epub 2010/07/14. doi: 10.1016/j.cmet.2010.05.012. PubMed PMID: 20620995; PMCID: PMC2910420.
4. Okada K, LeClair KB, Zhang Y, Li Y, Ozdemir C, Krisko TI, Hagen SJ, Betensky RA, Banks AS, Cohen DE. Thioesterase superfamily member 1 suppresses cold thermogenesis by limiting the oxidation of lipid droplet-derived fatty acids in brown adipose tissue. Molecular metabolism. 2016;5(5):340-51. Epub 2016/04/26. doi: 10.1016/j.molmet.2016.02.002. PubMed PMID: 27110486; PMCID: PMC4837299.
5. Zhang Y, Li Y, Niepel MW, Kawano Y, Han S, Liu S, Marsili A, Larsen PR, Lee CH, Cohen DE. Targeted deletion of thioesterase superfamily member 1 promotes energy expenditure and protects against obesity and insulin resistance. Proc Natl Acad Sci U S A. 2012;109(14):5417-22. Epub 2012/03/20. doi: 10.1073/pnas.1116011109. PubMed PMID: 22427358; PMCID: PMC3325675.
6. Cao J, Xu H, Zhao H, Gong W, Dunaway-Mariano D. The mechanisms of human hotdog-fold thioesterase 2 (hTHEM2) substrate recognition and catalysis illuminated by a structure and function based analysis. Biochemistry. 2009;48(6):1293-304. Epub 2009/01/28. doi: 10.1021/bi801879z. PubMed PMID: 19170545; PMCID: PMC2929599.
7. Swarbrick CM, Roman N, Cowieson N, Patterson EI, Nanson J, Siponen MI, Berglund H, Lehtio L, Forwood JK. Structural basis for regulation of the human acetyl-CoA thioesterase 12 and interactions with the steroidogenic acute regulatory protein-related lipid transfer (START) domain. J Biol Chem. 2014;289(35):24263-74. Epub 2014/07/09. doi: 10.1074/jbc.M114.589408. PubMed PMID: 25002576; PMCID: PMC4148856.
8. Han S, Cohen DE. Functional characterization of thioesterase superfamily member 1/Acyl-CoA thioesterase 11: implications for metabolic regulation. J Lipid Res. 2012;53(12):2620-31. Epub 2012/09/21. doi: 10.1194/jlr.M029538. PubMed PMID: 22993230; PMCID: PMC3494255.
9. Li YA, L.H.; Hagen, S.J.; Cohen, D.E. N-Terminal Phosphorylation of Thioesterase Superfamily Member 1 (Them1) Regulates its Subcellular Localization in Brown Adipocytes. FASEB Journal2017.
10. Bienert S, Waterhouse A, de Beer TA, Tauriello G, Studer G, Bordoli L, Schwede T. The SWISS-MODEL Repository-new features and functionality. Nucleic acids research. 2017;45(D1):D313-d9. Epub 2016/12/03. doi: 10.1093/nar/gkw1132. PubMed PMID: 27899672; PMCID: PMC5210589.
11. Waterhouse A, Bertoni M, Bienert S, Studer G, Tauriello G, Gumienny R, Heer FT, de Beer TAP, Rempfer C, Bordoli L, Lepore R, Schwede T. SWISS-MODEL: homology modelling

of protein structures and complexes. Nucleic acids research. 2018;46(W1):W296-w303. Epub 2018/05/23. doi: 10.1093/nar/gky427. PubMed PMID: 29788355; PMCID: PMC6030848.
12. Guex N, Peitsch MC, Schwede T. Automated comparative protein structure modeling with SWISS-MODEL and Swiss-PdbViewer: a historical perspective. Electrophoresis. 2009;30 Suppl 1:S162-73. Epub 2009/06/12. doi: 10.1002/elps.200900140. PubMed PMID: 19517507.
13. Benkert P, Biasini M, Schwede T. Toward the estimation of the absolute quality of individual protein structure models. Bioinformatics (Oxford, England). 2011;27(3):343-50. Epub 2010/12/08. doi: 10.1093/bioinformatics/btq662. PubMed PMID: 21134891; PMCID: PMC3031035.
14. Bertoni M, Kiefer F, Biasini M, Bordoli L, Schwede T. Modeling protein quaternary structure of homo- and hetero-oligomers beyond binary interactions by homology. Scientific reports. 2017;7(1):10480. Epub 2017/09/07. doi: 10.1038/s41598-017-09654-8. PubMed PMID: 28874689; PMCID: PMC5585393.
15. Forwood JK, Thakur AS, Guncar G, Marfori M, Mouradov D, Meng W, Robinson J, Huber T, Kellie S, Martin JL, Hume DA, Kobe B. Structural basis for recruitment of tandem hotdog domains in acyl-CoA thioesterase 7 and its role in inflammation. Proc Natl Acad Sci U S A. 2007;104(25):10382-7. Epub 2007/06/15. doi: 10.1073/pnas.0700974104. PubMed PMID: 17563367; PMCID: PMC1965522.
16. Kohlstaedt M, von der Hocht I, Hilbers F, Thielmann Y, Michel H. Development of a Thermofluor assay for stability determination of membrane proteins using the Na(+)/H(+) antiporter NhaA and cytochrome c oxidase. Acta Crystallogr D Biol Crystallogr. 2015;71(Pt 5):1112-22. Epub 2015/05/07. doi: 10.1107/s1399004715004058. PubMed PMID: 25945577.
17. Khandokar YB, Srivastava P, Cowieson N, Sarker S, Aragao D, Das S, Smith KM, Raidal SR, Forwood JK. Structural insights into GDP-mediated regulation of a bacterial acyl-CoA thioesterase. J Biol Chem. 2017;292(50):20461-71. Epub 2017/10/04. doi: 10.1074/jbc.M117.800227. PubMed PMID: 28972175; PMCID: PMC5733585.
18. Goh LL, Lee Y, Tan ES, Lim JSC, Lim CW, Dalan R. Patient with multiple acyl-CoA dehydrogenase deficiency disease and ETFDH mutations benefits from riboflavin therapy: a case report. BMC medical genomics. 2018;11(1):37. Epub 2018/04/05. doi: 10.1186/s12920-018-0356-8. PubMed PMID: 29615056; PMCID: PMC5883299.
19. Moutin MJ, Cuillel M, Rapin C, Miras R, Anger M, Lompre AM, Dupont Y. Measurements of ATP binding on the large cytoplasmic loop of the sarcoplasmic reticulum Ca(2+)-ATPase overexpressed in Escherichia coli. J Biol Chem. 1994;269(15):11147-54. Epub 1994/04/15. PubMed PMID: 8157641.
20. Schuck P. Size-distribution analysis of macromolecules by sedimentation velocity ultracentrifugation and lamm equation modeling. Biophysical journal. 2000;78(3):1606-19. Epub 2000/02/29. doi: 10.1016/s0006-3495(00)76713-0. PubMed PMID: 10692345; PMCID: PMC1300758.
21. Laue TMS, B.D., Ridgeway, T.M.; Pelletier, S.L. Computer-aided interpretation of analytical sedimentation data for proteins. Royal Society of Chemistry, Cambridge. 1992;Analytical ultracentrifugation in biochemistry and polymer science:90–125.

CHAPTER 5: DISCUSSION

This work contributes to our understanding of how lipid transfer proteins (LTPs) recognize specific lipids, and how lipids regulate LTP activity. This study counters the notion that LTPs are simply passive carriers of lipids. We provide multiple lines of evidence that LTPs are active participants in lipid signaling events, tuned to respond to specific lipids. Using structural and biochemical techniques, we showed that a lipid chaperone LTP plays a vital role in regulating aging (**Chapter 2**) and a lipid sensor LTP is responsible for controlling thermogenesis in brown adipose tissue (**Chapter 3**). These mechanistic insights help us understand the diverse physiological effects of lipids and enables us to better pharmacologically regulate these processes. In this concluding chapter, we will review the findings from the previous chapters, making connections with other relevant research, and end through outlining future directions for the field as a whole.

Lipid Chaperone the Extends Life

In **Chapter 2**, we investigated how Lipid Binding Protein 8 (LBP-8) extends lifespan in *C. elegans* (Fig. 1). LBP-8 was previously identified to mediate the life extending properties of lysosomal acid lipase (LIPL-4) through carrying lysosomal lipids to nuclear receptors to regulate transcription of life extending genes [1]. We solved the first structure of LBP-8, allowing us to identify residues putatively involved in lipid binding and a nuclear localization signal (NLS) that enables LBP-8 to control the expression of life-extending genes. Additionally, we discovered that LBP-8 binds to saturated and unsaturated long-chain fatty acids, showing a preference for oleic acid (18:1). Though LBP-8 binds a range of lipids, only select lipids activate its life prolonging properties. Oleoylethanolamide (OEA), a monounsaturated fatty amide, was previously shown to bind LBP-8 with high affinity and extend lifespan in *C. elegans* [1]. In

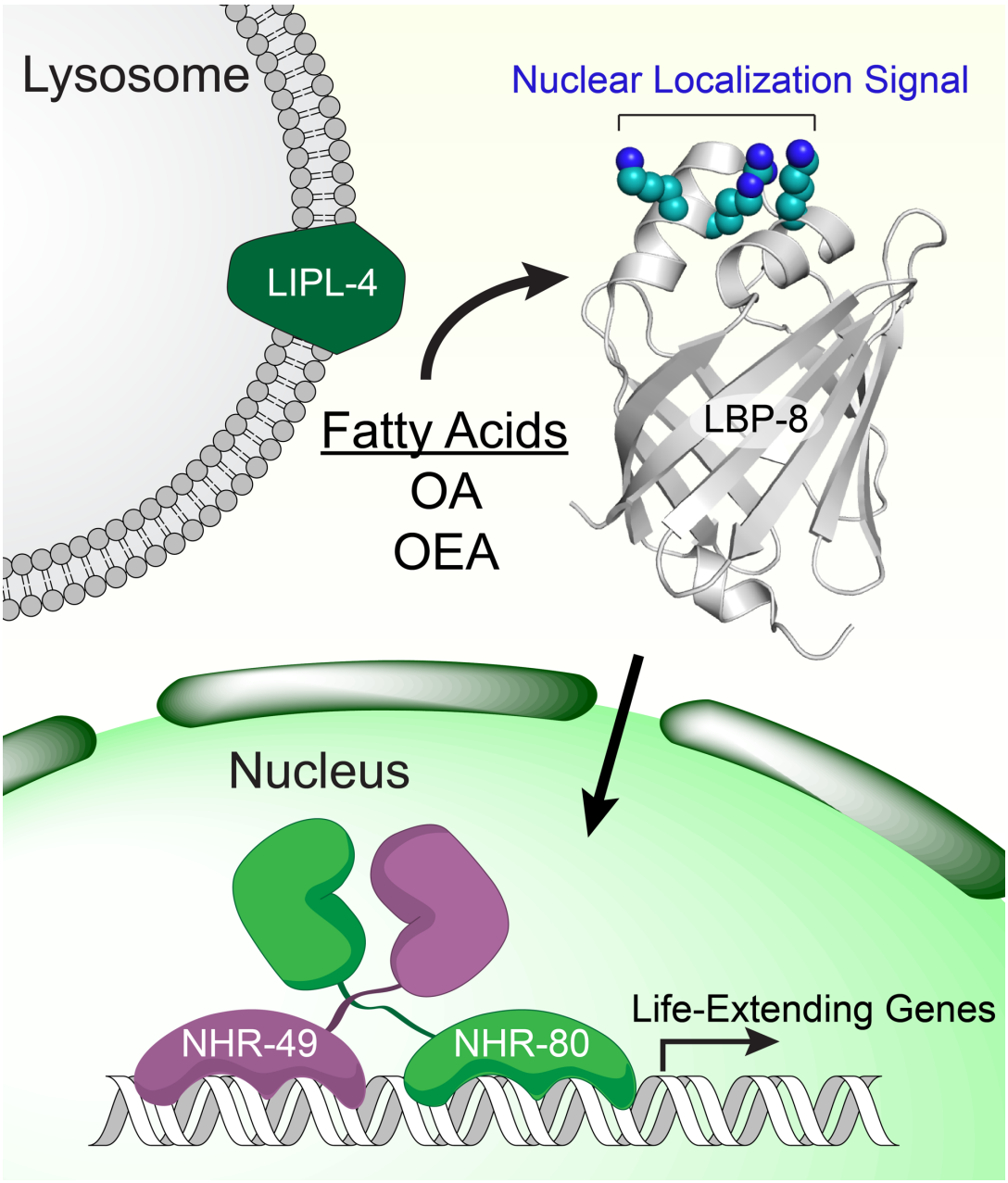

Figure 1. LBP-8 extends lifespan in *C. elegans* through carrying lysosomal fatty acids to nuclear receptors. LIPL-4 frees fatty acids from the lysosome, such as oleic acid (OA) and oleoylethanolamide (OEA). These life-extending fatty acids bind to LBP-8, activating the nuclear localization signal to stimulate nuclear transport of the fatty acids. While in the nucleus, LBP-8 regulates the activity of NHR-49 and NHR-80 to control expression of life-extending genes.

conjunction with this, oleic acid is also reported to extend lifespan in *C. elegans* [2], putatively through LBP-8.

The mechanism by which certain lipids activate FABP translocation to the nucleus to carry ligands to nuclear receptors has been investigated prior [3-7]. CRABPII [3], FABP4 [4], and FABP5 [5] all contain an NLS, similar to LBP-8, that is stabilized upon ligand binding, enabling interaction with importins for nuclear transport [8]. This process only occurs when "activating" ligands bind: retinoic acid activates CRABPII [3], PPARγ agonists activate FABP4 [4], and PPARβ/δ agonist activate FABP5 [5]. Furthermore, CRABPII transfers retinoic acid to retinoic acid receptor through a transient interaction mediated by an electrostatic patch on the surface of CRABPII [9, 10]. FABP1 and FABP2 also transfer lipids to the nucleus to regulate transcription, but through a different mechanism independent of an NLS. FABP1 and FABP2 passively diffuse into the nucleus and accumulate there due to decreased egress driven by specific lipids [6]. Similar to CRABPII, lipid binding to FABP1 induces a conformational change in an electrostatic surface patch that enables interaction with PPARα [7]. Up to this point, these are the only human FABPs that have been characterized to signal to the nucleus; however, more human FABPs, like FABP12 and FABP8, contain a putative NLS that remains to be verified.

Additional Lipid Chaperones that Extend Life

Given the life-extending properties of LBP-8, it is possible additional FABPs extend lifespan in *C. elegans*. Recently, our collaborator, Dr. Meng Wang of Baylor College of Medicine, identified LBP-2 and LBP-3 in *C. elegans* also extend lifespan in coordination with LIPL-4, similar to LBP-8 (all data regarding LBP-2 and LBP-3 is shown in appendix). We show that both LBP-2 and LBP-3 directly bind to C20-PUFAs, lipids necessary for life extension in *C.*

elegans. Additionally, we solved the first structure of LBP-3, which shows a novel dimeric state, potentially revealing how FABPs interact with each other. Both LBP-2 and LBP-3 contain a secretory sequence, and putatively extend lifespan by carrying C20-PUFAs from the muscle and fat storage tissue respectively to neurons to regulate expression of neuronal life-extending genes. As a whole, this cumulative work on LBPs in *C. elegans* has uncovered novel mechanisms by which these lipid chaperones propagate lipid signals intra- and extracellularly to extend lifespan.

As humans age, autophagy processes begin to slow, which can lead to a variety of diseases [11]. However, enhancement of autophagy through caloric restriction [12] or through genetic means, for instance through overexpression of LIPL-4 [13], which plays a key role in autophagy within the lysosome of *C. elegans*, extends lifespan. LBP-2, LBP-3, and LBP-8 [1] are necessary for the life extending properties of LIPL-4, suggesting these LBPs mediate the lipid driven downstream effects of autophagy in *C. elegans*. Similarly, overexpression of a FABP in *Drosophila melanogaster* leads to lifespan extension that is through a similar mechanism as caloric restriction [14]. These data suggest FABPs function during fasting and when autophagy is activated to extend lifespan.

Interestingly, FABPs in mice and humans are linked to the pathophysiology of metabolic disorders rather than promoting healthy aging [15, 16]. Elevated levels of FABP4 is linked to obesity and a variety of metabolic disorders [17]. Furthermore, inhibition of FABP4 and FABP5 with small molecules has proven effective at treating many of these disorders [18]. Deletion of FABP4 and FABP5 in mice improves metabolic health into old age similarly to caloric restriction, but deletion of these FABPs surprisingly does not extend lifespan like caloric restriction [19]. Though removal FABPs improves metabolic parameters in mammals, they may still be necessary to extend lifespan through caloric restriction as seen in *C. elegans* and *D. melanogaster*. The

difference between the advantageous effects of FABPs in studies with *C. elegans* and *D. melanogaster* and deleterious effects of FABPs observed in mammals may be explained by the difference in nutritional states and biological readouts between these studies. FABPs likely evolved a useful role in conditions of fasting and stress to propagate autophagy, mobilize needed metabolic resources, and activate key inflammatory pathways, which together extend lifespan as seen in *C. elegans* and *D. melanogaster*; however, these roles are deleterious in the common state of overnutrition within our society leading to obesity and metabolic disorders.

Lipid Sensor that Regulates Thermogenesis

Thioesterase superfamily member 1 (Them1) suppresses thermogenesis in brown adipose tissue in order to conserve energy reserves [20]. It does so through hydrolyzing acyl-CoA, preventing the utilization of the substrate as fuel for thermogenesis [21, 22]. Since Them1 expression is highly upregulated in brown adipose tissue upon adrenergic stimulation of the tissue [23], we suspected there were post-translational mechanisms to regulate Them1 activity in order to relieve Them1 inhibition of thermogenesis when needed. We recently identified that phosphorylation of the N-terminus regulates Them1 localization and in turn alters Them1's ability to suppress thermogenesis. When brown adipose tissue is activated through adrenergic stimulation, PKCβ phosphorylates S15 of Them1, which disrupts Them1 puncta localized at the lipid droplet – mitochondrial interface, and distributes Them1 throughout the cell, thus relieving Them1 suppression of thermogenesis [24]. In **Chapter 4**, we investigated how ADP and ATP inversely regulate Them1 activity through directly binding and altering the stability of Them1. This allows Them1 to sense the energetic state of the cell and finetune its activity. In **Chapter 3**, we elucidated the role of the StAR-related lipid transfer domain (StarD) of Them1 to control

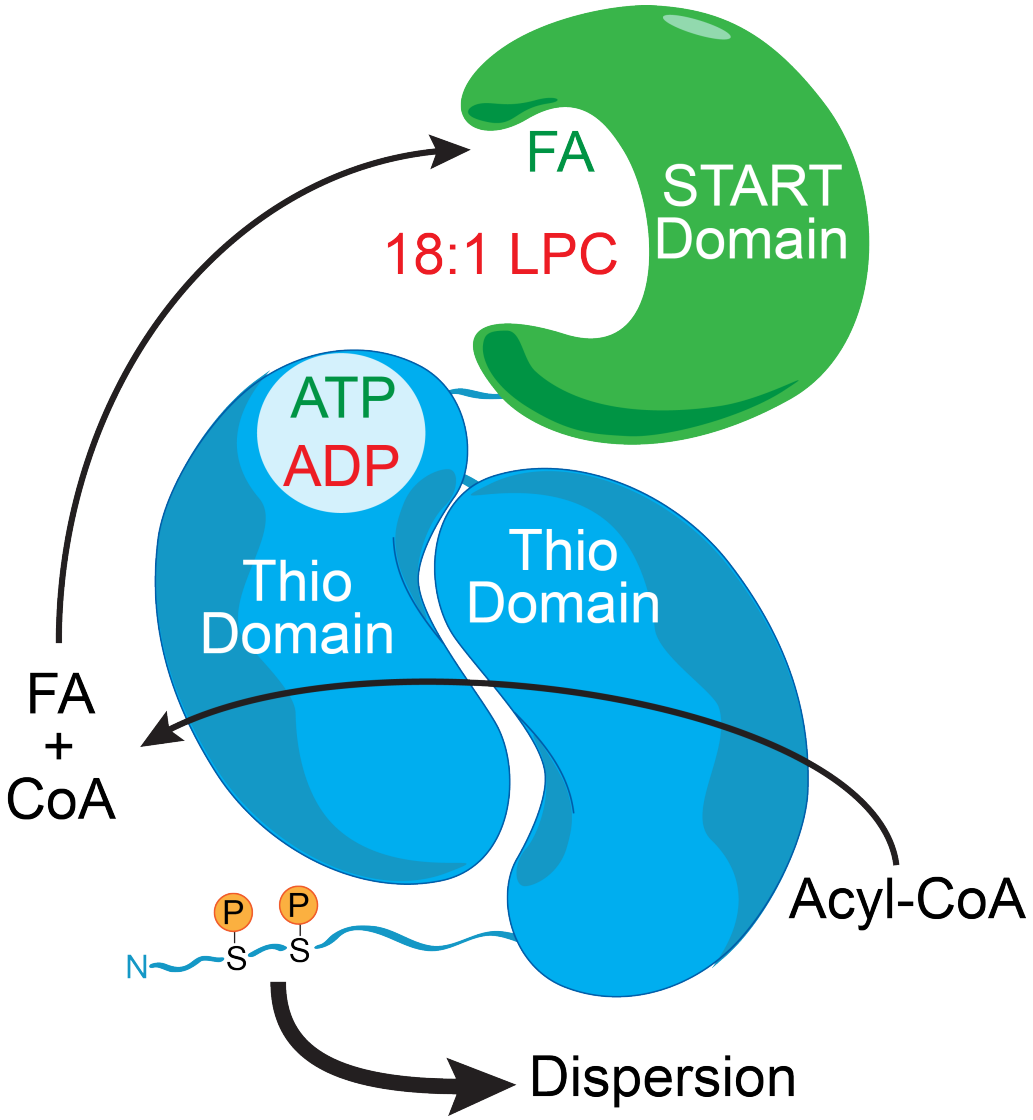

Figure 2. Schematic of the multiple layers of regulation of Them1 activity. There are three identified mechanisms that regulate Them1 activity. One, phosphorylation of serines in the N-terminus leads to dispersion of Them1 throughout the cell, which lowers Them1 mediated suppression of thermogenesis. Two, ATP and ADP bind to the thioesterase domains and allosterically regulate Acot activity (**Chapter 4**). Third, fatty acids and 18:1 LPC bind to the START domain and differentially regulate Acot activity (**Chapter 3**). Them1 ligands colored green enhance Acot activity, while red colored ligands inhibit Acot activity. Orange circle enclosing a "P" signifies serine phosphorylation.

thermogenesis. We identified that long-chain fatty acids, which are the products of Them1's enzymatic reaction [21], and lysophosphatidylcholine (LPC) bind to the StarD and inversely regulate Them1's enzymatic activity. Palmitic acid and myristic acid enhance, while 18:1 LPC inhibits Them1's activity. Furthermore, the lipids alter the stability of Them1; fatty acids stabilize, and 18:1 LPC destabilizes. Additionally, 18:1 LPC inhibited Them1 activity in an immortalized brown adipocytes cell line, relieving Them1 mediated suppression of thermogenesis. These data describe the StarD as a lipid sensor, evolved to recognize specific lipids to fine tune Them1 activity. These three mechanisms act as molecular switches, allowing for tight control of Them1 function, activating the enzyme when energy conservation is needed, and inhibiting the enzyme when there is a need for heat production.

In addition to the StarD of Them1 serving as a lipid sensor, we show it also regulates Them1 localization. Wild-type Them1 localizes in puncta near the surface of the lipid droplet and mitochondria. However, when the StarD is removed, Them1 puncta are no longer present at the lipid droplet – mitochondrial interface but are dispersed within the cytosol. A previous study showed Them1 attaches to a lipid coated surface through the StarD [25], though we were unable to experimentally show Them1 directly interacts with a membrane surface. The functional purpose of this localization is currently not understood since removal of the StarD did not prevent Them1 from suppressing thermogenesis. The StarD could potentially act as a lipid chaperone or lipid transporter at the lipid droplet surface, as many StarDs are involved in transporting specific lipids to cellular compartments [26, 27]. Given that Them1 distributes throughout the cell upon phosphorylation of its N-terminus [24], the StarD is a prime candidate to transfer lipids from the lipid droplet to other organelles. In line with this, the StarD of Them1 localizes to the nucleus where it possibly regulates transcription [28].

Additional Lipid Sensors that Regulate Thioesterase Activity

Acyl-CoA thioesterase 12 (ACOT12) is a close paralog of Them1, also containing two N-terminal hot-dog fold thioesterase domains and a C-terminal StarD. ACOT12 similarly is regulated by ADP/ATP [29] and the StarD putatively binds to lipids [30], though its endogenous ligand is not identified. ACOT12 differs from Them1 in that it preferentially hydrolyzes acetyl-CoA and does not contain an intrinsically disordered N-terminus that is phosphorylated like Them1 [31, 32]. Removal of the StarD significantly attenuates ACOT12 activity, suggesting the StarD allosterically controls ACOT12 activity, similar to Them1. It was previously shown that phosphatidic acid and lysophosphatidic acid inhibited ACOT12 activity through interaction with the StarD, though these lipids were not detected to bind *in vitro* [30].

Phosphatidylcholine transfer protein (PCTP, StarD2) contains a single StarD and no thioesterase domains, though it binds to thioesterase superfamily member 2 (Them2) and regulates its enzymatic activity [33, 34]. Them2 contains a single hot-dog fold thioesterase domain that oligomerizes in order to hydrolyze long-chain acyl-CoA [35]. PCTP enhances Them2 activity to the greatest extent at a PCTP:Them2 ratio of 1:2 [34], which is consistent with Them1 and ACOT12 containing two thioesterase domains and one StarD. Interestingly, PCTP also enhances the activity of the thioesterase domains of Them1 when added in *trans*, suggesting this StarD allosteric control of hot-dog fold thioesterase activity is a shared mechanism across Them1, ACOT12, and PCTP/Them2.

In this work, we propose the StarD of Them1 controls thioesterase activity through altering the stability of the enzyme. StarD ligands influence stability and in turn alter enzymatic activity. Moving forward, it should be tested if the StarD of ACOT12 and StarD2 alter the stability of the ACOT12 and Them2 enzymes respectively. Additionally, StarD ligands should be

identified and examined if they alter stability and enzyme activity. Enhancing our understanding of how StarDs regulate thioesterase enzymes will aid in our goal to pharmacologically perturb these systems. In **Chapter 4**, we show that Them1, ACOT12, and Them2 all share the same enzymatic mechanism; therefore, creating a specific competitive inhibitor for these enzymes would be technically difficult. However, generating allosteric inhibitors that specifically target the StarDs could be effective.

Future Directions of the Field

This study has focused on what lipids bind to specific LTPs and how these lipids alter LTP activity. This work is necessary, as many endogenous ligands for LTPs remain unidentified, though this can be tedious because LTPs commonly bind many lipids but are only activated by a select few. Therefore, LTP activity assays must be utilized to probe the effect of all binding lipids. This, however, only touches one aspect of LTP biology. A major future direction for LTP research is identifying downstream effectors of LTPs. This is the next step in uncovering how lipids signal and the physiological roles of LTPs.

Some protein effectors of LTPs have already been identified. As already discussed, nuclear receptors (NRs) are known downstream effectors of FABPs, though only a few FABP/NR interactions have been investigated. Some lines of evidence suggest that NRs are also downstream effectors of StarDs. For one, many NRs are activated by the cargo of StarDs: oxysterols activate liver X receptors (LXR) [36] and phosphatidylcholines activate liver receptor homolog-1 (LRH-1) [37]. Second, the activity of some NRs is altered in the presence of StarDs [38, 39]. Third, mammalian StarDs activate transcription when fused to a DNA binding domain in

yeast [40]. Lastly, StarDs in plants serve as transcription factors [41]. In light of the limited amount of current evidence, there is need for a comprehensive analysis into which LTPs and NRs interact.

There are many routes that can be taken to identify LTP/NR interactions. Yeast two-hybrid and affinity purification-mass spectrometry techniques can effectively identify interacting partners, but both have their caveats as they use an unnatural cell system and can miss transient interactions respectively. Protein-fragment complementation assays (PCAs) are an efficient alternative that allow for the detection of protein-protein interactions (PPIs) in a live cellular environment [42]. We used this system [42], in which we fused a split NanoLuc luciferase enzyme to the N-terminus of LTPs and NRs, in order to probe LTP/NR PPIs (Fig. 1A). As LTPs and NRs interact, the split NanoLuc luciferase will reversibly form an active enzyme, allowing us to identify and quantify the strength of these PPIs (Fig. 1A). We carried out this PPI screen with a large number of FABPs, StarDs, NRs, and other potential LTP effectors, such as acyl-CoA thioesterases. As expected, we identified a number of PPIs that were previously identified, such as CRABPII strongly interacting with RAR-β [9, 10] and FABP5 interacting with PPAR-δ [5] (Fig. 1B). Interestingly, we discovered several novel interactions. Many of these novel PPIs were logical as the LTP and effector bind to similar ligands, such as StAR interacting with LXR-α (both can bind sterols [36, 43, 44]) and PCTP interacting with PPAR-δ (both can bind phospholipid [45, 46]) (Fig. 1B). Some interactions were unexpected, such as the multiple LTPs that interacted with the steroid receptors (GR and AR) (Fig. 1B). Moving forward, these PPIs should be verified with a corresponding PPI experiment.

We tested the functional significance of PCTP interacting with PPAR-δ and found PCTP suppresses the transcriptional activity of PPAR-δ. Silencing PCTP expression in Huh7 cells enhanced the transcriptional activity of PPAR-δ as determined through qRT-PCR (Fig. 2A).

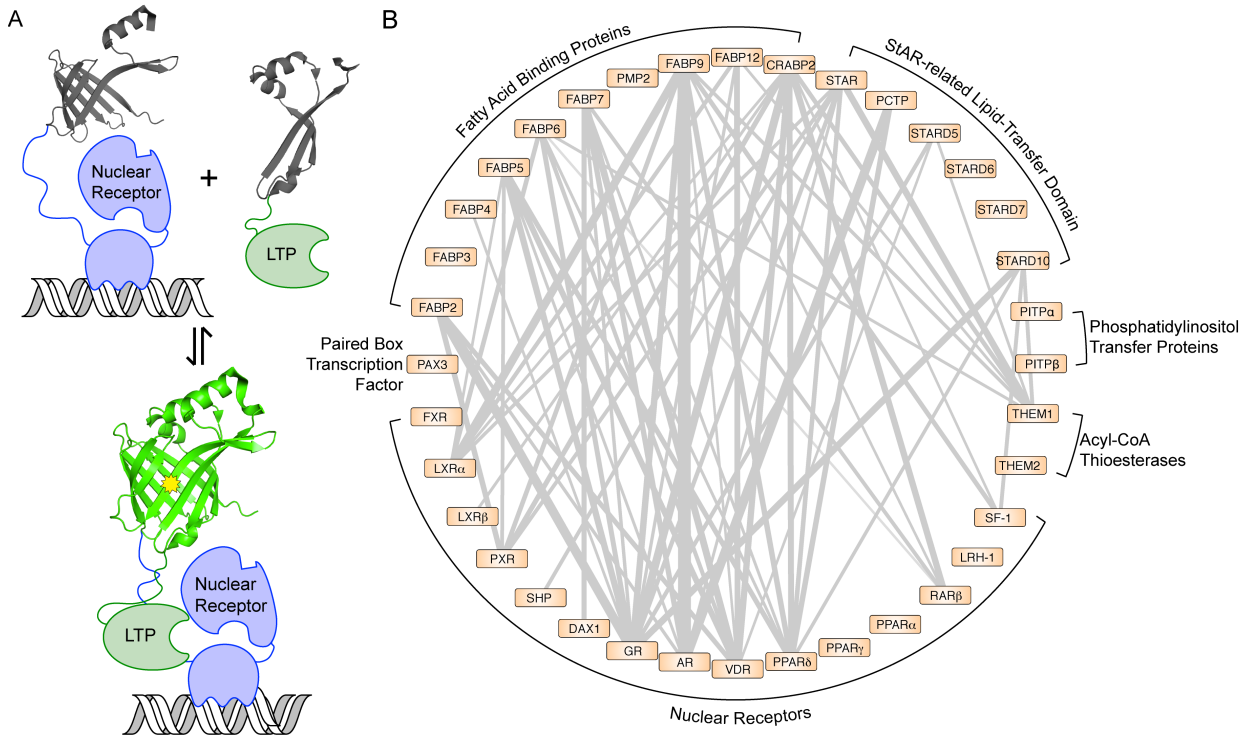

Figure 3. LTPs interact with a diverse array of effector proteins. *A.* Schematic of LTP-nuclear receptor (NR) NanoLuc luciferase PCA. N-terminal half of NanoLuc luciferase enzyme (residues 1-67) is fused to N-terminus of LTP, while C-terminal half of NanoLuc luciferase enzyme (residues 67-171) is fused to N-terminus of NR. When LTP and NR interact, NanoLuc protein fragments join to form active NanoLuc luciferase enzyme, allowing for a quantitative readout of the interaction through measuring luminescence. *B.* LTP-Effector PCA screen. Width of lines depict strength of interaction; fold change of 10 over negative control (enzyme fragment alone) is needed to display line. Proteins are grouped by protein families. Experiment performed with four replicates.

Furthermore, genetically deleting PCTP in mice increases the expression of known PPAR-δ target genes in the liver as compared to wild-type mice (Fig. 2B). This novel PPI example displays the effectiveness and utility of the NanoLuc luciferase PCA screen to identify LTP effectors. Additionally, this screen can be expanded to include more LTPs and possible effectors to further probe LTP biology.

The PPI screen is useful in identifying LTP effectors, yet the mechanism by which LTPs interact with these effectors remains to be explored. In the context of NR effectors, it is presumed that LTPs transfer NR ligands to the NR ligand binding pocket to regulate their activity; however, this has never been experimentally shown. To test this, nuclear magnetic resonance could be utilized to detect the loss of lipid from a lipid pre-loaded LTP upon interaction with a NR, moreover lipid transfer to apo-NR could also be detected. It is possible LTPs do not transfer lipids to NRs but still regulate their activity. LTPs could alter NR post-translational modifications or bind and allosterically regulate NR activity, acting as a lipid sensor to control NR function.

Utility of LTPs as Drug Targets

Disruption of some LTPs contributes to the pathophysiology of diseases. For instance, mutations in StAR leads to lipoid adrenal hyperplasia, which is characterized by disruptions in adrenal and gonadal steroidogenesis [47]. Multiple studies have shown a positive correlation between circulating FABP4 and obesity and diabetes [17, 48]. Furthermore, genetic deletion or overexpression of LTPs in mice leads to disease-like phenotypes [16, 49]. These studies show LTPs play a key role in disease progression, and pharmacologically targeting them could prove beneficial. As evidence of this, a small molecule inhibitor of FABP4 protected genetically obese

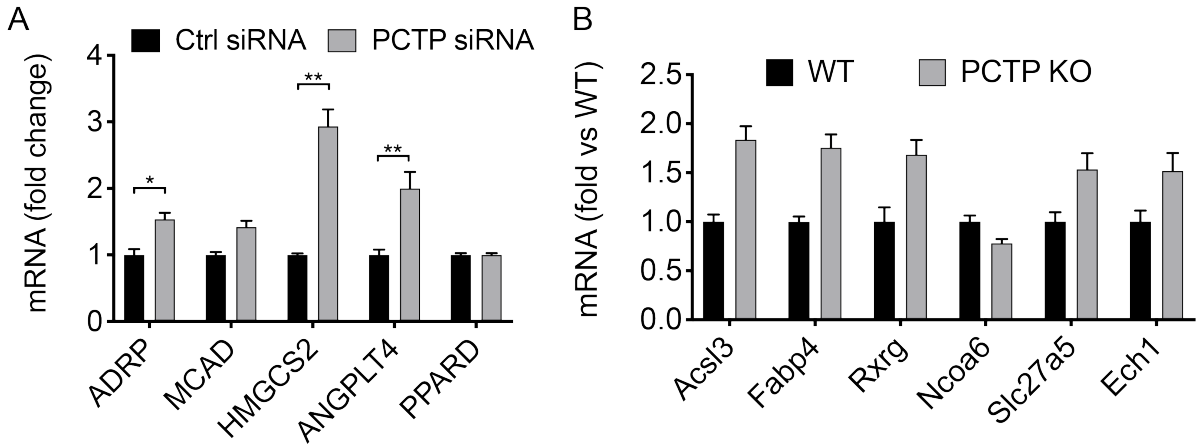

Figure 4. PCTP suppresses PPAR-δ transcriptional activity. *A.* Knock down of PCTP in Huh7 cells increases expression of PPAR-δ target genes as determined through qRT-PCR. Bars depict average from three replicates. Error bars represent standard error of the mean. Two-way ANOVA with a Sidak multiple comparisons test was used to analyze the data. * $P<0.05$, ** $P<0.0001$. *B.* Preliminary data of qRT-PCR microarray of PPAR controlled genes in liver tissue. Expression of PPAR target genes are elevated in mice lacking PCTP. Bars depict average from three mice. Error bars show standard error of the mean. Data credited to Dr. Suzanne Mays.

mice from hepatic steatosis, insulin insensitivity, and adipose tissue inflammation [18]. Many LTPs are prime drug targets because they are tissue specifically expressed, allowing for better drug pharmacokinetics [50]. Since many NRs are ubiquitously expressed, like PPAR-δ [51], a NR drug could be targeted to a specific tissue through designing it to signal through an LTP. This underscores the importance of identifying LTP effectors, which enables us to better pharmacologically manipulate these systems.

Final Thoughts

In this work, we show how lipids and LTPs regulate vital biological processes. Lipids serve more than a structural and metabolic role, but they are also signaling molecules. LTPs, placed at the interface between lipids and their physiological effects, mediate these lipid signals through transporting and sensing lipids. We shed some light on how lipid metabolism, aging, and homeostasis is regulated by lipids and LTPs. This is just one small facet of the complex orchestra of signaling and regulation that occurs to maintain and drive forward life.

References

1. Folick A, Oakley HD, Yu Y, Armstrong EH, Kumari M, Sanor L, Moore DD, Ortlund EA, Zechner R, Wang MC. Aging. Lysosomal signaling molecules regulate longevity in Caenorhabditis elegans. Science (New York, NY). 2015;347(6217):83-6. Epub 2015/01/03. doi: 10.1126/science.1258857. PubMed PMID: 25554789; PMCID: PMC4425353.
2. Han S, Schroeder EA, Silva-Garcia CG, Hebestreit K, Mair WB, Brunet A. Mono-unsaturated fatty acids link H3K4me3 modifiers to C. elegans lifespan. Nature. 2017;544(7649):185-90. Epub 2017/04/06. doi: 10.1038/nature21686. PubMed PMID: 28379943; PMCID: PMC5391274.
3. Sessler RJ, Noy N. A ligand-activated nuclear localization signal in cellular retinoic acid binding protein-II. Mol Cell. 2005;18(3):343-53. Epub 2005/05/04. doi: 10.1016/j.molcel.2005.03.026. PubMed PMID: 15866176.
4. Gillilan RE, Ayers SD, Noy N. Structural basis for activation of fatty acid-binding protein 4. Journal of molecular biology. 2007;372(5):1246-60. Epub 2007/09/01. doi: 10.1016/j.jmb.2007.07.040. PubMed PMID: 17761196; PMCID: PMC2032018.
5. Armstrong EH, Goswami D, Griffin PR, Noy N, Ortlund EA. Structural basis for ligand regulation of the fatty acid-binding protein 5, peroxisome proliferator-activated receptor beta/delta (FABP5-PPARbeta/delta) signaling pathway. J Biol Chem. 2014;289(21):14941-54. Epub 2014/04/03. doi: 10.1074/jbc.M113.514646. PubMed PMID: 24692551; PMCID: PMC4031543.
6. Hughes ML, Liu B, Halls ML, Wagstaff KM, Patil R, Velkov T, Jans DA, Bunnett NW, Scanlon MJ, Porter CJ. Fatty Acid-binding Proteins 1 and 2 Differentially Modulate the Activation of Peroxisome Proliferator-activated Receptor alpha in a Ligand-selective Manner. J Biol Chem. 2015;290(22):13895-906. Epub 2015/04/08. doi: 10.1074/jbc.M114.605998. PubMed PMID: 25847235; PMCID: PMC4447964.
7. Patil R, Mohanty B, Liu B, Chandrashekaran IR, Headey SJ, Williams ML, Clements CS, Ilyichova O, Doak BC, Genissel P, Weaver RJ, Vuillard L, Halls ML, Porter CJH, Scanlon MJ. A ligand-induced structural change in fatty acid-binding protein 1 is associated with potentiation of peroxisome proliferator-activated receptor alpha agonists. J Biol Chem. 2019;294(10):3720-34. Epub 2019/01/02. doi: 10.1074/jbc.RA118.006848. PubMed PMID: 30598509; PMCID: PMC6416440.
8. Amber-Vitos O, Kucherenko N, Nachliel E, Gutman M, Tsfadia Y. The Interaction of FABP with Kapalpha. PLoS One. 2015;10(8):e0132138. Epub 2015/08/19. doi: 10.1371/journal.pone.0132138. PubMed PMID: 26284534; PMCID: PMC4540411.
9. Budhu A, Gillilan R, Noy N. Localization of the RAR interaction domain of cellular retinoic acid binding protein-II. Journal of molecular biology. 2001;305(4):939-49. Epub 2001/02/13. doi: 10.1006/jmbi.2000.4340. PubMed PMID: 11162104.
10. Dong D, Ruuska SE, Levinthal DJ, Noy N. Distinct roles for cellular retinoic acid-binding proteins I and II in regulating signaling by retinoic acid. J Biol Chem. 1999;274(34):23695-8. Epub 1999/08/14. doi: 10.1074/jbc.274.34.23695. PubMed PMID: 10446126.
11. Barbosa MC, Grosso RA, Fader CM. Hallmarks of Aging: An Autophagic Perspective. Frontiers in endocrinology. 2018;9:790. Epub 2019/01/29. doi: 10.3389/fendo.2018.00790. PubMed PMID: 30687233; PMCID: PMC6333684.

12. Escobar KA, Cole NH, Mermier CM, VanDusseldorp TA. Autophagy and aging: Maintaining the proteome through exercise and caloric restriction. Aging cell. 2019;18(1):e12876. Epub 2018/11/16. doi: 10.1111/acel.12876. PubMed PMID: 30430746; PMCID: PMC6351830.
13. Hansen M, Rubinsztein DC, Walker DW. Autophagy as a promoter of longevity: insights from model organisms. Nature reviews Molecular cell biology. 2018;19(9):579-93. Epub 2018/07/15. doi: 10.1038/s41580-018-0033-y. PubMed PMID: 30006559.
14. Lee SH, Lee SK, Paik D, Min KJ. Overexpression of fatty-acid-beta-oxidation-related genes extends the lifespan of Drosophila melanogaster. Oxidative medicine and cellular longevity. 2012;2012:854502. Epub 2012/09/22. doi: 10.1155/2012/854502. PubMed PMID: 22997544; PMCID: PMC3446750.
15. Furuhashi M. Fatty Acid-Binding Protein 4 in Cardiovascular and Metabolic Diseases. Journal of atherosclerosis and thrombosis. 2019;26(3):216-32. Epub 2019/02/07. doi: 10.5551/jat.48710. PubMed PMID: 30726793; PMCID: PMC6402888.
16. Hotamisligil GS, Bernlohr DA. Metabolic functions of FABPs--mechanisms and therapeutic implications. Nature reviews Endocrinology. 2015;11(10):592-605. Epub 2015/08/12. doi: 10.1038/nrendo.2015.122. PubMed PMID: 26260145; PMCID: PMC4578711.
17. Xu A, Wang Y, Xu JY, Stejskal D, Tam S, Zhang J, Wat NM, Wong WK, Lam KS. Adipocyte fatty acid-binding protein is a plasma biomarker closely associated with obesity and metabolic syndrome. Clinical chemistry. 2006;52(3):405-13. Epub 2006/01/21. doi: 10.1373/clinchem.2005.062463. PubMed PMID: 16423904.
18. Furuhashi M, Tuncman G, Gorgun CZ, Makowski L, Atsumi G, Vaillancourt E, Kono K, Babaev VR, Fazio S, Linton MF, Sulsky R, Robl JA, Parker RA, Hotamisligil GS. Treatment of diabetes and atherosclerosis by inhibiting fatty-acid-binding protein aP2. Nature. 2007;447(7147):959-65. Epub 2007/06/08. doi: 10.1038/nature05844. PubMed PMID: 17554340; PMCID: PMC4076119.
19. Charles KN, Li MD, Engin F, Arruda AP, Inouye K, Hotamisligil GS. Uncoupling of Metabolic Health from Longevity through Genetic Alteration of Adipose Tissue Lipid-Binding Proteins. Cell reports. 2017;21(2):393-402. Epub 2017/10/12. doi: 10.1016/j.celrep.2017.09.051. PubMed PMID: 29020626; PMCID: PMC5682597.
20. Zhang Y, Li Y, Niepel MW, Kawano Y, Han S, Liu S, Marsili A, Larsen PR, Lee CH, Cohen DE. Targeted deletion of thioesterase superfamily member 1 promotes energy expenditure and protects against obesity and insulin resistance. Proc Natl Acad Sci U S A. 2012;109(14):5417-22. Epub 2012/03/20. doi: 10.1073/pnas.1116011109. PubMed PMID: 22427358; PMCID: PMC3325675.
21. Han S, Cohen DE. Functional characterization of thioesterase superfamily member 1/Acyl-CoA thioesterase 11: implications for metabolic regulation. J Lipid Res. 2012;53(12):2620-31. Epub 2012/09/21. doi: 10.1194/jlr.M029538. PubMed PMID: 22993230; PMCID: PMC3494255.
22. Okada K, LeClair KB, Zhang Y, Li Y, Ozdemir C, Krisko TI, Hagen SJ, Betensky RA, Banks AS, Cohen DE. Thioesterase superfamily member 1 suppresses cold thermogenesis by limiting the oxidation of lipid droplet-derived fatty acids in brown adipose tissue. Molecular metabolism. 2016;5(5):340-51. Epub 2016/04/26. doi: 10.1016/j.molmet.2016.02.002. PubMed PMID: 27110486; PMCID: PMC4837299.
23. Adams SH, Chui C, Schilbach SL, Yu XX, Goddard AD, Grimaldi JC, Lee J, Dowd P, Colman S, Lewin DA. BFIT, a unique acyl-CoA thioesterase induced in thermogenic brown

adipose tissue: cloning, organization of the human gene and assessment of a potential link to obesity. Biochem J. 2001;360:135-42. doi: 10.1042/0264-6021:3600135. PubMed PMID: WOS:000172466900015.
24. Li YA, L.H.; Hagen, S.J.; Cohen, D.E. N-Terminal Phosphorylation of Thioesterase Superfamily Member 1 (Them1) Regulates its Subcellular Localization in Brown Adipocytes. FASEB Journal2017.
25. Chen D, Latham J, Zhao H, Bisoffi M, Farelli J, Dunaway-Mariano D. Human brown fat inducible thioesterase variant 2 cellular localization and catalytic function. Biochemistry. 2012;51(35):6990-9. Epub 2012/08/18. doi: 10.1021/bi3008824. PubMed PMID: 22897136; PMCID: PMC4066737.
26. Horibata Y, Sugimoto H. StarD7 mediates the intracellular trafficking of phosphatidylcholine to mitochondria. J Biol Chem. 2010;285(10):7358-65. Epub 2010/01/01. doi: 10.1074/jbc.M109.056960. PubMed PMID: 20042613; PMCID: PMC2844184.
27. Olayioye MA, Vehring S, Muller P, Herrmann A, Schiller J, Thiele C, Lindeman GJ, Visvader JE, Pomorski T. StarD10, a START domain protein overexpressed in breast cancer, functions as a phospholipid transfer protein. J Biol Chem. 2005;280(29):27436-42. Epub 2005/05/25. doi: 10.1074/jbc.M413330200. PubMed PMID: 15911624.
28. Baqai ML, Yue; Tillman, Matthew C; Ortlund, Eric A.; Cohen, David E.; Hagen, Susan J. The Them1 START Domain Regulates Nuclear Trafficking in Brown Adipocytes. FASEB J. 2020.
29. Swarbrick CM, Roman N, Cowieson N, Patterson EI, Nanson J, Siponen MI, Berglund H, Lehtio L, Forwood JK. Structural basis for regulation of the human acetyl-CoA thioesterase 12 and interactions with the steroidogenic acute regulatory protein-related lipid transfer (START) domain. J Biol Chem. 2014;289(35):24263-74. Epub 2014/07/09. doi: 10.1074/jbc.M114.589408. PubMed PMID: 25002576; PMCID: PMC4148856.
30. Horibata Y, Ando H, Itoh M, Sugimoto H. Enzymatic and transcriptional regulation of the cytoplasmic acetyl-CoA hydrolase ACOT12. J Lipid Res. 2013;54(8):2049-59. Epub 2013/05/28. doi: 10.1194/jlr.M030163. PubMed PMID: 23709691; PMCID: PMC3708356.
31. Suematsu N, Isohashi F. Molecular cloning and functional expression of human cytosolic acetyl-CoA hydrolase. Acta biochimica Polonica. 2006;53(3):553-61. Epub 2006/09/05. PubMed PMID: 16951743.
32. Suematsu N, Okamoto K, Shibata K, Nakanishi Y, Isohashi F. Molecular cloning and functional expression of rat liver cytosolic acetyl-CoA hydrolase. Eur J Biochem. 2001;268(9):2700-9. Epub 2001/04/27. PubMed PMID: 11322891.
33. Kanno K, Wu MK, Agate DS, Fanelli BJ, Wagle N, Scapa EF, Ukomadu C, Cohen DE. Interacting proteins dictate function of the minimal START domain phosphatidylcholine transfer protein/StarD2. J Biol Chem. 2007;282(42):30728-36. Epub 2007/08/21. doi: 10.1074/jbc.M703745200. PubMed PMID: 17704541.
34. Wei J, Kang HW, Cohen DE. Thioesterase superfamily member 2 (Them2)/acyl-CoA thioesterase 13 (Acot13): a homotetrameric hotdog fold thioesterase with selectivity for long-chain fatty acyl-CoAs. Biochem J. 2009;421(2):311-22. Epub 2009/05/02. doi: 10.1042/bj20090039. PubMed PMID: 19405909; PMCID: PMC3086008.
35. Cao J, Xu H, Zhao H, Gong W, Dunaway-Mariano D. The mechanisms of human hotdog-fold thioesterase 2 (hTHEM2) substrate recognition and catalysis illuminated by a structure and function based analysis. Biochemistry. 2009;48(6):1293-304. Epub 2009/01/28. doi: 10.1021/bi801879z. PubMed PMID: 19170545; PMCID: PMC2929599.

36. Janowski BA, Willy PJ, Devi TR, Falck JR, Mangelsdorf DJ. An oxysterol signalling pathway mediated by the nuclear receptor LXR alpha. Nature. 1996;383(6602):728-31. Epub 1996/10/24. doi: 10.1038/383728a0. PubMed PMID: 8878485.
37. Lee JM, Lee YK, Mamrosh JL, Busby SA, Griffin PR, Pathak MC, Ortlund EA, Moore DD. A nuclear-receptor-dependent phosphatidylcholine pathway with antidiabetic effects. Nature. 2011;474(7352):506-10. Epub 2011/05/27. doi: 10.1038/nature10111. PubMed PMID: 21614002; PMCID: PMC3150801.
38. Kang HW, Kanno K, Scapa EF, Cohen DE. Regulatory role for phosphatidylcholine transfer protein/StarD2 in the metabolic response to peroxisome proliferator activated receptor alpha (PPARalpha). Biochimica et biophysica acta. 2010;1801(4):496-502. Epub 2010/01/05. doi: 10.1016/j.bbalip.2009.12.013. PubMed PMID: 20045742; PMCID: PMC2826570.
39. Kohn J. Novel Allosteric Communication in Nuclear Receptor Activation 2018-08-28 14:53:52 -0400.
40. Schrick K, Bruno M, Khosla A, Cox PN, Marlatt SA, Roque RA, Nguyen HC, He C, Snyder MP, Singh D, Yadav G. Shared functions of plant and mammalian StAR-related lipid transfer (START) domains in modulating transcription factor activity. BMC biology. 2014;12:70. Epub 2014/08/28. doi: 10.1186/s12915-014-0070-8. PubMed PMID: 25159688; PMCID: PMC4169639.
41. Schrick K, Nguyen D, Karlowski WM, Mayer KF. START lipid/sterol-binding domains are amplified in plants and are predominantly associated with homeodomain transcription factors. Genome biology. 2004;5(6):R41. Epub 2004/06/10. doi: 10.1186/gb-2004-5-6-r41. PubMed PMID: 15186492; PMCID: Pmc463074.
42. Mo X, Qi Q, Ivanov AA, Niu Q, Luo Y, Havel J, Goetze R, Bell S, Moreno CS, Cooper LA, Johns MA, Khuri FR, Du Y, Fu H. AKT1, LKB1, and YAP1 Revealed as MYC Interactors with NanoLuc-Based Protein-Fragment Complementation Assay. Molecular pharmacology. 2017;91(4):339-47. Epub 2017/01/15. doi: 10.1124/mol.116.107623. PubMed PMID: 28087810; PMCID: PMC5363710.
43. Reitz J, Gehrig-Burger K, Strauss JF, 3rd, Gimpl G. Cholesterol interaction with the related steroidogenic acute regulatory lipid-transfer (START) domains of StAR (STARD1) and MLN64 (STARD3). The FEBS journal. 2008;275(8):1790-802. Epub 2008/03/12. doi: 10.1111/j.1742-4658.2008.06337.x. PubMed PMID: 18331352.
44. Janowski BA, Grogan MJ, Jones SA, Wisely GB, Kliewer SA, Corey EJ, Mangelsdorf DJ. Structural requirements of ligands for the oxysterol liver X receptors LXRalpha and LXRbeta. Proc Natl Acad Sci U S A. 1999;96(1):266-71. Epub 1999/01/06. doi: 10.1073/pnas.96.1.266. PubMed PMID: 9874807; PMCID: PMC15128.
45. Kanno K, Wu MK, Scapa EF, Roderick SL, Cohen DE. Structure and function of phosphatidylcholine transfer protein (PC-TP)/StarD2. Biochimica et biophysica acta. 2007;1771(6):654-62. Epub 2007/05/15. doi: 10.1016/j.bbalip.2007.04.003. PubMed PMID: 17499021; PMCID: PMC2743068.
46. Musille PM, Kohn JA, Ortlund EA. Phospholipid--driven gene regulation. FEBS letters. 2013;587(8):1238-46. Epub 2013/01/22. doi: 10.1016/j.febslet.2013.01.004. PubMed PMID: 23333623; PMCID: PMC3632008.
47. Bose HS, Sugawara T, Strauss JF, 3rd, Miller WL. The pathophysiology and genetics of congenital lipoid adrenal hyperplasia. N Engl J Med. 1996;335(25):1870-8. Epub 1996/12/19. doi: 10.1056/nejm199612193352503. PubMed PMID: 8948562.

48. Kaess BM, Enserro DM, McManus DD, Xanthakis V, Chen MH, Sullivan LM, Ingram C, O'Donnell CJ, Keaney JF, Vasan RS, Glazer NL. Cardiometabolic correlates and heritability of fetuin-A, retinol-binding protein 4, and fatty-acid binding protein 4 in the Framingham Heart Study. The Journal of clinical endocrinology and metabolism. 2012;97(10):E1943-7. Epub 2012/08/03. doi: 10.1210/jc.2012-1458. PubMed PMID: 22855337; PMCID: PMC3674297.
49. Clark BJ. The mammalian START domain protein family in lipid transport in health and disease. J Endocrinol. 2012;212(3):257-75. Epub 2011/10/04. doi: 10.1530/joe-11-0313. PubMed PMID: 21965545.
50. Chiapparino A, Maeda K, Turei D, Saez-Rodriguez J, Gavin AC. The orchestra of lipid-transfer proteins at the crossroads between metabolism and signaling. Prog Lipid Res. 2016;61:30-9. Epub 2015/12/15. doi: 10.1016/j.plipres.2015.10.004. PubMed PMID: 26658141.
51. Higashiyama H, Billin AN, Okamoto Y, Kinoshita M, Asano S. Expression profiling of peroxisome proliferator-activated receptor-delta (PPAR-delta) in mouse tissues using tissue microarray. Histochemistry and cell biology. 2007;127(5):485-94. Epub 2007/03/03. doi: 10.1007/s00418-007-0279-5. PubMed PMID: 17333240.

APPENDIX

LIPID BINDING PROTEIN 2 AND LIID BINDING PROTEIN 3 EXTEND LIFESPAN IN CAENORHABDITIS ELEGANS THROUGH CARRYING POLYUNSATURATED FATTY ACIDS TO NEURONAL TISSUE

Marzia Savini[1], Matthew C Tillman[2], Andre' Cuevas[2], Eric A. Ortlund[2], Meng Wang[1,3]

From the [1]Huffington Center on Aging and Department of Molecular and Human Genetics, Baylor College of Medicine, Houston, Texas; [2]Department of Biochemistry, Emory University School of Medicine, 1510 Clifton Road, Atlanta, GA 30322; [3]Howard Hughes Medical Institute, Baylor College of Medicine, Houston, TX 77030, USA

Preface

All data collected from *C. elegans* was conducted by M.S. in Dr. Meng Wang's lab at Baylor College of Medicine. M.C.T. and A.C. collected lipid binding data and solved the LBP-3 structure. M.C.T. wrote this report.

Introduction

Lipids play an essential signaling role intra- and extra-cellularly to regulate metabolism, inflammation, and aging [1, 2]. Since lipids are hydrophobic, they utilize alternative means than passive diffusion to travel through the hydrophilic cellular environment. One such means is through lipid transfer proteins, such as fatty acid binding proteins (FABPs) [3]. Fatty acid binding proteins act as lipid chaperones, solubilizing fatty acids and other lipid molecules, and carrying them to proteins or membranes [4]. Recently, Lipid Binding Protein 8 (LBP-8), a fatty acid binding protein in *C. elegans*, was also shown to extend lifespan in worms [5]. LBP-8 extends lifespan through shuttling lysosomal lipids derived from lysosomal acid lipase (LIPL-4) into the nucleus to regulate the activity of NHR-49 and NHR-80 to induce expression of life extending genes. This process was driven by a specific lipid, oleoylethanolamine, showing lipids and FABPs work intricately together to signal.

There are nine *C. elegans* FABPs, while humans have ten FABPs. Most mammalian FABPs are cytosolic, but FABP4 is secreted and putatively transfers lipids between tissues [6, 7]. LBP-8 was the first *C. elegans* FABP identified to extend lifespan, but it is unknown if other FABPs extend lifespan. In this study, we identify that LBP-2 and LBP-3 also extend lifespan similar to LBP-8 but are secreted from their respective tissues and regulate gene expression in neuronal tissue. This is potentially mediated through LBP-2 and LBP-3 binding to C20 polyunsaturated fatty acids (PUFAs). Additionally, we solve the first structure of LBP-3, shedding light on the molecular mechanism by which LBP-3 extends lifespan.

Results & Discussion

LBP-2 and LBP-3 extend lifespan

Given the life-extending properties of LBP-8, we were motivated to test if other FABPs in *C. elegans* extend lifespan. There are eight FABPs in addition to LBP-8 present in *C. elegans*; therefore, we tested if these FABPs also extend lifespan, and we identified LBP-2 and LBP-3 prolong aging in a similar manner. Removing LBP-8 suppresses the life-extension yielded from overexpressing LIPL-4, while overexpressing LBP-8 alone extends lifespan in *C. elegans* [5]. Similarly, silencing LBP-2 or LBP-3 reduces the prolonged aging obtained from overexpressing LIPL-4, and overexpressing these LBPs extends lifespan (Fig. 1A-D). LBP-3 extends lifespan when overexpressed in intestines, while LBP-2 prolongs life when overexpressed in muscle; however, both LBPs contain N-terminal secretion peptides, suggesting they could mediate their effect in a cell non-autonomous manner. In conjunction with this, overexpression of LIPL-4 induces expression of EGL-21, a neuropeptide processing gene expressed in neurons, which is also necessary for the life-extending properties of LIPL-4 (Fig 2A-B). Given the specific expression of LIPL-4 in fat storage tissues and EGL-21 in neurons, we suspected that LBP-2 and LBP-3 could mediate this tissue crosstalk to extend lifespan. Interestingly, silencing LBP-2 or LBP-3 suppressed the induction of EGL-21 in neurons of worms overexpressing LIPL-4 (Fig. 2C). Additionally, overexpression of intestinal LBP-3, but not LBP-2, increased the expression of EGL-21 (Fig. 2D). These data suggest that LBP-2 and LBP-3 act as endocrine messengers, potentially carrying lipid signals from the fat storage tissues and muscle to neurons to extend lifespan.

LBP-2 and LBP-3 bind to C20-PUFAs

In order to identify if this tissue crosstalk mediated by LBP-2 and LBP-3 is driven by specific lipids, we investigated the binding preference of these LBPs. Lipidomic analysis of *C.*

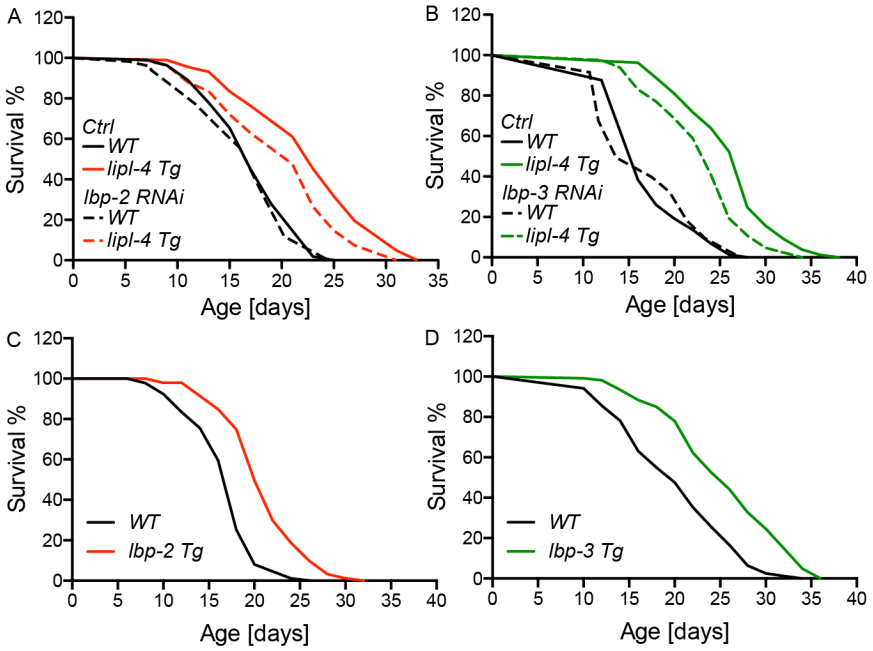

Figure 1. LBP-2 and LBP-3 extend lifespan of *C. elegans*. *A-B*. RNAi inactivation of *lbp-2* or *lbp-3* suppresses the lifespan extension in *lipl-4 Tg*. *C-D.* Overexpression of *lbp-2* or *lbp-3* is sufficient to extend lifespan.

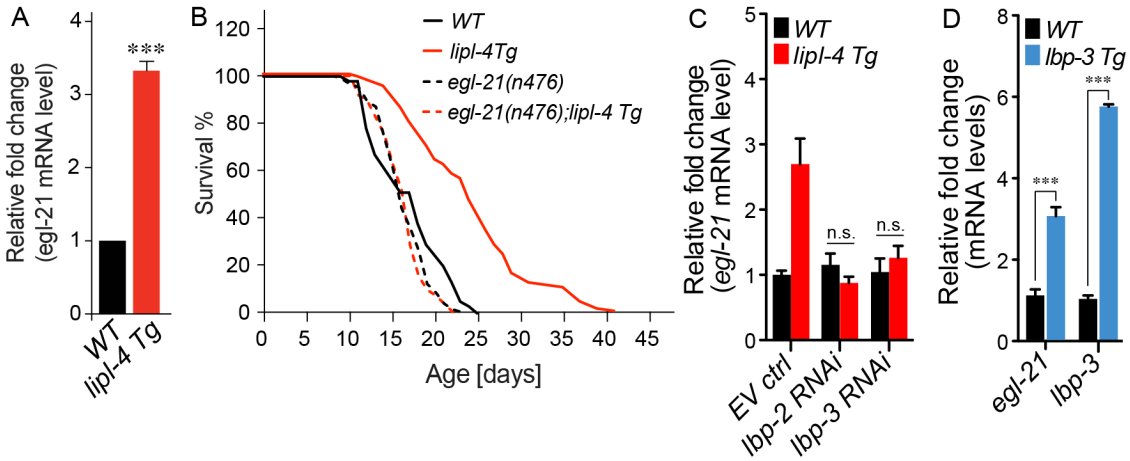

Figure 2. LBP-2 and LBP-3 mediate induction of EGL-21 by LIPL-4 overexpression to extend lifespan. *A. egl-21*, a neuropeptide processing gene, is transcriptionally up-regulated in *lilp-4 Tg* worms. *B.* Inactivation of *egl-21* suppresses the longevity effect of *lipl-4 Tg. C.* Inactivation of *lbp-2* or *lbp-3* suppresses the *egl-21* induction in *lilp-4 Tg. D. lbp-3* overexpression sufficiently induces *egl-21* expression.

elegans overexpressing LIPL-4 revealed levels of C20 polyunsaturated fatty acids (PUFAs) were significantly elevated [5]; therefore, we hypothesized LBP-2 and LBP-3 bind to C20-PUFAs. To determine if LBP-2 and LBP-3 bind to C20-PUFAs, we utilized a fluorescent based competition binding assay using the probe 1,8-ANS (1-anilinonaphthalene- 8-sulfonic acid), which fluoresces upon binding to a protein [8]. We were unable to use this assay for LBP-2 because it did not bind to 1,8-ANS, but LBP-3 bound to the probe with high affinity, enabling us to perform the competition assay. LBP-3 bound to *all-cis* 5,8,11,14-ETA (ω-6 ETA), DGLA, and EPA with low μM affinity, but did not bind to *all-cis* 8,11,14,17-ETA (ω-3 ETA) (Fig. 3A). Interestingly, LBP-3 can decipher between the placement of double bonds within the fatty acyl chain as evidence by ω-6 ETA binding but not ω-3 ETA. These data verify that LBP-3 can bind to C20-PUFAs and potentially carry them extracellularly.

Since we were unable to utilize the fluorescent based competition assay to determine if LBP-2 binds to C20-PUFAs, we used affinity purification and mass spectrometry to identify fatty acids derived from *C. elegans* that bind to LBP-2 [9]. Briefly, we recombinantly expressed His-tagged LBP-2 and purified through nickel affinity chromatography and size exclusion chromatography. We generated apo protein through unfolding/refolding the protein through step-wise dialysis [10]. Apo-LBP-2 was then exposed to *C. elegans* lipid liposomes and subsequently purified with size exclusion chromatography to remove nonspecifically bound lipids. Bound lipids were extracted and then identified and quantified through mass spectrometry. LBP-2 predominantly copurified with unsaturated fatty acids, namely linoleic acid (18:2, LA), oleic acid (18:1, OA), and eicosatetraenoic acid (20:4, ETA) (Fig. 3B). Since there is relatively low

abundance of C20 PUFAs in *C. elegans*, we supplemented worms with dihomo-γ-linolenic acid (20:3, DGLA) and exposed LBP-2 to lipid extracts from these worms. Interestingly, LBP-2 was

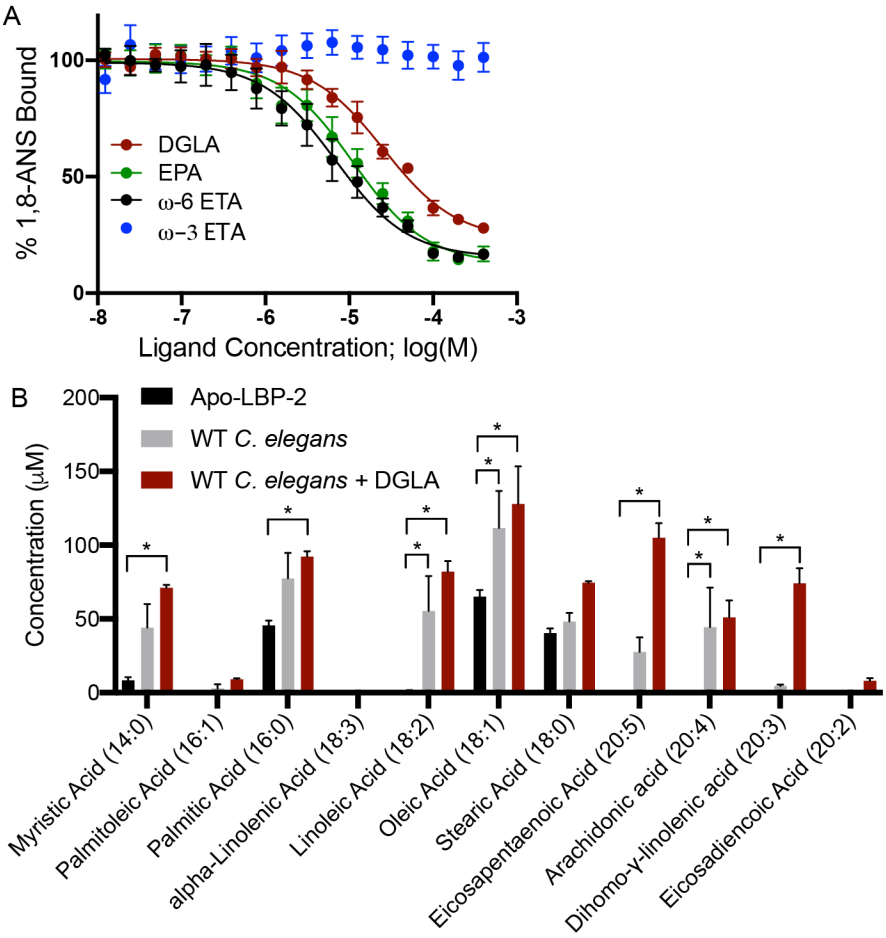

Figure 3. LBP-2 and LBP-3 bind to C20-PUFAs. *A.* Fluorescent ligand, 1,8-ANS, bound to LBP-3 was competed off with increasing amounts of DGLA (red) and EPA (green), ω-6 ETA (black), or ω-3 ETA (blue). Curves represent average of three independent replicates +/− SEM, conducted in triplicate, followed by normalization of curves. *B.* LBP-2 binds to C20-PUFAs. Affinity purification-mass spectrometry analysis of LBP-2 exposed to lipid liposomes from WT *C. elegans* (gray) or WT *C. elegans* supplemented with DGLA (red). Apo-LBP2 (black) was used as a negative control to account for non-specifically bound lipids.

enriched with eicosapentaenoic acid (20:5, EPA) and DGLA in addition to LA, OA, and ETA when exposed to lipid extracts from worms supplemented with DGLA (Fig. 3B), verifying LBP-2 binds to C20-PUFAs.

To test if C20-PUFAs alter longevity and EGL-21 expression, we generated *C. elegans* deficient in FAT-1 and FAT-3, desaturases essential for C20-PUFA synthesis (Fig. 4A). Deletion of FAT-1 or FAT-3 prevented the life extension and induction of EGL-21 from overexpression of LIPL-4 (Fig. 4B-C). Furthermore, supplementation with EPA rescued induction of EGL-21 in worms lacking FAT-1 and overexpressing LIPL-4 (Fig. 4D). However, silencing LBP-3 prevented this induction of EGL-21 expression in worms supplemented with EPA, suggesting LBP-3 is downstream of EPA and required for EPA induction of EGL-21 expression (Fig. 4D). These data support a model that LBP-3 extends lifespan through carrying C20-PUFAs derived from the fat storage tissue to neurons to regulate expression of EGL-21.

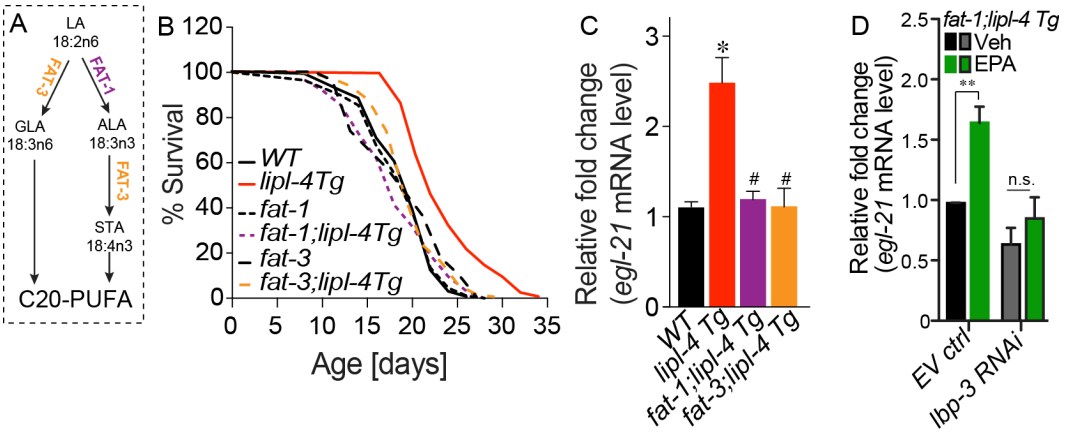

Figure 4. C20-PUFAs are required for induction of EGL-21 to extend lifespan. *A.* C20-PUFA biosynthesis requires FAT-1 and FAT-3. *B-C.* Inactivation of either *fat-1* or *fat-3* specifically in the intestine suppresses the *egl-21* induction and lifespan extension in *lipl-4 Tg*. *D.* EPA supplementation restores *egl-21* induction in *fat-1*;*lilp-4 Tg*, which is dependent on *lbp-3.*

Structural Insight into LBP-3

We set out to structurally characterize LBP-3 in order elucidate the mechanism by which it binds to lipids and extends lifespan. We were able to solve the first structure of LBP-3 to a resolution of 2.18 Å. We solved the structure with molecular replacement using a nematode extracellular FABP as the starting search model (PDB code: 6I8X) [11]. The LBP-3 structure was solved in the $P2_12_12_1$ space group, with the asymmetric unit containing two protein chains (Fig. 5A). The two LBP-3 chains form a dimer that adopt a novel FABP fold. The structure contains features characteristic of the FABP fold, including the N-terminal 3_{10}-like helix, the α-helical lid, and a β-barrel consisting of 10 β-strands; however, the β-barrels of the two LBP-3 chains are joined together, forming one large β-barrel. The fourth β-strand, which typically interacts with the fifth β-strand, interacts instead with the fourth β-strand of the dimeric partner. This displaces the fifth β-strand, inserting it and the loop between β5-β6 into the interior cavity of the adjacent LBP-3 molecule. The inserted loop into the interior cavity pushes open the α-helical lid, creating a large opening at the mouth of the pocket (Fig. 5B). This large opening extends across both protein chains, producing a large internal cavity that is exposed to solvent. There is no fatty acid present in the structure, despite attempts to soak EPA into the crystals.

We used the DALI server [12] to identify structures similar to LBP-3. The structure of *A. suum* As-p18, an extracellular nematode FABP, bound to oleate (PDB code: 6I9F) [11] shares the most structural similarity to LBP-3; however, there are significant differences between these structures. The largest difference is the location of the loop between β5-β6; this loop folds onto the mouth of the cavity in the As-p18 structure, but not in LBP-3 (Fig. 5C). Additionally, in the LBP-3 dimer, this loop is inserted into the interior cavity of the adjacent LBP-3 and sterically clashes with the oleate in the As-p18 structure, suggesting the LBP-3 dimer is incompatible with

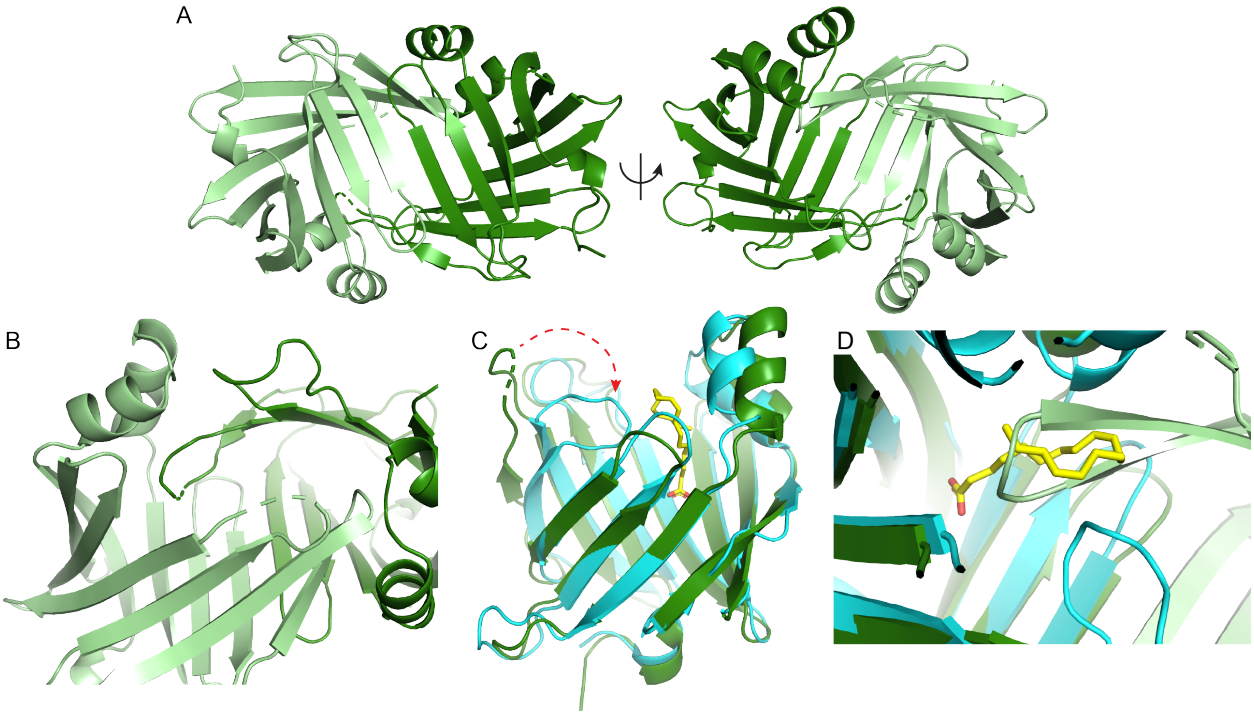

Figure 5. Crystal structure of LBP-3 reveals dimer unable to bind fatty acid. *A.* Crystal structure of LBP-3. LBP-3 forms a dimer. *C.* Loop between β5-β6 is inserted into interior cavity of dimeric partner, displacing the α-helical lid. *D.* Structural alignment with *A. suum* As-p18 (PDB code: 6I9F) (cyan) bound to oleic acid (yellow). Red arrow indicated the large structural difference in the location of the loop between β5-β6 in both structures. *E.* Loop between β5-β6 of dimeric partner sterically clashes with the placement of oleic acid (yellow) in the pocket.

lipid binding (Fig. 5D). Furthermore, incubation with ω-6 ETA prevented crystal formation in the same crystallization conditions.

Though LBP-3 crystallizes as a dimer, it is a monomer in solution as determined by size exclusion chromatography and analytical ultracentrifugation (Fig. 6A-B). It is possible the dimer is a transient state stabilized during crystal packing, but further testing is needed to determine if this dimer can form *in vivo*. Moving forward, we plan to perform a protein-protein interaction assay in cell culture to test this. LBP-3 is not the first FABP dimer, as FABP4 was crystalized as a potential dimer [13], and FABP5 crystallized as a domain-swapped dimer [14]. The functional significance of these structures remains to be explored, but these findings verify there is conformational flexibility within the highly conserved FABP fold. It is possible these dimeric structures provide a snapshot of how FABPs interact with one another. In the LBP-3 structure, a tunnel is formed between the two β barrels, which could allow passage of lipid from one LBP-3 chain to another. It remains to be determined if this same dimer fold can form between two distinct FABP paralogs.

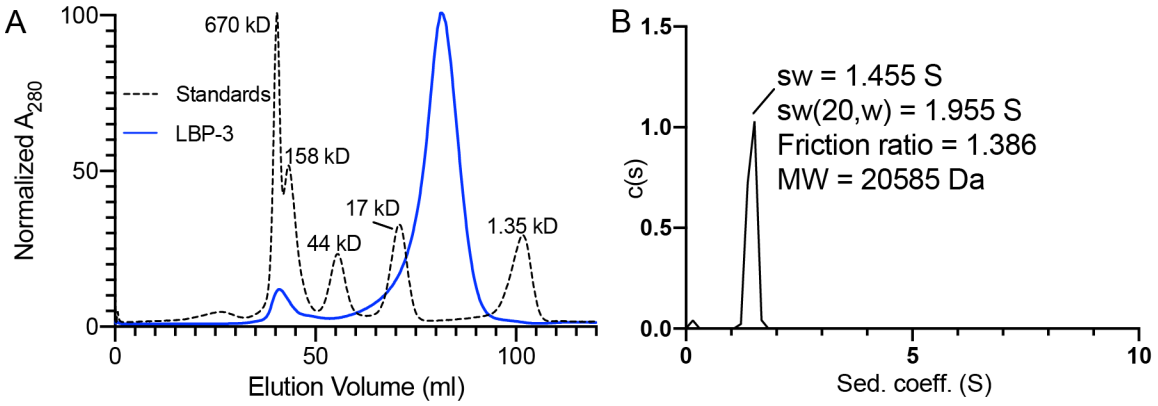

Figure 6. LBP-3 purifies as a monomer. *A.* Size exclusion chromatography of LBP-3 (blue) ran over S75 16/60 column. LBP-3 is predicted to be a monomer based on standards (dashed black). *B. c(s)* distribution from sedimentation velocity analytical ultracentrifugation of LBP-3.

To test the functional significance of the LBP-3 dimer, we plan to form an obligate dimer through mutagenesis. In the LBP-3 dimer structure, the proteins interface at the β4 strand of each chain. Threonine 70 on each chain lie close together; therefore, we propose mutating threonine 70 to a cystine, which would likely form a disulfide bond, creating an obligate dimer. If the LBP-3 T70C mutant purifies as a dimer, this would be an effective tool to probe the functional effect of the dimer on lipid binding and life extension in *C. elegans.*

As a whole, this cumulative work on LBPs in *C. elegans* has uncovered novel mechanisms by which these lipid chaperones propagate lipid signals extracellularly to extend lifespan. We determine that LBP-2 and LBP-3 both bind C20 PUFAs and potentially shuttle these lipids to neuronal tissues to induce expression of neural peptide processing genes. Additionally, we show the first structure of LBP-3, which reveals a novel dimeric fold. Moving forward, the functional significance of the dimer should be investigated through mutagenesis.

Materials & Methods

Materials and reagents—Chemicals were purchased from Sigma, Fisher or Acros Organics. The vector for His-tagged tobacco etch virus (TEV) was a gift from John Tesmer (University of Texas at Austin). The pMCSG7 (LIC_HIS) vector was provided by John Sondek (University of North Carolina at Chapel Hill). DNA oligonucleotide primers were synthesized by IDT (Coralville, IA).

Protein expression and purification—Wild-type *Caenorhabditis elegans* LBP-2 (residues 19-161) and LBP-3 (residues 16-165) were subcloned into pMCSG7-His vector. LBP-2 and LBP-3 in the pMCSG7 vector was transformed into *Escherichia coli* strain BL21 (DE3) cells and expressed as a His_6 fusion containing a tobacco etch virus protease cleavage site to facilitate tag removal. Cultures (1 liters in LB) were grown to an A_{600} of ~0.6 and induced with 0.5 mM isopropyl β-d-1-thiogalactopyranoside at 30 °C for 4 hours then harvested. For affinity purification/mass spectrometry studies with LBP-2, cells were lysed through sonication in a buffer containing 20 mM Tris HCl pH 7.4, 500 mM NaCl, 25 mM imidazole, 5% glycerol, 5 mM 2-mercaptoethanol, and 8 M urea. Unfolded LBP-2 was purified by nickel affinity chromatography in buffers containing 8 M urea. LBP-2 was refolded through stepwise dialysis over multiple days to remove urea. Refolded LBP-2 was further purified through size exclusion chromatography using a HiLoad 16/60 Superdex 75 column into a buffer containing 20 mM Hepes pH 7.5, 150 mM NaCl, and 5 % glycerol, 0.5 mM tris(2-carboxyethyl)phosphine (TCEP). For ligand binding assays and crystallography with LBP-3, cells were lysed through sonication in a buffer containing 20 mM Tris HCl pH 7.4, 500 mM NaCl, 25 mM imidazole, 5% glycerol, 5 mM 2-mercaptoethanol, lysozyme, Dnase A, and 100 uM phenylmethylsulfonyl fluoride. LBP-3

was purified by nickel affinity chromatography and the His tag was cleaved by tobacco etch virus protease at 4 °C overnight with simultaneous dialysis into a buffer containing 20 mM Tris HCl pH 7.4, 150 mM NaCl, and 5% glycerol. Cleaved LBP-3 were purified from His tag through nickel affinity chromatography followed by gel filtration chromatography using a HiLoad 16/60 Superdex 75 column.

Crystallization, data collection, structural refinement—Pure wild-type LBP-3 was concentrated to 2 mg mL^{-1} in 20 mM Hepes pH 7.5, 150 mM NaCl, and 5 % glycerol, 0.5 mM tris(2-carboxyethyl)phosphine (TCEP). Crystals of LBP-3 were grown via hanging drop vapor diffusion at 16 °C from solutions containing 1 µL LBP-3, 1 µL mother liquor (0.1 M citric acid pH 4.5, 0.16 M NaCl, and 14 % PEG 3350). Crystals were cryoprotected by immersion in 0.1 M citric acid pH 4.5, 0.24 M NaCl, and 20 % PEG 3350, and 20 % glycerol and flash frozen with liquid nitrogen. Data were collected remotely from the Southeast Regional Collaborative Access Team at the Advanced Photon Source, 22ID beamline (Argonne National Laboratories, Chicago, IL). Data were processed and scaled using HKL-2000 (HKL Research, Inc., Charlottesville, VA) [15] and phased by molecular replacement using Phaser-MR (Phenix, Berkeley, CA) [16]. The structure was phased using a previously solved crystal structure of As-p18 (PDB code: 6I8X) as a search model [11]. Structure refinement and validation was performed using PHENIX (Phenix, Berkeley, CA) (version 1.11.1), and model building was performed in COOT (MRC Laboratory of Molecular Biology, Cambridge, UK) [16, 17]. PyMOL (version 1.8.2; Schrödinger, New York, NY) was used to visualize structures and generate figures.

LBP-2 lipid exchange with C. elegans lipids—A synchronous population of approximately 500,000 day 1, N2 worms were grown at 20°C on OP50. Worms were washed 3x in PBS, frozen into small pellets in liquid Nitrogen, and stored at -80°C. The worms were later cracked using a Cellcrusher. The cracked worms were then ground using a pestle and mortar, which had been chilled with liquid Nitrogen, until no intact worms remained. Liquid nitrogen was added to the sample in both the Cellcrusher and pestle and mortar as needed to maintain a cold temperature. Lipids were extracted from the *C. elegans* lysates using the Bligh and Dyer method [18]. Briefly, homogenized *C. elegans* lysates was resuspended in 5 ml of PBS, 5 ml methanol, and 2.5 ml chloroform and vortexed for 30 minutes. Undissolved material was removed, followed by the addition of chloroform to separate the aqueous and organic phase. The organic phase was collected and dried with nitrogen gas. Dried lipid extracts (~20 mg) were resuspended in LBP-2 sizing buffer (20 mM Hepes pH 7.5, 150 mM NaCl, 5% glycerol, and 0.5 mM TCEP) and vortexed and sonicated in a bath sonicator to form liposomes. The lipid vesicles were incubated with purified apo-LBP-2 at 4 °C overnight. Nonspecifically bound lipids were removed through gel filtration chromatography using a HiLoad 16/60 Superdex 75 column.

Lipid derivatization and mass spectrometry—Lipids were extracted from LBP-2 before and after exchange with *C. elegans* lipid extracts using the Bligh and Dyer method as described above [18]. Fatty acid derivatives were generated as previously described here [19]. Briefly, dried lipid extracts were incubated with 200 μL of oxalyl chloride (2 M in dichloromethane) at 65 °C for 5 minutes, and then dried down with nitrogen gas. Then, 3-picolylamide fatty acid derivatives were formed through incubation with 3-picolylamine at room temperature for 5 minutes and then dried down with nitrogen gas. The fatty acid derivatives were resuspended in methanol for mass spec

analysis. 5 μL of sample was injected onto a ThermoScientific Accucore C18 (4.6 x 100mm, 2.6μm) column using the ExionLC AD UPLC system at a 0.8 ml/min flow rate, and a gradient solvent system containing 10mM ammonium acetate, pH=7 in H_2O (*solvent A*) and 100% Acetonitrile (*solvent B*). Samples were chromatographically resolved using a step wise gradient starting at 40 % *solvent B* for 3 minutes, 100 % *solvent B* for 5 minutes, and then 65 % *solvent B* for 2 minutes. Derivatized fatty acids were detected using ABSciex QTrap5500 triple quadrupole mass spectrometer in positive ion mode. The following multiple reaction-monitoring (MRM) transitions were used to detect the most abundant derivatized fatty acids: myristic acid (14:0, 319.3/109.0), palmitic acid (16:0, 347.3/109), palmitoleic acid (16:1, 345.3/109.0), stearic acid (18:0, 375.3/109.0), oleic acid (18:1, 373.3/109.0), linoleic acid (18:2, 371.3/109.0), alpha-linolenic acid (18:3, 369.3/109.0), eicosadienoic acid (20:2, 399.3/109.0), DGLA (20:3, 397.3/109.0), arachidonic acid (20:4, 395.3/109.0), eicosapentaenoic acid (20:5, 393.3/109.0), docosapentaenoic acid (22:5, 421.3/109.0), and docosahexaenoic acid (22:6, 419.3/109.0). Derivatized fatty acids were quantified in Multiquant 3.0.2 software using a calibration curve with the following fatty acids: myristic acid, palmitic acid, oleic acid, linoleic acid, arachidonic acid, and docosahexaenoic acid.

Competitive fluorescence-based binding assay— Quantification of ligand binding to LBP-3 was conducted via competition with the probe 1-anilinonaphthalene-8-sulfonic acid (1,8-ANS), a small molecule whose fluorescence increases drastically when surrounded by a hydrophobic environment and which has been shown to bind an array of iLBPs with varying affinity [8]. Briefly, binding of 1,8-ANS was carried out in a buffer containing 20 mM Tris HCl pH 7.4, 150 mM NaCl, 5 % glycerol, and 0.5 mM TCEP with a constant amount of 1,8-ANS (500 nM) and

increasing amounts of pure LBP-3 (40 nM – 400 μM). Blank measurements containing LBP-3 alone were subtracted from each protein concentration tested, and the resulting values were fit with a one site binding curve to determine the binding constant, K_d. Competition assays were then carried out in the same buffer using a constant concentration of 500 nM protein and 10 μM 1,8-ANS, with ligand added via 50X ethanol stocks to maintain an ethanol concentration of 2%. Following a one-hour incubation at 37 °C, data were collected on a BioTek Synergy NEO plate reader using an excitation wavelength of 360 nm and an emission wavelength of 525 nm. Blank wells containing only ligand and 1,8-ANS were subtracted from wells with protein at each ligand concentration tested. Background subtracted values were fit with a one site (Fit Ki) curve to calculate the K_i in GraphPad Prism 8. All curves are the average of three independent experiments.

Analytical Ultracentrifugation—Analytical ultracentrifugation experiments were carried out using a Beckman Coulter ProteomeLab™ XLI analytical ultracentrifuge equipped with both absorbance and interference optics and a four-hole An-60 Ti analytical rotor. Sedimentation velocity experiments were carried out at 10 °C and 50,000 rpm (200,000 × g) using 120-mm two-sector charcoal-filled Epon centerpieces with quartz windows. LBP-3 was scanned at 0-min time intervals for ~ 200 scans. LBP-3 was run at 0.2 mg/mL in PBS. Sedimentation boundaries were analyzed by the continuous distribution (c(s)) method using the program SEDFIT [56]. The program SEDNTERP, version 1.09, was used to correct the experimental s value (s*) to standard conditions at 20 °C in water ($s_{20,w}$) and to calculate protein partial specific volume [57]. Corrected $s_{20,w}$ was used for molecular weight calculation.

References

1. Kennedy BK, Lamming DW. The Mechanistic Target of Rapamycin: The Grand ConducTOR of Metabolism and Aging. Cell Metab. 2016;23(6):990-1003. Epub 2016/06/16. doi: 10.1016/j.cmet.2016.05.009. PubMed PMID: 27304501; PMCID: PMC4910876.
2. Wymann MP, Schneiter R. Lipid signalling in disease. Nature reviews Molecular cell biology. 2008;9(2):162-76. Epub 2008/01/25. doi: 10.1038/nrm2335. PubMed PMID: 18216772.
3. Chiapparino A, Maeda K, Turei D, Saez-Rodriguez J, Gavin AC. The orchestra of lipid-transfer proteins at the crossroads between metabolism and signaling. Prog Lipid Res. 2016;61:30-9. Epub 2015/12/15. doi: 10.1016/j.plipres.2015.10.004. PubMed PMID: 26658141.
4. Storch J, McDermott L. Structural and functional analysis of fatty acid-binding proteins. J Lipid Res. 2009;50 Suppl:S126-31. Epub 2008/11/20. doi: 10.1194/jlr.R800084-JLR200. PubMed PMID: 19017610; PMCID: PMC2674722.
5. Folick A, Oakley HD, Yu Y, Armstrong EH, Kumari M, Sanor L, Moore DD, Ortlund EA, Zechner R, Wang MC. Aging. Lysosomal signaling molecules regulate longevity in Caenorhabditis elegans. Science (New York, NY). 2015;347(6217):83-6. Epub 2015/01/03. doi: 10.1126/science.1258857. PubMed PMID: 25554789; PMCID: PMC4425353.
6. Villeneuve J, Bassaganyas L, Lepreux S, Chiritoiu M, Costet P, Ripoche J, Malhotra V, Schekman R. Unconventional secretion of FABP4 by endosomes and secretory lysosomes. The Journal of cell biology. 2018;217(2):649-65. Epub 2017/12/08. doi: 10.1083/jcb.201705047. PubMed PMID: 29212659; PMCID: PMC5800802.
7. Josephrajan A, Hertzel AV, Bohm EK, McBurney MW, Imai SI, Mashek DG, Kim DH, Bernlohr DA. Unconventional Secretion of Adipocyte Fatty Acid Binding Protein 4 Is Mediated By Autophagic Proteins in a Sirtuin-1-Dependent Manner. Diabetes. 2019;68(9):1767-77. Epub 2019/06/07. doi: 10.2337/db18-1367. PubMed PMID: 31171562; PMCID: PMC6702637.
8. Kane CD, Bernlohr DA. A simple assay for intracellular lipid-binding proteins using displacement of 1-anilinonaphthalene 8-sulfonic acid. Anal Biochem. 1996;233(2):197-204. Epub 1996/01/15. doi: 10.1006/abio.1996.0028. PubMed PMID: 8789718.
9. Tillman MC, Khadka M, Duffy J, Wang MC, Ortlund EA. Structural characterization of life-extending Caenorhabditis elegans Lipid Binding Protein 8. Scientific reports. 2019;9(1):9966. Epub 2019/07/12. doi: 10.1038/s41598-019-46230-8. PubMed PMID: 31292465; PMCID: PMC6620326.
10. Cabrita LD, Bottomley SP. Protein expression and refolding--a practical guide to getting the most out of inclusion bodies. Biotechnology annual review. 2004;10:31-50. Epub 2004/10/27. doi: 10.1016/s1387-2656(04)10002-1. PubMed PMID: 15504702.
11. Ibanez-Shimabukuro M, Rey-Burusco MF, Gabrielsen M, Franchini GR, Riboldi-Tunnicliffe A, Roe AJ, Griffiths K, Cooper A, Corsico B, Kennedy MW, Smith BO. Structure and ligand binding of As-p18, an extracellular fatty acid binding protein from the eggs of a parasitic nematode. Bioscience reports. 2019;39(7). Epub 2019/07/06. doi: 10.1042/bsr20191292. PubMed PMID: 31273060; PMCID: PMC6646235.
12. Holm L, Rosenstrom P. Dali server: conservation mapping in 3D. Nucleic acids research. 2010;38(Web Server issue):W545-9. Epub 2010/05/12. doi: 10.1093/nar/gkq366. PubMed PMID: 20457744; PMCID: PMC2896194.
13. Gillilan RE, Ayers SD, Noy N. Structural basis for activation of fatty acid-binding protein 4. Journal of molecular biology. 2007;372(5):1246-60. Epub 2007/09/01. doi: 10.1016/j.jmb.2007.07.040. PubMed PMID: 17761196; PMCID: PMC2032018.

14. Sanson B, Wang T, Sun J, Wang L, Kaczocha M, Ojima I, Deutsch D, Li H. Crystallographic study of FABP5 as an intracellular endocannabinoid transporter. Acta Crystallogr D Biol Crystallogr. 2014;70(Pt 2):290-8. Epub 2014/02/18. doi: 10.1107/s1399004713026795. PubMed PMID: 24531463; PMCID: PMC3940194.
15. Otwinowski Z, Minor W. [20] Processing of X-ray diffraction data collected in oscillation mode. Methods in enzymology. 1997;276:307-26. Epub 1997/01/01. doi: 10.1016/s0076-6879(97)76066-x. PubMed PMID: 27799103.
16. Adams PD, Afonine PV, Bunkoczi G, Chen VB, Davis IW, Echols N, Headd JJ, Hung LW, Kapral GJ, Grosse-Kunstleve RW, McCoy AJ, Moriarty NW, Oeffner R, Read RJ, Richardson DC, Richardson JS, Terwilliger TC, Zwart PH. PHENIX: a comprehensive Python-based system for macromolecular structure solution. Acta Crystallogr D Biol Crystallogr. 2010;66(Pt 2):213-21. Epub 2010/02/04. doi: 10.1107/s0907444909052925. PubMed PMID: 20124702; PMCID: PMC2815670.
17. Emsley P, Lohkamp B, Scott WG, Cowtan K. Features and development of Coot. Acta Crystallogr D Biol Crystallogr. 2010;66(Pt 4):486-501. Epub 2010/04/13. doi: 10.1107/s0907444910007493. PubMed PMID: 20383002; PMCID: PMC2852313.
18. Bligh EG, Dyer WJ. A rapid method of total lipid extraction and purification. Can J Biochem Physiol. 1959;37(8):911-7. Epub 1959/08/01. PubMed PMID: 13671378.
19. Li X, Franke AA. Improved LC-MS method for the determination of fatty acids in red blood cells by LC-orbitrap MS. Analytical chemistry. 2011;83(8):3192-8. Epub 2011/03/25. doi: 10.1021/ac103093w. PubMed PMID: 21428294; PMCID: PMC4439250.